

Electronic Thesis and Dissertation Repository

12-9-2016 12:00 AM

Synthesis of Metal-Containing Polymers and Stable Organic Radical-Containing Polymers and Their Use as Advanced Functional Materials


Joseph A. Paquette, *The University of Western Ontario*

Supervisor: Joe B Gilroy, *The University of Western Ontario*

A thesis submitted in partial fulfillment of the requirements for the Doctor of Philosophy degree in Chemistry

© Joseph A. Paquette 2016

Follow this and additional works at: <https://ir.lib.uwo.ca/etd>

 Part of the [Inorganic Chemistry Commons](#), [Materials Chemistry Commons](#), [Organic Chemistry Commons](#), and the [Polymer Chemistry Commons](#)

Recommended Citation

Paquette, Joseph A., "Synthesis of Metal-Containing Polymers and Stable Organic Radical-Containing Polymers and Their Use as Advanced Functional Materials" (2016). *Electronic Thesis and Dissertation Repository*. 4275.

<https://ir.lib.uwo.ca/etd/4275>

This Dissertation/Thesis is brought to you for free and open access by Scholarship@Western. It has been accepted for inclusion in Electronic Thesis and Dissertation Repository by an authorized administrator of Scholarship@Western. For more information, please contact wlsadmin@uwo.ca.

Abstract

The work presented in this thesis details the synthesis and characterization of two different families of multifunctional polymers. The first family involved the incorporation of stable 6-oxoverdazyl radicals into polymer scaffolds. This was originally achieved by the polymerization of the radical precursors, phenyl- and *isopropyl*-6-oxotetrazanes, followed by post-polymerization oxidation to afford the phenyl- and *isopropyl*-6-oxoverdazyl polymers. A second methodology involved the direct polymerization of *isopropyl*-6-oxoverdazyl radicals using ring-opening metathesis polymerization (ROMP) to afford polymers with controlled molecular weights and narrow molecular weight distributions. The polymers were characterized by the close comparison of the physical and spectroscopic properties to related model compounds. The semiconducting behaviour of the latter polymer was explored and ultimately exploited in flash memory devices.

The second family included redox-active Ni(II) complexes of Goedken's macrocycle. This macrocycle was incorporated into main-chain polymers via a step growth mechanism involving Sonogashira cross-coupling with π -conjugated solubilizing organic spacers and into side-chain polymers via a chain growth polymerization using ROMP. The resulting polymers spectroscopic and physical properties were characterized and compared to a variety of model compounds. Main-chain Ni(II) complexes of Goedken's macrocycle and fluorene copolymers were further functionalized with $\text{Co}_2(\text{CO})_8$ via the alkyne synthetic handle to yield heterobimetallic copolymers that yielded metal-rich nanomaterials upon pyrolysis in a reducing atmosphere.

Combined, this work represents a significant advance in the synthesis, characterization and application of synthetic multifunctional polymers.

Keywords

Stable Radical Polymers, Free Radical Polymerization, Ring-Opening Metathesis Polymerization, Semiconductivity, Organic Electronics, Electrochemistry, Redox Chemistry, Heterocycle Chemistry, Metallopolymers, Goedken's Macrocycle, Pyrolysis, π -Conjugated Polymers.

Co-Authorship Statement

The work described in this thesis contains contributions from the author as well as co-workers Dr. Jacquelyn T. Price, Christopher S. Harrison, Reg Bauld, Stephanie M. Barbon, Sabastine Ezugwu, Ethan R. Sauv , Prof. Giovanni Fanchini, and my supervisor Prof. Joe B. Gilroy. The contributions of each are described below.

Chapter 1 was written by the author and edited by Prof. Joe Gilroy

Chapter 2 describes a project that was in large part a collaborative effort between the author and Dr. Price. The author was responsible for the synthesis and characterization of the phenyl-substituted 6-oxoverdazyl polymer, and Dr. Price was responsible for the synthesis and characterization of the *isopropyl*-substituted 6-oxoverdazyl polymer and the solid state structures presented in the chapter. Initial efforts toward the synthesis of these materials was undertaken by Christopher Harrison. The KPFM measurements and assistance with EPR measurements were done by Reg Bauld and Prof. Fanchini from the Department of Physics. The chapter was written by the author, Dr. Price and Prof. Gilroy and edited by Prof. Fanchini.

Chapter 3 describes the synthesis and characterization of a 6-oxoverdazyl polymer performed by the author. Data acquisition for the solid-state structure and assistance with EPR measurements was done by Stephanie Barbon. Thin-film measurements and subsequent memsistor studies were performed in collaboration with Sabastin Egzugwu and Prof. Fanchini from the Department of Physics. The chapter was written by the author and edited by Prof. Gilroy.

Chapter 4 describes a project for which most of the experimental work and characterization was performed by the author. As a work-study student, Ethan Sauv  aided in the preparation and purification of synthetic materials up to and including the monomer. The solid-state structure was elucidated by Stephanie Barbon. The chapter was written by the author and edited by Prof. Joe Gilroy.

Chapter 5 details a project designed by the author and Prof. Joe Gilroy. The experimental work and characterization was performed by the author. The chapter was written by the author and edited by Prof. Joe Gilroy.

Acknowledgments

I want to begin by expressing my never ending gratitude to Professor Joe Gilroy, who has – by far – contributed the most towards the completion of my degree. I am grateful that you have given me the opportunity to join your group four years ago and I believe this is one of the best decisions I have ever made. Under Joe’s tutelage I have become a better chemist, communicator, presenter, and mentor, which will be essential tools for my future endeavours. Joe’s support, encouragement, and life lessons have pushed me to improve everyday and be the best researcher possible.

This degree would not have been possible without lots of help from the members of the Gilroy Group. The people who have been there since the start: Steph, who has always been willing to lend a helping hand and Amir a steadfast friend who was always willing to talk about anything. The new grad students: Ryan, who’s passion for science and desire to learn was appreciated and Sam for putting up with me and doing it with a smile. Jackie, John, and Ana you have been great mentors and friends. Thanks to the students I have mentored along the way, Ethan, Jordan, Jasmine, and Devin, it was truly a pleasure. I especially want to thank all my friends I have made over the years including everyone from the Alibi crew, to my ‘Ohana’, and to everyone on the many sports teams.

I have been fortunate to study at a university where there was ample interest in collaborations. I appreciate the opportunity to work with Sivayini Kandeepan and Professor Mittler on the gold precursor project and with Professor Fanchini and Sabastine Ezugwu who were instrumental in device fabrication of my polymers. These collaborations have been fruitful and have taught me a lot about teamwork. I must also thank the Ragogna and Gillies Groups that have been so collegial when our group was new and as it grows.

The Department of Chemistry is made up of many awesome staff that have helped along the way. Mat Willans’ expertise was always valuable when elucidating new structures in the NMR room. Doug Harsine always managed to find my ion peak no matter how mixed the sample seemed to be. The office staff were always helpful, especially Darlene who answered any and all questions with a smile and Clara who was always willing to help. The ChemBio Stores for the help over the years: Marylou, Monica, Yuhua, and Sherrie.

A special thanks to my committee members Professors Brian Pagenkopf, Dick Puddephatt, Paul Charpentier, and Martin Lemaire for taking the time to read this thesis and providing important feedback.

I cannot forget to thank my parents Claude and Bizz who have given me so much over the years. It seems the older I get, the more I appreciate them. I will always strive to be as hardworking, fun-loving, kind, and selfless as they are. I also want to thank my sisters, Michelle, Peekie, and Renee, and my new brothers Tony, Adam, and Sam whom are some of my favourite people.

Lastly, I want to thank Rebecca for the never ending support, for sharing in the struggle, and for always being patient and standing by me all these years, even though I can be super annoying.

Table of Contents

Abstract.....	i
Co-Authorship Statement.....	ii
Acknowledgments.....	iii
Table of Contents.....	v
List of Tables.....	x
List of Figures.....	xi
List of Schemes.....	xvii
List of Appendices.....	xix
List of Abbreviations.....	xx
Chapter 1.....	1
1 Introduction.....	1
1.1 π -Conjugated, Stable Radical, and Metal-Containing Multifunctional Polymers ..	1
1.2 Organic Polymers.....	2
1.2.1 Polyacetylene.....	3
1.2.2 Polythiophene, its Derivatives, and Organosulfur Compounds.....	6
1.2.3 Heteroatom and Carbonyl-Containing Polymers.....	8
1.2.4 Stable Organic Radical Polymers.....	10
1.3 Metal-Containing Polymers.....	14
1.3.1 π -Conjugated MCPs.....	15
1.3.2 Non-Conjugated MCPs.....	20
1.4 Scope of Thesis.....	23
1.5 References.....	25
Chapter 2.....	37
2 6-Oxoverdazyl Radical Polymers with Tunable Electrochemical Properties.....	37

2.1	Introduction.....	37
2.2	Experimental.....	38
2.2.1	General considerations.....	38
2.2.2	Electrochemical Methods.....	39
2.2.3	Electron Paramagnetic Resonance (EPR) Spectroscopy	39
2.2.4	Kelvin Probe Force Microscopy (KPFM).....	40
2.2.5	X-ray Crystallography Details	41
2.2.6	Synthetic Procedures.....	42
2.3	Results and Discussion	52
2.3.1	Synthesis of Monomers.....	52
2.3.2	Polymerization	53
2.3.3	Macromolecular Properties.....	55
2.3.4	Synthesis of Model Compounds	57
2.3.5	Spectroscopic Characterization.....	58
2.3.6	Electrochemical Properties	60
2.3.7	Solid-State Behaviour	62
2.3.8	Thin-Film Studies	64
2.4	Conclusion	65
2.5	References.....	66
	Chapter 3.....	70
3	Synthesis, Characterization, and Thin-Film Properties of 6-Oxoverdazyl Polymers Prepared by Ring-Opening Metathesis Polymerization.....	70
3.1	Introduction.....	70
3.2	Experimental.....	72
3.2.1	General Considerations.....	72
3.2.2	Gel Permeation Chromatography (GPC).....	72

3.2.3	Thermal Analysis	73
3.2.4	Cyclic Voltammetry	73
3.2.5	Electron Paramagnetic Resonance Spectroscopy	73
3.2.6	X-ray Crystallography	74
3.2.7	Thin-Film Preparation and Electrical Conductivity Measurements	75
3.2.8	Synthetic Procedures.....	77
3.2.9	Kinetic Studies of the ROMP of Monomer 3.12	79
3.3	Results and Discussion	80
3.3.1	Synthesis	80
3.3.2	Polymer Characterization.....	84
3.3.3	Electrical Properties of Thin Films of Polymer 3.13	86
3.3.4	Ultrathin Memistor Device.....	89
3.4	Conclusion	90
3.5	References.....	91
Chapter 4.....		96
4	Synthesis, Characterization, and Preceramic Properties of π -Conjugated Polymers Based on Ni(II) Complexes of Goedken's Macrocycle	96
4.1	Introduction.....	96
4.2	Experimental.....	97
4.2.1	General Considerations.....	97
4.2.2	Microwave Reactions.....	98
4.2.3	Gel Permeation Chromatography (GPC).....	98
4.2.4	Thermal Analysis and Pyrolysis Studies.....	99
4.2.5	Electrochemical Methods.....	100
4.2.6	X-ray Crystallography Details	100
	Synthetic Procedures.....	101

4.3 Results and Discussion	108
4.3.1 Monomer Synthesis	108
4.3.2 Copolymer Synthesis	110
4.3.3 Model Compound Synthesis	113
4.3.4 UV-vis Absorption Spectroscopy	114
4.3.5 Cyclic Voltammetry	116
4.3.6 Post-Polymerization Functionalization	118
4.3.7 Thermal Analysis	119
4.3.8 Pre-Ceramic Properties	120
4.4 Conclusion	122
4.5 References	123
Chapter 5	130
5 Side-Chain Polymers bearing Ni(II) Complexes of Goedken's Macrocycle	130
5.1 Introduction	130
5.2 Experimental	131
5.2.1 General Considerations	131
5.2.2 Gel Permeation Chromatography (GPC)	132
5.2.3 Thermal Analysis and Pyrolysis Studies	132
5.2.4 Electrochemical Methods	133
5.2.5 Synthesis	133
5.3 Results and Discussion	138
5.3.1 Monomer Synthesis	138
5.3.2 Polymerization	139
5.3.3 Kinetic Studies	140
5.3.4 Polymer Characterization	143
5.4 Conclusion	146

5.5 References.....	147
Chapter 6.....	151
6 Conclusions and Future Work.....	151
6.1 Conclusions.....	151
6.2 Future Work.....	154
6.2.1 6-Oxoverdazyl Radical Polymers	154
6.2.2 Incorporation of Goedken’s Macrocycle into Copolymers	156
6.3 References.....	158
Appendices.....	160
Appendix 1 – Permission to Reuse Copyrighted Material.....	160
Appendix 2 – Supporting Information for Chapter 2.....	170
Appendix 3 – Supporting Information for Chapter 3.....	185
Appendix 4 – Supporting Information for Chapter 4.....	190
Appendix 5 – Supporting Information for Chapter 5.....	206
Curriculum Vitae	213

List of Tables

Table 2.1 Crystallographic data for compounds 2.11a , 2.11c , and 2.12c	42
Table 2.2 Polymer characterization data.	56
Table 2.3 Electrochemical data for verdazyl polymers 2.7a,b and verdazyl radicals 2.11a,b	61
Table 2.4 Selected bond lengths (Å) and angles (°) for 6-oxoverdazyl 2.11a,c and cation 2.12c	64
Table 3.1 Selected X-ray diffraction data collection and refinement details for monomer 3.12	75
Table 3.2 Electrochemical data for 6-oxoverdazyl monomer 3.12 and polymer 3.13	86
Table 4.1 Crystallography data for compound solid state structure of 4.7	101
Table 4.2 Reaction conditions for the production of polymer 4.10F (optimized conditions shown in bold).....	112
Table 4.3 Summary of GPC data for copolymers 4.10F , 4.10F-[Co₂(CO)₆]₂ , 4.10B , and 4.10T	113
Table 4.4 UV-vis absorption spectroscopy data for copolymers 4.10F , 4.10F-[Co₂(CO)₆]₂ , 4.10T , and 4.10B , and model compounds 4.13 and 4.14 in CH ₂ Cl ₂	116
Table 4.5 Cyclic voltammetry data for polymers 4.10F , 4.10T , 4.10B and model compounds 4.13 and 4.14 . ^a	117
Table 5.1 MW data for the polymer 5.11 produced in different solvents.	140
Table 5.2 Cyclic voltammetry data for monomer 5.10 and polymer 5.11	145

List of Figures

Figure 1.1 Image and schematic of a polymer light emitting diode using PPV.	3
Figure 1.2 Frontier orbitals of atomic orbitals of ethene, butadiene, and polyacetylene.	4
Figure 1.3 Range of conductivities covered by PA compared to other relevant materials.	4
Figure 1.4 Positive charge propagation during the oxidation of <i>p</i> -type radical polymers in electrolyte solution. Figure adapted from Ref. [71].	12
Figure 1.5 Energy diagram of <i>p</i> -type (red) and <i>n</i> -type (blue) radical polymers, and redox-active polymers for comparison (black). Figure adapted from Ref. [71].	12
Figure 1.6 (a) Representation of polymer-based flow battery that includes two reservoir tanks, the first including the TEMPO containing copolymer and the second including a redox-active viologen based copolymer. The reservoirs are separated by a size-exclusion membrane that allows the electrolytes to permeate but not the macromolecules. (b) The fundamental electrode reactions are shown of the TEMPO radical and viologen. Reproduced with permission from Ref. [77].	13
Figure 1.7 Radical polymer-based memory architecture and electron movement of the device. Reproduced with permission from Ref. [83].	14
Figure 1.8 Representation of Type I-III MCPs. Figure adapted from Ref. [90].	15
Figure 1.9 Structure of Zn-porphyrin nanorings and scanning tunneling microscopy images of a 30 repeat unit nanoring deposited on a gold surface. Figure reproduced with permission from Ref. [102].	17
Figure 1.10 STM image of polymer 1.54 formed on a Ag(111) surface. Image reproduced with permission from Ref. [103].	18
Figure 1.11 (a) Pyrolyzed pentagon shaped polymers derived from PFS, (b) PFS microparticle, (c) PFS micelles with complex fluorescent patterning (scale = 5µm). Images reproduced with permission from (a) [129], (b) [130], and (c) [131].	21

Figure 1.12 (left) Calculated singly occupied molecular orbital (SOMO, DFT; B3LYP/6-31G), ¹⁴³ (right) corresponding molecular drawing for 6-oxoverdazyl 1.72	23
Figure 2.1 ¹ H NMR spectra of (a) monomer 2.5b and (b) polymer 2.6b . The squares indicate H ₂ O signals, circles indicate EtOAc, and triangles indicate residual DMSO.....	55
Figure 2.2 Normalized GPC traces recorded in DMF containing 10 mM LiBr and 1 % (v/v) triethylamine at 85 °C for (a) tetrazane polymer 2.6a (black) and 6-oxoverdazyl polymer 2.7a (red), and (b) for tetrazane polymer 2.6b (black), tetrazane polymer 2.6b after air oxidation for 24 h (blue), tetrazane polymer 2.6b after air oxidation for 48h (green), and 6-oxoverdazyl polymer 2.7b (red).	56
Figure 2.3 IR spectra for tetrazane polymer 2.6a (black), verdazyl polymer 2.7a (red), and verdazyl model compound 2.11a (green). The baselines are offset for ease of comparison. .	59
Figure 2.4 EPR spectra of (a) 6-oxoverdazyl 2.11a (g = 2.0043, black) and 6-oxoverdazyl polymer 2.7a (g = 2.0050, red) and (b) triaryl-6-oxoverdazyl 2.11b (g = 2.0038, black) and triaryl-6-oxoverdazyl polymer 2.7b (g = 2.0043, red) in CH ₂ Cl ₂ . (See Figures A17,18 for simulation of the spectrum of 2.11a,b).	60
Figure 2.5 UV-vis absorption spectrum of 6-oxoverdazyl 2.7b (red) and model 2.11b (black).	60
Figure 2.6 Cyclic voltammograms of 6-oxoverdazyl polymer 2.7b (red) and model 6-oxoverdazyl 2.11b (black) recorded at scan rate 100 mV s ⁻¹ in THF solutions of 1 mM analyte and 0.1 M <i>n</i> Bu ₄ NPF ₆	61
Figure 2.7 Solid-state structures of 6-oxoverdazyl 2.11c (left) and tetrazinium cation 2.12c (right). Anisotropic displacement ellipsoids are shown at 50% probability level. Hydrogen atoms have been omitted for clarity.....	63
Figure 2.8 Solid-state structure of 2.11a . Anisotropic displacement ellipsoids are shown at 50 % probability level. Hydrogen atoms have been omitted for clarity.	63
Figure 2.9 AFM topography (top) and KPFM image (bottom) of 6-oxoverdazyl polymer 2.7a referenced to ITO (work function: 4.7 eV ⁴⁰). The inset is a histogram of the KPFM image	

showing a work function of 4.9 ± 0.1 eV for **2.7a**. The small peak on the right is a KPFM artifact due to lateral contact of the tip with the film edge. 65

Figure 3.1 Solid-state structure of monomer **3.12**. Anisotropic displacement ellipsoids are shown at 50% probability and hydrogen atoms have been omitted for clarity. Selected bond lengths (Å): N1-N2 1.3558(15), N3-N4 1.3595(15), N1-C2 1.3819(16), N2-C1 1.3319(16), N3-C2 1.3802(16), N4-C1 1.3315(16), C24-C25 1.318(2). Selected bond angles (deg): N1-N2-C1 115.00(10), N3-N4-C1 114.96(10), N1-C2-N3 114.35(11), N2-C1-N4 127.20(11).. 81

Figure 3.2 Representative GPC traces for (a) a typical sample of polymer **3.13** ($M_n = 46,100$ g mol⁻¹, $M_w = 49,300$ g mol⁻¹, $D = 1.07$) and (b) a GPC trace for a polymer containing a minor fraction of high molecular weight polymer **3.13** ($M_n = 51,100$ g mol⁻¹, $M_w = 57,750$ g mol⁻¹, $D = 1.13$). (c) Relationship of feed molar ratio and DP_n determined by GPC. The black line represents the theoretical relationship between DP_n and feed molar ratio. (d) Molecular weight (M_n) as a function of reaction time. 83

Figure 3.3 (a) UV-vis absorption spectra acquired for CH₂Cl₂ solutions of monomer **3.12** (red line) and polymer **3.13** (black line). (b) Magnified spectra from 350 to 475 nm. 84

Figure 3.4 Experimental EPR spectra of 6-oxoverdazyl monomer **3.12** (red line, $g = 2.0045$) and polymer **3.13** (black line, $g = 2.0043$). Simulation of the spectrum of monomer **3.12** yielded the following parameters: line width = 0.089 mT, $a_{N1,3} = 0.529$ mT, $a_{N2,4} = 0.640$ mT, $a_H = 0.140$ mT (Figure A3.8). 85

Figure 3.5 CVs of 6-oxoverdazyl monomer **3.12** (red line) and polymer **3.13** (black line) recorded at a scan rate of 100 mV s⁻¹ in CH₂Cl₂/MeCN (1:1) solution containing 1 mM analyte and 0.1 M *n*Bu₄NPF₆ as supporting electrolyte..... 86

Figure 3.6 (a) Sandwich-type configuration for measuring the I-V characteristics of polymer **3.13** thin films, showing bistable electrical transport. (b) I-V curves of thin films at four different thicknesses in high conductivity state, which were fitted with straight lines to demonstrate ohmic transport and (c) I-V curves of thin films in low conductivity state showing non-ohmic, Poole-Frenkel like, behavior. Solid line fits were performed using eq. (2). (d) Film resistivity values obtained from the low-voltage portions of I-V curves..... 88

Figure 3.7 (a) Schematic representation of the electron hopping mechanism from repeating unit to repeating unit, in a Poole-Frenkel mechanism in the high conductivity and in an extended states mechanism for low conductivity. (b) The structural schematic of sandwich memristors from **3.13** thin film formed by spin coating 12.5 mg mL^{-1} of **3.13** dissolved in anhydrous chlorobenzene, four identical pre-patterned bottom electrodes and thermally evaporated Ca/Al top electrodes. 90

Figure 4.1 (a) Side view, and (b) top view of the solid-state structure of monomer **4.7**. Anisotropic displacement ellipsoids are shown at 50% probability. Hydrogen atoms and co-crystallized solvent molecules omitted for clarity. Selected bond lengths (Å): N1-C2 1.335(2), N1-C35 1.417(2), N1-Ni 1.8543(15), N2-C4 1.336(2), N2-C29 1.4156(19), N2-Ni 1.8590(13), N3-C16 1.333(2), N3-C34 1.4140(19), N3-Ni 1.8533(15), N4-C18 1.329(2), N4-C40 1.414(2), N4-Ni 1.8533(13), C2-C3 1.411(2), C3-C4 1.411(2), C16-C17 1.418(2), C17-C18 1.414(2). Selected bond angles (°): N1-Ni-N2 94.35(6), N2-Ni-N3 85.97(6), N3-Ni-N4 93.93(6), N1-Ni-N4 85.69(6)..... 110

Figure 4.2 ^1H NMR spectra of comonomers **4.7** (blue), **4.11** (black), and polymer **4.10F** (red) recorded in CDCl_3 (asterisks denote residual CHCl_3 and H_2O). 113

Figure 4.3 UV-vis absorption spectra recorded in CH_2Cl_2 . (a) Comparison of copolymers **4.10F**, **4.10T**, and **4.10B**. (b) Comparison of model compounds **4.13**, **4.14**, and copolymer **4.10F**. 115

Figure 4.4 Cyclic voltammograms of **4.10F**, **4.10T**, and **4.10B** recorded at a scan rate of 100 mV s^{-1} in CH_2Cl_2 solutions containing $1 \times 10^{-3} \text{ M}$ analyte and 0.1 M $[\text{nBu}_4\text{N}][\text{PF}_6]$ as supporting electrolyte..... 117

Figure 4.5 FT-IR spectra of **4.10F** (black) and **4.10F**- $[\text{Co}_2(\text{CO})_6]_2$ (purple). The dashed boxes highlight the energy regions of specific interest. 119

Figure 4.6 TGA data demonstrating the thermal decomposition of **4.10F** (black) and **4.10F**- $[\text{Co}_2(\text{CO})_6]_2$ (purple). 120

Figure 4.7 SEM of the nanomaterials resulting from pyrolysis of A) **4.10F** and B) **4.10F**- $[\text{Co}_2(\text{CO})_6]_2$. Elemental maps (EDX spectroscopy) of the nanomaterials resulting from the

pyrolysis of C) 4.10F and D) 4.10F -[Co ₂ (CO) ₆] ₂ . Light areas indicate a positive response for the elements in question.....	121
Figure 5.1 (a) Number average molecular weight (M_n) as a function of time from GPC, (b) semilogarithmic plot for the consumption of monomer 5.10 as a function of time. $[M]_0/[M]$ was determined using ¹ H NMR integration data.	142
Figure 5.2 (a) GPC traces of polymer samples at different catalyst loadings. The graphs have been colour coded for ease of comparison. (b) Relationship of feed molar ratio and DP_n determined by GPC using conventional calibration. The black line depicts ideal behaviour.	143
Figure 5.3 (a) UV-vis absorption spectra recorded in CH ₂ Cl ₂ of monomer 5.10 (black) and polymer 5.11 (red). (b) UV-vis absorption spectra of polymer 5.11 in CH ₂ Cl ₂ (red) and as a thin-film (blue).....	144
Figure 5.4 CVs of 5.10 (black) and 5.11 (red) recorded at a scan rate of 250 mV s ⁻¹ in CH ₂ Cl ₂ solutions containing 1 × 10 ⁻³ M analyte and 0.1 M [<i>n</i> Bu ₄ N][PF ₆] as supporting electrolyte.	145
Figure 5.5 CVs of polymer 5.11 in THF (green) and THF/CH ₂ Cl ₂ (1:1) solvent mixture (purple) recorded at a scan rate of 250 mV s ⁻¹ in CH ₂ Cl ₂ solutions containing 1 × 10 ⁻³ M analyte and 0.1 M [<i>n</i> Bu ₄ N][PF ₆] as supporting electrolyte.	146
Figure 6.1 Graphical summary of Chapter 1.....	151
Figure 6.2 Graphical summary of Chapter 2.....	152
Figure 6.3 Graphical summary of Chapter 4.....	153
Figure 6.4 Graphical summary of Chapter 5.....	154
Figure 6.5 Plot of mean intersite distance (δ_{AV}) versus redox capacities for various redox active polymers. Polymers from left to right: 3.13 , 1.2 , 6.3 , poly(vinylferrocene), poly(ethernitroxide), and 6.6 . The dotted curve represents the mean intersite distance calculated per repeating unit. Inset: R represents redox-active sites.	156

Figure 6.6 Synthesis of a block copolymer based on Goedken's macrocycle, followed by their self-assembly into micelles and targeted payload release.....	157
Figure 6.7 (a) Synthesis of an asymmetric Goedken's macrocycle and (b) potential template molecule 6.12	158
Figure 6.8 Template synthesis of cyclic oligomers composed of M(II) complexes of Goedken's macrocycle (6.11) with template molecule (6.12). i) PdCl ₂ (PPh ₃) ₂ , CuI, Et ₃ N, THF. ii) pyridine.....	158

List of Schemes

Scheme 1.1 Synthesis of PAs from acetylene precursors.....	5
Scheme 1.2 General synthetic method for regioregular P3AT using GRIM.	6
Scheme 1.3 The nitroxide radical can be reversibly oxidized and reduced.	10
Scheme 1.4 Synthesis of PFS from ferrocene.	21
Scheme 1.5 Templated synthesis of a Ni(II) complex of Goedken's macrocycle. ¹⁴⁴	24
Scheme 2.1 (a) Synthesis of monomer 2.5a and (b) synthesis of monomer 2.5b	53
Scheme 2.2 (a) Synthesis of polymers 2.6a,b and (b) verdazyl radicals polymers 2.7a,b	54
Scheme 2.3 Synthesis of <i>i</i> Pr-substituted model compounds 2.11a and 2.12a	58
Scheme 2.4 Synthesis of phenyl-substituted model compound 2.11b	58
Scheme 2.5 Synthesis and oxidation of 6-oxoverdazyl radical 2.11c	62
Scheme 3.1 Synthesis of 6-oxoverdazyl monomer 3.12 and polymer 3.13	81
Scheme 4.1 Synthesis of monomer 4.7 and macrocycle 4.9	109
Scheme 4.2 Synthesis of copolymers 4.10F , 4.10B , and 4.10T	111
Scheme 4.3 Synthesis of model compounds 4.13 and 4.14	114
Scheme 4.4 Synthesis of 4.10F -[Co ₂ (CO) ₆] ₂	118
Scheme 5.1 Synthesis of monomer 5.10	139
Scheme 5.2 ROMP of monomer 5.10 using Grubbs' 3 rd generation catalyst.	140
Scheme 6.1 Proposed synthesis of an <i>isopropyl</i> -6-oxoverdazyl polymer with higher radical content using ROMP.	155

Scheme 6.2 Proposed synthetic route towards 6-oxoverdazyl polymers with higher radical content metal-catalyzed polymerization.	155
--	-----

List of Appendices

Appendix 1 – Permission to Reuse Copyrighted Material.....	160
Appendix 2 – Supporting information for Chapter 2.....	170
Appendix 3 – Supporting Information for Chapter 3.....	185
Appendix 4 – Supporting Information for Chapter 4.....	190
Appendix 5 – Supporting Information for Chapter 5.....	206

List of Abbreviations

°	degree
°C	degrees Celsius
¹³ C	carbon-thirteen
¹ H	proton
2D	two-dimensional
3D	three-dimensional
A	absorbance
Å	angstrom
a.u.	arbitrary units
AC	alternating current
AcOH	acetic acid
AFM	atomic force microscopy
ATR	attenuated total reflectance
br	broad
Bu	butyl
<i>ca.</i>	approximately
CCDC	the Cambridge crystallographic data centre
cm	centimeter
cm ⁻¹	wavenumber
Cp	cyclopentadienyl
CuAAC	copper(I)-catalyzed azide-alkyne cycloaddition reaction
CV	cyclic voltammetry
<i>D</i>	dispersity
d	doublet
DCC	dicyclohexylcarbodiimide
dd	doublet of doublets
DI	deionized water
DIPA	<i>diisopropylamine</i>
DMAP	dimethylaminopyridine
DMF	dimethylformamide

DMSO	dimethylsulfoxide
DNA	deoxyribonucleic acid
DP _n	degree of polymerization
DSC	differential scanning calorimetry
E	potential
E _{1/2}	half-wave potential
EA	elemental analysis
EDX	energy dispersive X-ray
E _g	band-gap
EI	electron-impact ionization
E _{pa}	anodic peak potential
E _{pc}	cathodic peak potential
EPR	electron paramagnetic resonance
equiv.	equivalent(s)
ESI-MS	electrospray ionization mass spectrometry
Et	ethyl
Et ₂ O	diethyl ether
Et ₃ N	triethylamine
EtOAc	ethyl acetate
EtOH	ethanol
eV	electron volts
EVE	ethyl vinyl ether
Fc	ferrocene
FT-IR	Fourier transform infra-red spectroscopy
FW	formula weight
g	grams
<i>g</i>	electron spin g-factor
G3	Grubbs' third generation catalyst
GPC	gel permeation chromatography
GRIM	Grignard metathesis
h	hours
hex	hexanes

HOMO	highest-occupied molecular orbital
HRMS	high-resolution mass spectroscopy
HT	heat-to-tail
Hz	hertz
ITO	indium tin oxide
I-V	current-voltage
<i>J</i>	NMR coupling constant
K	Kelvin
kg	kilograms
kHz	kilohertz
KPFM	Kelvin-probe force microscopy
LED	light emitting diode
LUMO	lowest-unoccupied molecular orbital
M	molar
m	multiplet
mA	milliamps
max	maximum
Mc	macrocycle
MCP	metal-containing polymer
Me	methyl
MeCN	acetonitrile
mg	milligram
MHz	megahertz
min	minute/minutes
mL	milliliters
MLCT	metal-to-ligand charge transfer
mm	millimeter
mM	millimolar
mmol	millimoles
M_n	number average molecular weight
mol	moles
mV	millivolts

MW	molecular weight
M_w	weight average molecular weight
nm	nanometers
NMR	nuclear magnetic resonance
<i>n</i> -type	electron transport layer
OAc	acetate
OFET	organic field effect transistor
OLED	organic light-emitting diode
OPV	organic photovoltaic
<i>p</i>	para
P3AT	poly(3-alkylthiophene)
P3HT	poly(3-hexylthiophene)
PA	poly(acetylene)
PEDOT	poly(3,4-ethylenedioxythiophene)
PEG	poly(ethyleneglycol)
PEV	poly(vinylether)
PFS	poly(ferrocenylsilane)
Ph	phenyl
PMA	poly(methacrylate)
PNB	poly(norbornene)
ppm	parts per million
PPV	poly(phenylenebinylene)
PROXYL	2,2,5,5-tetramethyl-1-pyrrolidinyloxy
PS	poly(styrene)
PSS	poly(styrene sulfonic acid)
PT	poly(thiophene)
PXRD	powder X-ray diffraction
py	pyridine
q	quartet
r.t.	room temperature
R•	stable radical group
RI	refractive index

RMS	root mean squared
ROMP	ring-opening metathesis polymerization
ROP	ring-opening polymerization
RPM	rotations per minute
S	Siemens
s	singlet
SEM	scanning electron microscopy
sh	shoulder
SOMO	singly-occupied molecular orbital
t	triplet
TEMPO	(2,2,6,6-tetramethylpiperidin-1-yl)oxyl
T _g	glass transition temperature
TGA	thermal gravimetric analysis
THF	tetrahydrofuran
TMS	trimethylsilane
TTF	tetrathiafulvalene
UHV	ultra-high vacuum
UV	ultraviolet
UV-vis	ultraviolet-visible
V	volts
v/v	volume to volume ratio
viol	viologen
w	weak
<i>x</i>	Cartesian axis
XRD	X-ray diffraction
<i>y</i>	Cartesian axis
<i>z</i>	Cartesian axis
α	crystallographic lattice constant, torsional angle
β	crystallographic lattice constant, torsional angle
γ	crystallographic lattice constant, torsional angle
δ	chemical shift, partial charge
ϵ	molar absorptivity

θ	theta (range for crystallographic data collection)
λ	wavelength
λ_{\max}	wavelength of maximum absorption
μA	microamps
ρ	resistivity
Ω	ohm

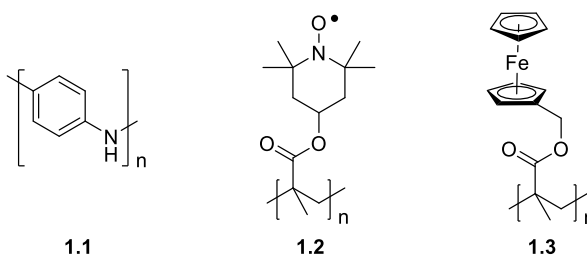
Chapter 1

1 Introduction

A polymer is a macromolecule that is made up of many repeating units (*i.e.* building blocks) called monomers. The properties of macromolecules change once they reach molecular weights above the critical entanglement molecular weight, meaning their physical, chemical, and optical properties can change relative to their monomeric starting materials. Polymers range from polystyrene used to make plastic containers to DNA macromolecules used by our bodies as the building blocks of life. Since the development of the first synthetic polymer over 100 years ago, they have become ubiquitous in everyday life.¹ The discovery that polymers can behave as more than simple commodity materials (plastics) has led to the study of multifunctional materials, including π -conjugated, stable radical, and metal containing polymers.

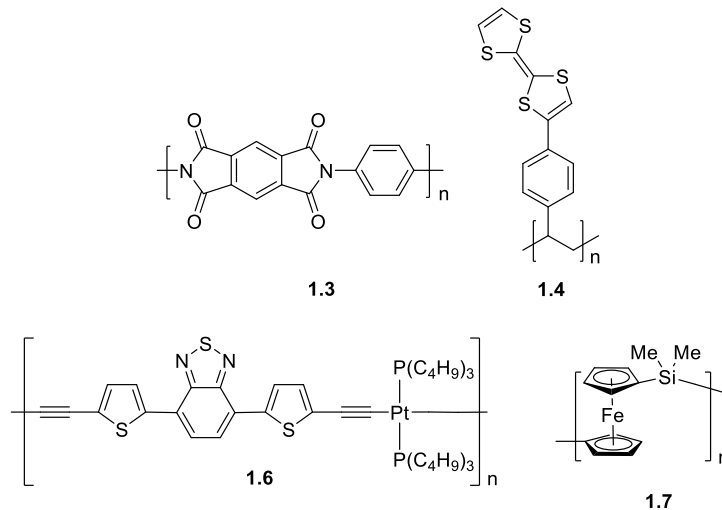
1.1 π -Conjugated, Stable Radical, and Metal-Containing Multifunctional Polymers

The variety of applications associated with multifunctional polymers can be partly attributed to the redox active sites and/or the electronic communication that can be introduced within or pendant to the polymer backbone. These redox active groups range from conjugated polymer backbones (*e.g.* polyaniline, **1.1**), electroactive organic (*e.g.* stable organic radicals, **1.2**) or inorganic moieties (*e.g.* **1.3**).²⁻³



These polymers have been classified many different ways, but for the purposes of this thesis, they will be organized in two broad categories: firstly, as organic polymers, which consists of functional main-chain (*e.g.* **1.4**) or side-chain (*e.g.* **1.5**) polymers, as well as

polymers containing pendant stable radical groups (*e.g.* **1.2**). The second group will consist of functional polymers containing transition metals, which will be further divided into π -conjugated (*e.g.* **1.6**) and non-conjugated (*e.g.* **1.7**) architectures.



Since the discovery of multifunctional polymers, a significant amount of research has been devoted to their development with the goal of producing materials that combine the electrical and optical properties of organic or metallic components with the processability and mechanical advantages associated with polymers.

1.2 Organic Polymers

Historically, the functional polymer field began in the 1970s when it was discovered that polyacetylene (PA), that was understood to be insulating, demonstrated electronic conductivity in the partially oxidized state. As is often the case, this discovery was accidental. A student in the Shirakawa lab had prepared a molar concentration of catalyst instead of millimolar for the polymerization reaction. The result was a metallic foil instead of the usual grey powder. Through collaboration with MacDiarmid and Heeger, they discovered that upon partial doping PA (oxidation or reduction) the conductivity of this material increased a billion fold. In fact, this discovery and subsequent research into the conductive polymer field was significant enough to deserve a Nobel Prize in chemistry in the year 2000. It was awarded to the three collaborating scientists, Alan MacDiarmid, Alan J. Heeger, and Hideki Shirakawa “for the discovery and development of conductive

polymers".⁴⁻⁶ Unfortunately, the first conductive polymer was difficult to process and unstable towards oxygen. This, however, led to the investigation of more stable conjugated polymers. One notable example is the use of poly(phenylenevinylene) (PPV) as the electroactive emissive material in light emitting diodes (LEDs)⁷ (Figure 1.1).

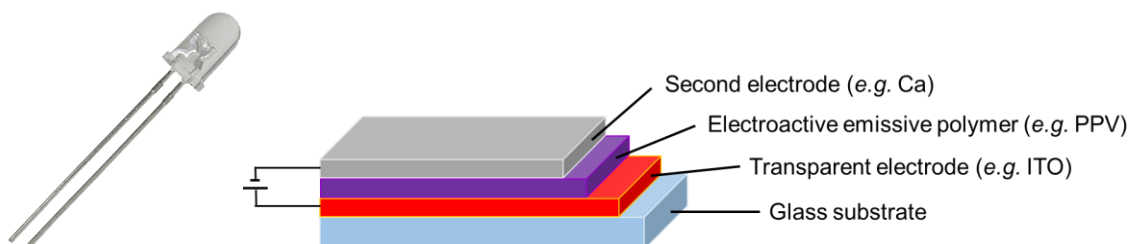


Figure 1.1 Image and schematic of a polymer light emitting diode using PPV.

Initial research into functional polymers consisted largely of aromatic π -conjugated building blocks incorporated into the main-chain of polymer backbones. The metallic conductivity seen with these polyaromatic materials has spurred much interest as scientists were now able to produce synthetic metals. These organic polymers afford the ability to replace metal-based electronic materials with “plastic electronics” as conductors and more recently as semiconductors.⁸

1.2.1 Polyacetylene

PA is the classic example of a π -conjugated polymer, or metal-like plastic. In a conjugated carbon chain each carbon has 3 sp^2 -hybridized orbitals, forming two σ C-C bonds and one C-H bond. The remaining p orbital is responsible for the formation of π bonds and for the conjugation. Looking at the frontier orbitals of a simple system, an ethylene group, there is a bonding orbital (the highest occupied molecular orbital; HOMO) and an antibonding orbital (the lowest unoccupied molecular orbital; LUMO). As additional π -bonds are introduced, there is a splitting of the bonding and antibonding orbitals and the HOMO-LUMO gap becomes smaller. In a conjugated system with many repeating units the HOMO-LUMO gap approaches zero and the material would theoretically behave as a conductive metal (Figure 1.2). However, due to Peierls distortion, the structure is unstable, which leads to the localization of single and double bonds removing degeneracy and opening the band gap (E_g) to usually larger than 1.5 eV.⁷

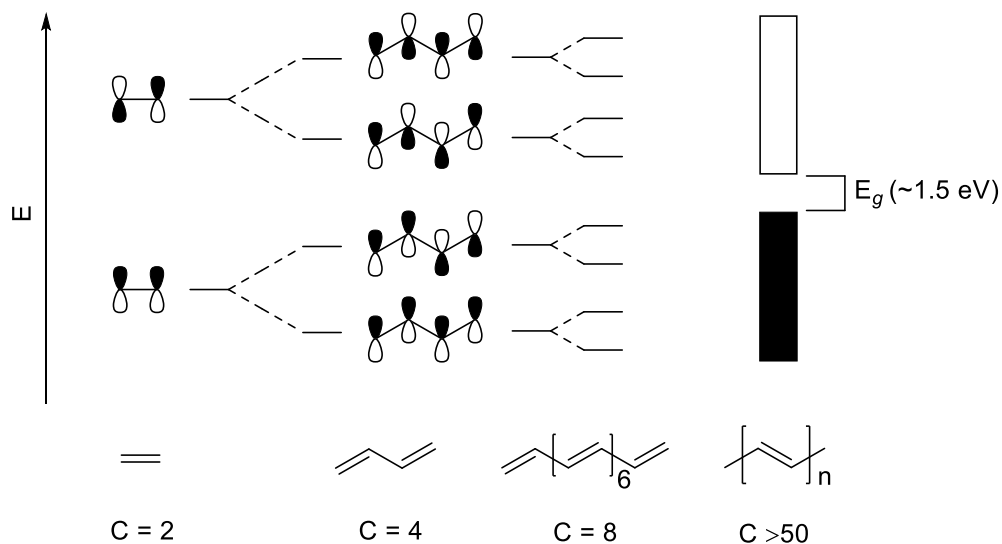


Figure 1.2 Frontier orbitals of ethene, butadiene, and polyacetylene.

This problem was originally overcome upon doping PA with halogens or AsF_5 . In this case, PA becomes conducting due to the introduction of a negatively charged species (n -doping). The resulting anion is stabilized by resonance throughout the polymer chain and this creates an open site where electrons can move along the PA chains and within the bulk of the polymer. The propagation of charge from one PA chain to the next is explained by the bipolaron hopping mechanism.⁹ Depending on the dopant used for PA, different conductivities can be achieved, ranging from metal-like behavior to an insulating material (Figure 1.3).⁷

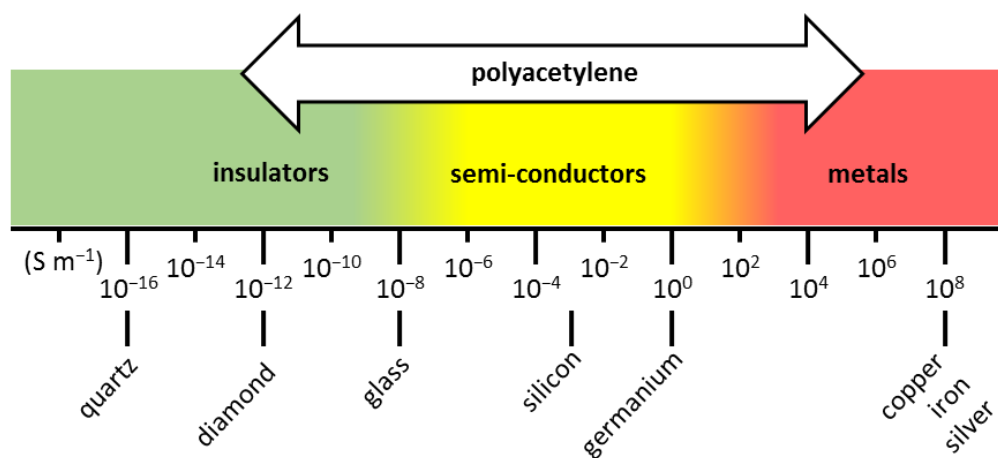
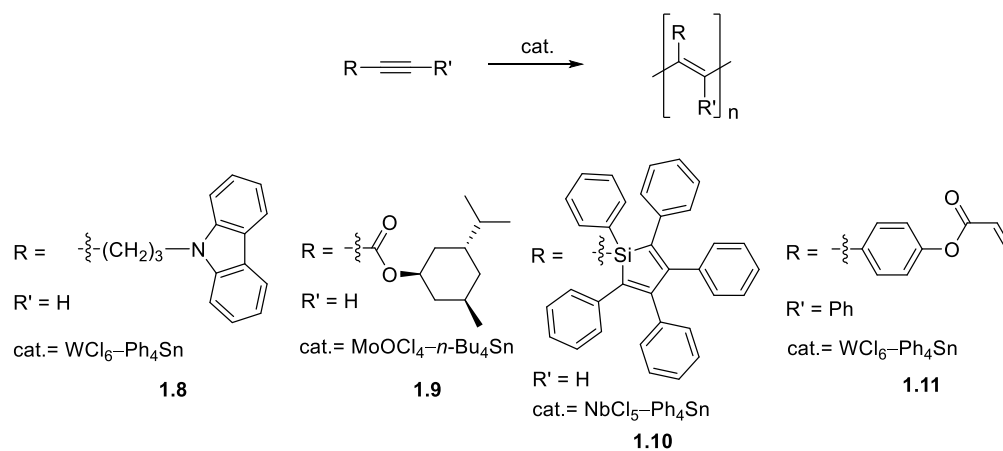


Figure 1.3 Range of conductivities covered by PA compared to other relevant materials.

PA is a linear polyene chain with two C-H bonds present on the backbone. These bonds allow for substitution along the backbone to produce the monosubstituted or disubstituted PAs (Scheme 1.1). The interplay between the backbone and pendant functionalities can afford new properties such as electro-optic activity, photo-responsiveness, and biological compatibility.⁸

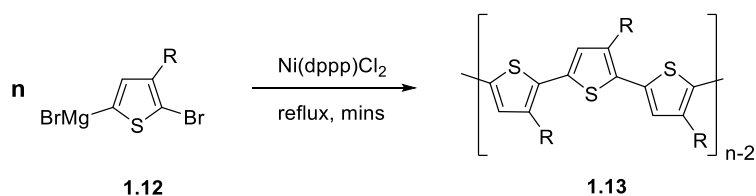
Considerable effort was devoted to the synthesis of substituted PAs in order to study their properties.¹⁰⁻¹² However, in the early stages of the synthesis of PA, integration of polar groups proved difficult. That was caused by the poisoning of the Ziegler-Natta catalysts by the functional groups present.¹³ The discovery of different metal based catalysts for the synthesis of PA allowed for the introduction of more varied functional groups appended to acetylene.¹⁴⁻¹⁵ Although many applications have been developed for functionalized PAs, I will only highlight a few interesting examples. A PA derivative containing a carbazole group (**1.8**) has high conductivity while simultaneously being a good hole transporter.¹⁶ When a bulky chiral core is appended to the PA backbone, a macromolecule with a helical conformation was created (**1.9**).¹⁷ When a silolyl functionality is present on the PA backbone (**1.10**) a strongly luminescent species is created due to aggregation induced emission.¹⁸ Finally, if a second polymerizable group is introduced, such as methacrylate (**1.11**), photo-polymerization of the methacrylate group can produce a well-defined photoresist and the patterns glow under UV irradiation due to the poly(phenylacetylene) backbone.¹⁹



Scheme 1.1 Synthesis of PAs from acetylene precursors.

1.2.2 Polythiophene, its Derivatives, and Organosulfur Compounds

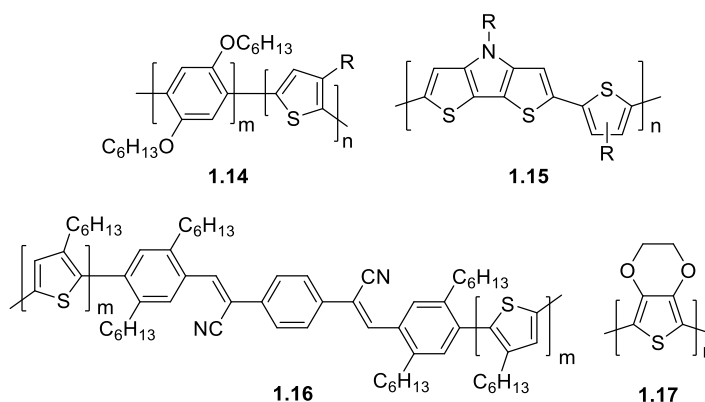
Polythiophenes (PTs) are an important class of π -conjugated polymers because of their optical properties, processability, and charge-transport properties.²⁰⁻²¹ The first syntheses of unsubstituted PT was reported in 1980 by the Yamamoto²² and Lin and Dudek²³ groups. This polymer demonstrated relatively good electrical semiconductivity when doped (1 S cm^{-1}),²⁴ high thermal and chemical stability, but was plagued by a lack of control during polymerization and proved to be insoluble in all organic solvents even at low molecular weights. Eventually, flexible and solubilizing alkyl chains were introduced and these monomers (**1.12**) were used to create the first poly(3-alkylthiophene) (P3AT) by electrochemical methods²⁵ and subsequently by catalysis using a Grignard reagent,²⁶ which was soluble in common organic solvents. The synthesis was then developed to produce regioregular head-to-tail coupled P3AT (**1.13**) which led to conformational ordering along the backbone, π -stacking of planar polymer backbones and lamellar stacking between adjacent backbones (Scheme 1.2).²⁷ All of these features led to improved electrical performance of the materials and, in turn, better device performance (600 S cm^{-1} for regioregular P3AT).²⁷ It was not until 1999 that the current technology for the synthesis of P3AT was reported, known as Grignard metathesis (GRIM) polymerization.²⁸⁻²⁹ This polymerization yielded P3AT with 99% HT coupling, a number average molecular weight (M_n) of 20–35 kg mol^{-1} and dispersities (D) of 1.2–1.4.



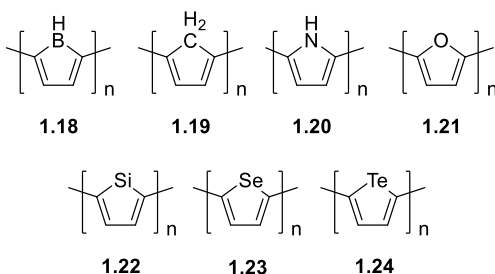
Scheme 1.2 General synthetic method for regioregular P3AT using GRIM.

P3ATs have become ubiquitous in organic electronics, especially in organic field effect transistors and organic photovoltaics. The band gap of P3AT is relatively large (2.85 eV), so considerable efforts have gone toward lowering this band gap. Conjugated polymers including PT have been expanded to produce copolymers with many organic conjugated spacers in order to tune their electrical and optical properties. These polymers include, for

example, benzene-³⁰ (**1.14**), dithienothiophene-³¹ (**1.15**), and cyano-substituted PPV³² (**1.16**). Perhaps the most common derivative of PT would be poly-(3,4-ethylenedioxythiophene) (PEDOT) (**1.17**).³³⁻³⁴ PEDOT was beneficial as it had high conductivity (*ca.* 300 S cm⁻¹), was almost transparent in a thin oxidized film, and was highly stable.³⁵⁻³⁶ PEDOT in conjunction with poly(styrene sulfonic acid) yielded a water-soluble polyelectrolyte system useful in organic electronics being the most successful commercially used conducting polymer.³⁷



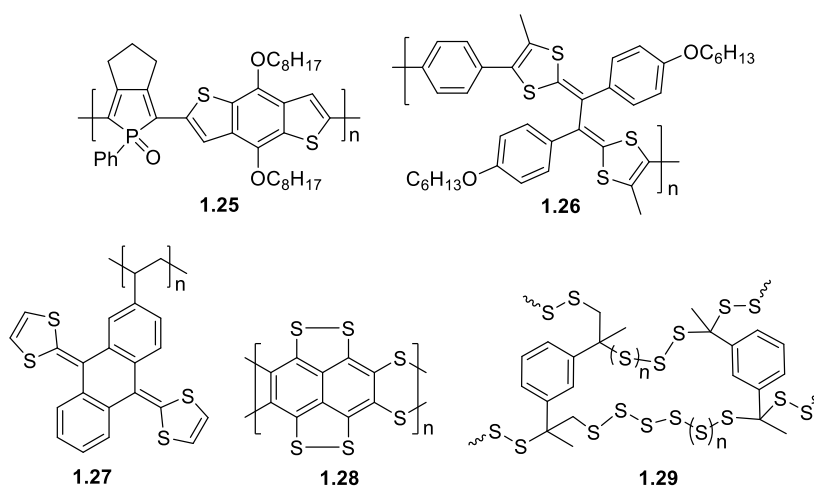
As PT showed great promise as an organic electronic material and in order to further understand the structure-property relationship of PT, many derivatives of the π -conjugated heteroatomic five-membered rings were explored. Among these were polyborole (**1.18**), polycyclopentadiene (**1.19**), polypyrrole (**1.20**), polyfuran (**1.21**), polysilole (**1.22**), polyselenophene (**1.23**), and polytellurophene (**1.24**).³⁸



These polymers have vastly different electrical properties, chemical stability, and syntheses. For example, the conductivity of PT and polyfuran are relatively high at 2000 and 500 S cm⁻¹, respectively. Polyselenophene and polytellurophene have a low conductivity of 3.7×10^{-2} and 7.6×10^{-6} S cm⁻¹, respectively. This shows that even though

the band gap of the polymer systems has been reduced, from 2.85 to 2.0 eV for PT compared to polyselenophene, the electrical properties are not conserved.

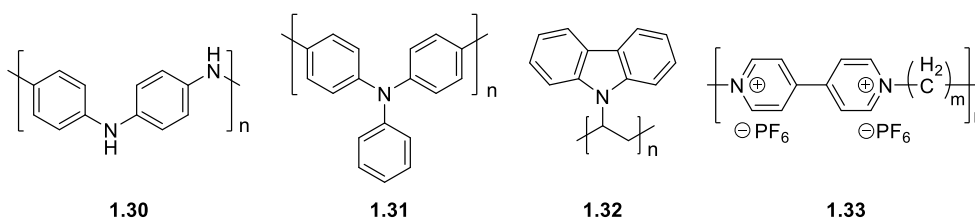
Polymers with disulfide or polysulfide groups show much promise in the field of organic photovoltaics (OPV), energy storage, and drug delivery. By creating a polymer such as **1.25**³⁹ with an electron-rich thiophene and electron-poor phosphole units, greater power conversion efficiencies can be achieved. Tetrathiafulvalene (TTF) is an important π -electron donor due to its ability to readily oxidize to the radical cation and the dicationic states. The incorporation of these units into polymer materials can improve both their electronic and mechanical properties while introducing the processability of macromolecules. To date, these materials have been incorporated into main-chain (**1.26**),⁴⁰ side-chain⁴¹ (**1.27**),⁴² and conjugated⁴³ polymers. Further to this, TTF has also been incorporated into polymers for charge storage applications. Compound **1.28**⁴⁴ had an observed capacity of 122 mA h g⁻¹ and the redox response remains essentially unchanged for 20 cycles. Compound **1.29**⁴⁵⁻⁴⁷ is a promising material as it is produced by a facile polymerization method taking advantage of elemental sulfur with vinylic monomers. It possesses good thermomechanical properties, and maintained high capacity (823 mA h g⁻¹) after 100 cycles.



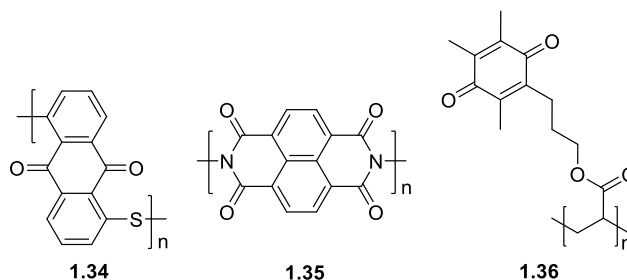
1.2.3 Heteroatom and Carbonyl-Containing Polymers

Polyaniline (**1.30**) was first synthesized in 1834, but it wasn't until the 1980s that the conductive properties of polyaniline were recognized and research dealing with the

conductivity was undertaken.⁴⁸ Over the years, many derivatives of polyaniline have been synthesized and many chemical syntheses have been developed in order to produce these polymers.⁴⁹ Another interesting heteroatomic polymer is polytriphenylamine (**1.31**) and its derivatives, which have useful hole-transport abilities. To date, they have been studied in organic light-emitting diodes (OLEDs), solar cells, organic field effect transistors (OFETs) and photorefractive holographic materials.⁵⁰ Similar to the other heteroatom-based materials, carbazole-based materials, such as compound **1.32**, have also been explored for their electrical and optical properties.⁵¹ For example, their hole-transporting ability has been used in xerographic applications⁵² and lithium-ion batteries.⁵³ Another interesting class of heteroatomic redox polymers are poly(viologen)s (**1.33**).⁵⁴ These polymers combine redox and electrochromic properties useful in sensor and catalyst applications.⁵⁵⁻⁵⁶



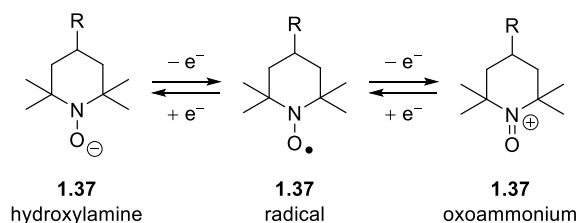
The family of functional π -conjugated polymers that contain carbonyl groups are another relevant class. Architectures that have been investigated for their redox properties include anthroquinones, quinones, anhydrides, and imides. Some examples of this group are anthroquinone polymer **1.34**,⁵⁷ and naphthalene derivative **1.35**⁵⁸ which have been explored for their use as charge storage materials in lithium batteries. Polymer **1.36**, which contains a quinone, has been used as an actuating material.⁵⁹ Upon reduction, this material forms either a mono- or dianionic species, and the associated solvent and counterions then induce the desired swelling for actuation.



Redox-active carbonyl containing polymers have exciting potential for further development in the energy storage field, as quinone moieties are found in biopolymers and are an abundant natural resource.⁶⁰

1.2.4 Stable Organic Radical Polymers

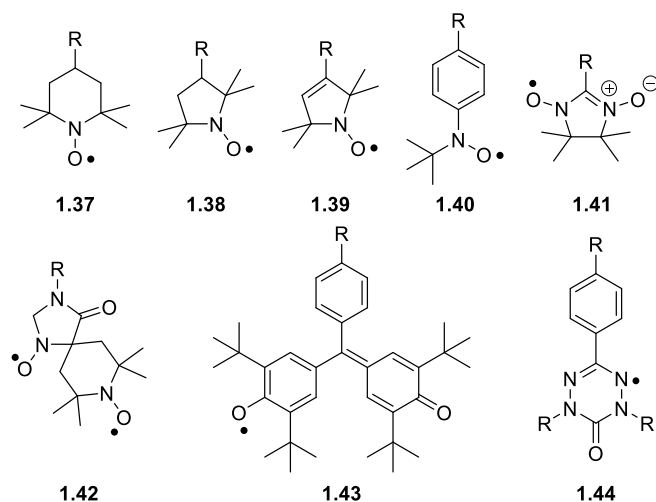
A promising class of organic redox polymers consist of stable radical groups appended to a non-conjugated polymer backbone. Although this family of polymers are relatively new, persistent organic radicals were discovered over 100 years ago by Gomberg.⁶¹ Since then, many different types of organic radicals have been synthesized and subsequently incorporated into polymeric materials. These types of materials prove interesting to the scientific community because they afford the advantage of reversible oxidation and reduction of the radical species (Scheme 1.3) and they allow the tailoring of redox potential of the resulting polymer by modifying the radical group used or by synthetically modifying the radical functionality.



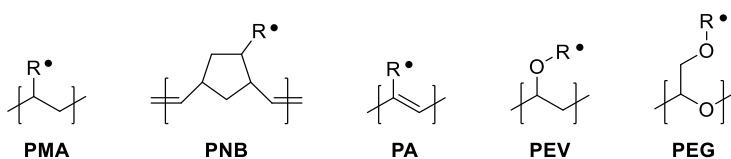
Scheme 1.3 The nitroxide radical can be reversibly oxidized and reduced.

Stable organic radicals typically gain their stability from the distribution of the unpaired electron over electronegative heteroatoms and the introduction of functional groups that inhibit side-reactions such as disproportionation, and reactions with other radicals or impurities. 2,2,6,6-tetramethylpiperidinyloxy (TEMPO, **1.37**) is the most widely studied of the nitroxide group of stable radicals.⁶² Other members of the nitroxide family include 2,2,5,5-tetramethyl-1-pyrrolidinyloxy (PROXYL, **1.38**),⁶³ unsaturated PROXYL (**1.39**),⁶⁴ *N-tert*-butyl-*N*-oxy-aminobenzene (**1.40**),⁶⁵ nitronyl nitroxide (**1.41**),⁶⁶ and spirobisnitroxide (**1.42**).⁶⁷ Occuring less often in the literature, radicals stabilized by delocalization over an aromatic system, steric bulk surrounding the radical species, and

distribution of electron density over several nitrogen atoms can be found. These radicals include galvinoxyl (**1.43**)⁶⁸ and verdazyl (**1.44**)⁶⁹ radicals.



One of the advantages of using stable radicals as the functional component of polymers is that they can be synthetically modified to include different polymerizable groups. Some of the more common backbone architectures include polymethacrylate (PMA), polynorbornene (PNB), PA, polyvinyl ether (PEV), and polyethyleneglycol (PEG) using either step growth or chain growth polymerization pathways.⁷⁰



The majority of research in the field of organic radical polymers is focused on their utility as electrode materials for use in batteries.⁷¹ Stable radical polymers are ideal materials for their use as electrode materials in battery applications because of their high charge capacity (although limited by molecular weight of the repeating unit) and a self-exchange mechanism that is fast and efficient (Figure 1.4).

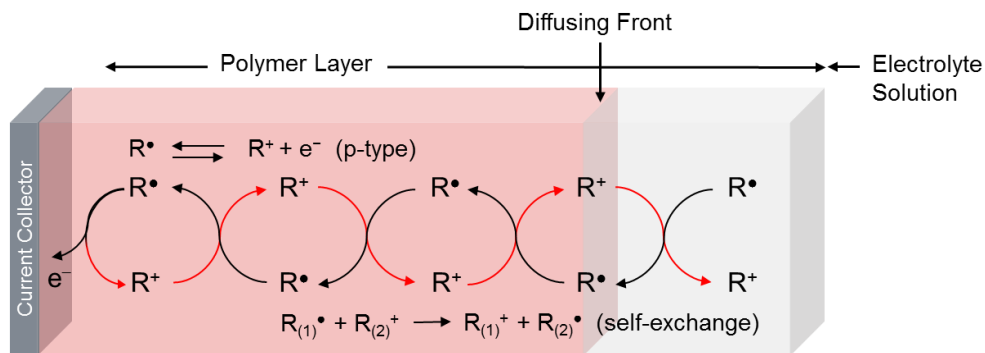


Figure 1.4 Positive charge propagation during the oxidation of *p*-type radical polymers in electrolyte solution. Figure adapted from Ref. [71].

Stable radical polymers have been developed as both *p*-type and *n*-type materials. The recent growth in this field has led to the creation of a library of stable radical polymers that can be utilized for various applications. In Figure 1.5 they are organized by redox-capacity versus the weight-based capacities.⁷¹

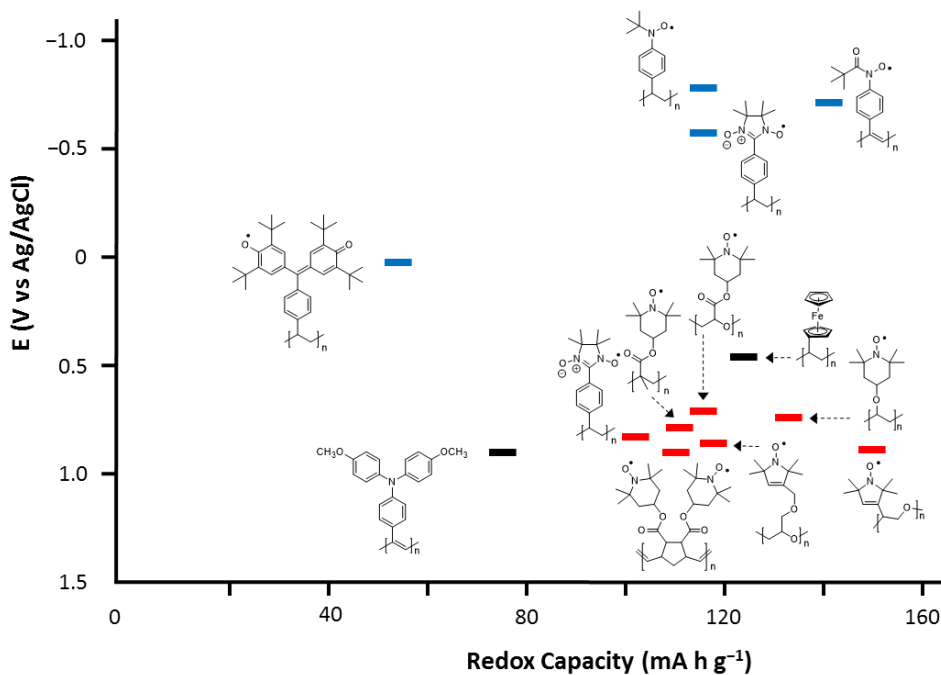


Figure 1.5 Energy diagram of *p*-type (red) and *n*-type (blue) radical polymers, and redox-active polymers for comparison (black). Figure adapted from Ref. [71].

Recent advances in this field have led to batteries that have improved performance by introduction of carbon nano-fillers⁷²⁻⁷⁴ and the creation of zinc hybrid batteries with enhanced performance and cyclability.⁷⁵⁻⁷⁶ Most recently, stable radical polymer based flow batteries soluble in aqueous medium were developed.⁷⁵⁻⁷⁷ With an emphasis on renewable energy sources such as solar and wind, there is a requirement for flexible and scalable energy-storage solutions. Schubert and co-workers were able to design an aqueous polymer-based battery using low cost materials (Figure 1.6).⁷⁷ This represents a significant advance in the field of radical polymers for charge storage applications.

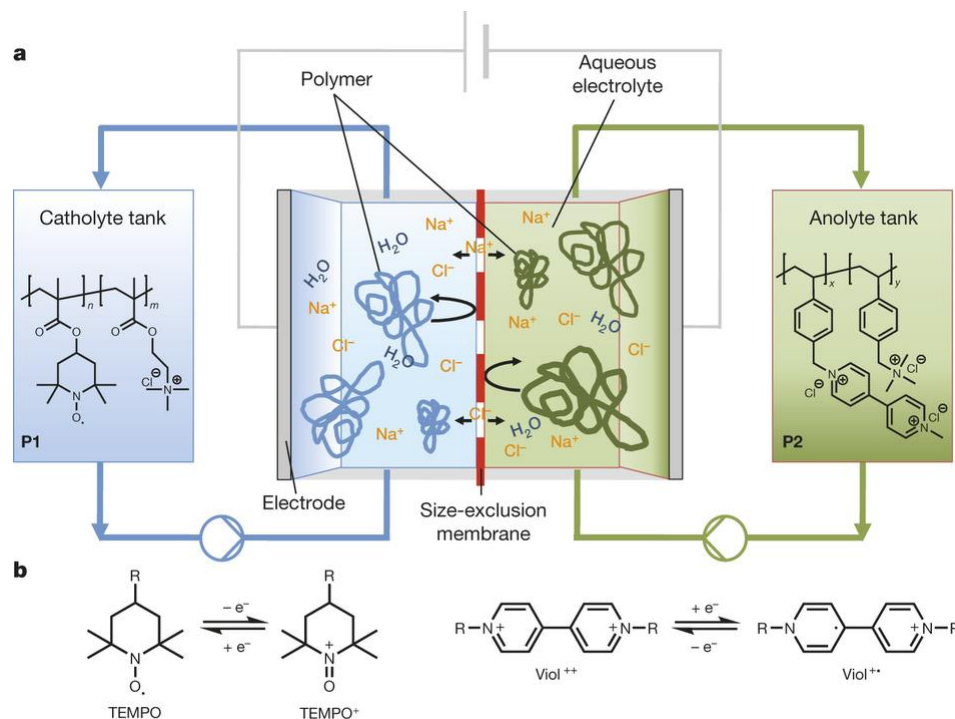


Figure 1.6 (a) Representation of polymer-based flow battery that includes two reservoir tanks, the first including the TEMPO containing copolymer and the second including a redox-active viologen based copolymer. The reservoirs are separated by a size-exclusion membrane that allows the electrolytes to permeate but not the macromolecules. (b) The fundamental electrode reactions are shown of the TEMPO radical and viologen. Reproduced with permission from Ref. [77].

Other areas of research for radical polymers include applications as (co)catalysts for the selective oxidation of alcohols,⁷⁸ solid-state conductive materials,⁷⁹⁻⁸¹ inhibitors of self-polymerization materials,⁸² and the functional component of memory architectures.⁸³⁻⁸⁴

Nishide and co-workers have developed a rewritable memory architecture using a TEMPO radical polymer as the *p*-type layer and a galvinoxyl polymer as the *n*-type layer (Figure 1.7).⁸³ They reported a difference of four orders of magnitude between the ON-OFF ratio and good cyclability.

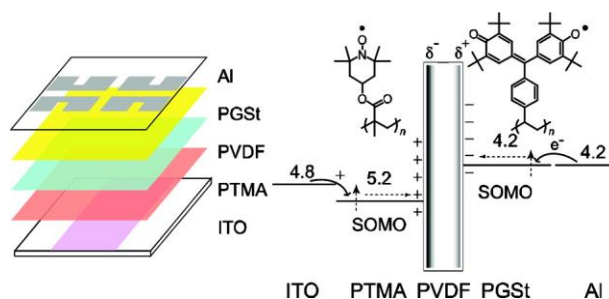
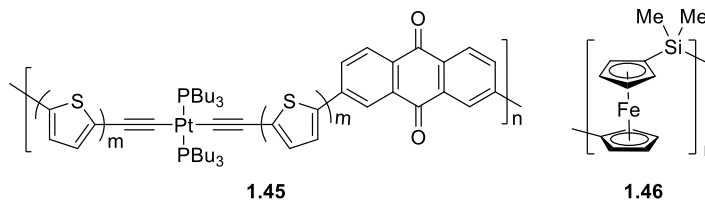


Figure 1.7 Radical polymer-based memory architecture and electron movement of the device. Reproduced with permission from Ref. [83].

1.3 Metal-Containing Polymers

The introduction of transition metals into synthetic polymers allows for processable materials with properties and functions comparable to their organic counterparts. The type of metal incorporated into the polymer can introduce important redox chemistry, emission properties, conductivity, magnetism, and can also be an important structural component to the primary or secondary structure. The binding motif of the metal to the polymer structure are varied. The metal can be covalently bound, connected through weak or labile coordination bonds, or non-covalently coordinated to afford dynamic materials in solution. Over the last couple of decades, effective approaches to the synthesis of metal-containing polymers (MCPs) have been developed. Crucially, the synthetic methods developed had to be compatible with the metal centres present in the monomer or with the binding sites present for the subsequent introduction of metals into polymers.⁸⁵⁻⁸⁸ For the purposes of this thesis, MCPs will be divided into two broad categories: π -conjugated MCPs (*e.g.* a Pt-polyne polymer, **1.45**)⁸⁹ which contain the metal within the main-chain or appended to a conjugated backbone. The other category consists of non-conjugated MCPs [*e.g.* polyferrocenylsilanes (PFSs), **1.46**] where the metal is present in the main-chain or side-chain, but the polymer backbone is non-conjugated.



1.3.1 π -Conjugated MCPs

π -Conjugated MCPs have gained considerable interest over the last 30 years. Within this class of materials, the transition metal used strongly affects the π -conjugation within the polymer backbone, and results in unique functional materials that offer properties that cannot be achieved with either metals or π -conjugated polymer alone. Wolf has described the classification of π -conjugated MCPs (Figure 1.8).⁹⁰ Type I polymers have a pendant metal centre connected to a conjugated organic backbone through an electronically isolated linker. Type II polymers have electronic interaction between the backbone and the metal and Type III polymers contain the metal within the polymer backbone.

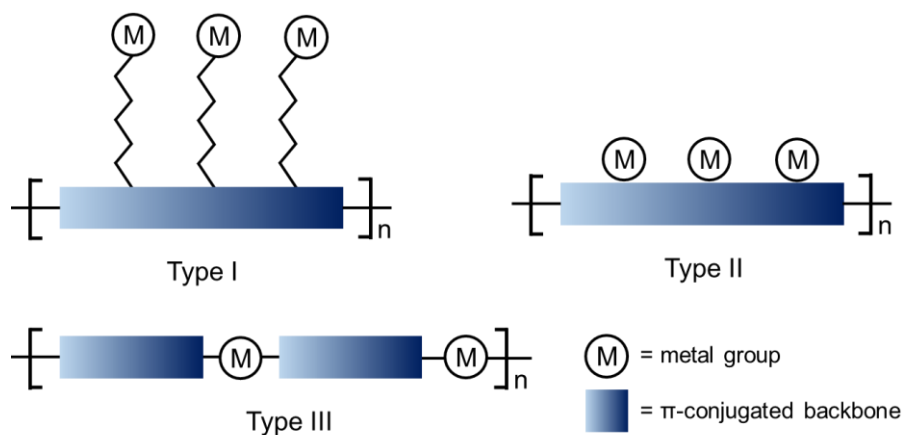
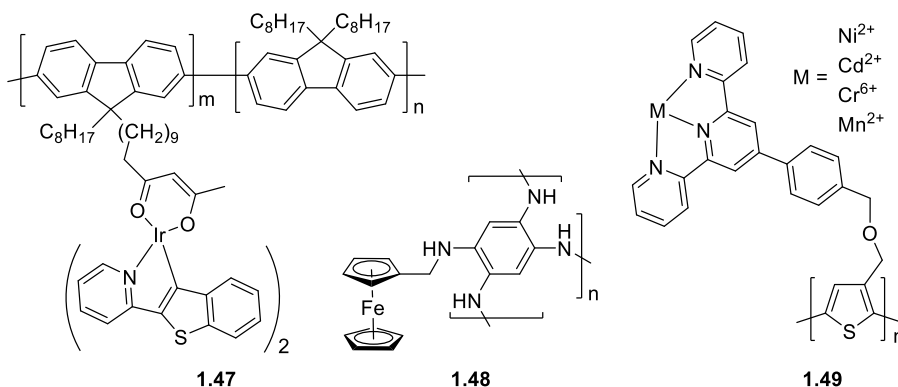


Figure 1.8 Representation of Type I-III MCPs. Figure adapted from Ref. [90].

1.3.1.1 Wolf Type I Polymers

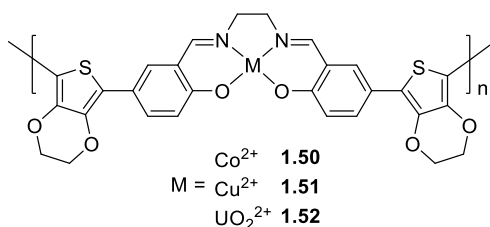
In Wolf Type I polymers, the metal is tethered to a conjugated backbone. The polymer typically behaves as a conductive support while the metal behaves electronically, optically, and chemically as if it were untethered. These types of polymers usually tether the metal centre to the conjugated backbone via an alkyl linker. The Chen group utilized this polymer motif to design a material for a LED with the highest external quantum efficiency of a

polymer LED at the time (1.59%). This polymer uses a conjugated polyfluorene backbone and the iridium complex as a phosphorescent dopant which displays red-light emission from a the cyclometalated iridium complex (**1.47**).⁹¹⁻⁹² Another example includes a polyaniline derivative with a ferrocene group appended to the polymer backbone (**1.48**).⁹³ The polymers exhibit a colour transition when the ferrocene functionality undergoes a reduction or oxidation. This produced a polymer with three electronically different states. A third example of this type of polymer utilized a polythiophene backbone with an oligopyridine ligand as a metal coordination site (**1.49**).⁹⁴ The polymer can detect the presence of different metals, such as Cd^{2+} , Cr^{6+} , Mn^{2+} and Ni^{2+} upon metal coordination as the emission intensity of the polymer varies. This allowed polymer **1.49** to be used as a chemosensor.⁹⁴



1.3.1.2 Wolf Type II Polymers

A Wolf Type II polymer contains a metal that is electronically coupled to a π -conjugated backbone. However, the existence of the polymer backbone does not require the transition metal to be present. The backbone and metal groups can be redox-active and this leads to systems that can be electronically tuned. An interesting example of a Type II polymer was synthesized by the Swager group, and includes a Salen-type ligand with a series of metal centres, including Co^{2+} (**1.50**), Cu^{2+} (**1.51**), and UO_2^{2+} (**1.52**).⁹⁵⁻⁹⁶



The cobalt containing variation of this polymer system is able to detect a change in oxidation potential of 0.1 V when the cobalt metal centre is ligated to nitric oxide.⁹⁷ This allowed for the detection of nitric oxide, a molecule present in many cascade pathways within the body, when this polymer system was appended to an electrode.⁹⁵

Metal complexes of macrocyclic ligands such as porphyrin and phthalocyanine with metals coordinated are an important class of compounds.⁹⁸⁻¹⁰¹ An example of a Zn-porphyrin polymer (**1.53**) uses a template-directed synthesis in order to create a macromolecule that has the ability to self-organize into a cyclic polymer and display a high degree of order. The cyclic polymer nanoring can then stack or nest when deposited onto a gold surface (Figure 1.9).¹⁰²

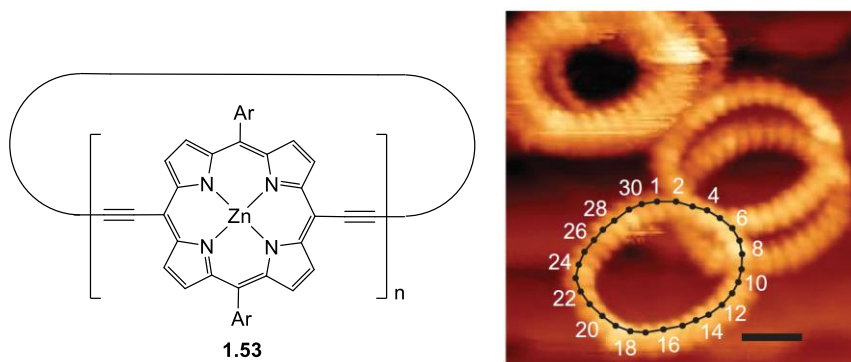


Figure 1.9 Structure of Zn-porphyrin nanorings and scanning tunneling microscopy images of a 30 repeat unit nanoring deposited on a gold surface. Figure reproduced with permission from Ref. [102].

Phthalocyanin macrocycles are structurally similar to porphyrins, with the inclusion of 4 additional nitrogens in the backbone. One notable example includes an iron metal centre coordinated to the phthalocyanine (**1.54**) within a well-ordered two-dimensional polymer matrix (Figure 1.10).¹⁰³ This polymer represents a fully delocalized 2D matrix with paramagnetic metal atoms evenly distributed throughout. This provided a scaffold for the

introduction of many different metal centres in order to tune the structure, chemical composition, and magnetic properties.

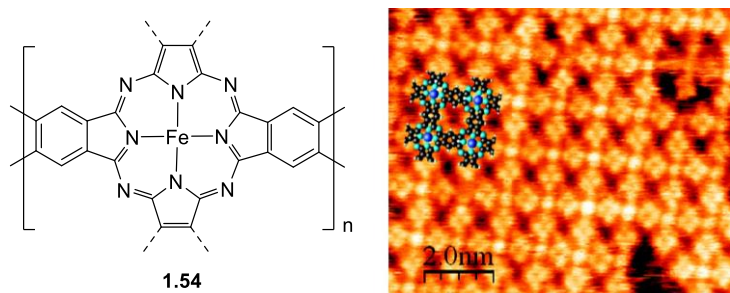
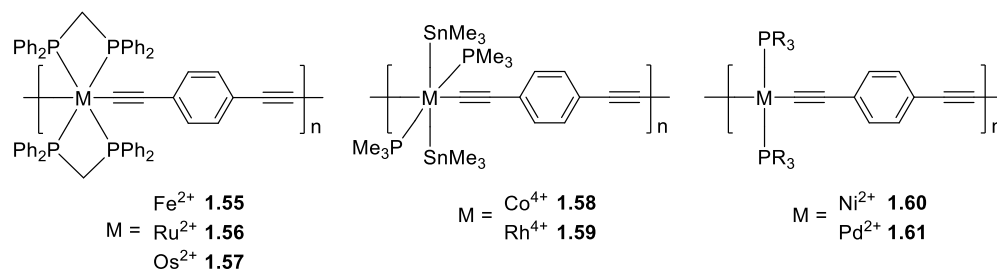


Figure 1.10 STM image of polymer **1.54** formed on a Ag(111) surface. Image reproduced with permission from Ref. [103].

1.3.1.3 Wolf Type III MCPs

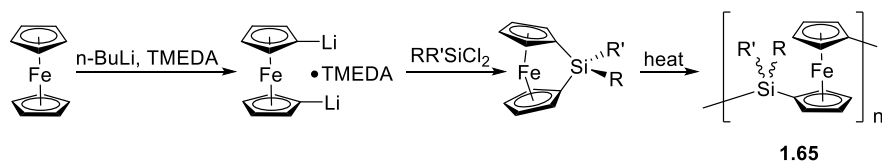
Wolf Type III MCPs contain metals embedded in the main-chain, typically with the metal connected by a single, double, or triple bond. The metal centre can interact with the conjugated backbone so that the properties of the resulting material is a combination of both parts. One notable example of a Wolf Type III polymer includes a platinum polyynes (*e.g.* **1.45**).¹⁰⁴ This polymer is characterized by a low-band gap utilizing a donor-acceptor copolymer approach in order to improve the charge-transfer properties. The polymer demonstrated impressive power conversion efficiencies of 4.1% when blended with poly(3-hexylthiophene) (P3HT) and fullerene to produce a photovoltaic device.

The study of transition-metal alkynyl complexes has been an intense area of research for many years, with thousands of research papers published since the 1980s.¹⁰⁵⁻¹⁰⁹ Computational studies of these polymers show that the highest occupied molecular orbital is primarily d orbital in character and delocalized along the entire chain through the metal-ligand groups. Different syntheses were developed and the incorporation of many transition metals was achieved. Some examples include octahedral metal centres including Fe²⁺ (**1.55**),¹¹⁰ Ru²⁺ (**1.56**),¹¹¹ Os²⁺ (**1.57**),¹¹² Co⁴⁺ (**1.58**),¹¹³ and Rh⁴⁺ (**1.59**),¹¹⁴ as well as square planar metal centres Ni²⁺ (**1.60**),¹¹⁵ Pd²⁺ (**1.61**),¹¹⁶ and Pt²⁺ (**1.45**).¹¹⁷



The synthesis of a zinc(II)-salen polymer was performed by Peng and co-workers (**1.61**).¹¹⁸ This polymer exhibited some interesting thin-film properties. The photoluminescence was measured to be *ca.* 50% and the creation of light-emitting diodes with this material produced efficient green emitters. The ability to tailor the conjugated backbone of the metallopolymer in order to achieve the desired electronic properties is a powerful synthetic tool. Khan and co-workers were able to tune the optical bandgap of the platinum alkynyl polymer by introducing one, two or three thiophenes within the polymer backbone, (**1.62**).¹¹⁹

Iridium-based complexes are attractive candidates for device applications (*e.g.* **1.63**) due to the ease of fabrication and high quantum efficiency.¹²⁰ Unfortunately, when these small molecules are incorporated into a polymer network the resulting devices experience fast decay due to phase separation. By incorporating the Ir into the polymer main-chain, the stability was increased and the polymers realized high efficiency emission. The combination of the strong charge-transfer character of a transition metal paired with the conductive properties of an organic conjugated polymer can produce polymers ideal for photoelectronic applications. One such example, polymer **1.64**,¹²¹ showed promising short circuit currents and open circuit voltages in the 8.9–15.0 $\mu\text{A cm}^{-2}$ and 0.76–0.84 V ranges, respectively when incorporated into a photovoltaic device.



Scheme 1.4 Synthesis of PFS from ferrocene.

The incorporation of ferrocene into different polymer systems allows for the tailoring of the physical, chemical, and optical properties. The tailoring of these properties relies mostly on the ability to control the redox activity of the ferrocene/ferrocenium couple. In Figure 1.11a–c, we can see the production of a ceramic network resulting from the pyrolysis of PFS molded to a pentagon shape that has tunable magnetic properties,¹²⁸⁻¹²⁹ the synthesis of microbeads using microfluidics that are redox responsive,¹³⁰ and the synthesis of colour-tunable fluorescent micelles utilizing block copolymer self-assembly,¹³¹ respectively.

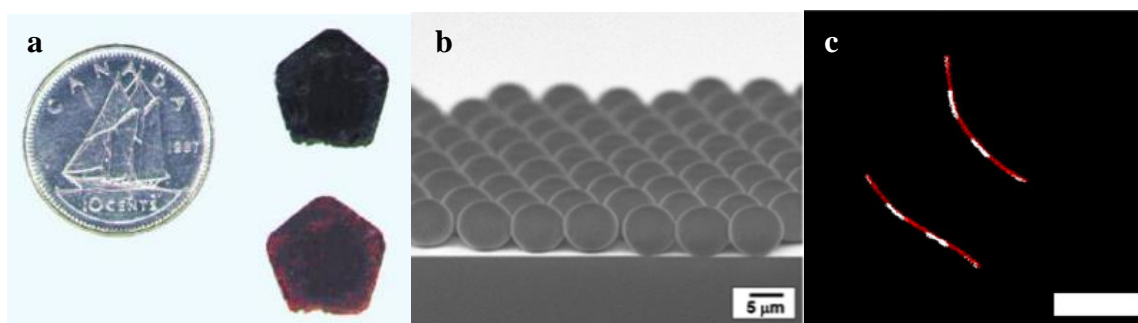
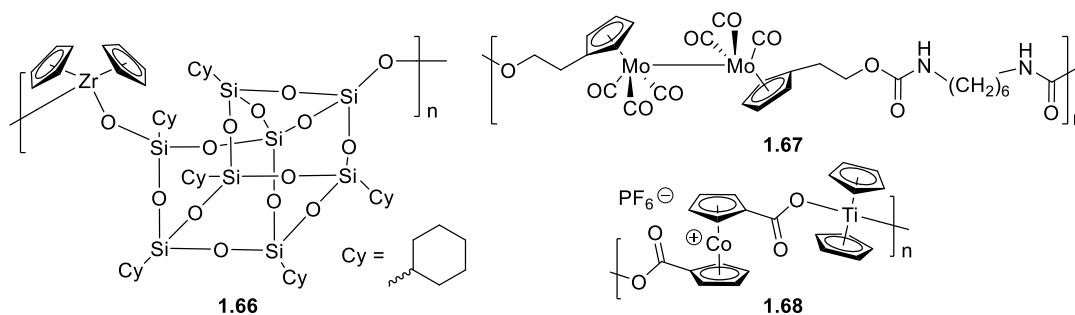


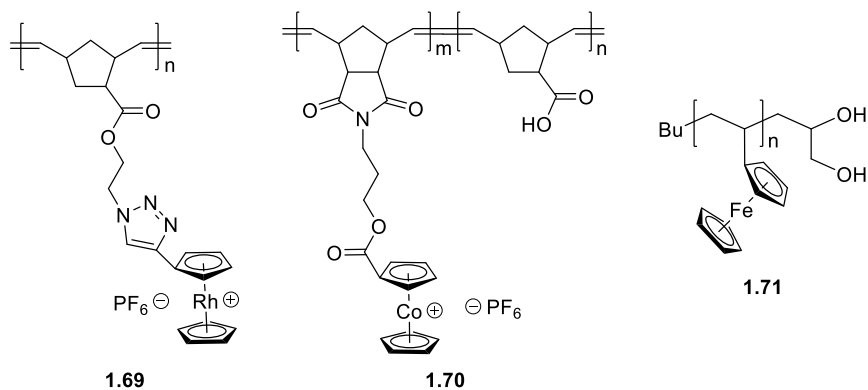
Figure 1.11 (a) Pyrolyzed pentagon shaped polymers derived from PFS, (b) PFS microparticle, (c) PFS micelles with complex fluorescent patterning (scale = 5 μ m). Images reproduced with permission from (a) [129], (b) [130], and (c) [131].

Further to the ferrocene family of polymers, there exists many different types of metallocene polymers contained within the main-chain. For example, a zirconocene-containing polymer that uses a silsesquioxane macromonomer in the backbone (**1.66**). This polymer was one of the first reported zirconocene complexes that was stable to both air and methanol.¹³² A half-sandwich molybdenum complex was incorporated into a urethane monomer to produce polymer **1.67**, synthesized by Wang and co-workers.¹³³⁻¹³⁴ Lastly, Carraher and co-workers were able to synthesize a colbatocene- and titanocene-containing copolymer (**1.68**) that has potential applications as an antitumor agent.¹³⁵⁻¹³⁶



1.3.2.2 Non-Conjugated Side-Chain MCPs

When incorporating metallocenes as pendant groups on a polymer scaffold, there exists the ability to tune both the backbone and the redox-active metallocene group. In terms of the backbone, scientists are afforded the advantage of using many different backbone structures as the monomers are typically more tolerant of different polymerization methods. For example, ring-opening metathesis polymerization (ROMP) can be used, which is a well understood, highly amenable to different functional groups, and a living polymerization method.¹³⁷ The Yan group was able to synthesize a rhodocenium based side-chain polymer (**1.69**) utilizing the ROMP protocol.¹³⁸ The self-assembly and ion-exchange properties of this class of rhodocenium-based polymers opens the door for potential applications. ROMP was also used to synthesize cobaltocenium side-chain polymers (**1.70**).¹³⁹ The benefit of this method is the ability to create diblock copolymers in a fast and efficient manner in order to produce polymers with higher-order functionality. The investigators designed a system in which the copolymer self-assembled to form a micelle, followed by the creation of a cobalt nanoparticles resulting from pyrolysis.¹⁴⁰ A final example of side-chain polymers incorporates a ferrocene functional group that was polymerized using a carbanionic polymerization (**1.71**). The researchers were able to create block copolymers with this system and selectively tune the size of vesicle-like materials that resulted by changing the solvents used for block copolymer self-assembly.¹⁴¹



1.4 Scope of Thesis

This thesis will focus of the synthesis of functional monomers including 6-oxoverdazyl stable radical group and Ni(II) complexes of Goedken's macrocycle and their subsequent incorporation into polymers that demonstrate reversible redox behaviour. The resulting optical, electronic, and physical properties of these macromolecules will be explored and compared, in certain cases, to model compounds.

The 6-oxoverdazyl molecule was chosen to be incorporated into a polymer material due to several desirable features. The verdazyl radical affords tunability of the reduction and oxidation potentials by modifying the substituents present on the 1 and 5 position (Figure 1.12). Simply by changing the group from an alkyl to an aryl, a change of *ca.* 0.5 V was observed for the reduction potential and 0.2 V for the oxidation potential, for example.¹⁴² Verdazyl radicals also exhibit stabilities towards oxygen and water that rivals the most stable organic radicals reported in the literature (*e.g.* TEMPO), and allow modification at the 3 position in order to incorporate a variety of polymerizable groups.

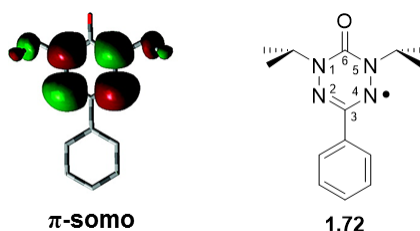
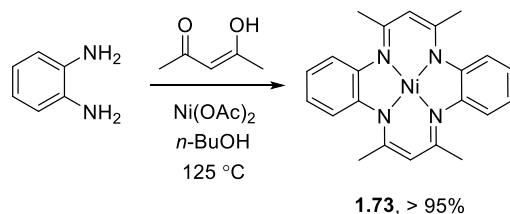


Figure 1.12 (left) Calculated singly occupied molecular orbital (SOMO, DFT; B3LYP/6-31G),¹⁴³ (right) corresponding molecular drawing for 6-oxoverdazyl **1.72**.

The second family of molecules chosen to be incorporated into polymer scaffolds were nickel complexes of Goedken's macrocycle. This π -conjugated macrocycle offers the advantage of being relatively easy to synthesize when templated with $\text{Ni}(\text{OAc})_2$ in a high yielding and scalable reaction.¹⁴⁴ Chemical modification of the C-H on the macrocycle backbone will allow the introduction of polymerizable groups or reactive moieties to allow polymerization.¹⁴⁵



Scheme 1.5 Templated synthesis of a Ni(II) complex of Goedken's macrocycle.¹⁴⁴

Chapter 2 will focus on the synthesis of 6-oxoverdazyl radical polymers and their resulting redox properties in solution and the solid-state. The chapter details the post-polymerization conversion of the pendant 6-oxotetrazane moiety to 6-oxoverdazyl in the polymers produced, as confirmed by spectroscopic studies and comparison to closely related model compounds. Kelvin probe force microscopy studies also highlight the potential utility of 6-oxoverdazyl polymers as redox-active thin films.

Chapter 3 includes discussion on the ring-opening metathesis polymerization methods used to directly prepare novel side-chain polymer bearing 6-oxoverdazyl stable radicals. Detailed characterization, including FT-IR, UV-vis absorption, and electron paramagnetic resonance (EPR) spectroscopy quantitatively and qualitatively confirmed the large radical content within the polymer backbone. The polymers exhibited ambipolar redox properties in solution, and the resistivity of thin-films varied dramatically when an external potential of 5 V was applied ($10^{10} \Omega \cdot \text{m} \rightarrow 10^4 \Omega \cdot \text{m}$). This behaviour led to the development of bistable memory devices.

Chapter 4 describes the optimized copolymerization of 2,7-dibromo-9,9-dihexylfluorene and ethynyl functionalized Goedken's macrocycle and the subsequent copolymerization with 1,4-dibromo-2,5-dihexyloxybenzene and 2,5-dibromo-3-hexylthiophene. These polymers were characterized in detail and their redox and optical properties were studied.

The post-polymerization functionalization of the initial polymer at the alkyne position with cobalt carbonyl produced a heterobimetallic polymer. Upon pyrolysis in a reducing atmosphere, nanoparticles with the metallic content influenced by the polymer composition were obtained.

Chapter 5 highlights the controlled polymerization of norbornene-based side-chain monomers of Ni(II) complexes of Goedken's macrocycle. The title polymer was characterized and the redox and optical properties were studied. Differences in the electrochemical reduction behaviour of Ni species were observed in the macromolecule when compared to the discrete monomer unit.

1.5 References

1. Constitution and Architecture of Chains. In *The Physics of Polymers: Concepts for Understanding Their Structures and Behavior*, Strobl, G., Ed. Springer Berlin Heidelberg: Berlin, Heidelberg, 2007; p 1–13.
2. Casado, N.; Hernández, G.; Sardon, H.; Mecerreyes, D. *Prog. Polym. Sci.* **2016**, *52*, 107–135.
3. Gracia, R.; Mecerreyes, D. *Polym. Chem.* **2013**, *4*, 2206–2214.
4. Heeger, A. J. *Angew. Chem. Int. Ed.* **2001**, *40*, 2591–2611.
5. MacDiarmid, A. G. *Angew. Chem. Int. Ed.* **2001**, *40*, 2581–2590.
6. Shirakawa, H. *Angew. Chem. Int. Ed.* **2001**, *40*, 2574–2580.
7. Conjugated Polymers. In *The Physics of Polymers: Concepts for Understanding Their Structures and Behavior*, Springer Berlin Heidelberg: Berlin, Heidelberg, 2007; p 287–312.
8. Liu, J.; Lam, J. W. Y.; Tang, B. Z., Synthesis and Functionality of Substituted Polyacetylenes. In *Design and Synthesis of Conjugated Polymers*, Wiley-VCH Verlag GmbH & Co. KGaA: 2010; p 1–43.

9. MacDiarmid, A. G.; Mammone, R. J.; Kaner, R. B.; Porter, S. J.; Pethig, R.; Heeger, A. J.; Rosseinsky, D. R. *Philos. Trans. R. Soc., A* **1985**, *314*, 3–15.
10. Lam, J. W. Y.; Tang, B. Z. *Acc. Chem. Res.* **2005**, *38*, 745–754.
11. Moore, J. S.; Gorman, C. B.; Grubbs, R. H. *J. Am. Chem. Soc.* **1991**, *113*, 1704–1712.
12. Schrock, R. R.; Luo, S.; Lee, J. C.; Zanetti, N. C.; Davis, W. M. *J. Am. Chem. Soc.* **1996**, *118*, 3883–3895.
13. Masuda, T.; Higashimura, T. *Acc. Chem. Res.* **1984**, *17*, 51–56.
14. Furlani, A.; Licocchia, S.; Russo, M. V.; Camus, A.; Marsich, N. *J. Polym. Sci., Part A: Polym. Chem.* **1986**, *24*, 991–1005.
15. Yang, W.; Tabata, M.; Kobayashi, S.; Yokota, K.; Shimizu, A. *Polym. J.* **1991**, *23*, 1135–1138.
16. Tang, B. Z.; Chen, H. Z.; Xu, R. S.; Lam, J. W. Y.; Cheuk, K. K. L.; Wong, H. N. C.; Wang, M. *Chem. Mater.* **2000**, *12*, 213–221.
17. Nakako, H.; Nomura, R.; Tabata, M.; Masuda, T. *Macromolecules* **1999**, *32*, 2861–2864.
18. Chen, J.; Xie, Z.; Lam, J. W. Y.; Law, C. C. W.; Tang, B. Z. *Macromolecules* **2003**, *36*, 1108–1117.
19. Yuan, W. Z.; Qin, A.; Lam, J. W. Y.; Sun, J. Z.; Dong, Y.; Häussler, M.; Liu, J.; Xu, H. P.; Zheng, Q.; Tang, B. Z. *Macromolecules* **2007**, *40*, 3159–3166.
20. Osaka, I.; McCullough, R. D. *Acc. Chem. Res.* **2008**, *41*, 1202–1214.
21. Skotheim, T. A.; Reynolds, J. R. *Handbook of conducting polymers. Conjugated polymers : theory, synthesis, properties, and characterization*. 3rd ed.; CRC Press: Boca Raton, 2007.

22. Yamamoto, T.; Sanechika, K.; Yamamoto, A. *J. Polym. Sci., Part A: Polym. Chem.* **1980**, *18*, 9–12.
23. Lin, J. W. P.; Dudek, L. P. *J. Polym. Sci., Part A: Polym. Chem.* **1980**, *18*, 2869–2873.
24. McCullough, R. D.; Lowe, R. D. *J. Chem. Soc., Chem. Commun.* **1992**, 70–72.
25. Sato, M.-a.; Tanaka, S.; Kaeriyama, K. *J. Chem. Soc., Chem. Commun.* **1986**, 873–874.
26. Jen, K.-Y.; Miller, G. G.; Elsenbaumer, R. L. *J. Chem. Soc., Chem. Commun.* **1986**, 1346–1347.
27. McCullough, R. D.; Tristram-Nagle, S.; Williams, S. P.; Lowe, R. D.; Jayaraman, M. *J. Am. Chem. Soc.* **1993**, *115*, 4910–4911.
28. Loewe, R. S.; Khersonsky, S. M.; McCullough, R. D. *Adv. Mater.* **1999**, *11*, 250–253.
29. Loewe, R. S.; Ewbank, P. C.; Liu, J.; Zhai, L.; McCullough, R. D. *Macromolecules* **2001**, *34*, 4324–4333.
30. Miyakoshi, R.; Yokoyama, A.; Yokozawa, T. *Chem. Lett.* **2008**, *37*, 1022–1023.
31. Liu, J.; Zhang, R.; Sauv e, G.; Kowalewski, T.; McCullough, R. D. *J. Am. Chem. Soc.* **2008**, *130*, 13167–13176.
32. Tu, G.; Li, H.; Forster, M.; Heiderhoff, R.; Balk, L. J.; Scherf, U. *Macromolecules* **2006**, *39*, 4327–4331.
33. Groenendaal, L.; Jonas, F.; Freitag, D.; Pielartzik, H.; Reynolds, J. R. *Adv. Mater.* **2000**, *12*, 481–494.
34. Kirchmeyer, S.; Reuter, K. *J. Mater. Chem.* **2005**, *15*, 2077–2088.

35. Dietrich, M.; Heinze, J.; Heywang, G.; Jonas, F. *J. Electroanal. Chem.* **1994**, *369*, 87–92.
36. Jonas, F.; Schrader, L. *Synth. Met.* **1991**, *41*, 831–836.
37. Patra, A.; Bendikov, M.; Chand, S. *Acc. Chem. Res.* **2014**, *47*, 1465–1474.
38. Salzner, U.; Lagowski, J. B.; Pickup, P. G.; Poirier, R. A. *Synth. Met.* **1998**, *96*, 177–189.
39. Matano, Y.; Ohkubo, H.; Miyata, T.; Watanabe, Y.; Hayashi, Y.; Umeyama, T.; Imahori, H. *Eur. J. Inorg. Chem.* **2014**, *2014*, 1620–1624.
40. Bigot, J.; Charleux, B.; Cooke, G.; Delattre, F.; Fournier, D.; Lyskawa, J.; Stoffelbach, F.; Woisel, P. *Macromolecules* **2010**, *43*, 82–90.
41. Häupler, B.; Burges, R.; Friebe, C.; Janoschka, T.; Schmidt, D.; Wild, A.; Schubert, U. S. *Macromol. Rapid Commun.* **2014**, *35*, 1367–1371.
42. Inagi, S.; Naka, K.; Iida, D.; Chujo, Y. *Polym. J.* **2006**, *38*, 1146–1151.
43. Bryce, M. R.; Chissel, A.; Gopal, J.; Kathirgamanathan, P.; Parker, D. *Synth. Met.* **1991**, *39*, 397–400.
44. Sarukawa, T.; Oyama, N. *J. Electrochem. Soc.* **2010**, *157*, F23–F29.
45. Chung, W. J.; Griebel, J. J.; Kim, E. T.; Yoon, H.; Simmonds, A. G.; Ji, H. J.; Dirlam, P. T.; Glass, R. S.; Wie, J. J.; Nguyen, N. A.; Guralnick, B. W.; Park, J.; SomogyiÁrpád; Theato, P.; Mackay, M. E.; Sung, Y.-E.; Char, K.; Pyun, J. *Nat. Chem.* **2013**, *5*, 518–524.
46. Simmonds, A. G.; Griebel, J. J.; Park, J.; Kim, K. R.; Chung, W. J.; Oleshko, V. P.; Kim, J.; Kim, E. T.; Glass, R. S.; Soles, C. L.; Sung, Y.-E.; Char, K.; Pyun, J. *ACS Macro Lett.* **2014**, *3*, 229–232.

47. Griebel, J. J.; Li, G.; Glass, R. S.; Char, K.; Pyun, J. *J. Polym. Sci., Part A: Polym. Chem.* **2015**, *53*, 173–177.
48. Geniès, E. M.; Boyle, A.; Lapkowski, M.; Tsintavis, C. *Synth. Met.* **1990**, *36*, 139–182.
49. Stejskal, J.; Sapurina, I.; Trchová, M. *Prog. Polym. Sci.* **2010**, *35*, 1420–1481.
50. Iwan, A.; Sek, D. *Prog. Polym. Sci.* **2011**, *36*, 1277–1325.
51. Blouin, N.; Leclerc, M. *Acc. Chem. Res.* **2008**, *41*, 1110–1119.
52. Grazulevicius, J. V.; Strohmriegl, P.; Pielichowski, J.; Pielichowski, K. *Prog. Polym. Sci.* **2003**, *28*, 1297–1353.
53. Yao, M.; Senoh, H.; Sakai, T.; Kiyobayashi, T. *J. Power Sources* **2012**, *202*, 364–368.
54. Ogoshi, T.; Nishida, Y.; Yamagishi, T.-a.; Nakamoto, Y. *Macromolecules* **2010**, *43*, 7068–7072.
55. Lampert, C. M. *Sol. Energy Mater.* **1984**, *11*, 1–27.
56. Somani, P. R.; Radhakrishnan, S. *Mater. Chem. Phys.* **2003**, *77*, 117–133.
57. Song, Z.; Zhan, H.; Zhou, Y. *Chem. Commun.* **2009**, 448–450.
58. Hernandez, G.; Casado, N.; Coste, R.; Shanmukaraj, D.; Rubatat, L.; Armand, M.; Mecerreyes, D. *RSC Adv.* **2015**, *5*, 17096–17103.
59. Goswami, S. K.; McAdam, C. J.; Lee, A. M. M.; Hanton, L. R.; Moratti, S. C. *J. Mater. Chem.* **2013**, *1*, 3415–3420.
60. Milczarek, G.; Inganäs, O. *Science* **2012**, *335*, 1468–1471.
61. Gomberg, M. *J. Am. Chem. Soc.* **1900**, *22*, 757–771.

62. Nishide, H.; Iwasa, S.; Pu, Y. J.; Suga, T.; Nakahara, K.; Satoh, M. *Electrochim. Acta* **2004**, *50*, 827–831.
63. Qu, J.; Fujii, T.; Katsumata, T.; Suzuki, Y.; Shiotsuki, M.; Sanda, F.; Satoh, M.; Wada, J.; Masuda, T. *J. Polym. Sci., Part A: Polym. Chem.* **2007**, *45*, 5431–5445.
64. Nakahara, K.; Iwasa, S.; Iriyama, J.; Morioka, Y.; Suguro, M.; Satoh, M.; Cairns, E. J. *Electrochim. Acta* **2006**, *52*, 921–927.
65. Suga, T.; Pu, Y.-J.; Kasatori, S.; Nishide, H. *Macromolecules* **2007**, *40*, 3167–3173.
66. Suga, T.; Sugita, S.; Ohshiro, H.; Oyaizu, K.; Nishide, H. *Adv. Mater.* **2011**, *23*, 751–754.
67. Nesvadba, P.; Bugnon, L.; Maire, P.; Novák, P. *Chem. Mater.* **2010**, *22*, 783–788.
68. Suga, T.; Ohshiro, H.; Sugita, S.; Oyaizu, K.; Nishide, H. *Adv. Mater.* **2009**, *21*, 1627–1630.
69. Price, J. T.; Paquette, J. A.; Harrison, C. S.; Bauld, R.; Fanchini, G.; Gilroy, J. B. *Polym. Chem.* **2014**, *5*, 5223–5226.
70. Janoschka, T.; Hager, M. D.; Schubert, U. S. *Adv. Mater.* **2012**, *24*, 6397–6409.
71. Oyaizu, K.; Nishide, H. *Adv. Mater.* **2009**, *21*, 2339–2344.
72. Choi, W.; Ohtani, S.; Oyaizu, K.; Nishide, H.; Geckeler, K. E. *Adv. Mater.* **2011**, *23*, 4440–4443.
73. Choi, W.; Endo, S.; Oyaizu, K.; Nishide, H.; Geckeler, K. E. *J. Mater. Chem.* **2013**, *1*, 2999–3003.
74. Aqil, A.; Vlad, A.; Piedboeuf, M.-L.; Aqil, M.; Job, N.; Melinte, S.; Detrembleur, C.; Jérôme, C. *Chem. Commun.* **2015**, *51*, 9301–9304.

75. Winsberg, J.; Janoschka, T.; Morgenstern, S.; Hagemann, T.; Muench, S.; Hauffman, G.; Gohy, J.-F.; Hager, M. D.; Schubert, U. S. *Adv. Mater.* **2016**, *28*, 2238–2243.
76. Winsberg, J.; Muench, S.; Hagemann, T.; Morgenstern, S.; Janoschka, T.; Billing, M.; Schacher, F. H.; Hauffman, G.; Gohy, J.-F.; Hoeppener, S.; Hager, M. D.; Schubert, U. S. *Polym. Chem.* **2016**, *7*, 1711–1718.
77. Janoschka, T.; Martin, N.; Martin, U.; Friebe, C.; Morgenstern, S.; Hiller, H.; Hager, M. D.; Schubert, U. S. *Nature* **2015**, *527*, 78–81.
78. Saito, K.; Hirose, K.; Okayasu, T.; Nishide, H.; Hearn, M. T. W. *RSC Adv.* **2013**, *3*, 9752–9756.
79. Kunz, T. K.; Wolf, M. O. *Polym. Chem.* **2011**, *2*, 640–644.
80. Rostro, L.; Baradwaj, A. G.; Boudouris, B. W. *ACS Appl. Mater. Interfaces* **2013**, *5*, 9896–9901.
81. Rostro, L.; Wong, S. H.; Boudouris, B. W. *Macromolecules* **2014**, *47*, 3713–3719.
82. Liu, S.; Chu, X.; Wang, H.; Zhao, F.; Tang, E. *Ind. Eng. Chem. Res.* **2015**, *54*, 5475–5480.
83. Yonekuta, Y.; Susuki, K.; Oyaizu, K.; Honda, K.; Nishide, H. *J. Am. Chem. Soc.* **2007**, *129*, 14128–14129.
84. Yonekuta, Y.; Honda, K.; Nishide, H. *Polym. Adv. Technol.* **2008**, *19*, 281–284.
85. Schubert, U. S.; Eschbaumer, C. *Angew. Chem. Int. Ed.* **2002**, *41*, 2892–2926.
86. Williams, K. A.; Boydston, A. J.; Bielawski, C. W. *Chem. Soc. Rev.* **2007**, *36*, 729–744.
87. Abd-El-Aziz, A. S.; Shipman, P. O.; Boden, B. N.; McNeil, W. S. *Prog. Polym. Sci.* **2010**, *35*, 714–836.

88. Whittell, G. R.; Hager, M. D.; Schubert, U. S.; Manners, I. *Nat. Mater.* **2011**, *10*, 176–188.
89. Li, L.; Chow, W.-C.; Wong, W.-Y.; Chui, C.-H.; Wong, R. S.-M. *J. Organomet. Chem.* **2011**, *696*, 1189–1197.
90. Wolf, M. O. *Adv. Mater.* **2001**, *13*, 545–553.
91. Chen, X.; Liao, J.-L.; Liang, Y.; Ahmed, M. O.; Tseng, H.-E.; Chen, S.-A. *J. Am. Chem. Soc.* **2003**, *125*, 636–637.
92. Evans, N. R.; Sudha Devi, L.; Mak, C. S. K.; Watkins, S. E.; Pascu, S. I.; Köhler, A.; Friend, R. H.; Williams, C. K.; Holmes, A. B. *J. Am. Chem. Soc.* **2006**, *128*, 6647–6656.
93. Gülce, H.; Yetkin, A.; Akgül, E.; Gülce, A. *Thin Solid Films* **2013**, *545*, 81–88.
94. Zhang, Y.; Murphy, C. B.; Jones, W. E. *Macromolecules* **2002**, *35*, 630–636.
95. Kingsborough, R. P.; Swager, T. M. *J. Am. Chem. Soc.* **1999**, *121*, 8825–8834.
96. Kingsborough, R. P.; Swager, T. M. *Chem. Mater.* **2000**, *12*, 872–874.
97. Shioya, T.; Swager, T. M. *Chem. Commun.* **2002**, 1364–1365.
98. Eichhorn, H.; Sturm, M.; Wöhrle, D. *Macromol. Chem. Phys.* **1995**, *196*, 115–131.
99. McKeown, N. B. *J. Mater. Chem.* **2000**, *10*, 1979–1995.
100. Colson, J. W.; Dichtel, W. R. *Nat. Chem.* **2013**, *5*, 453–465.
101. Ding, X.; Guo, J.; Feng, X.; Honsho, Y.; Guo, J.; Seki, S.; Maitarad, P.; Saeki, A.; Nagase, S.; Jiang, D. *Angew. Chem. Int. Ed.* **2011**, *50*, 1289–1293.
102. Kondratuk, D. V.; Perdigão, L. M. A.; Esmail, A. M. S.; O'Shea, J. N.; Beton, P. H.; Anderson, H. L. *Nat. Chem.* **2015**, *7*, 317–322.

103. Abel, M.; Clair, S.; Ourdjini, O.; Mossoyan, M.; Porte, L. *J. Am. Chem. Soc.* **2011**, *133*, 1203–1205.
104. Wong, W.-Y.; Wang, X.-Z.; He, Z.; Djurišić, A. B.; Yip, C.-T.; Cheung, K.-Y.; Wang, H.; Mak, C. S. K.; Chan, W.-K. *Nat. Mater.* **2007**, *6*, 521–527.
105. Nast, R. *Coord. Chem. Rev.* **1982**, *47*, 89–124.
106. Kingsborough, R. P.; Swager, T. M., Transition Metals in Polymeric π -Conjugated Organic Frameworks. In *Prog. Inorg. Chem.*, John Wiley & Sons, Inc.: 2007; p 123–231.
107. Schwab, P. F. H.; Levin, M. D.; Michl, J. *Chem. Rev.* **1999**, *99*, 1863–1934.
108. Nguyen, P.; Gómez-Elipe, P.; Manners, I. *Chem. Rev.* **1999**, *99*, 1515–1548.
109. Manners, I. *Angew. Chem. Int. Ed.* **1996**, *35*, 1602–1621.
110. Johnson, B. F. G.; Kakkar, A. K.; Khan, M. S.; Lewis, J. *J. Organomet. Chem.* **1991**, *409*, C12–C14.
111. Davies, S. J.; Johnson, B. F. G.; Lewis, J.; Raithby, P. R. *J. Organomet. Chem.* **1991**, *414*, C51–C53.
112. Younus, M.; Long, N. J.; Raithby, P. R.; Lewis, J.; Page, N. A.; White, A. J. P.; Williams, D. J.; Colbert, M. C. B.; Hodge, A. J.; Khan, M. S.; Parker, D. G. *J. Organomet. Chem.* **1999**, *578*, 198–209.
113. Khan, M. S.; Pasha, N. A.; Kakkar, A. K.; Raithby, P. R.; Lewis, J.; Fuhrmann, K.; Friend, R. H. *J. Mater. Chem.* **1992**, *2*, 759–760.
114. Davies, S. J.; Johnson, B. F. G.; Khan, M. S.; Lewis, J. *J. Chem. Soc., Chem. Commun.* **1991**, 187–188.
115. Sonogashira, K.; Ohga, K.; Takahashi, S.; Hagihara, N. *J. Organomet. Chem.* **1980**, *188*, 237–243.

116. Masai, H.; Sonogashira, K.; Hagihara, N. *Bull. Chem. Soc. Jpn.* **1971**, *44*, 2226–2230.
117. Abe, A.; Kimura, N.; Tabata, S. *Macromolecules* **1991**, *24*, 6238–6243.
118. Peng, Q.; Xie, M.; Huang, Y.; Lu, Z.; Cao, Y. *Macromol. Chem. Phys.* **2005**, *206*, 2373–2380.
119. Chawdhury, N.; Köhler, A.; Friend, R. H.; Wong, W.-Y.; Lewis, J.; Younus, M.; Raithby, P. R.; Corcoran, T. C.; Al-Mandhary, M. R. A.; Khan, M. S. *J. Chem. Phys.* **1999**, *110*, 4963–4970.
120. Zhen, H.; Jiang, C.; Yang, W.; Jiang, J.; Huang, F.; Cao, Y. *Chem. Eur. J.* **2005**, *11*, 5007–5016.
121. Man, K. Y. K.; Wong, H. L.; Chan, W. K.; Djurišić, A. B.; Beach, E.; Rozeveld, S. *Langmuir* **2006**, *22*, 3368–3375.
122. Manners, I. *Polyhedron* **1996**, *15*, 4311–4329.
123. Neuse, E. W.; Rosenberg, H. J. *Macromol. Sci., Polym. Rev.* **1970**, *4*, 1–145.
124. Manners, I. *Chem. Commun.* **1999**, 857–865.
125. Musgrave, R. A.; Russell, A. D.; Manners, I. *Organometallics* **2013**, *32*, 5654–5667.
126. Hailes, R. L. N.; Oliver, A. M.; Gwyther, J.; Whittell, G. R.; Manners, I. *Chem. Soc. Rev.* **2016**, *45*, 5358–5407.
127. Pietschnig, R. *Chem. Soc. Rev.* **2016**, *45*, 5216–5231.
128. MacLachlan, M. J.; Ginzburg, M.; Coombs, N.; Coyle, T. W.; Raju, N. P.; Greedan, J. E.; Ozin, G. A.; Manners, I. *Science* **2000**, *287*, 1460–1463.

129. Ginzburg, M.; MacLachlan, M. J.; Yang, S. M.; Coombs, N.; Coyle, T. W.; Raju, N. P.; Greedan, J. E.; Herber, R. H.; Ozin, G. A.; Manners, I. *J. Am. Chem. Soc.* **2002**, *124*, 2625–2639.
130. Sui, X.; Shui, L.; Cui, J.; Xie, Y.; Song, J.; van den Berg, A.; Hempenius, M. A.; Julius Vancso, G. *Chem. Commun.* **2014**, *50*, 3058–3060.
131. Hudson, Z. M.; Lunn, D. J.; Winnik, M. A.; Manners, I. *Nat. Commun.* **2014**, *5*.
132. Haddad, T. S.; Lichtenhan, J. D. *J. Inorg. Organomet. Polym. Mater.* **1995**, *5*, 237–246.
133. Cao, K.; Murshid, N.; Wang, X. *Macromol. Rapid Commun.* **2015**, *36*, 586–596.
134. Tyler, D. R. *Coord. Chem. Rev.* **2003**, *246*, 291–303.
135. Carraher, C. E.; Sheats, J. E. *Makromol. Chem.* **1973**, *166*, 23–29.
136. Roner, M. R.; Carraher, C. E.; Shahi, K.; Ashida, Y.; Barot, G. *BMC Cancer* **2009**, *9*, 1–9.
137. Bielawski, C. W.; Grubbs, R. H. *Prog. Polym. Sci.* **2007**, *32*, 1–29.
138. Yan, Y.; Deaton, T. M.; Zhang, J.; He, H.; Hayat, J.; Pageni, P.; Matyjaszewski, K.; Tang, C. *Macromolecules* **2015**, *48*, 1644–1650.
139. Ren, L.; Zhang, J.; Bai, X.; Hardy, C. G.; Shimizu, K. D.; Tang, C. *Chem. Sci.* **2012**, *3*, 580–583.
140. Ren, L.; Zhang, J.; Hardy, C. G.; Ma, S.; Tang, C. *Macromol. Rapid Commun.* **2012**, *33*, 510–516.
141. Morsbach, J.; Natalello, A.; Elbert, J.; Winzen, S.; Kroeger, A.; Frey, H.; Gallei, M. *Organometallics* **2013**, *32*, 6033–6039.
142. Gilroy, J. B.; McKinnon, S. D. J.; Koivisto, B. D.; Hicks, R. G. *Org. Lett.* **2007**, *9*, 4837–4840.

143. Gilroy, J. B.; McKinnon, S. D. J.; Kennepohl, P.; Zsombor, M. S.; Ferguson, M. J.; Thompson, L. K.; Hicks, R. G. *J. Org. Chem.* **2007**, *72*, 8062–8069.
144. Niewahner, J. H.; Walters, K. A.; Wagner, A. *J. Chem. Educ.* **2007**, *84*, 477.
145. Huang, H.-H.; Chao, C.-G.; Lee, S.-L.; Wu, H.-J.; Chen, C.-H.; Luh, T.-Y. *Org. Biomol. Chem.* **2012**, *10*, 5948–5953.

Chapter 2

2 6-Oxoverdazyl Radical Polymers with Tunable Electrochemical Properties

Adapted from:

J.T. Price, **J.A. Paquette**, C.S Harrison, R. Bauld, G. Fanchini,* and J.B. Gilroy* *Polym. Chem.* **2014**, *5*, 5223–5226.

2.1 Introduction

Organic radicals have fascinated scientists since the discovery of the persistent triphenyl methyl radical by Gomberg in 1900.¹ Since then, many families of stable radicals have been discovered and their properties widely explored across a number of applications.²⁻³

More recently, polymers containing stable radicals within or appended to a variety of polymer backbones have been prepared as part of efforts towards combining the processability of polymers with the functionality (*i.e.*, magnetic and redox properties) of stable organic radicals. Based on the combination of these traits, stable radical polymers have shown application as host materials in Li-ion batteries,⁴ silica-grafted catalysts for the oxidation of alcohols,⁵ ferromagnetic organic materials,⁶ solid-state conductive materials,⁷⁻⁸ redox mediators in transparent conducting materials,⁹ the functional component of rewritable memory devices,¹⁰ and electrode materials in stable radical polymer batteries.^{11-12,13-17}

Although advances in the stable radical polymer field have been impressive, examples that exhibit readily tunable properties through structural variation have remained elusive. 6-Oxoverdazyl radicals (**2.1**: X = CO) represent one of the only classes of stable radicals with stabilities rivaling nitroxide (**2.2**) and nitronyl nitroxide radicals (**2.3**). The ability to tune the properties of 6-oxoverdazyl radicals through structural variation (**2.1**: R, R', and X) has led to their use as mediators for controlled radical polymerization,¹⁸⁻¹⁹ in model coordination complexes for molecule-based magnets,^{20,21-25} as photoconductive liquid-crystalline materials,²⁶ and in tunable redox-active molecular materials.²⁷⁻³⁰ However, the

Varian Mercury instrument. ^1H NMR spectra were referenced to CHCl_3 (7.26 ppm), $\text{CD}_3\text{SOCD}_2\text{H}$ (2.50 ppm), or CD_2HCN (1.93 ppm) and $^{13}\text{C}\{^1\text{H}\}$ NMR spectra were referenced to CDCl_3 (77.2 ppm) or CD_3SOCD_3 (39.5 ppm). Mass spectrometry data were recorded in positive-ion mode using a high resolution Finnigan MAT 8200 spectrometer using electron impact ionization. UV-vis spectra were recorded in CH_2Cl_2 solutions and recorded using a Cary 300 Scan instrument. Four separate concentrations were run for each sample, and molar extinction coefficients were determined from the slope of a plot of absorbance against concentration. IR spectra were recorded as KBr pellets using a Bruker Vector 33 FT-IR spectrometer. Gel permeation chromatography (GPC) was carried out at a flow rate of 1 mL min^{-1} in *N,N*-dimethylformamide (DMF) with 10 mM LiBr and 1% (v/v) Et_3N added at a regulated temperature of $85 \text{ }^\circ\text{C}$ using a Waters 515 pump, equipped with a Wyatt Optilab REx detector and two PLgel $5 \text{ }\mu\text{m}$ mixed-D ($300 \text{ mm} \times 7.5 \text{ mm}$) columns from Polymer Laboratories connected in series. Calibration was performed using monodisperse polystyrene standards supplied by Polymer Lab. Elemental analyses (C, H, N) were carried out by Laboratoire d'Analyse Élémentaire de l'Université de Montréal, Montréal, QC, Canada.

2.2.2 Electrochemical Methods

Cyclic voltammetry experiments were performed with a Bioanalytical Systems Inc. (BASi) Epsilon potentiostat and analyzed using BASi Epsilon software. Typical electrochemical cells consisted of a three-electrode setup including a glassy carbon working electrode, platinum wire counter electrode, and silver wire *pseudo*-reference electrode. Experiments were run at variable scan rates in degassed tetrahydrofuran (THF) solutions of the analyte ($\sim 1 \text{ mM}$) and electrolyte ($0.1 \text{ M } n\text{Bu}_4\text{N PF}_6$). Cyclic voltammograms were referenced against the ferrocene/ferrocenium redox couple ($\sim 1 \text{ mM}$ internal standard) and corrected for internal cell resistance using the BASi Epsilon software.

2.2.3 Electron Paramagnetic Resonance (EPR) Spectroscopy

EPR measurements were made on *ca.* 10^{-5} M CH_2Cl_2 solutions of verdazyl radical polymers **2.7a,b** and verdazyl radicals **2.11a,b** that had been subjected to three freeze-

pump-thaw cycles in 0.4 mm quartz tubes using a JEOL JES-FA200 EPR spectrometer. All measurements were made at 20 °C and *g*-factors were referenced relative to a built-in manganese dioxide marker within the resonant cavity of the instrument.

2.2.4 Kelvin Probe Force Microscopy (KPFM)

Thin films of polymer **2.7a** were spun under atmospheric conditions using a Laurell WS40-6NPP spin coater from a 15 mg mL⁻¹ solution in anhydrous chlorobenzene (Sigma-Aldrich). A spinning speed of 1,000 RPM produced a polymeric thin film of approximately 166±10 nm thickness. The topography and work function of thin films of 6-oxoverdazyl polymer **2.7a** were determined in one single scan by intermittent contact mode Atomic Force Microscopy (AFM) and Kelvin Probe Force Microscopy (KPFM), respectively. Images were recorded on a Witec Alpha 300S atomic force microscope specifically modified for KPFM experiments with the attachment of a Stanford DS 345 function generator. This generator is locked-in at the second-order resonance frequency of the AFM cantilever using a Stanford SR844-RF lock-in amplifier that transfers the data directly to the digital controller of the Witec system. The AFM/KPFM microscope is contained in a sealed enclosure for controlling the temperature and humidity of the atmosphere during measurements. For each pixel of an AC-mode AFM scan, the voltage V_{b0} resulting in the minimum force between the tip and the sample is optimized in the $V_b = \pm 10$ V range using an integral-proportional feedback loop. Under those conditions, $e \cdot V_{b0}$ represents the work function of the sample relative to the tip.³⁹ Conducting cantilevers (~75 kHz first-order resonance frequency, ~425 kHz second-order resonance frequency, from Nanosensors Inc.) were used for AFM/KPFM imaging. For KPFM, the work function of the polymeric thin film was determined from its shift from the work function of ITO recorded on a portion of the sample in which the polymer film was removed. The work function of the used ITO reference was assumed to be 4.7 eV.⁴⁰ In order to determine the uncertainty associated with such a work function estimate, the conducting AFM tip was also calibrated by scanning highly doped *p*- and *n*-type silicon wafers of known work functions and determined to be $\sim 4.6 \pm 0.1$ eV. With this crosscheck we determined the uncertainty associated to our KPFM measurements to be ± 0.1 eV, or better. KPFM histograms were directly extracted from the recorded images using the Witec Project 2.04 software and analyzed using a model

comprising three Gaussian peaks, one for the signal from the polymeric film surface, one for the signal from the ITO film surface and one minor peak related to the signal related to the edge of the film, as shown in the inset of Figure 2.9.

2.2.5 X-ray Crystallography Details

Crystals suitable for X-ray diffraction were grown by slow cooling ($-20\text{ }^{\circ}\text{C}$) a saturated toluene solution of **2.11a**, slow cooling ($-20\text{ }^{\circ}\text{C}$) a saturated EtOAc solution of **2.11c**, or vapor diffusion of Et_2O into a saturated acetonitrile solution of **2.12c** at $-35\text{ }^{\circ}\text{C}$. X-ray diffraction data were collected on a Nonius KappaCCD or a Bruker ApexII CCD area detector using graphite-monochromated Mo $\text{K}\alpha$ radiation ($\lambda = 0.71073\text{ \AA}$). Single crystals were selected under Paratone-N, mounted on MiTeGen polyimide micromount, and immediately placed under a cold stream of N_2 . Structures were solved by direct methods and refined using full-matrix least squares on F^2 .⁴¹ See Table 2.1 for crystallographic data and the CCDC (991914-991916) for structural data.

Table 2.1 Crystallographic data for compounds **2.11a**, **2.11c**, and **2.12c**.

	2.11a	2.11c	2.12c
Chemical Formula	C ₁₉ H ₂₇ N ₄ O ₃	C ₁₄ H ₁₉ N ₄ O	C ₁₄ H ₁₉ BFN ₄ O
FW (g/mol)	359.44	259.33	346.14
Crystal Dimensions (mm)	0.51 x 0.17 x 0.052	0.4 x 0.3 x 0.3	0.24 x 0.22 x 0.18
Crystal Habit	Red, block	Red, block	Red, block
Crystal System	Monoclinic	Orthorhombic	Monoclinic
Space Group	<i>P</i> 2 ₁ / <i>c</i>	<i>P</i> <i>na</i> 2 ₁	<i>P</i> 2 ₁ / <i>c</i>
Temperature (K)	110	150(2)	150(2)
<i>a</i> (Å)	18.930(7)	16.219(7)	8.1059(16)
<i>b</i> (Å)	5.8718(19)	15.484(9)	13.501(5)
<i>c</i> (Å)	18.364(5)	5.7192(14)	15.435(6)
α (°)	90	90	90
β (°)	105.364(12)	90	99.864(10)
γ (°)	90	90	90
<i>V</i> (Å ³)	1968.3(11)	1436.4(11)	1664.3(10)
<i>Z</i>	4	4	4
ρ (g/cm ³)	1.213	1.199	1.381
λ , Å, (Mo K α)	0.71073	0.71073	0.71073
μ (cm ⁻¹)	0.084	0.079	0.119
Diffractometer Type	Bruker APEX-II CCD	Nonius KappaCCD	Nonius KappaCCD
<i>R</i> _{merge}	0.0548	0.0269	0.0376
^a <i>R</i> ₁ [$2\sigma I > 2$]	0.0515	0.0313	0.0580
^b <i>wR</i> ₂ [$2\sigma I > 2$]	0.1282	0.0735	0.1489
<i>R</i> ₁ (all data)	0.0891	0.0378	0.0818
<i>wR</i> ₂ (all data)	0.1527	0.0767	0.1685
GOF	1.041	1.045	1.048

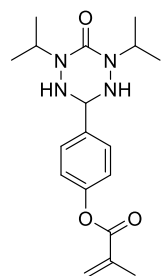
$$^a R_1 = \frac{\sum (|F_o| - |F_c|)}{\sum F_o}$$

$$^b wR_2 = \left[\frac{\sum (w(F_o^2 - F_c^2)^2)}{\sum (w F_o^4)} \right]^{1/2}$$

$$\text{GOF} = \left[\frac{\sum (w(F_o^2 - F_c^2)^2)}{(\text{No. of reflns.} - \text{No. of params.})} \right]^{1/2}$$

2.2.6 Synthetic Procedures

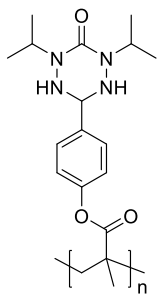
Synthesis of 1,5-di-isopropyl-3-(4-phenylmethacryloyl)-6-oxotetrazane **2.5a**



A sample of tetrazane **2.4** (2.20 g, 7.90 mmol) was added to a Schlenk flask equipped with a stir bar and combined with dry CH₂Cl₂ (150 mL) and dry Et₃N (1.1 mL, 0.79 g, 7.9 mmol). Methacryloyl chloride (0.70 mL, 0.75 g, 7.9 mmol) was then added drop wise via syringe to the suspension of tetrazane **2.4** causing dissolution. After stirring for 3 h at 20 °C, deionized H₂O (10 mL) was transferred to the reaction flask via syringe and the reaction mixture was stirred for 5 min to consume any remaining methacryloyl chloride. The reaction mixture was then transferred to a separatory funnel and washed with deionized H₂O (3 x 100 mL). The organic layer was dried over MgSO₄ before the solvent was

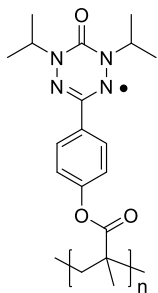
removed to yield a light yellow powder. Recrystallization from a saturated EtOAc solution afforded tetrazane **2.5a** as a soft, fibrous white solid. Yield = 1.75 g, 65 %. ^1H NMR (400.1 MHz, d_6 -DMSO): δ 7.61 (d, 2H, $^3J_{\text{HH}} = 8$ Hz, aryl CH), 7.20 (d, 2H, $^3J_{\text{HH}} = 8$ Hz, aryl CH), 6.28 (s, 1H, =CH), 5.91 (s, 1H, =CH), 5.00 (d, 2H, $^3J_{\text{HH}} = 12$ Hz, NH), 4.50 (sept, 1H, $^3J_{\text{HH}} = 7$ Hz, CH), 4.39 (t, 1H, $^3J_{\text{HH}} = 12$ Hz, CH), 2.00 (s, 3H, CH_3), 1.07 (d, 6H, $^3J_{\text{HH}} = 7$ Hz, CH_3), 1.04 (d, 6H, $^3J_{\text{HH}} = 7$ Hz, CH_3). $^{13}\text{C}\{^1\text{H}\}$ NMR (100.6 MHz, d_6 -DMSO): δ 165.3, 153.4, 150.4, 135.2, 134.1, 127.9, 121.7, 71.1, 46.7, 19.5, 18.4, 18.0. FT-IR (ranked intensity), KBr pellet: 724(10), 916(7), 1129(2), 1205(9), 1317(8), 1429(6), CO tetrazane 1583(1), CO ester 1735(3), 2977(4), NH tetrazane 3232(5) cm^{-1} . Mass Spec. (EI, +ve mode): exact mass calculated for $\text{C}_{18}\text{H}_{26}\text{N}_4\text{O}_3$: 346.2005; found: 346.1992; difference: -3.8 ppm. Anal. Calcd. (%) for $\text{C}_{18}\text{H}_{26}\text{N}_4\text{O}_3$: C, 62.41; H, 7.56; N, 16.17. Found: C, 62.40; H, 7.61; N, 16.01.

Synthesis of isopropyl-substituted tetrazane polymer **2.6a**



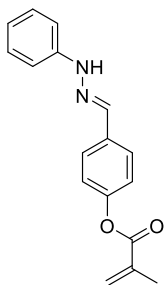
A sample of tetrazane **2.5a** (3.0 g, 8.64 mmol) was added degassed MeOH (15 mL) in a greaseless Schlenk flask equipped with a stir bar under N_2 . AIBN (0.075 g, 0.43 mmol) was added to the reaction flask under a flow of nitrogen and the reaction mixture was further degassed by 2 more freeze-pump-thaw cycles. The reaction was then heated to 65°C for 22 h at which time the solvent was removed *in vacuo* yielding a white solid. The white solid was then washed with EtOAc (3×30 mL) to remove trace amounts of tetrazane **2.5a**. Tetrazane polymer **2.6a** was isolated as a white solid by centrifugation and dried at 20°C *in vacuo* for 16 h before it was stored at 20°C to avoid undesirable oxidation. Yield = 2.47 g, 83%. ^1H NMR (400.1 MHz, d_6 -DMSO): 7.57 (br, s, 2H, aryl CH), 7.15 (br, s, 2H, aryl CH), 4.97 (br, s, 2H, NH), 4.45 (br, s, 2H, $\text{CH}(\text{CH}_3)$), 4.35 (br, s, 1H, CH), 2.50–2.20 overlaps residual NMR solvent signal (v. br, s, 2H, CH_2), 1.41–1.33 (br, m, 3H, CH_3), 0.99 (br, s, 12H, CH_3). FT-IR (ranked intensity), KBr pellet: 728(8), 879(5), 1017(9), 1166(2), 1416(4), 1507(10), CO tetrazane 1613(1), CO ester 1751(6), 2917(3), NH tetrazane 3244(7) cm^{-1} . GPC: $M_n = 25,260$ g mol^{-1} , $M_w = 46,230$ g mol^{-1} , $D = 1.83$.

Synthesis of *isopropyl*-substituted 6-oxoverdazyl polymer **2.7a**



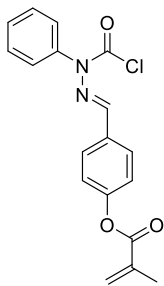
A sample of **2.6a** (1.50 g, 4.30 mmol) and *p*-benzoquinone (0.72 g, 6.6 mmol) were added to a mixture of THF (30 mL) and MeOH (30 mL) and heated to 85 °C for 15 h. Upon heating, the reaction mixture changed from yellow to bright red/orange in colour. The reaction was cooled to 20 °C and concentrated *in vacuo*. The resulting red residue was taken up in CH₂Cl₂ (60 mL) and purified by column chromatography (neutral alumina, CH₂Cl₂ eluent). The orange solution was then collected and concentrated *in vacuo*. The polymer was further purified by precipitating (in triplicate) concentrated CH₂Cl₂ solutions into pentane. 6-Oxoverdazyl polymer **2.7a** was isolated as an orange solid by centrifugation and dried at 35 °C under reduced pressure for 16 h. Yield = 1.15 g, 78%. FT-IR (ranked intensity), KBr pellet: 657(8), 877(9), 722(6), 1016(7), 1164(2), 1387(3), 1510(5), CO verdazyl 1685(1), CO ester 1753(10), 2979(4) cm⁻¹. UV-vis (CH₂Cl₂): λ_{max} 417 nm (ε = 1,649 M⁻¹ cm⁻¹). GPC: M_n = 25,750 g mol⁻¹, M_w = 48,670 g mol⁻¹, Đ = 1.89.

Synthesis of 4-methacryloylbenzaldehyde phenylhydrazone **2.8**



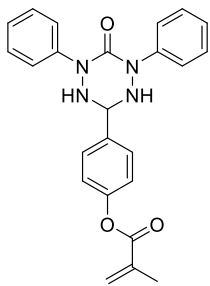
The preparation was adapted from a procedure by Milcent and co-workers.⁴² To a solution of 4-formylphenyl methacrylate (4.00 g, 21.0 mmol) in EtOH (50 mL) was added phenylhydrazine (2.49 mL, 2.73 g, 25.2 mmol). A yellow precipitate quickly formed, and was left to stir for 1 h. The solution was poured into ice-cold H₂O (200 mL) and the resulting white precipitate was filtered before it was recrystallized in *i*PrOH to give **2.8** as lustrous white crystals. Yield = 5.01 g, 85%. ¹H NMR (599.5 MHz, *d*₆-DMSO): δ 10.36 (s, 1H, NH), 7.89 (s, 1H, N=CH), 7.70 (d, 2H, ³J_{HH} = 9 Hz, aryl CH), 7.22 (m, 4H, aryl CH), 7.09 (d, 2H, ³J_{HH} = 7 Hz, aryl CH), 6.75 (t, 1H, ³J_{HH} = 7 Hz, aryl CH), 6.29 (s, 1H, C=CH₂), 5.90 (s, 1H, C=CH₂), 2.01 (s, 3H, CH₃). ¹³C{¹H} NMR (150.8 MHz, *d*₆-DMSO): δ 165.2, 150.1, 145.2, 135.5, 135.2, 133.6, 129.1, 127.7, 126.5, 122.0, 118.8, 112.0, 18.0. Mass Spec. (EI, +ve mode): exact mass calculated for C₁₇H₁₆N₂O₂: 280.1212; exact mass found: 280.1211; difference: -0.43 ppm.

Synthesis of 4-methacryloylbenzaldehyde α -chloroformylphenylhydrazone **2.9**



This procedure was adapted from a preparation by Milcent and co-workers.⁴² To a cooled solution of phosgene (2.94 mL, 4.46 mmol, 15 wt % in toluene) was added dropwise hydrazone **2.8** (1.00 g, 3.57 mmol) dissolved in a minimum amount of dry EtOAc/benzene (1:1, 20 mL) containing dry pyridine (0.32 mL, 0.33 g, 3.9 mmol) under N₂. Once the addition was complete, the pink mixture was heated to 60 °C for 1 h. The solvent was then removed *in vacuo*. The pink impurity was removed by column chromatography (silica gel, CH₂Cl₂ eluent). The resulting solid was recrystallized in cyclohexane to give **2.9** as a white microcrystalline solid. Yield = 1.19 g, 98%. ¹H NMR (399.8 MHz, CDCl₃): δ 7.67 (m, 2H, aryl CH), 7.56 (m, 3H, aryl CH), 7.32 (s, 1H, N=CH), 7.26 (m, 2H, aryl CH), 7.15 (m, 2H, aryl CH), 6.34 (s, 1H, C=CH₂), 5.77 (m, 1H, C=CH₂), 2.04 (s, 3H, CH₃). ¹³C{¹H} NMR (100.6 MHz, CDCl₃): δ 165.3, 152.6, 144.7 (bs, COCl), 135.9, 135.5, 130.8, 130.5, 130.2, 128.8, 128.7, 127.6, 122.0, 18.2. Note: The ¹³C NMR spectra were initially gathered in *d*₆-DMSO, which resulted in rapid decomposition of **2.9**. Therefore, CDCl₃ was used, but this caused broadening of several signals and certain peaks could not be resolved. Mass Spec. (EI, +ve mode): exact mass calculated for C₁₈H₁₅ClN₂O₃: 342.0771; exact mass found: 342.0769; difference: -0.68 ppm.

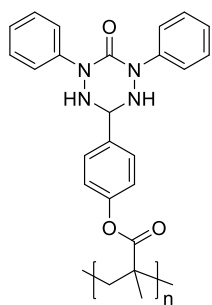
Synthesis of 1,5-diphenyl-3-(4-phenylmethacryloyl)-6-oxotetrazane **2.5b**



This procedure was adapted from a previous synthesis by Milcent and co-workers.⁴² To a stirred solution of phenylhydrazine (0.23 mL, 0.25 g, 2.3 mmol) in EtOH (10 mL) was added the α -chloroformylphenylhydrazone **2.9** (0.40 g, 1.2 mmol) in small portions over 15 min. After the addition was complete, the solution was heated to 55 °C and left to stir for 3 h. The solution began clear and became opaque as the reaction proceeded. The warm mixture was then poured into ice cold H₂O (30 mL). The precipitate was filtered, dried *in vacuo* overnight and the grey solid was recrystallized in *n*-PrOH to give **2.5b** as a white powder. Yield = 0.31 g, 64%. ¹H NMR (399.8 MHz, *d*₆-DMSO): δ 7.60 (m, 6H, aryl CH), 7.33 (t, 4H, ³J_{HH} = 7 Hz, aryl CH), 7.17 (d, 2H, ³J_{HH} =

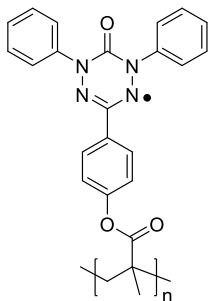
9 Hz, aryl *CH*), 7.08 (t, 2H, $^3J_{\text{HH}} = 7$ Hz, aryl *CH*), 6.43 (d, 2H, $^3J_{\text{HH}} = 9$, *NH*), 6.27 (s, 1H, $\text{C}=\text{CH}_2$), 5.89 (s, 1H, $\text{C}=\text{CH}_2$), 5.42 (t, 1H, $^3J_{\text{HH}} = 9$ Hz, *N-CH*), 1.99 (s, 3H, CH_3). $^{13}\text{C}\{^1\text{H}\}$ NMR (100.5 MHz, d_6 -DMSO): δ 165.6, 157.4, 150.8, 143.1, 135.7, 135.6, 128.6, 128.4, 128.2, 123.7, 122.1, 121.5, 72.8, 18.4. FT-IR (ranked intensities) KBr pellet: 692(10), 742(11), 922(12), 1124(3), 1167(4), 1310(6), 1202(7), 1375(2), 1501(8), CO tetrazane 1625(1), CO ester 1735(5), NH tetrazane 3233(9) cm^{-1} . Mass Spec. (EI, +ve mode): exact mass calculated for $\text{C}_{24}\text{H}_{22}\text{N}_4\text{O}_3$: 414.1692; exact mass found: 414.1682; difference: -2.4 ppm. Anal. Calcd. (%) for $\text{C}_{24}\text{H}_{22}\text{N}_4\text{O}_3$: C, 69.55; H, 5.35; N, 13.52. Found: C, 69.20; H, 5.39; N, 13.40.

Synthesis of phenyl-substituted tetrazane polymer **2.6b**



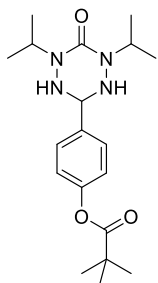
A dry solution of THF/MeOH (1:1, 10 mL) was degassed using the freeze-pump-thaw technique 3 times, followed by the addition of AIBN (0.050 g, 0.30 mmol, 5 mol %) to THF. 2 mL of this AIBN solution was then transferred to a greaseless Schlenk flask containing 6-oxotetrazane **2.5b** (0.50 g, 1.21 mmol). The mixture was shielded from light and heated to 65 °C in a temperature controlled oil bath in a sealed flask and stirred for 48 h. The solution was removed from the oil bath and precipitated into ethyl acetate (3 x 20 mL), then dried *in vacuo* to afford **5b** as a white solid. Yield = 0.38 g, 76 %. ^1H NMR (599.4 MHz, d_6 -DMSO): δ 7.55 (bs, 6H, aryl *CH*), 7.22 (bs, 4H, aryl *CH*), 7.01 (bs, 4H, aryl *CH*), 6.35 (bs, 2H, *NH*), 5.32 (bs, 1H, *CH*), 2.21 (bs, 2H, CH_2), 1.27 (bs, 3H, CH_3). FT-IR (ranked intensities) KBr pellet: 692(10), 756(9), 883(12), 1105(7), 1166(3), 1363(2), 1497(1), 1596(8), CO tetrazane 1666(5), CO ester 1750(4), NH tetrazane 3248(11) cm^{-1} . GPC: $M_n = 20,280$ g mol^{-1} , $M_w = 25,450$ g mol^{-1} , $D = 1.49$. Anal. Calcd. (%) for $[\text{C}_{24}\text{H}_{22}\text{N}_4\text{O}_3]_n$: C, 69.55; H, 5.35; N, 13.52 Found: C, 69.33; H, 5.44; N, 13.52.

Synthesis of phenyl-substituted 6-oxoverdazyl polymer **2.7b**



A sample of **2.6b** (0.15 g, 0.36 mmol) and freshly sublimed *p*-benzoquinone (0.060 g, 0.54 mmol) were dissolved in THF (20 mL). Once dissolved, MeOH (10 mL) was added and the solution was heated to 85 °C for 21 h. Upon heating, the reaction mixture changed from yellow to dark red. The reaction was cooled to 20 °C and concentrated *in vacuo*. The resulting red residue was taken up in CH₂Cl₂ (10 mL) and purified by column chromatography (neutral alumina, CH₂Cl₂ followed by THF as eluent). The second fraction, a dark red solution, was collected and concentrated *in vacuo*. The solid was further dried at 40 °C *in vacuo* for 36 h, to obtain **2.7b** as a dark red solid. Yield = 0.12 g, 81%. FT-IR (ranked intensities) KBr pellet: 688(9), 748(8), 1101(3), 1162(2), 1266(4), 1251(7), 1464(5), CO verdazyl 1701(1), CO ester 1750(6), 2953(10) cm⁻¹. UV-vis (CH₂Cl₂): λ_{max} 566 nm (ε = 1,667 M⁻¹ cm⁻¹), 319 nm (ε = 9,760 M⁻¹ cm⁻¹), 262 nm (ε = 21,314 M⁻¹ cm⁻¹). GPC: M_n = 12,000 g mol⁻¹, M_w = 14,500 g mol⁻¹, Đ = 1.46.

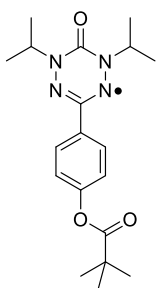
Synthesis of 1,5-diisopropyl-3-(4-trimethylacetylphenyl)-6-oxotetrazane **2.10a**



A sample of tetrazane **2.4** (2.80 g, 10.1 mmol) was added to a Schlenk flask equipped with a stir bar and combined with CH₂Cl₂ (200 mL) and Et₃N (1.41 mL, 1.02 g, 10.1 mmol). Trimethylacetyl chloride (1.24 mL, 1.21 g, 10.1 mmol) was then added drop wise via syringe to the suspension of tetrazane **2.4** causing complete dissolution after a few min. After stirring for 3 h at 20 °C, deionized H₂O (10 mL) was transferred to the reaction flask via syringe and the mixture was allowed to stir for 5 min to ensure any remaining trimethylacetyl chloride was consumed. The reaction mixture was transferred to a separatory funnel and washed with deionized H₂O (3 × 100 mL). The organic layer was dried over MgSO₄ before the solvent was removed *in vacuo* to yield a light yellow powder. Recrystallization from a saturated EtOAc solution afforded tetrazane **2.10a** as an off-white solid. Yield = 2.08 g, 57%. ¹H NMR (400.1 MHz, *d*₆-DMSO): δ 7.59 (d, 2H, ³J_{HH} = 8 Hz, aryl CH), 7.12 (d, 2H, ³J_{HH} = 8 Hz, aryl CH), 4.99 (d, 2H, ³J_{HH} = 11 Hz, NH), 4.50 (sept. 2H, ³J_{HH} = 6.61 Hz, CH), 4.39 (t, 1H, ³J_{HH} = 11 Hz, CH), 1.31 (s, 9H, CH₃), 1.05 (d, 6H, ³J_{HH} = 7 Hz, CH₃),

1.03 (d, 6H, $^3J_{\text{HH}} = 7$ Hz, CH_3). $^{13}\text{C}\{^1\text{H}\}$ NMR (100.6 MHz, d_6 -DMSO): δ 176.6, 153.6, 150.8, 134.2, 128.1, 121.7, 71.3, 46.9, 26.9, 19.7, 18.6. FT-IR (ranked intensity), KBr pellet: 619(7), 640(10), 726(5), 894(3), 1115(4), 1426(8), CO tetrazane 1579(1), CO ester 1751(9), 2975(2), NH tetrazane 3236(6) cm^{-1} . Mass Spec. (EI, +ve mode): exact mass calculated for $\text{C}_{19}\text{H}_{30}\text{N}_4\text{O}_3$: 362.2318; exact mass found: 362.2315; difference: -0.8 ppm. Anal. Calcd. (%) for $\text{C}_{19}\text{H}_{30}\text{N}_4\text{O}_3$: C, 62.96; H, 8.34; N, 15.46. Found: C, 62.95; H, 8.44; N, 15.44.

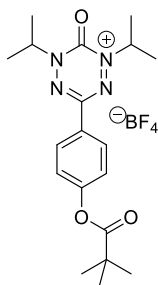
Synthesis of 1,5-di-isopropyl-3-(4-trimethylacetylphenyl)-6-oxoverdazyl **2.11a**



A sample of tetrazane **2.10a** (2.40 g, 6.20 mmol) was combined with freshly sublimed *p*-benzoquinone (1.08 g, 9.40 mmol) in a 250 mL round bottom flask equipped with a stir bar and a reflux condenser. To this flask, toluene (35 mL) was added before it was immersed in an oil bath, stirred, and heated at 120 °C for 30 min. The orange-red reaction mixture was cooled to 20 °C causing *p*-hydroquinone to precipitate from solution. The reaction mixture was filtered and the toluene removed from the filtrate *in vacuo* to afford an orange-red residue. Purification via flash column chromatography (neutral alumina, toluene eluent) followed by removal of the solvent afforded 6-oxoverdazyl **2.11a** as a bright orange microcrystalline solid. Yield = 1.90 g, 85%. FT-IR (ranked intensity), KBr: 658(9), 720(8), 895(10), 1116(2), 1165(7), 1227(4), 1366(3), CO verdazyl 1681(1), CO ester 1757(6), 2983(5) cm^{-1} . UV-vis (CH_2Cl_2): λ_{max} 417 nm ($\epsilon = 1,648 \text{ M}^{-1} \text{ cm}^{-1}$). Mass Spec. (EI, +ve mode): exact mass calculated for $\text{C}_{19}\text{H}_{27}\text{N}_4\text{O}_3$: 359.2083; exact mass found: 359.2078; difference -1.4 ppm. Anal. Calcd. (%) for $\text{C}_{19}\text{H}_{27}\text{N}_4\text{O}_3$: C, 63.49; H, 7.57; N, 15.59. Found: C, 63.65; H, 7.76; N, 15.33.

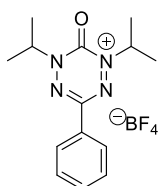
Synthesis of 1,5-di-isopropyl-3-(4-trimethylacetylphenyl)-6-oxotetrazinium cation

2.12a



A sample of 6-oxoverdazyl **2.11a** (0.40 g, 1.10 mmol) was added to a 20 mL glass vial equipped with a stir bar and dissolved in 3 mL of MeCN. An MeCN (5 mL) solution of NOBF₄ (0.13 g, 1.1 mmol) was then added drop wise to the reaction mixture over 5 min. During the reaction, the mixture changed from dark red to dark purple and the evolution of NO_(g) was observed. The reaction mixture stirred at 20 °C for 30 min and then concentrated *in vacuo*. The resulting purple powder was washed with Et₂O (3 × 10 mL) and then concentrated affording tetrazinium cation **2.12a** as a dark purple solid. Yield: 0.47 g, 96%; ¹H NMR (400.1 MHz, CDCl₃): δ 7.97 (br s, 2H, aryl CH), 7.20 (br s, 3H, aryl CH), 5.23 (br s, 2H, (CH₃)₂CH), 1.52 (br s, 12H, CH₃), 1.38 (s, 9H, CH₃); ¹⁹F NMR (376.1 MHz, CDCl₃): δ -153.4; ¹¹B NMR (128.3 MHz, CDCl₃): δ -2.1. FT-IR (ranked intensity), KBr pellet: 657(4), 789(9), 899(5), 1118(1), 1209(10), 1277(8), 1402(3), CO tetrazinium cation 1605(7), CO ester 1751(2), 2975(6) cm⁻¹. UV-vis (CH₂Cl₂): λ_{max} 287 nm (ε = 21,400 M⁻¹ cm⁻¹), 355 nm (ε = 3,100 M⁻¹ cm⁻¹), 530 nm (ε = 1,600 M⁻¹ cm⁻¹). Mass Spec. (EI, +ve mode): exact mass calculated for C₁₉H₂₇N₄O₃: 359.2083; exact mass found: 359.2074; difference: -2.5 ppm. Anal. Calcd. (%) for C₁₉H₂₇B₁F₄N₄O₃: C, 51.14; H, 6.10; N, 12.56. Found: C, 50.15; H, 6.20; N, 12.78.

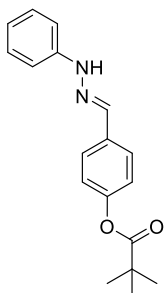
Synthesis of 1,5-di-isopropyl-3-phenyl-6-oxotetrazinium cation 2.12c



A sample of 6-oxoverdazyl **2.11c** (0.30 g, 1.14 mmol) was added to a 20 mL glass vial equipped with a stir bar and dissolved in 3 mL of MeCN. An MeCN (5 mL) solution of NOBF₄ (0.13 g, 1.1 mmol) was then added drop wise to the reaction mixture over 5 min. During the reaction, the mixture changed from dark red to dark purple and the evolution of NO_(g) was observed. The reaction mixture stirred at 20 °C for 30 min and then concentrated under reduced pressure. The resulting bright orange powder was washed with Et₂O (3 × 10 mL) and then concentrated affording tetrazinium cation **2.12c** as a bright orange/red powder. Yield: 0.32 g, 79%; ¹H NMR (400.1 MHz, CD₃CN, 40 °C): δ 8.22 (br s, 2H, aryl CH), 7.76 (br s, 3H, aryl CH),

5.41 (br s, 2H, $(\text{CH}_3)_2\text{CH}$), 1.62 (br s, 12H, CH_3); ^{19}F NMR (376.1 MHz, CD_3CN , -40°C): δ 151.3; ^{11}B NMR (128.3 MHz, CD_3CN , 40°C): δ 1.4. FT-IR (ranked intensities), KBr pellet: 659(8), 692(5), 782(4), 900(9), 1037(1), 1276(6), 1400(3), CO tetrazinium 1603(10), 751(2), 998(7) cm^{-1} . UV-vis (CH_2Cl_2): λ_{max} 280 nm ($\epsilon = 14,700 \text{ M}^{-1} \text{ cm}^{-1}$), 350 nm ($\epsilon = 1,900 \text{ M}^{-1} \text{ cm}^{-1}$), 510 nm ($\epsilon = 1,600 \text{ M}^{-1} \text{ cm}^{-1}$). Mass Spec. (EI, +ve mode): exact mass calculated for $\text{C}_{14}\text{H}_{10}\text{N}_4\text{O}_1$: 259.1559 exact mass found: 259.1562; difference: +1.15 ppm. Anal. Calcd. (%) for $\text{C}_{14}\text{H}_{19}\text{B}_1\text{F}_4\text{N}_4\text{O}_1$: C, 48.58; H, 5.53; N, 16.19. Found: C, 48.65; H, 5.65; N, 16.19.

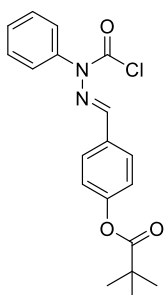
Synthesis of 4-pivaloylbenzaldehyde phenylhydrazone **2.13**



The preparation was adapted from a procedure by Milcent and co-workers.⁴² To a solution of 4-formylphenyl pivalate (3.00 g, 14.6 mmol) in EtOH (50 mL) was added phenylhydrazine (1.72 mL, 18 g, 17.5 mmol). A yellow precipitate quickly formed, and was left to stir for 1 h. The solution was poured into ice-cold water (200 mL). The grey precipitate was filtered before it was recrystallized in 2-propanol to give **2.13** as an off-white solid.

Yield = 2.34 g, 54 %. ^1H NMR (399.8 MHz, d_6 -DMSO): δ 10.36 (s, 1H, NH), 7.89 (s, 1H, N=CH), 7.69 (d, 2H, $^3J_{\text{HH}} = 8.6 \text{ Hz}$, aryl CH), 7.23 (m, 2H, aryl CH), 7.10 (m, 2H, aryl CH), 6.76 (t, 1H, $^3J_{\text{HH}} = 7$, aryl CH), 1.31 (s, 9H, CH_3). $^{13}\text{C}\{^1\text{H}\}$ NMR (100.5 MHz, d_6 -DMSO): δ 176.3, 150.3, 145.2, 135.5, 135.5, 133.5, 129.1, 126.5, 126.4, 121.9, 118.7, 112.0, 38.5, 26.8, 26.7. Three extra signals were present in the ^{13}C NMR due to restricted rotation of phenylpivalate moiety. Mass Spec. (EI, +ve mode): exact mass calculated for $\text{C}_{18}\text{H}_{20}\text{N}_2\text{O}_2$: 296.1525; exact mass found: 296.1531; difference: +2.03 ppm.

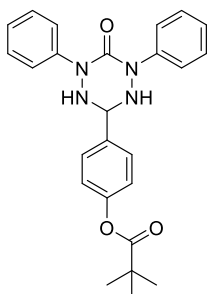
4-pivaloylbenzaldehyde α -chloroformylphenylhydrazone **2.14**



This procedure was adapted from a preparation by Milcent and co-workers.⁴² To a cooled solution of phosgene (4.17 mL, 6.33 mmol, 15 wt % in toluene) was added dropwise phenylhydrazone **2.13** (1.50 g, 5.06 mmol) that was dissolved in minimum amount of dry EtOAc/benzene (1:1, 20 mL) with distilled pyridine (0.45 mL, 0.44 g, 5.6 mmol) under N_2 . Once the addition was complete, the pink mixture was heated to 60°C for 1 h. The

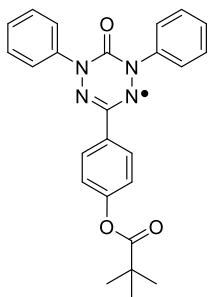
solvent was then removed *in vacuo*. The pink impurity was removed by a short silica column in CH₂Cl₂. The clear colourless oil was precipitated in EtOH, followed by recrystallization in EtOH to give **2.14** as a white solid. Yield = 1.53 g, 84%. ¹H NMR (399.8 MHz, CDCl₃): δ 7.67 (d, 2H, ³J_{HH} = 9 Hz, aryl CH), 7.59 (m, 3H, aryl CH), 7.33 (s, 1H, N=CH), 7.28 (d, 2H, ³J_{HH} = 7.43 Hz, aryl CH), 7.09 (d, 2H, ³J_{HH} = 9 Hz, aryl CH), 1.36 (s, 9H, (CH₃)₃). ¹³C{¹H} NMR (100.6 MHz, CDCl₃): δ 176.6, 153.0, 144.9 (bs, COCl), 136.1, 130.7, 130.5, 130.2, 128.9, 122.0, 39.1, 27.0. Note: The ¹³C NMR spectra were initially gathered in *d*₆-DMSO, which resulted in rapid decomposition of product. Therefore, CDCl₃ was used, but this caused broadening of several signals and certain signals could not be resolved. Mass Spec. (EI, +ve mode): exact mass calculated for C₁₉H₁₉ClN₂O₃: 358.1084; exact mass found: 358.1087; difference: +1.01 ppm.

1,5-diphenyl-3-(4-pivaloylphenyl)-6-oxotetrazane **2.10b**



To a stirred solution of phenylhydrazine (0.22 mL, 0.24 g, 2.2 mmol) in EtOH (10 mL) was added α-chloroformylphenylhydrazone **2.14** (0.40 g, 1.1 mmol), in small portions over 15 min. After the addition was complete, the solution was heated to 55 °C and left to stir for 1 h. The solution began clear and became opaque as precipitate formed. The warm mixture was poured into ice cold H₂O (30 mL). The off-white precipitate was filtered, dried *in vacuo* overnight and recrystallized in *n*-PrOH to give **2.10b** as a white powder. Yield = 0.39 g, 80%. ¹H NMR (399.8 MHz, *d*₆-DMSO): δ 7.66 (d, 4H, ³J_{HH} = 8 Hz, aryl CH), 7.62 (d, 2H, ³J_{HH} = 8 Hz, aryl CH), 7.34 (t, 4H, ³J_{HH} = 7 Hz, aryl CH), 7.10 (m, 4H, aryl CH), 6.33 (d, 2H, ³J_{HH} = 9 Hz, NH), 5.43 (t, 1H, ³J_{HH} = 9 Hz, CH), 1.33 (s, 9H, CH₃). ¹³C{¹H} NMR (100.5 MHz, *d*₆-DMSO): δ 176.1, 156.4, 150.5, 142.7, 134.9, 128.0, 127.8, 123.1, 121.3, 121.1, 72.1, 38.3, 26.6. FT-IR (ranked intensity), KBr pellet: 692(7), 742(10), 757(11), 899(13), 918(12), 1118(1), 1165(4), 1310(8), 1200(9), 1373(3), 1500(5), CO tetrazane 1628(2), CO ester 1751(6), NH tetrazane 3241(14) cm⁻¹. Mass Spec. (EI, +ve mode): exact mass calculated for C₂₅H₂₆N₄O₃: 430.2005; exact mass found: 430.2011; difference: +1.39 ppm. Anal. Calcd. (%) for C₂₅H₂₆N₄O₃: C, 69.75; H, 6.09; N, 13.01. Found: C, 69.41; H, 6.21; N, 12.93.

1,5-diphenyl-3-(4-pivaloylphenyl)-6-oxoverdazyl **2.11b**

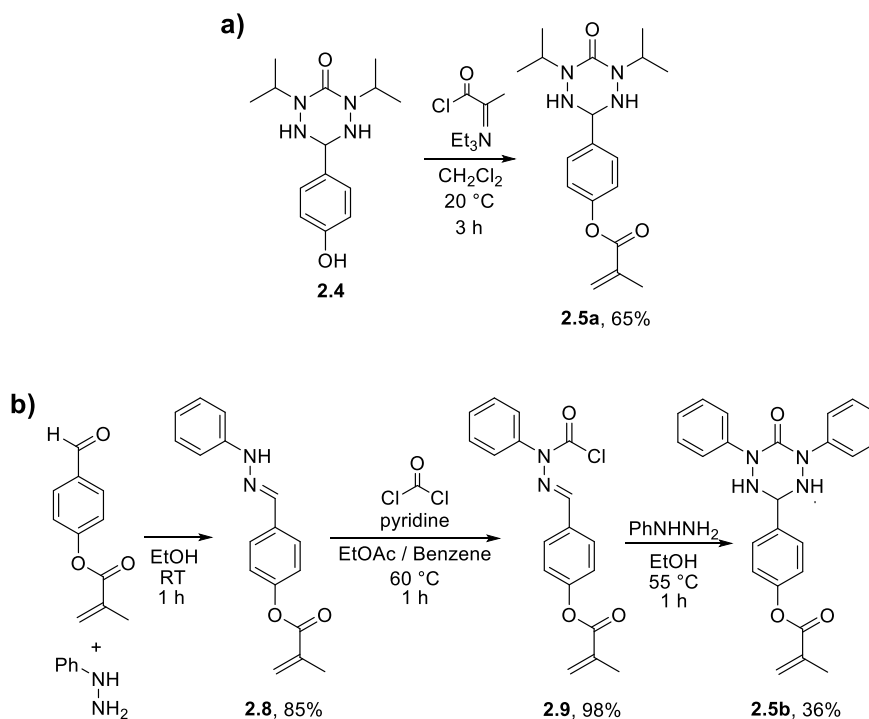


This procedure was adapted from a report published by Hicks and co-workers.²⁷ Celite (0.10 g) and Ag₂CO₃ (0.19 g) were combined in MeOH (10 mL) and allowed to stir for 10 min. 6-oxotetrazane **2.10b** (0.15 g, 0.35 mmol) was then added to the suspension and the mixture was left to stir for 16 h at room temperature. The solution turned a dark red colour and darkened as the reaction proceeded. To the mixture was added CH₂Cl₂ to dissolve the product and a gravity filtration was performed to remove Celite/Ag_(s). The solid was recrystallized in MeOH/H₂O (9:1) to give **2.11b** as a dark red solid. Yield = 1.40 g, 94%. FT-IR (ranked intensity) KBr pellet: 689 (1), 749 (9), 1113 (2), 1161 (6), 1201 (5), 1249 (8), 1485 (7), CO verdazyl 1702 (3), CO ester 1746 (4), 2974 (10) cm⁻¹. UV-vis (CH₂Cl₂): λ_{max}: 563 nm (ε = 2,000 M⁻¹·cm⁻¹), 317 nm (ε = 11,800 M⁻¹·cm⁻¹), 258 nm (ε = 24,700 M⁻¹·cm⁻¹). Mass Spec. (EI, +ve mode): exact mass calculated for C₂₅H₂₃N₄O₃: 427.1770; exact mass found: 427.1757; difference: -3.00 ppm. Anal. Calcd. (%) for C₂₅H₂₃N₄O₃: C, 70.24; H, 5.42; N, 13.11. Found: C, 70.24; H, 5.46; N, 13.00.

2.3 Results and Discussion

2.3.1 Synthesis of Monomers

The synthesis towards **2.5a** involved the addition of a polymerizable methacrylate group using methacryloyl chloride to a previously reported *i*Pr-tetrazane compound (**2.4**) functionalized with an alcohol group. This reaction yielded compound **2.5a** in 65% yield (Scheme 2.1). The synthesis of phenyl-substituted monomer **2.5b** was synthetically more demanding (Scheme 2.1). The condensation of phenylhydrazine with 4-formylphenyl methacrylate afforded hydrazone **2.8** in 85% yield. The subsequent installation of a chloroformyl functionality to the α-nitrogen of the hydrazone with phosgene afforded compound **2.9** in 98% yield. The introduction of a second equivalent of phenylhydrazine produced monomer **2.5b** in 36% yield. The low yield in the final step of the monomer synthesis was due to the direct filtration of the precipitate formed during the reaction, which afforded very pure monomer that did not require further purification.

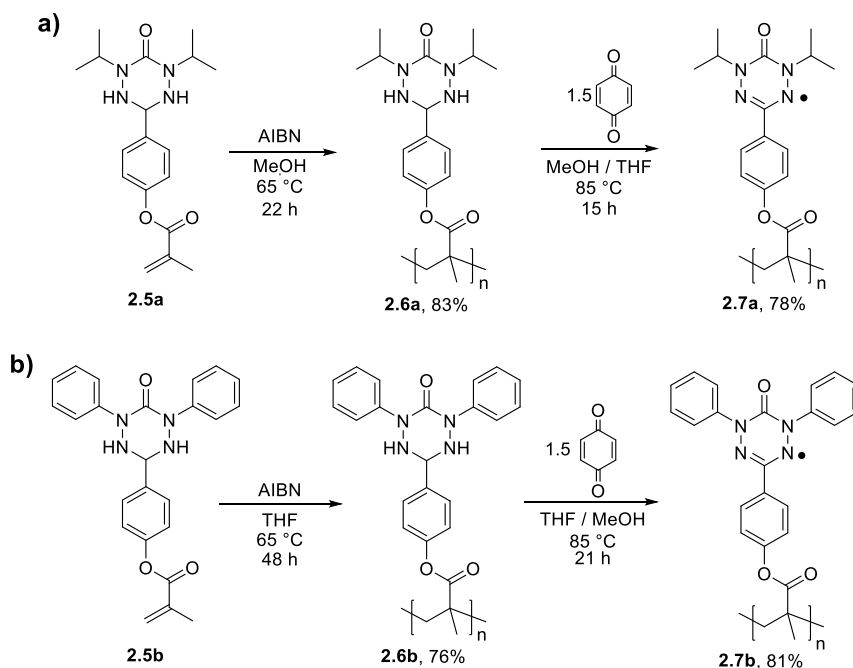


Scheme 2.1 (a) Synthesis of monomer **2.5a** and (b) synthesis of monomer **2.5b**.

The ^1H and $^{13}\text{C}\{^1\text{H}\}$ NMR spectra of compounds **2.5a** and **b** are shown in Figures 1, A2.1–2.2. d_6 -DMSO was used as it allowed for better resolution of the splitting patterns resulting from the coupling of protons in these molecules.

2.3.2 Polymerization

The polymerization method employed in this study (Scheme 2.2) began with the free radical polymerization of phenyl methacrylate-substituted tetrazanes **2.5a,b**, which afforded tetrazane polymers **2.6a,b** as white powders in 83% and 76% yield, respectively. Oxidation of tetrazane polymers **2.6a,b** with *p*-benzoquinone gave 6-oxoverdazyl polymers **2.7a,b** in 78% and 81% yield after purification by column chromatography and repeated precipitation. A summary of characterization data for polymers **2.6a,b** and **2.7a,b** can be found in Table 2.2 and additional details can be found in the supplementary information (Figures A2.4–2.12).



Scheme 2.2 (a) Synthesis of polymers **2.6a,b** and (b) verdazyl radicals polymers **2.7a,b**.

Characterization of polymer **2.6b** was carried out in the solution phase by NMR spectroscopy. The chemical shifts present in the ^1H NMR of **2.5b** (Figure 2.1a), clearly show aromatic CH signals at 7.61, 7.34, 7.16, and 7.08 ppm. The methacrylate vinyl signals were observed at 6.27 and 5.90 ppm. The signals for NH and CH are present at 6.43 and 5.43 ppm as a doublet and triplet, respectively (Figure 2.1). The coupling between NH and CH protons can be attributed to hydrogen bonding of the amine proton with the carbonyl present in dimethyl sulfoxide.

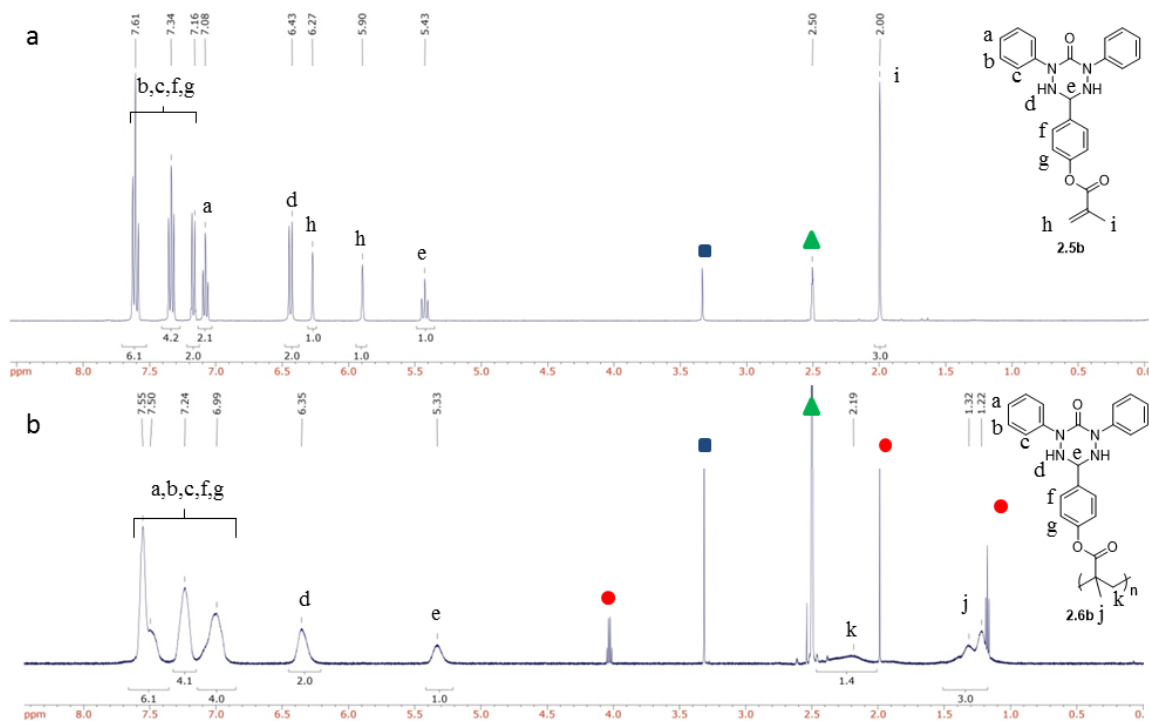


Figure 2.1 ^1H NMR spectra of (a) monomer **2.5b** and (b) polymer **2.6b**. The squares indicate H_2O signals, circles indicate EtOAc, and triangles indicate residual DMSO.

Tetrazane polymer **2.6b** shows broadened NMR signals (Figure 2.1b). The aromatic signals at 7.55, 7.50, 7.24, and 6.99 ppm generally shifted upfield due to the increased shielding from the polymeric system. The NH and CH signals are present at 6.35 and 5.22 ppm, respectively. The most diagnostic signals are the methacrylate vinyl signals at 6.27 and 5.90 ppm which disappear upon successful polymerization and the appearance of signals in the alkyl proton region at 2.19, 5.32, and 5.22 ppm, which are indicative of the saturated hydrocarbon polymer backbone.

2.3.3 Macromolecular Properties

The polymers presented herein, including tetrazane polymers **2.6a,b** and 6-oxoverdazyl polymers **2.7a,b**, all exhibit drastically different solubility profiles. In general, the tetrazane polymers are soluble only in highly polar solvents while 6-oxoverdazyl polymers are soluble in a wide range of solvents. We were unable to obtain reproducible GPC data for our polymers in THF, due to poor solubility of tetrazane polymers **2.6a,b**. However, we were able to obtain reproducible GPC data for all of our polymers in DMF containing 10

mM LiBr and 1 % (v/v) Et₃N at 85 °C using conventional calibration for the determination of molecular weight distributions (Table 2.2). Tetrazane polymer **2.6a** and 6-oxoverdazyl polymer **2.7a** gave rise to very similar GPC traces (Figure 2.2a). Tetrazane polymer **2.6b** and 6-oxoverdazyl polymer **2.7b** did not behave in the same way (Figure 2.2b).

Table 2.2 Polymer characterization data.

	M _n (g mol ⁻¹) ^a	<i>D</i> ^a	T _g (°C)	Onset of Decomposition (°C) ^b
2.6a	25,250	1.83	204	288
2.7a	25,750	1.89	203	188
2.6b	20,300	1.48	180	246
2.7b	12,000	1.46	174	236

^aConventional calibration GPC vs. polystyrene standards in DMF (10 mM LiBr and 1% (v/v) NEt₃) at 85°C. See supplementary information for additional discussion of GPC experiments. ^bCalculated at 2 % mass loss.

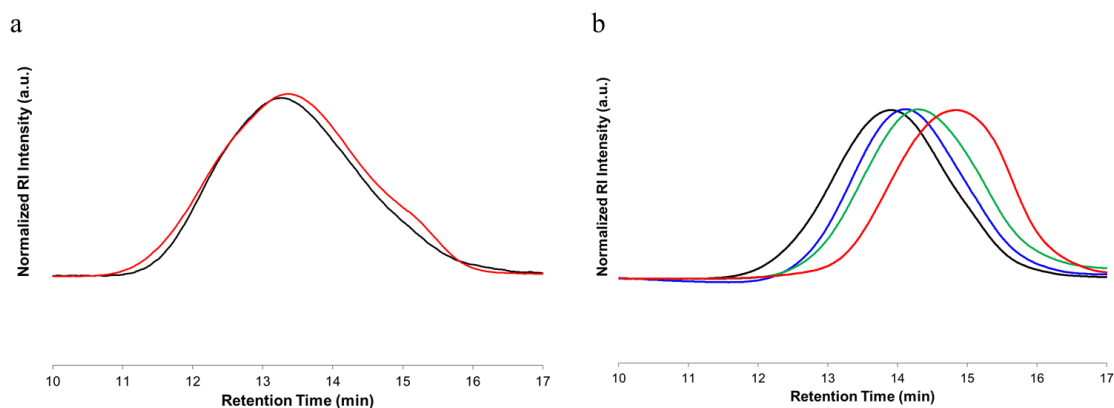


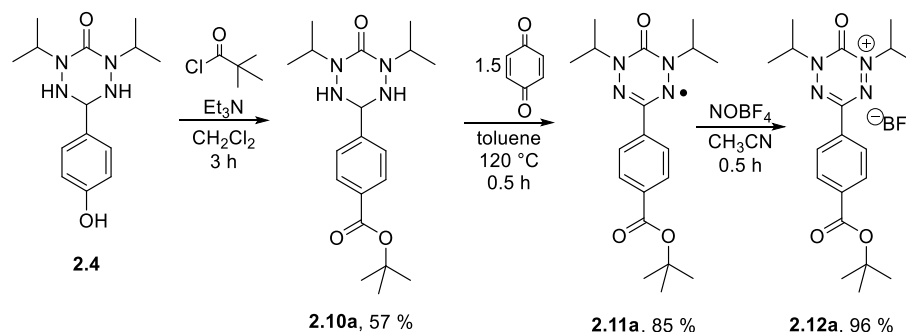
Figure 2.2 Normalized GPC traces recorded in DMF containing 10 mM LiBr and 1 % (v/v) triethylamine at 85 °C for (a) tetrazane polymer **2.6a** (black) and 6-oxoverdazyl polymer **2.7a** (red), and (b) for tetrazane polymer **2.6b** (black), tetrazane polymer **2.6b** after air oxidation for 24 h (blue), tetrazane polymer **2.6b** after air oxidation for 48h (green), and 6-oxoverdazyl polymer **2.7b** (red).

We initially suspected that the chemical oxidation of tetrazane polymer **2.6b** using *p*-benzoquinone as an oxidant in refluxing THF/MeOH may have resulted in chain scission. However, upon closer inspection of the distributions observed for **2.6b** and **2.7b**, we hypothesized that it was highly unlikely that chain scission had occurred based on the

remarkably similar shape and width of the distributions ($\mathcal{D} = 1.48$ for **2.6b**, $\mathcal{D} = 1.46$ for **2.7b**). To further probe this hypothesis, we allowed the GPC solution used for the analysis of **2.6b** to stand in air to partially oxidize. The sample, which becomes a random tetrazane/6-oxoverdazyl copolymer upon partial oxidation, was analyzed after 24 h and after 48 h of air exposure (Figure 2.2). As the radical content in the polymer increased with time, the centre of the GPC distributions shifted to longer retention times and the shape and width of the distributions did not change significantly ($\mathcal{D} = 1.40$ for **2.6b** after 24 h in air, $\mathcal{D} = 1.50$ for **2.6b** after 48h in air). The shape and width of the GPC traces obtained for 6-oxoverdazyl polymer **2.7b** after standing in air did not change. In our opinion, the difference in molecular weights observed for tetrazane polymer **2.6b** and 6-oxoverdazyl polymer **2.7b** arises due to limitations associated with the comparison of polymers with substantially different solubility profiles using conventional calibration GPC. It is likely that each of our polymers interact very differently with the solvent system and size-exclusion columns employed, and that their properties match those of the polystyrene standards employed to different extents [specifically the relationship between molecular weight and radius of gyration (R_g) in the solvent system employed].

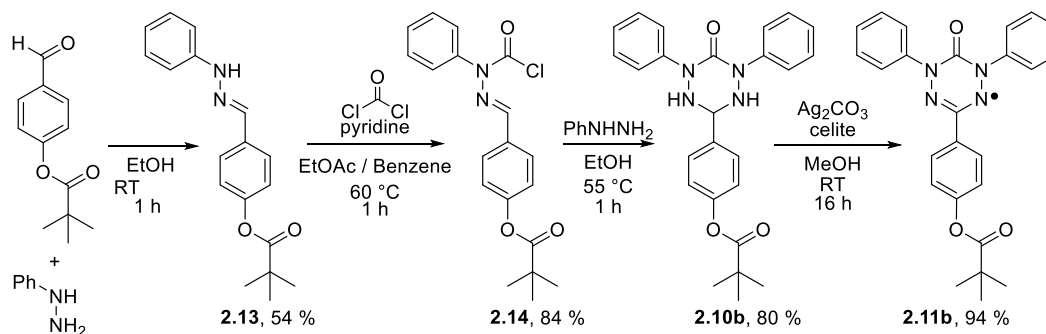
2.3.4 Synthesis of Model Compounds

Model compound **2.11a** and the corresponding oxoammonium cation **2.12a** were synthesized using a method similar to that of the monomer and polymer (Scheme 2.3). Compound **2.4** was treated with pivaloyl chloride in the presence of Et_3N to afford **2.10a** in 57% yield. From there, **2.10a** was oxidized using 1.5 equiv. of benzoquinone to give **2.11a** in 85% yield. Verdazyl radical **2.11a** was further oxidized using NOBF_4 in MeCN to afford oxoammonium cation **2.12a** in 96% yield, which was further investigated by X-ray crystallography (discussed later).



Scheme 2.3 Synthesis of *i*Pr-substituted model compounds **2.11a** and **2.12a**.

In order to synthesize model compound **2.11b**, pivalate benzaldehyde was synthesized and used in a condensation reaction with phenyl hydrazine to give hydrazone **2.13**, in 54% yield. Hydrazone **2.13** was treated with phosgene to give α -chloroformyl hydrazone **2.14** in 84% yield, followed by treatment with phenylhydrazine to give tetrazane **2.10b** in 80% yield. Once the tetrazane compound was synthesized, oxidation using Fetizon's reagent afforded pivalate substituted triphenyl-6-oxoverdazyl radical **2.11b** in 94% yield (Scheme 2.4). NMR data for compounds **2.10a,b** can be found in Figures A2.19–2.22.



Scheme 2.4 Synthesis of phenyl-substituted model compound **2.11b**.

2.3.5 Spectroscopic Characterization

The IR spectra of tetrazanes and 6-oxoverdazyls were found to be highly diagnostic (Figure 2.3, A2.13–2.16). In each case the spectra of the model compounds were in very close agreement with those collected for the corresponding polymers (Figure 2.3). Further comparison of the IR spectra qualitatively confirmed the complete conversion of tetrazane

polymers **2.6a,b** to 6-oxoverdazyl polymers **2.7a,b** as the NH stretches of **2.6a,b** disappeared completely and CO stretches shifted to higher energies (Figure 2.3).

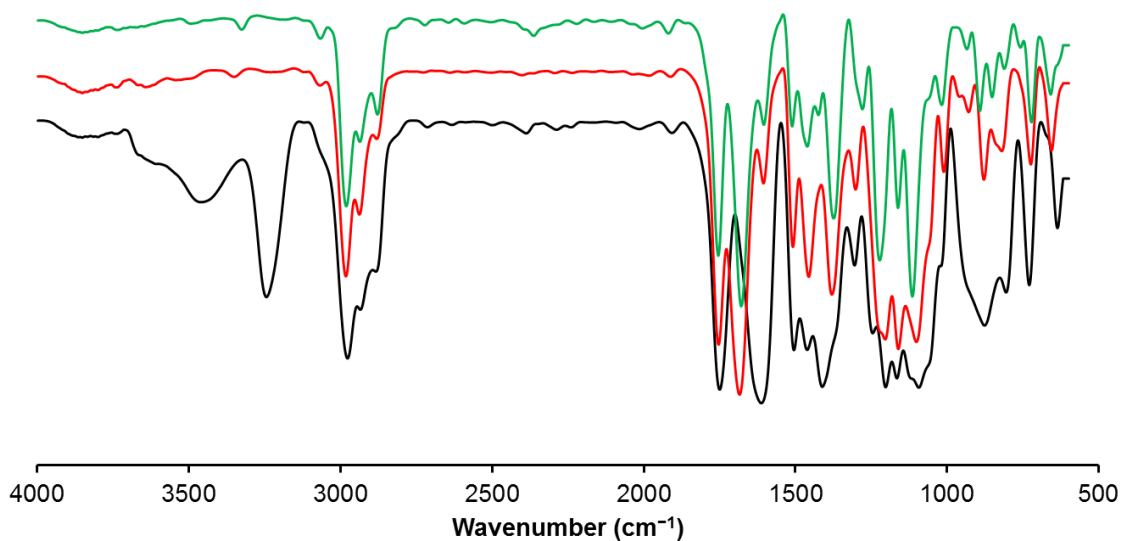


Figure 2.3 IR spectra for tetrazane polymer **2.6a** (black), verdazyl polymer **2.7a** (red), and verdazyl model compound **2.11a** (green). The baselines are offset for ease of comparison.

The radical content within the verdazyl polymer backbones was studied qualitatively using electron paramagnetic resonance (EPR) spectroscopy. Broad, isotropic signals were observed for radical polymers **2.7a,b** ($g = 2.0050$ and 2.0043) and complex signals were observed for model 6-oxoverdazyl radicals **2.11a,b** ($g = 2.0043$ and 2.0038) (Figures 2.4, A2.17-2.18). Broadening of the EPR spectra obtained for polymers **2.7a,b** is consistent with their proposed structures and macromolecular nature.

Quantitative analysis of the radical content in 6-oxoverdazyl polymers **2.7a,b** was performed using UV-vis absorption spectroscopy. The complex spectra obtained were in close agreement with model compounds **2.11a,b** indicating that $> 95\%$ of the repeating units within the polymer backbone contain a pendant radical unit (Figures 2.5, A2.23). To illustrate this point, the UV-vis absorption spectra of compounds **2.7b** and **2.11b** are compared in Figure 2.5, with the inset that shows the absorbances at 566 and 563 nm, respectively. The excitations at ca. 566 nm are the transitions of the radical species from the SOMO to the HOMO and the LUMO to the SOMO. The overlap of the absorptions in

these spectra suggest that there was an efficient conversion of the tetrazane polymer to the verdazyl radical polymer upon oxidation.

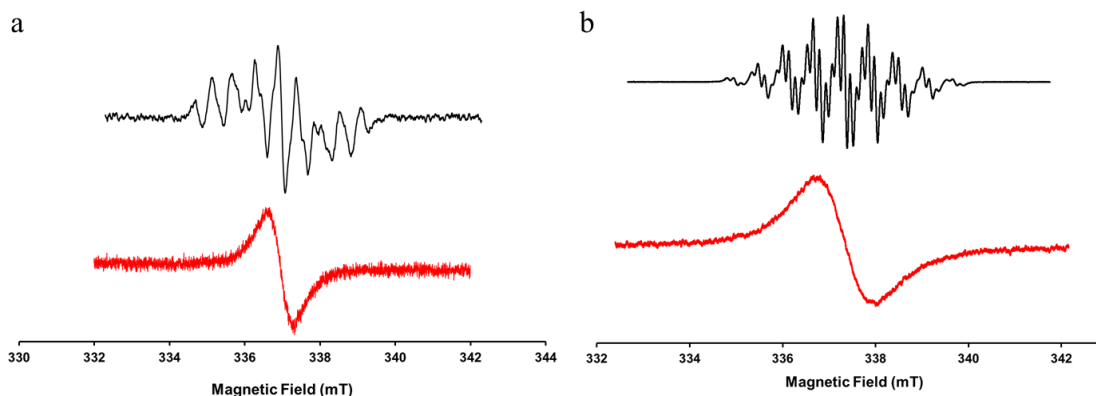


Figure 2.4 EPR spectra of (a) 6-oxoverdazyl **2.11a** ($g = 2.0043$, black) and 6-oxoverdazyl polymer **2.7a** ($g = 2.0050$, red) and (b) triaryl-6-oxoverdazyl **2.11b** ($g = 2.0038$, black) and triaryl-6-oxoverdazyl polymer **2.7b** ($g = 2.0043$, red) in CH_2Cl_2 . (See Figures A17,18 for simulation of the spectrum of **2.11a,b**).

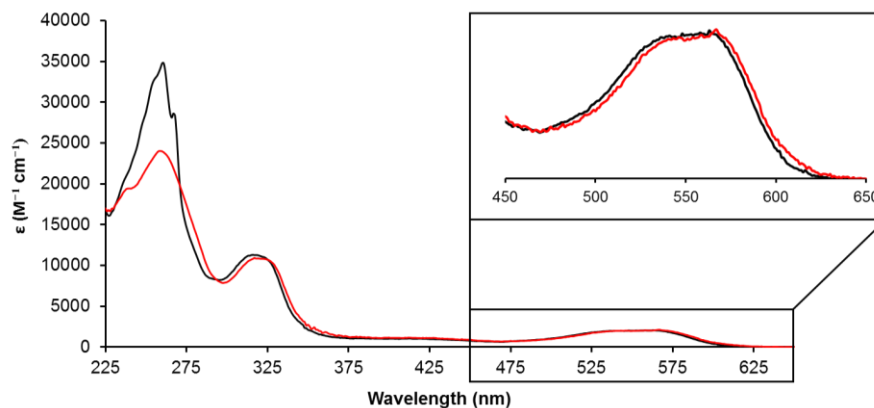


Figure 2.5 UV-vis absorption spectrum of 6-oxoverdazyl **2.7b** (red) and model **2.11b** (black).

2.3.6 Electrochemical Properties

The electrochemical properties of 6-oxoverdazyl polymer **2.7a,b** and the model 6-oxoverdazyls **2.11a,b** were studied using cyclic voltammetry in THF (Figure 2.6 and Table 2.3). Consistent with reports of similar compounds,²⁷ 6-oxoverdazyls **2.11a,b** were reversibly oxidized and reduced (one electron each). Polymers **2.7a,b** exhibited *pseudo*

reversible oxidation and reduction waves under similar conditions. It should be noted that, as a result of the loss of control associated with the slow diffusion of polymers in solution, sharp, asymmetric responses were observed in the CVs of **2.7a,b**. We were unable to study the thin film electrochemistry of 6-oxoverdazyl polymers **2.7a,b** due to our inability to find a common solvent for the neutral and charged forms of the polymers. Crucially, switching from *N*-isopropyl to *N*-phenyl substituents causes a shift in the half wave oxidation (E_{ox}°) and reduction (E_{red}°) potentials by 220 mV and 530 mV, respectively. Although the redox properties of verdazyl polymers **2.7a,b** are very similar to those of the model complexes studied, the incorporation of the radicals into polymers will allow them to be used in applications where film-forming properties are essential.

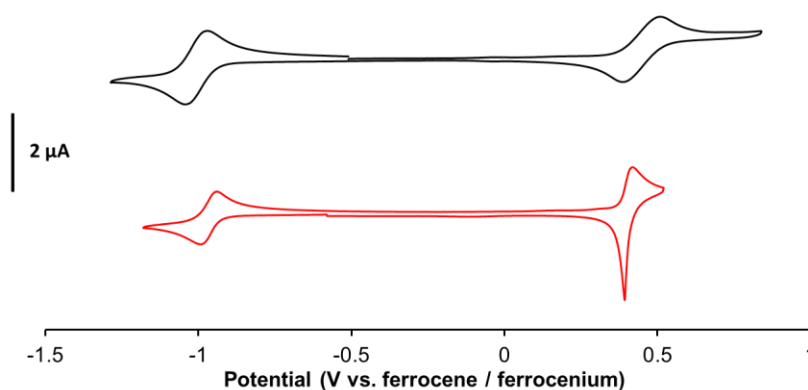


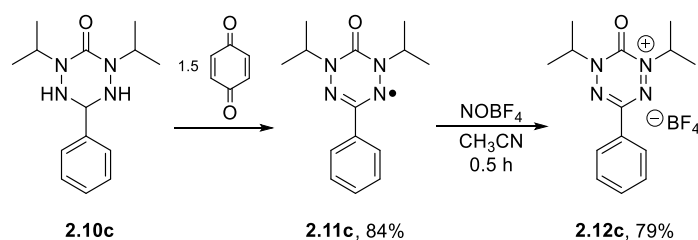
Figure 2.6 Cyclic voltammograms of 6-oxoverdazyl polymer **2.7b** (red) and model 6-oxoverdazyl **2.11b** (black) recorded at scan rate 100 mV s^{-1} in THF solutions of 1 mM analyte and 0.1 M $n\text{Bu}_4\text{NPF}_6$.

Table 2.3 Electrochemical data for verdazyl polymers **2.7a,b** and verdazyl radicals **2.11a,b**.

Compound	E_{ox}° (V vs. Fc/Fc ⁺)	E_{red}° (V vs. Fc/Fc ⁺)
2.7a	0.17	-1.50
2.11a	0.20	-1.49
2.7b	0.39	-0.97
2.11b	0.38	-1.01

2.3.7 Solid-State Behaviour

The ability of stable radical polymers to undergo redox reactions without significant structural change is advantageous for their use in organic electronics where changes in volume accompanying electron transfer are highly undesirable. In order to study potential structural changes accompanying oxidation, we chemically oxidized 6-oxoverdazyls **2.11a,c** with NOBF₄ (Scheme 2.5). Oxidation resulted in a red-shift in the wavelength of their maximum absorption (*e.g.*, from $\lambda_{\text{max}} = 414$ nm in **2.11c** to $\lambda_{\text{max}} = 510$ nm for **2.12c**) (Figures S2.24–2.27). The crude residues were washed with Et₂O to afford analytically pure samples of **2.12a,c**, which exhibited qualitatively similar electrochemical behavior to the corresponding neutral radicals (Figures A2.28, A2.29), in 96% and 79% yield. Attempts to chemically reduce 6-oxoverdazyls **2.11a,c** using Na/15-crown-5 and decamethylcobaltocene in an inert atmosphere glovebox (< 1 ppm O₂/H₂O) reproducibly resulted in decomposition of the verdazyl framework.



Scheme 2.5 Synthesis and oxidation of 6-oxoverdazyl radical **2.11c**.

The solid-state structures of 6-oxoverdazyls **2.11a**, **2.11c** and tetrazinium cation **2.12c** were determined by single crystal X-ray diffraction (Table 2.4, Figure 2.7Figure 2.8). Once synthesized, recrystallization was performed in order to produce crystals suitable to X-ray diffraction. In the solid-state structures of **2.11c** and **2.12c**, the N1-N2-C1-N4-N3-C2 heterocycle is planar, and twisted with respect to the phenyl substituents by 21.5° and 24.7°, respectively. Despite these similarities, a shortening of the N-N bonds in the nitrogen-rich heterocycle was observed upon oxidation. The average N-N bond distance decreases from 1.369(2) Å in **2.11c** to 1.299(2) Å in **2.12c**, while the average C-N bond lengths increased slightly upon removal of an electron from the antibonding singly

occupied molecular orbital (π -SOMO) of 6-oxoverdazyl **2.11c**. The structural metrics of 6-oxoverdazyl **2.11a** were found to be very similar to those of **2.11c**. The reversible nature of the electrochemical oxidation of 6-oxoverdazyl polymers **2.7a** and **2.7b** along with the structural similarities of model compounds **2.11c** and **2.12c** further illustrates the potential utility of the polymers produced in this study for use as redox-active materials for organic electronics.

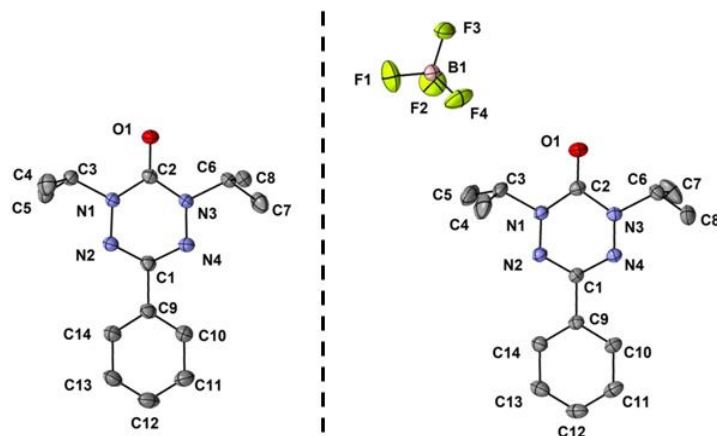


Figure 2.7 Solid-state structures of 6-oxoverdazyl **2.11c** (left) and tetrazinium cation **2.12c** (right). Anisotropic displacement ellipsoids are shown at 50% probability level. Hydrogen atoms have been omitted for clarity.

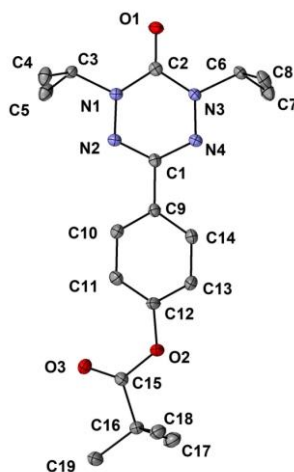


Figure 2.8 Solid-state structure of **2.11a**. Anisotropic displacement ellipsoids are shown at 50 % probability level. Hydrogen atoms have been omitted for clarity.

Table 2.4 Selected bond lengths (Å) and angles (°) for 6-oxoverdazyl **2.11a,c** and cation **2.12c**.

Bonds and Angles	2.11a	2.11c	2.12c
N1-N2, N3-N4	1.365(1), 1.368(1)	1.372(2), 1.366(2)	1.307(2), 1.291(2)
C1-N2, C1-N4	1.333(1), 1.331(1)	1.327(2), 1.334(2)	1.340(2), 1.344(2)
N1-C2, N3-C2	1.379(1), 1.379(1)	1.381(2), 1.372(2)	1.398(2), 1.414(2)
N1-N2-C1, N3-N4-C1	115.11(8), 115.24(7)	115.0(1), 115.1(1)	117.4(1), 117.7(1)
N2-C1-N4	126.66(8)	126.9(2)	123.2(1)
N2-C2-N3	113.74(8)	114.1(1)	111.4(1)

2.3.8 Thin-Film Studies

Kelvin probe force microscopy (KPFM),⁴³ a scanning probe technique able to image the work function (*i.e.*, the energy of the highest occupied molecular orbital) of materials at the nanoscale was employed in order to study thin films of 6-oxoverdazyl polymer **2.7a**. In this context, the KPFM measurements provided an estimate of the energy (relative to ITO, work function: 4.7 eV⁴⁰) of the π -SOMO of the 6-oxoverdazyl polymer studied. A 166 ± 10 nm thick film of **2.7a** was spin coated onto ITO glass from a 15 mg mL⁻¹ solution in chlorobenzene. The topography image shown in Figure 2.9 revealed a very smooth and uniform layer of polymer **2.7a** on ITO. The KPFM image of the polymer film (Figure 2.9) is also very uniform, suggesting the presence of few defects, and corroborating a very high radical content of polymer **2.7a**. The work function of the π -SOMO orbital was measured to be 4.9 ± 0.1 eV, which corresponds to an oxidation potential of *ca.* 0.20 V against ferrocene, which has a work function of 5.1 eV.⁴⁴ This number agrees well with the solution-phase electrochemical data collected for 6-oxoverdazyl polymer **2.7a** and 6-oxoverdazyl radical **2.11a**.

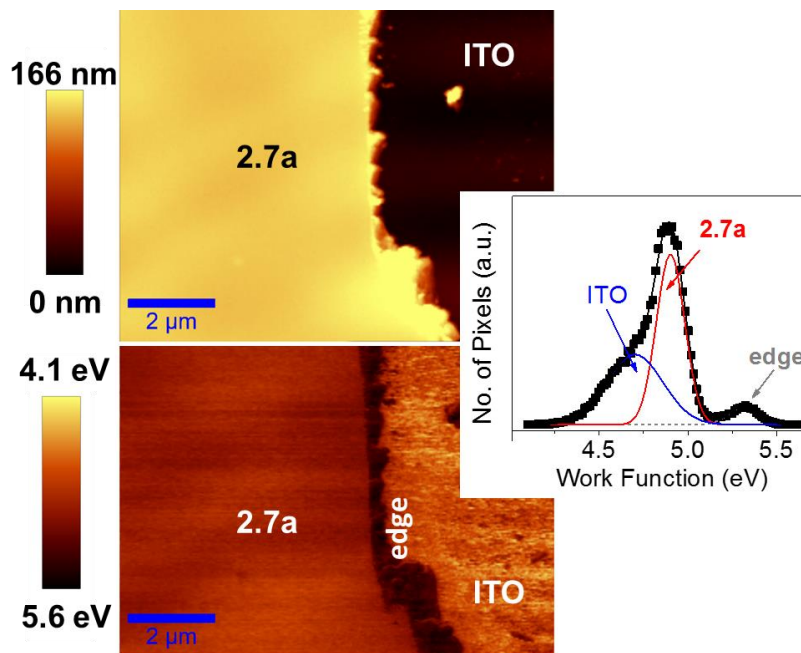


Figure 2.9 AFM topography (top) and KPFM image (bottom) of 6-oxoverdazyl polymer **2.7a** referenced to ITO (work function: 4.7 eV⁴⁰). The inset is a histogram of the KPFM image showing a work function of 4.9 ± 0.1 eV for **2.7a**. The small peak on the right is a KPFM artifact due to lateral contact of the tip with the film edge.

2.4 Conclusion

Two distinct synthetic routes were described in this chapter that have allowed for the first examples of alkyl- and aryl-6-oxotetrazene and -oxoverdazyl polymers to be realized. The polymers exhibited substituent-dependent, tunable, and reversible oxidation and reduction in solution and their oxidation was also studied in thin films using KPFM, confirming that the redox properties of the 6-oxoverdazyl polymers were retained. Structural characterization of model compounds further demonstrated the potential of 6-oxoverdazyl polymers as functional redox-active materials as several structural features, including planarity, of the neutral radical were retained upon oxidation. Future work in this area will aim to exploit the structural versatility of the 6-oxoverdazyl scaffold and to evaluate the utility of the polymers reported as functional redox-active thin films.

2.5 References

1. Gomberg, M. *J. Am. Chem. Soc.* **1900**, *22*, 757–771.
2. Hicks, R. G. *Org. Biomol. Chem.* **2007**, *5*, 1321–1338.
3. *Stable Radicals: Fundamentals and Applied Aspects of Odd-Electron Compounds*. John Wiley & Sons Ltd: Chichester, UK, 2010; p 588.
4. Chae, I. S.; Koyano, M.; Sukegawa, T.; Oyaizu, K.; Nishide, H. *J. Mater. Chem.* **2013**, *1*, 9608–9611.
5. Saito, K.; Hirose, K.; Okayasu, T.; Nishide, H.; Hearn, M. T. W. *RSC Adv.* **2013**, *3*, 9752–9756.
6. Rajca, A.; Wongsriratanakul, J.; Rajca, S. *Science* **2001**, *294*, 1503–1505.
7. Rostro, L.; Baradwaj, A. G.; Boudouris, B. W. *ACS Appl. Mater. Interfaces* **2013**, *5*, 9896–9901.
8. Kunz, T. K.; Wolf, M. O. *Polym. Chem.* **2011**, *2*, 640–644.
9. Choi, W.; Ohtani, S.; Oyaizu, K.; Nishide, H.; Geckeler, K. E. *Adv. Mater.* **2011**, *23*, 4440–4443.
10. Yonekuta, Y.; Susuki, K.; Oyaizu, K.; Honda, K.; Nishide, H. *J. Am. Chem. Soc.* **2007**, *129*, 14128–14129.
11. Oyaizu, K.; Nishide, H. *Adv. Mater.* **2009**, *21*, 2339–2344.
12. Janoschka, T.; Hager, M. D.; Schubert, U. S. *Adv. Mater.* **2012**, *24*, 6397–6409.
13. Suguro, M.; Iwasa, S.; Kusachi, Y.; Morioka, Y.; Nakahara, K. *Macromol. Rapid Commun.* **2007**, *28*, 1929–1933.
14. Bugnon, L.; Morton, C. J. H.; Novak, P.; Vetter, J.; Nesvadba, P. *Chem. Mater.* **2007**, *19*, 2910–2914.

15. Suga, T.; Sugita, S.; Ohshiro, H.; Oyaizu, K.; Nishide, H. *Adv. Mater.* **2011**, *23*, 751–754.
16. Hung, M.-K.; Wang, Y.-H.; Lin, C.-H.; Lin, H.-C.; Lee, J.-T. *J. Mater. Chem.* **2012**, *22*, 1570–1577.
17. Sukegawa, T.; Kai, A.; Oyaizu, K.; Nishide, H. *Macromolecules* **2013**, *46*, 1361–1367.
18. Chen, E. K. Y.; Teertstra, S. J.; Chan-Seng, D.; Otieno, P. O.; Hicks, R. G.; Georges, M. K. *Macromolecules* **2007**, *40*, 8609–8616.
19. Rayner, G.; Smith, T.; Barton, W.; Newton, M.; Deeth, R. J.; Prokes, I.; Clarkson, G. J.; Haddleton, D. M. *Polym. Chem.* **2012**, *3*, 2254–2260.
20. Koivisto, B. D.; Hicks, R. G. *Coord. Chem. Rev.* **2005**, *249*, 2612–2630.
21. Hicks, R. G.; Lemaire, M. T.; Thompson, L. K.; Barclay, T. M. *J. Am. Chem. Soc.* **2000**, *122*, 8077–8078.
22. Barclay, T. M.; Hicks, R. G.; Lemaire, M. T.; Thompson, L. K.; Xu, Z. *Chem. Commun.* **2002**, 1688–1689.
23. Norel, L.; Pointillart, F.; Train, C.; Chamoreau, L.-M.; Boubekeur, K.; Journaux, Y.; Brieger, A.; Brook, D. J. R. *Inorg. Chem.* **2008**, *47*, 2396–2403.
24. Brook, D. J. R.; Richardson, C. J.; Haller, B. C.; Hundley, M.; Yee, G. T. *Chem. Commun.* **2010**, *46*, 6590–6592.
25. Norel, L.; Chamoreau, L.-M.; Journaux, Y.; Oms, O.; Chastanet, G.; Train, C. *Chem. Commun.* **2009**, 2381–2383.
26. Jankowiak, A.; Pocięcha, D.; Szczytko, J.; Monobe, H.; Kaszyński, P. *J. Am. Chem. Soc.* **2012**, *134*, 2465–2468.

27. Gilroy, J. B.; McKinnon, S. D. J.; Koivisto, B. D.; Hicks, R. G. *Org. Lett.* **2007**, *9*, 4837–4840.
28. McKinnon, S. D. J.; Patrick, B. O.; Lever, A. B. P.; Hicks, R. G. *Chem. Commun.* **2010**, *46*, 773–775.
29. McKinnon, S. D. J.; Patrick, B. O.; Lever, A. B. P.; Hicks, R. G. *J. Am. Chem. Soc.* **2011**, *133*, 13587–13603.
30. Johnston, C. W.; McKinnon, S. D. J.; Parick, B. O.; Hicks, R. G. *Dalton Trans.* **2013**, *42*, 16829–16836.
31. Miura, Y.; Kinoshit.M; Imoto, M. *Makromol. Chem.* **1971**, *146*, 69–77.
32. Kamachi, M.; Enomoto, H.; Shibasaka, M.; Mori, W.; Kishita, M. *Polym. J.* **1986**, *18*, 439–441.
33. Bosch, J.; Rovira, C.; Veciana, J.; Castro, C.; Palacio, F. *Synth. Met.* **1993**, *55*, 1141–1146.
34. Lang, A.; Naarmann, H.; Rosler, G.; Gotschy, B.; Winter, H.; Dormann, E. *Mol. Phys.* **1993**, *79*, 1051–1062.
35. García-Acosta, B.; García, F.; García, J. M.; Martínez-Máñez, R.; Sancenón, F.; San-José, N.; Soto, J. *Org. Lett.* **2007**, *9*, 2429–2432.
36. Jiménez-González, L.; García-Muñoz, S.; Álvarez-Corral, M.; Muñoz-Dorado, M.; Rodríguez-García, I. *Chem. Eur. J.* **2007**, *13*, 557–568.
37. Paré, E. C.; Brook, D. J. R.; Brieger, A.; Badik, M.; Schinke, M. *Org. Biomol. Chem.* **2005**, *3*, 4258–4261.
38. Chemistruck, V.; Chambers, D.; Brook, D. J. R. *J. Org. Chem.* **2009**, *74*, 1850–1857.
39. Sharifi, F.; Bauld, R.; Fanchini, G. *J. Appl. Phys.* **2013**, *114*.

40. Schlaf, R.; Murata, H.; Kafafi, Z. H. *J. Electron Spectrosc. Relat. Phenom.* **2001**, *120*, 149–154.
41. Sheldrick, G. M. *Acta. Cryst.* **2008**, *A64*, 112–122.
42. Milcent, R.; Barbier, G. *J. Heterocycl. Chem.* **1994**, *31*, 319–324.
43. Melitz, W.; Shen, J.; Kummel, A. C.; Lee, S. *Surf. Sci. Rep.* **2011**, *66*, 1–27.
44. Cardona, C. M.; Li, W.; Kaifer, A. E.; Stockdale, D.; Bazan, G. C. *Adv. Mater.* **2011**, *23*, 2367–2371.

Chapter 3

3 Synthesis, Characterization, and Thin-Film Properties of 6-Oxoverdazyl Polymers Prepared by Ring-Opening Metathesis Polymerization

Adapted from:

J. A. Paquette, S. Ezugwu, V. Yadav, G. Fanchini*, J. B. Gilroy* *J. Polym. Sci., Part A: Polym. Chem.* **2016**, *54*, 1803–1813.

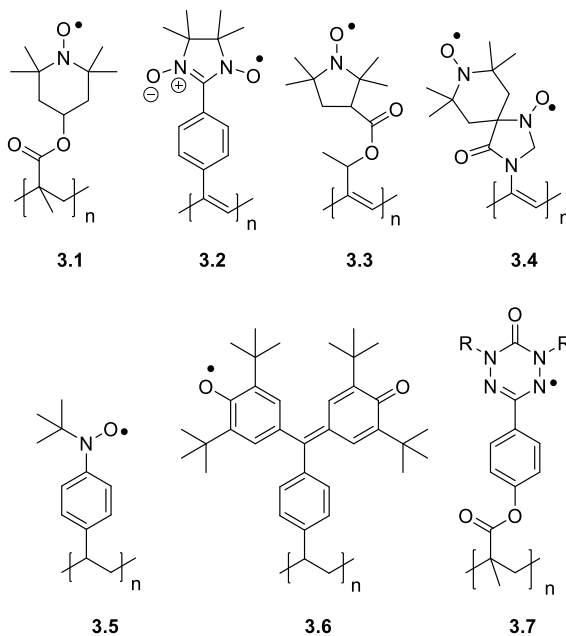
S. Ezugwu, **J. A. Paquette**, V. Yadav, J. B. Gilroy*, G. Fanchini* *Adv. Electron. Mater.* **2016**, *2*, 1600253.

3.1 Introduction

Functional polymers with potentially useful optical and electronic properties have received significant attention due to the ability of these materials to improve upon existing technologies by combining the unique properties of small functional molecules (*e.g.*, electron transfer, light absorption/emission, magnetic) with the processability, mechanical robustness, and flexibility associated with polymers.¹ An interesting subclass of functional polymers that has emerged in recent years contain stable organic radicals² in the repeating unit pendant to their backbones.³⁻⁵ The vast majority of research towards stable radical polymers has been motivated by their utility as electrode materials in batteries,^{3-4, 6} where the introduction of conductive (nano)fillers has led to enhanced performance.⁷⁻¹⁰ However, radical polymers have also shown application as high-spin ground state materials,¹¹ (co)catalysts for the selective oxidation of alcohols,¹² inhibitors of self-polymerization reactions,¹³ solid-state conductive materials,¹⁴⁻¹⁶ and the functional component of memory architectures.¹⁷⁻¹⁹

The most widely studied family of stable radical polymers is based on 2,2,6,6-tetramethylpiperidin-1-yl (TEMPO, **3.1**) radicals,^{14-15, 20-27} while examples based on other families of radicals, including nitronyl nitroxide (**3.2**),²⁸ 2,2,5,5-tetramethyl-1-pyrrolidinylloxy (PROXYL, **3.3**),²⁹ spirobisnitroxide (**3.4**),³⁰ aminoxy (**3.5**),³¹ galvinoxyl (**3.6**),³² and 6-oxoverdazyl (**7**)³³ radicals have received considerably less attention. Further expansion of

the stable radical polymer field to include examples based on these and other stable radicals will allow for the realization of materials with targeted properties that are suitable for the applications described above. 6-Oxoverdazyl radicals offer exceptional stability towards air and moisture, and, while their high molecular weights render them poor candidates for battery applications, their tunable ambipolar redox properties³³⁻³⁴ may allow for their future use as charge transport materials.



Most synthetic protocols, for example, those targeting nitroxide radical polymers, involve the polymerization of monomers based on radical precursors followed by post-polymerization reactions designed to generate the targeted stable radical polymers. These strategies are often hampered by difficulty surrounding the complete conversion of the radical precursor pendant units to their stable radical form, a factor that has recently been shown to affect their charge transport properties.¹⁶ Therefore, there remains a need for further development of polymerization protocols that allow for direct polymerization of stable radical-containing monomers^{25, 35-39} and to ensure a high degree of radical content along the polymer backbone.

Herein, the ring-opening metathesis polymerization (ROMP) behavior of a 6-oxoverdazyl radical monomer and the thorough characterization of the bulk, solution, and thin-film properties of the resulting polymers is reported.

3.2 Experimental

3.2.1 General Considerations

Reactions and manipulations were carried out under a nitrogen atmosphere using standard Schlenk techniques unless otherwise stated. Solvents were obtained from Caledon Laboratories, dried using an Innovative Technologies Inc. solvent purification system, collected under vacuum, and stored under a nitrogen atmosphere over 4 Å molecular sieves. Reagents were purchased from Sigma-Aldrich, Alfa Aesar, or Oakwood Chemicals and used as received unless otherwise stated. 2,4-Di-*isopropyl*carbonohydrazide bis-hydrochloride **3.8**,⁴⁰ *N*-(3-hydroxypropyl)-*cis*-5-norbornene-*exo*-2,3-dicarboximide **3.11**,⁴¹ and 3-bromopyridine derivative of Grubbs' 3rd generation catalyst⁴² were prepared according to published procedures. NMR spectra were recorded on a 400 MHz (¹H: 400.1 MHz, ¹³C{¹H}: 100.4 MHz) Varian INOVA instrument. ¹H NMR spectra were referenced to residual CD₃SOCD₂H (2.50 ppm) and ¹³C{¹H} NMR spectra were referenced to CD₃SOCD₃ (39.5 ppm). Mass spectrometry data were recorded in positive-ion mode using a high resolution Finnigan MAT 8200 spectrometer using electron impact ionization. UV-vis absorption spectra were recorded in CH₂Cl₂ solutions using a Cary 300 Scan instrument. Four separate concentrations were run for each sample, and molar extinction coefficients were determined from the slope of a plot of absorbance against concentration. FT-IR spectra were recorded on a PerkinElmer Spectrum Two FT-IR as KBr pellets. Elemental analysis (C, H, N) was carried out by Laboratoire d'Analyse Élémentaire, Université de Montréal, Montréal, QC, Canada.

3.2.2 Gel Permeation Chromatography (GPC)

GPC experiments were conducted in chromatography grade THF at concentrations of 5 mg mL⁻¹ using a Viscotek GPCmax VE 2001 GPC instrument equipped with an Agilent PolyPore guard column (PL1113-1500) and two sequential Agilent PolyPore GPC columns packed with porous poly(styrene-*co*-divinylbenzene) particles (MW range

200–2,000,000 g mol⁻¹; PL1113-6500) regulated at a temperature of 30 °C. Signal response was measured using a Viscotek VE 3580 RI detector, and molecular weights were determined by comparison of the maximum RI response with a calibration curve (10 points, 1,500–786,000 g mol⁻¹) established using monodisperse polystyrene purchased from Viscotek.

3.2.3 Thermal Analysis

Thermal degradation studies were performed using a TA Instruments Q600 SDT TGA and processed using TA Universal Analysis software. Samples were placed in an alumina cup and heated at a rate of 10 °C min⁻¹ from 25 to 800 °C under a flow of nitrogen (100 mL min⁻¹). Glass transition (T_g) temperatures were determined using differential scanning calorimetry (DSC) on a TA Instruments DSC Q20. The polymer samples were placed in an aluminum Tzero pan and heated from room temperature to 180 °C at a scan rate of 10 °C min⁻¹ under a flow of nitrogen (50 mL min⁻¹) and cooled down to 0 °C at a scan rate 10 °C min⁻¹ before they underwent two more heating/cooling cycles. The glass transition temperature was determined from the second heating/cooling cycle.

3.2.4 Cyclic Voltammetry

CV experiments were performed with a Bioanalytical Systems Inc. (BASi) Epsilon potentiostat and analyzed using BASi Epsilon software. Typical electrochemical cells consisted of a three-electrode setup including a glassy carbon working electrode, platinum wire counter electrode, and silver wire *pseudo*-reference electrode. Experiments were run at 100 mV s⁻¹ in degassed MeCN/CH₂Cl₂ (1:1) solutions of the analyte (~1 mM) and electrolyte (0.1 M *n*Bu₄NPF₆). Voltammograms were referenced internally against the ferrocene/ferrocenium redox couple (~1 mM internal standard) and corrected for internal cell resistance using the BASi Epsilon software.

3.2.5 Electron Paramagnetic Resonance Spectroscopy

EPR spectroscopy measurements were made on *ca.* 10⁻⁵ M CH₂Cl₂ solutions of 6-oxoverdazyl monomer **3.12** and polymer **3.13** that had been subjected to three freeze-pump-thaw cycles in 4 mm quartz tubes using a JEOL JES-FA200 EPR spectrometer. All

measurements were made at 20 °C and *g*-factors were referenced relative to a built-in manganese oxide marker within the resonant cavity of the instrument. Quantification of the number of unpaired electrons present in polymer **3.13** was done by comparing an EPR spectrum collected for a TEMPO solution of known concentration in CH₂Cl₂ that was compared to the manganese oxide marker signal as outlined above. The integration of the TEMPO signal with respect to the manganese oxide marker was compared to that of the radical polymer. By assuming one molecule of TEMPO contributes one unpaired electron, the number of unpaired electrons present in the radical polymer sample was determined.

3.2.6 X-ray Crystallography

Crystals of monomer **3.12** suitable for X-ray diffraction were grown by vapor diffusion of hexanes into a saturated CH₂Cl₂ solution at -30 °C. The sample was mounted on a MiTeGen polyimide micromount with a small amount of Paratone-N oil. All X-ray measurements were made on a Nonius KappaCCD Apex2 diffractometer at a temperature of 110 K. The frame integration was performed using SAINT.⁴³ The resulting raw data was scaled and absorption corrected using a multi-scan averaging of symmetry equivalent data using SADABS.⁴⁴ The structure was solved by using a dual space methodology using the SHELXT program.⁴⁵ All non-hydrogen atoms were obtained from the initial solution. The hydrogen atoms were introduced at idealized positions and the positional parameters but not the displacement parameters were allowed to refine. The structural model was fit to the data using full matrix least-squares based on F^2 . The calculated structure factors included corrections for anomalous dispersion from the usual tabulation. The structure was refined using the SHELXL-2014 program from the SHELX suite of crystallographic software.⁴⁶ Graphic plots were produced using the Mercury program suite. See Table 3.1 and CCDC 1428231 for X-ray diffraction data collection and refinement details.

Table 3.1 Selected X-ray diffraction data collection and refinement details for monomer **3.12**.

Compound	3.12
Chemical Formula	C ₂₇ H ₃₂ N ₅ O ₅
Formula Weight (g mol ⁻¹)	506.57
Crystal Dimensions (mm)	0.349 × 0.325 × 0.115
Crystal Color and Habit	Red prism
Crystal System	Triclinic
Space Group	P-1
Temperature (K)	110
<i>a</i> (Å)	10.063(2)
<i>b</i> (Å)	11.316(2)
<i>c</i> (Å)	12.516(2)
α (°)	100.839(4)
β (°)	112.235(5)
γ (°)	98.624(5)
<i>V</i> (Å ³)	1257.0(4)
<i>Z</i>	2
ρ (g cm ⁻¹)	1.338
λ (Å)	1.54178
μ (cm ⁻¹)	0.769
Diffractometer Type	Nonius KappaCCD Apex2
R _{merge}	0.0245
R ₁ ^a [2σI > 2]	0.0352
ωR ₂ ^b [2σI > 2]	0.0900
R ₁ (all data)	0.0391
ωR ₂ (all data)	0.0940
GOF ^c	1.028

$$^a R_1 = \Sigma(|F_o| - |F_c|) / \Sigma F_o$$

$$^b \omega R_2 = [\Sigma(\omega(F_o^2 - F_c^2)^2) / \Sigma(\omega F_o^4)]^{1/2}$$

$$^c \text{GOF} = [\Sigma(\omega(F_o^2 - F_c^2)^2) / (\text{No. of reflns.} - \text{No. of params.})]^{1/2}$$

3.2.7 Thin-Film Preparation and Electrical Conductivity Measurements

Thin films of various thickness were prepared from polymer **3.13** and their electrical properties were measured. Film preparation and electrical measurements were both carried out in a glove box loaded with N₂ (Nexus II, Vacuum Atmospheres Co.) attached to an ultra-high vacuum (UHV) chamber for sample metallization and contacting. Samples can be transferred to/from this chamber from/to the glove box without any direct exposure to air. O₂ and H₂O contents in the glove box were below 3 ppm during the entire fabrication and measurement process. To prepare the thin films, the polymer was dissolved at 12.5 mg mL⁻¹ in anhydrous chlorobenzene. The solution was stirred overnight at 50 °C, filtered through 0.8 μm pore size syringe filters and spun on glass substrates with pre-deposited indium tin-oxide (ITO) contacts (15 Ω/square sheet resistance, Sigma-Aldrich)

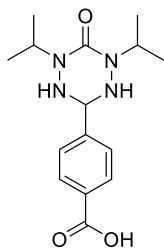
using a KW-4A spin coater (Chemat Technologies Inc.) located in the glove box. ITO substrate patterning on glass was previously obtained by coating the ITO area to be retained with KaptonTM tape and etching the remaining area in a 2:1:1 H₂O:HCl:HNO₃ mixture at 55 °C.

Different spinning speeds, from 500 to 3000 rpm, were used to obtain a set of thin films at thicknesses from 50 ± 4 nm to 10 ± 4 nm, respectively. These thicknesses were measured by atomic force microscopy (AFM) from samples identical to those used for electrical measurements. In order to perform the thickness measurements, part of the substrate was masked prior to spin coating the polymer solution. The mask was then removed and samples were extracted from the glove box and analyzed in contact-mode using a Witec Alpha300S AFM microscope, from which topography profiles of the step in the correspondence of the masked area were obtained. Additional AFM profiles were recorded in the correspondence of scratches made on the polymer film using soft probes that were known not to affect the substrate. AFM images showed that root mean squared (RMS) roughness of thin films of polymer **3.13** could be estimated to be about 2 nm, which was significantly less than the RMS roughness of ITO. This suggests the polymeric film is continuous with no outstanding ITO pinholes (Figure A3.1).

Electrical measurements were performed in a sandwich configuration in the glove box. To complete the sandwich structure, samples were transferred in the aforementioned UHV chamber directly accessible from the glove box and 100 nm thick aluminum contacts were thermally evaporated on top of the polymer films, with contact thickness measured *in situ* using a Sycom STM-2 thickness monitor. The temperature was kept below 50 °C during the entire thermal evaporation process. A first set of current voltage (I-V) characteristics of the thin films were recorded at ± 1 V using a computer automated Keithley 2400 source meter with 10 mV scan step. After this set of measurements a significantly higher voltage, $V_o = 5$ V, was applied to the samples, and electrical measurements were repeated. The breakdown voltage was determined to be 8–12 V for the thinnest sample and is therefore significantly higher than any voltages used during our experiments. Consistent electrical measurements were successfully reproduced on different sets of identically prepared samples.

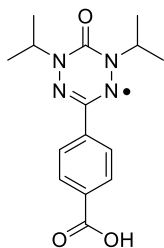
3.2.8 Synthetic Procedures

1,5-di-*isopropyl*-3-(4-carboxyphenyl)-6-oxotetrazane (3.9)



To a refluxing solution of 2,4-di-*isopropyl*carbazine (2.00 g, 8.09 mmol) and NaOAc (1.33 g, 16.2 mmol) in MeOH (50 mL) was added dropwise over a 3 h period, a solution of 4-carboxybenzaldehyde (1.21 g, 8.09 mmol) and NaOAc (0.66 g, 8.1 mmol) in MeOH (50 mL). The solution was stirred at reflux overnight, removed from the heat and allowed to cool to room temperature. The reaction mixture was then acidified to pH ~ 3 using 1 M HCl, followed by the removal of MeOH *in vacuo*. The white precipitate that crashed out of the resulting aqueous solution was filtered and washed with two portions of deionized H₂O (50 mL) to give tetrazane **3.9** as a white microcrystalline powder. Yield = 2.34 g, 94%. ¹H NMR (400.1 MHz, *d*₆-DMSO): δ 13.00 (s, 1H, COOH), 7.97 (d, 2H, ³J_{HH} = 6 Hz, aryl CH), 7.68 (d, 2H, ³J_{HH} = 6 Hz, aryl CH), 5.05 (d, 2H, ³J_{HH} = 11 Hz, NH), 4.50–4.43 (m, 3H, NCHN and CHMe₂), 1.06–1.04 (m, 12H, CH₃). ¹³C{¹H} NMR (100.6 MHz, *d*₆-DMSO): δ 167.0, 153.4, 141.1, 130.6, 129.3, 126.9, 72.2, 46.8, 19.6, 18.4. FT-IR (ranked intensity, assignment), KBr pellet: 3249 (13, NH), 2981 (7), 2935 (11), 2872 (12), 1694 (3, CO), 1586 (1, CO), 1423 (2), 1227 (5), 1125 (6), 1062 (8), 904 (9), 863 (10), 752 (4) cm⁻¹. Mass Spec. (EI, +ve mode): exact mass calculated for C₁₅H₂₂N₄O₃: 306.1692; found: 306.1688; difference: -1.3 ppm.

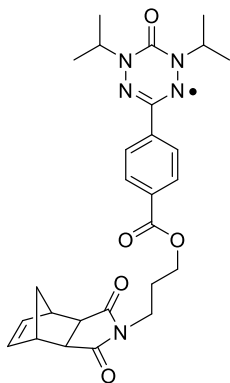
1,5-di-*isopropyl*-3-(4-carboxyphenyl)-6-oxoverdazyl (3.10)



To a deionized H₂O/THF (2:1, 45 mL) solution of 1,5-di-*i*Pr-3-(4-carboxyphenyl)-6-oxotetrazane **3.9** (2.34 g, 7.64 mmol) and NaOH (0.31 g, 7.6 mmol) open to air was added NaIO₄ (2.45 g, 11.5 mmol) in deionized H₂O (30 mL) dropwise over 30 min. The reaction was stirred at room temperature for 18 h and slowly turned a dark red colour. The mixture was then acidified to pH ~ 3 using 1 M HCl, followed by removal of THF *in vacuo*. The resultant dark-red precipitate was filtered and washed with two portions of deionized H₂O (50 mL) to give verdazyl **3.10** as a red microcrystalline powder. Yield = 2.15 g, 93%. FT-IR (ranked intensity, assignment), KBr pellet: 3434 (4, br, OH), 3198 (8),

2985 (6), 2937 (9), 1721 (3, CO), 1680 (1, CO), 1656 (2), 1612 (7), 1432 (12), 1386 (10), 1290 (11), 1219 (5) cm^{-1} . UV-vis (CH_2Cl_2): λ_{max} 419 nm ($\epsilon = 1,875 \text{ M}^{-1} \text{ cm}^{-1}$), 405 nm ($\epsilon = 1,600 \text{ M}^{-1} \text{ cm}^{-1}$), 270 nm ($\epsilon = 29,750 \text{ M}^{-1} \text{ cm}^{-1}$). Mass Spec. (EI, +ve mode): exact mass calculated for $\text{C}_{15}\text{H}_{19}\text{N}_4\text{O}_3$: 303.1457; found: 303.1459; difference: +0.7 ppm.

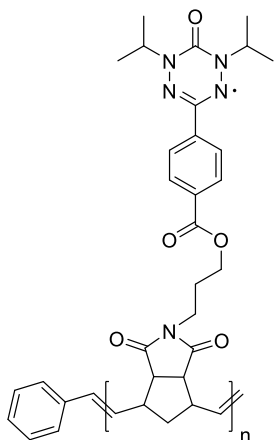
1,5-di-*isopropyl*-3-(*cis*-5-norbornene-*exo*-2,3-dicarboxiimide)-6-oxoverdazyl (**3.12**)



To a solution of *N,N'*-dicyclohexylcarbodiimide (DCC) (0.75 g, 3.6 mmol) and 4-dimethylaminopyridine (DMAP) (0.48 g, 4.0 mmol) in dry CH_2Cl_2 (20 mL) was added 1,5-di-*i*Pr-3-(4-carboxyphenyl)-6-oxoverdazyl **3.10** (1.00 g, 3.30 mmol) before the mixture was stirred for 10 min at room temperature. To this solution was added *N*-(3-hydroxypropyl)-*cis*-5-norbornene-*exo*-2,3-dicarboxiimide **3.11** (0.73 g, 3.3 mmol) and a further 10 mL of dry CH_2Cl_2 (for rinsing). The reaction mixture was stirred for 4 h at room temperature. The solution

was filtered to remove precipitated material, which was rinsed with dry CH_2Cl_2 (20 mL) before the organic phases were combined and taken to dryness *in vacuo*. The resulting orange oil was purified by column chromatography [75 mL neutral alumina, hexanes/EtOAc (35:65), $R_f = 0.45$], and recrystallized from a hot saturated solution of hexanes to give **3.12** as dark-red needles. Yield = 1.18 g, 71%. FT-IR (ranked intensity, assignment), KBr pellet: 2978 (11), 2935 (12), 2877 (14), 1770 (13, CO), 1697 (1, CO), 1679 (2, CO), 1611 (10), 1386 (9), 1367 (8), 1268 (2), 1230 (5), 1174 (6), 776 (7), 705 (4) cm^{-1} . UV-vis (CH_2Cl_2): λ_{max} 418 nm ($\epsilon = 1,900 \text{ M}^{-1} \text{ cm}^{-1}$), 403 nm ($\epsilon = 1,400 \text{ M}^{-1} \text{ cm}^{-1}$), 268 nm ($\epsilon = 31,025 \text{ M}^{-1} \text{ cm}^{-1}$). Mass Spec. (EI, +ve mode): exact mass calculated for $\text{C}_{27}\text{H}_{32}\text{N}_5\text{O}_5$: 506.2403; found: 506.2399; difference: -0.8 ppm. Anal. Calcd. (%) for $\text{C}_{27}\text{H}_{32}\text{N}_5\text{O}_5$: C, 64.02; H, 6.37; N, 13.82. Found: C, 63.88; H, 6.50; N, 13.65.

Representative synthesis of poly[1,5-di-isopropyl-3-(*cis*-5-norbornene-*exo*-2,3-dicarboxiimide)-6-oxoverdazyl] (3.13)



A grease-free Schlenk flask was charged with monomer **3.12** (0.50 g, 0.99 mmol) and degassed CH_2Cl_2 (12 mL, 3 freeze-pump-thaw cycles). The monomer solution was cooled to 0 °C in an ice bath for 10 min before a 1 mg mL^{-1} CH_2Cl_2 solution of Grubbs' 3rd generation catalyst (8.73 mL, 9.87×10^{-3} mmol) was rapidly added in one portion. The polymerization proceeded for 1 h before it was terminated with ethyl vinyl ether (2.37 mL, 24.7 mmol) and stirred for an additional 30 min while warming to room temperature. The crude mixture was filtered through a short neutral alumina column (20 mL, CH_2Cl_2) before the solvent was removed *in vacuo*. The resultant polymer, an orange oil was dissolved in THF (10 mL) and precipitated thrice into cold hexanes (90 mL) to afford **3.13** as an orange powder. Yield = 0.46 g, 92%. FT-IR (ranked intensity, assignment), KBr pellet: 2975 (13), 2939 (14), 2871 (16), CO ester 1775 (15), 1698 (1, CO), 1682 (2, CO), 1611 (12), 1387 (10), 1368 (8), 1270 (3), 1228 (9), 1173 (6), 1104 (7), 1101 (5), 776 (11), 705 (4) cm^{-1} . UV-vis (CH_2Cl_2): λ_{max} 419 nm ($\epsilon = 2,050 \text{ M}^{-1} \text{ cm}^{-1}$), 402 nm ($\epsilon = 1,475 \text{ M}^{-1} \text{ cm}^{-1}$), 270 nm ($\epsilon = 29,900 \text{ M}^{-1} \text{ cm}^{-1}$). GPC (THF, conventional calibration relative to polystyrene standards): $M_n = 46,100 \text{ g mol}^{-1}$, $M_w = 49,000 \text{ g mol}^{-1}$, $D = 1.07$).

3.2.9 Kinetic Studies of the ROMP of Monomer **3.12**

3.2.9.1 Catalyst Loading

Using 0.05 g of monomer **3.12** each, a series of five reactions were carried out according to the procedure described above. The catalyst molar feed stock ratios (monomer:catalyst) were: 20, 40, 60, 80, and 100. The polymerization times were held constant at 60 min. The degree of polymerization was measured by GPC analysis using conventional calibration relative to polystyrene (PS) standards.

3.2.9.2 Timed aliquots

A 1 mg mL⁻¹ CH₂Cl₂ solution of 3-bromopyridine derivative of Grubbs' 3rd generation catalyst (3.5 mL, 4.0 × 10⁻³ mmol) was rapidly added in one portion to a 42 mg mL⁻¹ CH₂Cl₂ solution of monomer **3.12** (4.8 mL, 0.40 mmol) and the mixture was stirred at 0 °C. Six samples were taken at 150 s intervals and added into separate reaction flasks containing ethyl vinyl ether (0.94 mL, 9.9 mmol) to terminate polymerization. The number average molecular weights (M_n) were measured by GPC analysis using conventional calibration relative to PS standards.

3.3 Results and Discussion

3.3.1 Synthesis

The synthesis of monomer **3.12** (Scheme 3.1) began with the condensation reaction between bis-hydrazide•2HCl salt **3.8** and 4-formylbenzoic acid to afford tetrazane **3.9** as a white powder in 94% yield (Figures A3.2 and A3.3). Tetrazane **3.9** was then oxidized in THF/deionized H₂O solution using NaIO₄ to yield 6-oxoverdazyl **3.10** as an orange powder in 93% yield. The reaction was monitored by FT-IR spectroscopy where the disappearance of the NH stretch at 3249 cm⁻¹ was observed (Figure A3.4). Verdazyl **3.10** was then coupled to *N*-(3-hydroxypropyl)-*cis*-5-norbornene-*exo*-2,3-dicarboximide **3.11** in the presence of DCC and DMAP to afford monomer **3.12** as dark-red crystals in 71% yield. The propyl-substituted *cis*-5-norbornene-*exo*-2,3-dicarboximide polymerizable group was chosen based on previous reports by Tang and co-workers describing the successful ROMP of monomers bearing redox-active cobaltocenium moieties.⁴²

X-ray diffraction studies of single crystals of monomer **3.12** afforded a solid-state structure (Figure 3.1 and Table 3.1). The bond lengths of N1-N2 1.3558(15) and N3-N4 1.3595(15) Å are intermediate between single and double N-N bonds.⁴⁷ Similarly, the N2-C1 1.3319(16) and N4-C1 1.3315(16) Å bond lengths fall between those expected for single and double N-C bonds,⁴⁷ confirming the delocalized nature of the bonding in the planar verdazyl radical. The dihedral angle between the verdazyl plane (N1-N2-C1-N4-N3-C2) and the plane defined by the phenyl ring (C9-C14) was found to be 6.13°. Furthermore, the bond length of C24-C25 of 1.318(2) Å is consistent with the preservation

of the alkene in the norbornene ring. The structural metrics observed for verdazyl monomer **3.12** are consistent with those of other 6-oxoverdazyl radicals.^{33, 48-52}

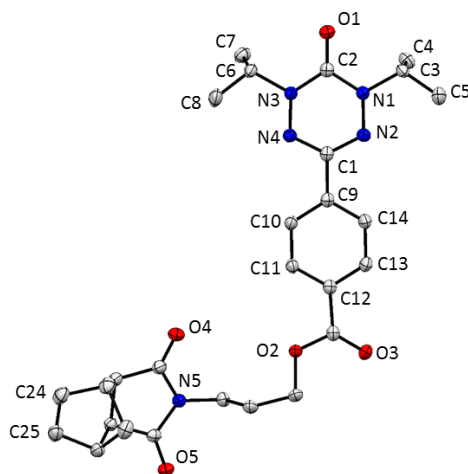
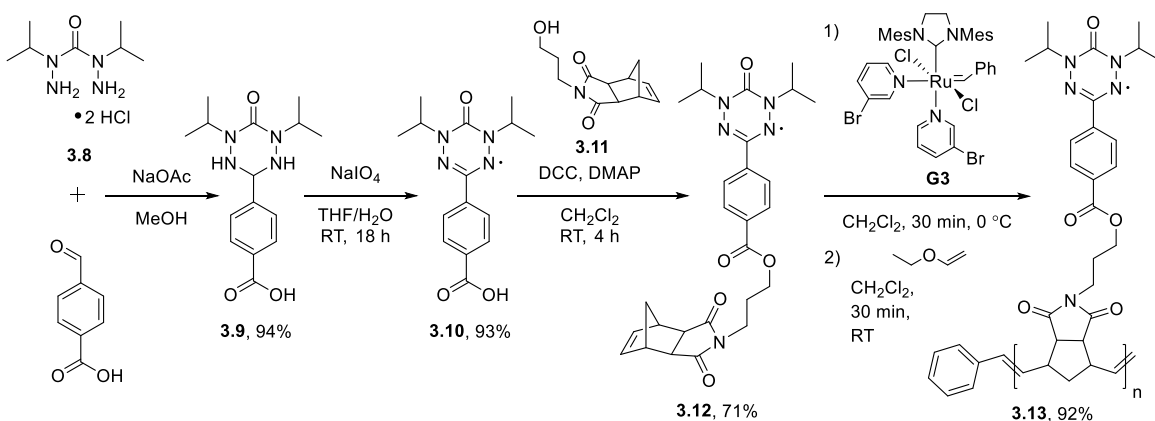


Figure 3.1 Solid-state structure of monomer **3.12**. Anisotropic displacement ellipsoids are shown at 50% probability and hydrogen atoms have been omitted for clarity. Selected bond lengths (Å): N1-N2 1.3558(15), N3-N4 1.3595(15), N1-C2 1.3819(16), N2-C1 1.3319(16), N3-C2 1.3802(16), N4-C1 1.3315(16), C24-C25 1.318(2). Selected bond angles (deg): N1-N2-C1 115.00(10), N3-N4-C1 114.96(10), N1-C2-N3 114.35(11), N2-C1-N4 127.20(11).



Scheme 3.1 Synthesis of 6-oxoverdazyl monomer **3.12** and polymer **3.13**.

With monomer **3.12** in hand, we began to explore its ROMP behavior. In a representative reaction, polymerization was initiated by the rapid introduction of a solution of 3-bromopyridine derivative of Grubbs' 3rd generation catalyst (G3) to a stirring solution of monomer **3.12** in dry and degassed CH_2Cl_2 at 0 °C with a feed molar ratio of 100 (monomer:catalyst = 100:1). Reaction progress was monitored by GPC, confirming the reaction was near completion after approximately 15 min. Nonetheless, the solution was stirred for an additional 45 min to ensure complete monomer conversion before a large excess of ethyl vinyl ether (EVE) was added to terminate the polymerization. The reaction mixture was passed through a plug of neutral alumina to remove residual catalyst. Subsequent precipitations from THF into cold hexanes, followed by centrifugation afforded polymer **3.13** as an orange powder in 92% yield. Figure 3.2a shows the GPC trace (typical) obtained for polymer **3.13** after purification ($M_n = 46,100 \text{ g mol}^{-1}$, $M_w = 49,300 \text{ g mol}^{-1}$, $D = 1.07$). Our best results were obtained when CH_2Cl_2 was employed as a solvent, while Nishide and co-workers have recently noted improved results when acetone was employed as solvent for the ROMP of a related bis nitroxide monomer.²⁶

It is worth noting that during our investigations of the ROMP of monomer **3.12**, approximately 20% of our reactions yielded polymer samples that contained a high molecular weight shoulder in their GPC chromatograms (*e.g.*, Figure 3.2b, $M_n = 51,100 \text{ g mol}^{-1}$, $M_w = 57,750 \text{ g mol}^{-1}$, $D = 1.13$). Based on the inconsistent appearance of this shoulder in our GPC data, we assume that the high molecular weight species are generated via chain coupling or related reactions during the termination step. The origin of the coupling remains unclear, however, molecular oxygen inadvertently introduced when EVE was introduced to the reaction flask via syringe may play a role in the observed reactivity.

We performed two separate experiments designed to further probe the ROMP of monomer **3.12**. Unfortunately, the scope of our studies were limited due to the paramagnetic nature of polymer **3.13**, which precluded the use of integration data obtained from ^1H NMR spectroscopy for the determination of the number average degree of polymerization (DP_n) and monomer consumption as a function of time. The first study involved ROMP of monomer **3.12** at five different molar feedstock ratios (Figure 3.2c).

As expected, the values of DP_n determined by GPC analysis increased significantly as the molar feedstock ratios were increased from 20 to 100. However, when high molecular weight polymers were targeted, we observed a deviation from ideal behavior, and lower than expected values of DP_n . This observation is indicative of well-behaved, but not formally living polymerization ROMP. A second study was performed, where a single ROMP reaction (monomer:catalyst 100:1) was studied at time intervals of 150 s (Figure 3.2d). The molecular weight of the isolated polymers increased in a non-linear fashion as a function of time due to a decrease in monomer concentration as the reaction proceeded. Again, this trend was consistent with a well-behaved ROMP reaction involving limited side reactions.

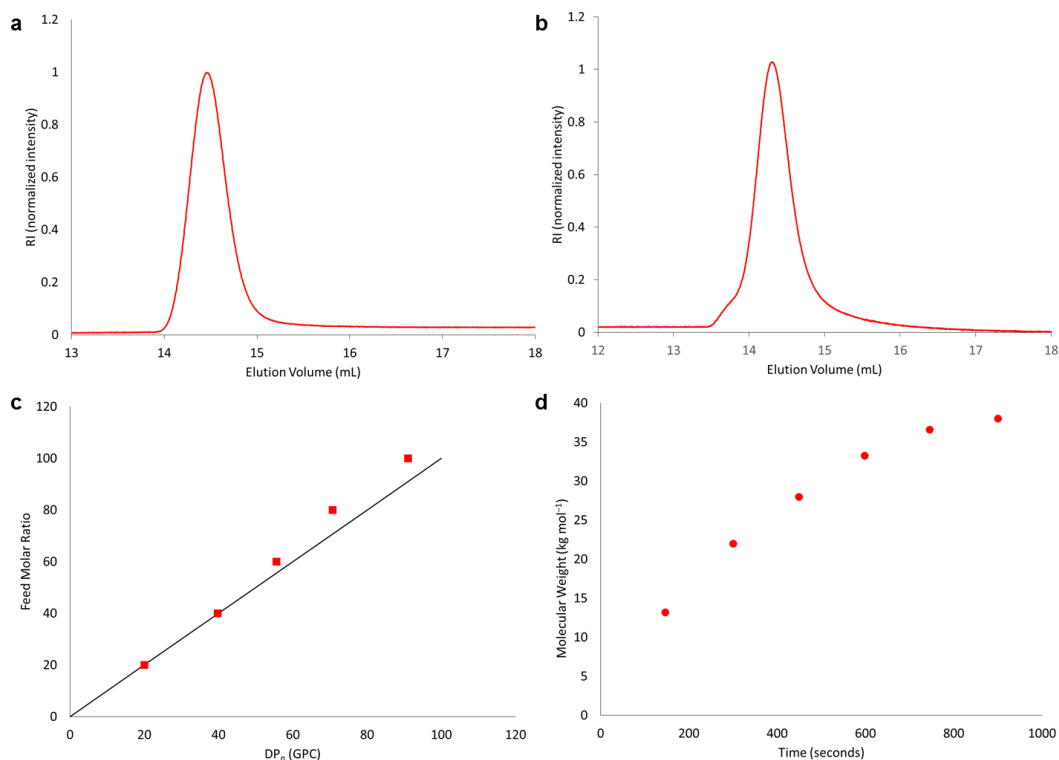


Figure 3.2 Representative GPC traces for (a) a typical sample of polymer **3.13** ($M_n = 46,100\ g\ mol^{-1}$, $M_w = 49,300\ g\ mol^{-1}$, $\mathcal{D} = 1.07$) and (b) a GPC trace for a polymer containing a minor fraction of high molecular weight polymer **3.13** ($M_n = 51,100\ g\ mol^{-1}$, $M_w = 57,750\ g\ mol^{-1}$, $\mathcal{D} = 1.13$). (c) Relationship of feed molar ratio and DP_n determined by GPC. The black line represents the theoretical relationship between DP_n and feed molar ratio. (d) Molecular weight (M_n) as a function of reaction time.

3.3.2 Polymer Characterization

Thermal gravimetric analysis (TGA) revealed that polymer **3.13** was thermally stable up to a temperature of 190 °C, where rapid degradation occurred in three steps (Figure A3.5). The first step (190–290 °C) involved a mass loss of 13%, the second (290–430 °C) 35%, and the third (430–800 °C) 40%, to give an overall char yield of 12%. Differential scanning calorimetry (DSC) studies of polymer **3.13** revealed a T_g of 152 °C (Figure A3.6).

To confirm the presence of 6-oxoverdazyl radicals in the polymer, careful comparison of the spectroscopic and electrochemical properties of monomer **3.12** and polymer **3.13** were made. The FT-IR spectrum of monomer **3.12** showed characteristic carbonyl peaks at 1679, 1697, 1770 cm^{-1} similar to the carbonyl peaks at 1682, 1698, and 1775 cm^{-1} of polymer **3.13** (Figure A3.7). Moreover, when we compared the UV-vis absorption spectra of monomer **3.12** and polymer **3.13** between 350 and 475 nm, we found that they were in very close agreement (Figure 3.3). Based on the IR and UV-vis absorption spectra, we conclude that nearly 100% of the repeating units in polymer **3.13** contain a 6-oxoverdazyl moiety, indicating that the ROMP reaction employed is indeed tolerant of such radicals.

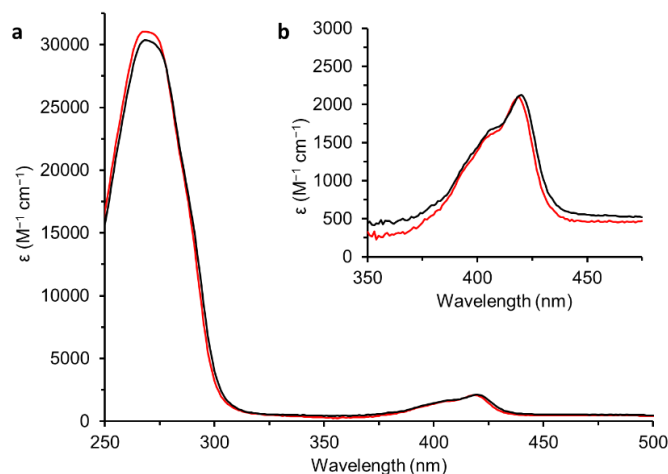


Figure 3.3 (a) UV-vis absorption spectra acquired for CH_2Cl_2 solutions of monomer **3.12** (red line) and polymer **3.13** (black line). (b) Magnified spectra from 350 to 475 nm.

In order to further support these findings, electron paramagnetic resonance (EPR) spectroscopy was performed to quantitatively determine the number of unpaired 6-oxoverdazyl units present in polymer **3.13**. This experiment showed that *ca.* 94% of the repeating units in the polymer contain an unpaired electron, supporting our IR and UV-vis absorption spectroscopy-based claims discussed above. An EPR spectrum of monomer **3.12** was also obtained and compared to the spectrum of polymer **3.13** (Figure 3.4). The spectrum of monomer **3.12** showed a typical pattern for 1,5-substituted 6-oxoverdazyls,⁴⁰ with the radical coupling to two unique pairs of nitrogen atoms and the CH protons of the *i*Pr groups [simulation data (Figure A3.8): $g = 2.0045$, line width = 0.089 mT, $a_{N1,3} = 0.529$ mT, $a_{N2,4} = 0.640$ mT, $a_H = 0.140$ mT]. The isotropic EPR spectrum of polymer **3.13** ($g = 2.0043$) was very broad and essentially featureless, as would be expected for a polymer containing stable radicals in random orientations and close proximity.

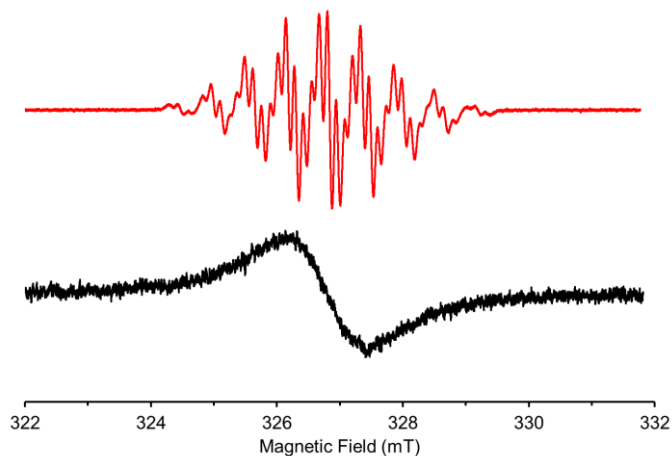


Figure 3.4 Experimental EPR spectra of 6-oxoverdazyl monomer **3.12** (red line, $g = 2.0045$) and polymer **3.13** (black line, $g = 2.0043$). Simulation of the spectrum of monomer **3.12** yielded the following parameters: line width = 0.089 mT, $a_{N1,3} = 0.529$ mT, $a_{N2,4} = 0.640$ mT, $a_H = 0.140$ mT (Figure A3.8).

The electrochemical properties of monomer **3.12** and polymer **3.13** were studied using cyclic voltammetry (CV) in a $\text{CH}_2\text{Cl}_2/\text{MeCN}$ (1:1) solvent mixture (Figure 3.5, Table 3.2). 6-Oxoverdazyl monomer **3.12** was reversibly oxidized and reduced at half-wave oxidation ($E_{1/2,\text{ox}}$) and reduction ($E_{1/2,\text{red}}$) potentials of 0.24 and -1.36 V relative to the ferrocene/ferrocenium redox couple, respectively. Similarly, the CV of polymer **3.13**

showed oxidation and reduction wave potentials at 0.25 V and -1.35 V, respectively. The current response for the polymer was lower than expected and the oxidation/reduction waves broadened as a result of a loss of diffusion control at the electrode interface, a commonly observed phenomenon for redox-active polymers.

Table 3.2 Electrochemical data for 6-oxoverdazyl monomer **3.12** and polymer **3.13**.

Compound	$E_{1/2,ox}$ (V vs. Fc/Fc ⁺)	$E_{1/2,red}$ (V vs. Fc/Fc ⁺)
3.12	0.24	-1.36
3.13	0.25	-1.35

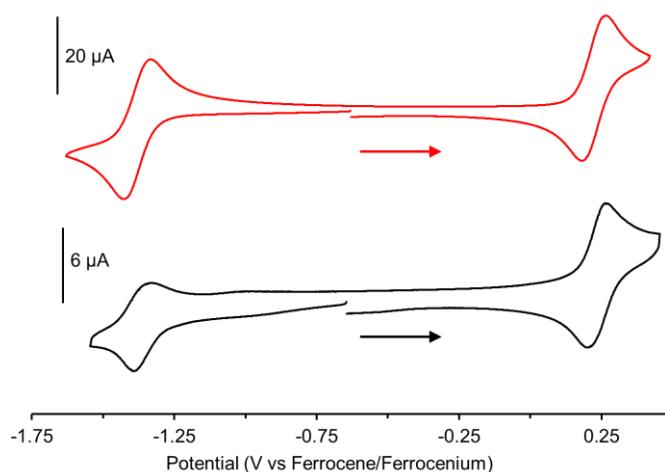


Figure 3.5 CVs of 6-oxoverdazyl monomer **3.12** (red line) and polymer **3.13** (black line) recorded at a scan rate of 100 mV s^{-1} in $\text{CH}_2\text{Cl}_2/\text{MeCN}$ (1:1) solution containing 1 mM analyte and 0.1 M $n\text{Bu}_4\text{NPF}_6$ as supporting electrolyte.

3.3.3 Electrical Properties of Thin Films of Polymer **3.13**

Based on the spectroscopic and electrochemical studies described above, we concluded that polymer **3.13** may have interesting and potentially unique thin-film properties. To this end, we investigated the electrical properties of thin solid films of this polymer, from approximately 10 nm to 50 nm in thickness, by using a sandwich architecture. Thin polymeric films may have very peculiar morphological and structural properties⁵³ as a consequence of the preferential alignment of the polymeric chains with respect to the substrate. Specifically, the alignment may be strongly dependent on the

thickness, which may sometimes lead to non-ohmic conductivity mechanisms and thickness-dependent resistivity in ultrathin polymeric films.⁵³

Figure 3.6a illustrates the configuration we used to measure the I-V characteristics of our films before and after the films were pretreated at high voltage ($V_o = 5$ V). In both cases, the film resistivity (ρ) was inferred from the I-V characteristics through the relationship

$$\rho = \frac{R \cdot A}{d} \quad (1)$$

where A is the area of the region in which the top and bottom contacts overlap, d is the film thickness and $R = V/I$ is the thin film resistance, obtained from the slope of the I-V characteristics in the proximity of the origin. The I-V curves recorded from our films of polymer **3.13** are reported in Figure 3.6b and 3.6c for measurements recorded after and before 5 V film treatment, respectively. In ohmic systems ρ is an inherent property of the material, independent of the thickness of the thin film that is being considered. After 5 V treatment, all films were electrically ohmic and exhibit a relatively high conductivity, with linear I-V characteristics in the entire ± 1 V range as can be observed in Figure 3.6b. The extracted resistivity value ($\rho \approx 1.7 \times 10^4 \Omega\cdot\text{m}$, Figure 3.6d) is thickness independent, as can be expected from ohmic systems. This value favorably compares with poly(2,2,6,6-tetramethylpiperidinyloxy methacrylate) **1** ($\rho \approx 1 \times 10^4 \Omega\cdot\text{m}$),¹⁵ the most widely studied stable radical polymer that has also shown defect-dependent thin-film properties.¹⁶ In contrast, Figure 3.6d also shows that these films are significantly more insulating before the high voltage treatment at 5 V. They revert to such a low-conductivity state after the effects of high-voltage treatment vanish, typically in 20–200 h.

Although a more complete understanding of the electrical properties of our films is beyond the scope of this thesis and will be the subject of future reports, it is noteworthy that the I-V characteristics before high-voltage treatment of our films are typically non-ohmic, as can be inferred from Figure 3.6c. As a consequence of non-ohmicity, the resistivity inferred from eq. (1) strongly increases as the thickness of the films decreases and could not be measured with our equipment at thicknesses below 20 nm. This suggests that ρ should be higher than $10^{12} \Omega\cdot\text{m}$ below this thickness value and, therefore, it may be approximately

comparable with that of glass ($\rho \approx 10^{12}\text{--}10^{14} \Omega\cdot\text{m}$).⁵⁴ It can be phenomenologically observed that the I-V curves shown in Figure 3.6c can be fitted using a Poole-Frenkel model for non-ohmic transport via localized trapped charges,⁵⁵ in which the current is related to the voltage by the following relationship:

$$I = \frac{A}{\rho_o d} V \exp\left\{\frac{-q\Delta\varphi + q^{3/2}\pi^{-1/2}[V/(\epsilon_m d)]^{1/2}}{k_B T}\right\} \quad (2)$$

where ρ_o corresponds to the polymer resistivity in the absence of traps, q is the electron charge, $\Delta\varphi$ is the voltage barrier electrons must cross at low voltage to hop from one charged trap to another, ϵ_m is the dielectric permittivity of the polymer relative to vacuum, and $k_B T = 0.025$ eV at room temperature.

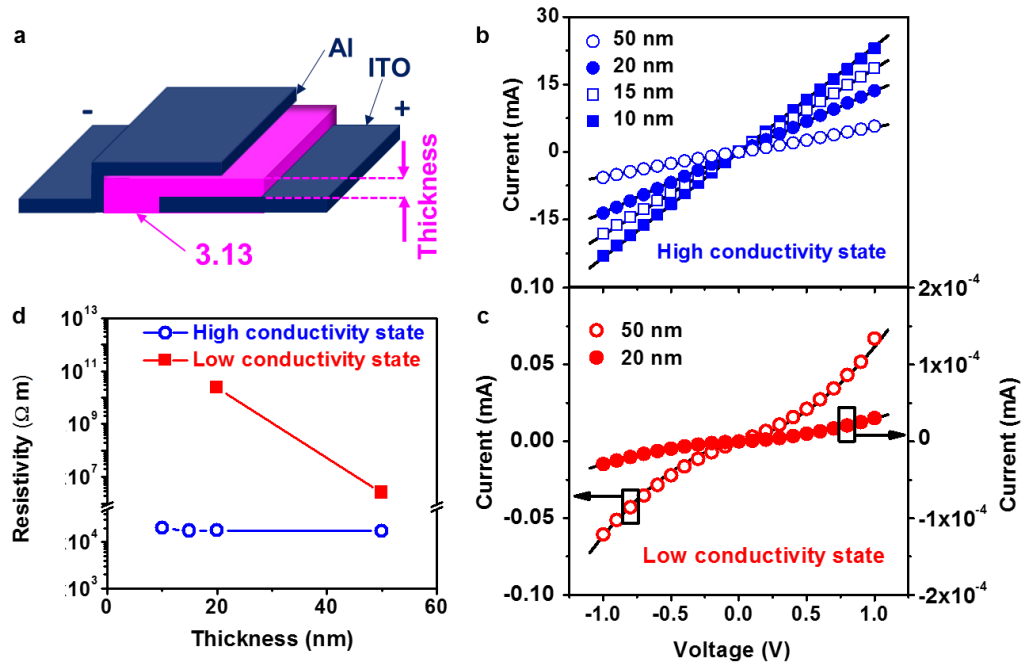


Figure 3.6 (a) Sandwich-type configuration for measuring the I-V characteristics of polymer **3.13** thin films, showing bistable electrical transport. (b) I-V curves of thin films at four different thicknesses in high conductivity state, which were fitted with straight lines to demonstrate ohmic transport and (c) I-V curves of thin films in low conductivity state showing non-ohmic, Poole-Frenkel like, behavior. Solid line fits were performed using eq. (2). (d) Film resistivity values obtained from the low-voltage portions of I-V curves.

While the high-conductivity state observed in Figure 3.6b can be attributed to extended-state transport via free electrons, the low-conductivity, Poole-Frenkel-like transport mechanism observed in Figure 3.6c can be assigned to hopping between localized states situated at specific charged monomers along a polymer filament. The hopping conditions may be strongly dependent on the degree of alignment of the polymer filaments along the substrate, in analogy to what previously observed in polythiophenes.⁵³ Specifically, if all of the polymer chains are aligned parallel to the substrate, hopping along the z-direction must occur through localized states situated on different polymer chains, thus explaining why the thinnest films, presumably containing polymer filaments more aligned along the substrate, are also more electrically insulating.

The switchable conductor-insulator transitions in thin films of polymer **3.13** and their relationship with the redox processes in this material requires further investigation. However, the observation of Poole-Frenkel type transport in the low conductivity state leads us to tentatively suggest that such a state corresponds to a situation in which only a few repeating units in a polymer chain are charged, while most of them are in a neutral state. At sufficiently high voltage (*i.e.*, $V \geq V_0 \approx 5$ V) charges may directly tunnel from the electrodes into some of the neutral repeating units, charging them either positively or negatively. When a sufficient concentration of charged repeating units is reached in a thin film, a percolating pathway may be established between such repeating units, leading to switching to the high conductivity state, dominated by transport between extended electronic states. This conductor-insulator transition makes polymer **3.13** uniquely positioned for several applications in bistable electronics and will be the subject of future reports.

3.3.4 Ultrathin Memristor Device

The quest for memristors with flash properties suitable to retain information without any external power source, but capable of satisfying the thinness requirements of next-generation electronics, demands the development of device architectures with a homogeneous layer of active material that can be made as thin as possible. An ultrathin memristor device was fabricated in which the active layer is formed by a 10 nm

homogeneous thin film of polymer **3.13** (Figure 3.7). To the best of our knowledge, these are the thinnest organic flash memristors obtained to date. Careful engineering of the anode and cathode work functions, specifically aligning them with the negative and positive energy levels of polymer **3.13** is vital to maximize the on/off current ratio and ensure flash operation. Conversely, devices in which the cathode work function aligns with the neutral energy level of **3.13** are writable only once. We assign the bistability of our memristors to two distinct transport regimes in organic polyradicals: extended states and Poole-Frenkel.

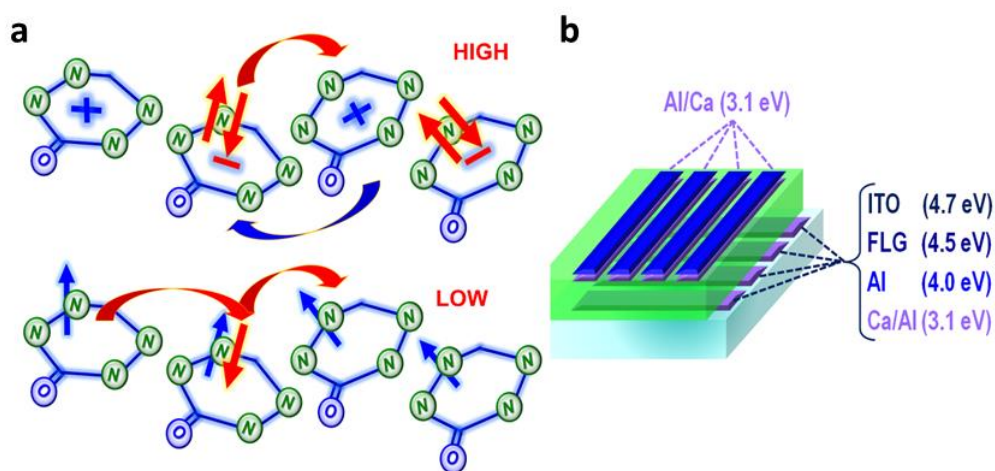


Figure 3.7 (a) Schematic representation of the electron hopping mechanism from repeating unit to repeating unit, in a Poole-Frenkel mechanism in the high conductivity and in an extended states mechanism for low conductivity. (b) The structural schematic of sandwich memristors from **3.13** thin film formed by spin coating 12.5 mg mL^{-1} of **3.13** dissolved in anhydrous chlorobenzene, four identical pre-patterned bottom electrodes and thermally evaporated Ca/Al top electrodes.

3.4 Conclusion

As a result of this work, we have demonstrated that ROMP using Grubbs' 3rd generation catalyst can produce 6-oxoverdazyl polymers with up to *ca.* 100 repeating units, narrow molecular weight distributions ($\mathcal{D} < 1.2$), and high radical content ($> 94\%$). A representative sample of the 6-oxoverdazyl polymers produced was thermally stable up to a temperature of $190 \text{ }^\circ\text{C}$ and had a glass transition temperature of $152 \text{ }^\circ\text{C}$. Comparison of the same polymer, which is stable towards air and moisture, to the monomer employed using several spectroscopic techniques, including IR, UV-vis, and EPR spectroscopy. CV

confirmed that the identity and properties of the pendant 6-oxoverdazyl groups were maintained after ROMP. The redox properties of the polymers described led us to explore their thin-film electrical transport properties, revealing a significant decrease in sheet resistance from 240 Ω to 26 M Ω upon application of a potential, $V_o = 5$ V. Our future work in this area will include expansion of the ROMP methods described to include other stable radical monomers and a detailed description of the electrical transport mechanism in 6-oxoverdazyl polymers in the solid state.

3.5 References

1. Meller, G.; Grasser, T. *Organic Electronics*. Springer: Berlin, 2010.
2. Hicks, R. G. *Stable radicals: fundamentals and applied aspects of odd-electron compounds*. Wiley: Chichester, UK, 2010; p xviii, 588 p.
3. Oyaizu, K.; Nishide, H. *Adv. Mater.* **2009**, *21*, 2339–2344.
4. Janoschka, T.; Hager, M. D.; Schubert, U. S. *Adv. Mater.* **2012**, *24*, 6397–6409.
5. Tomlinson, E. P.; Hay, M. E.; Boudouris, B. W. *Macromolecules* **2014**, *47*, 6145–6158.
6. Janoselika, T.; Martin, N.; Martin, U.; Friebe, C.; Morgenstern, S.; Hiller, H.; Hager, M. D.; Schubert, U. S. *Nature* **2015**, *527*, 78–81.
7. Choi, W.; Ohtani, S.; Oyaizu, K.; Nishide, H.; Geckeler, K. E. *Adv. Mater.* **2011**, *23*, 4440–4443.
8. Choi, W.; Endo, S.; Oyaizu, K.; Nishide, H.; Geckeler, K. E. *J. Mater. Chem.* **2013**, *1*, 2999–3003.
9. Sukegawa, T.; Sato, K.; Oyaizu, K.; Nishide, H. *RSC Adv.* **2015**, *5*, 15448–15452.
10. Aqil, A.; Vlad, A.; Piedboeuf, M.-L.; Aqil, M.; Job, N.; Melinte, S.; Detrembleur, C.; Jérôme, C. *Chem. Commun.* **2015**, *51*, 9301–9304.

11. Gallagher, N. M.; Olankitwanit, A.; Rajca, A. *J. Org. Chem.* **2015**, *80*, 1291–1298.
12. Saito, K.; Hirose, K.; Okayasu, T.; Nishide, H.; Hearn, M. T. W. *RSC Adv.* **2013**, *3*, 9752–9756.
13. Liu, S.; Chu, X.; Wang, H.; Zhao, F.; Tang, E. *Ind. Eng. Chem. Res.* **2015**, *54*, 5475–5480.
14. Kunz, T. K.; Wolf, M. O. *Polym. Chem.* **2011**, *2*, 640–644.
15. Rostro, L.; Baradwaj, A. G.; Boudouris, B. W. *ACS Appl. Mater. Interfaces* **2013**, *5*, 9896–9901.
16. Rostro, L.; Wong, S. H.; Boudouris, B. W. *Macromolecules* **2014**, *47*, 3713–3719.
17. Yonekuta, Y.; Susuki, K.; Oyaizu, K.; Honda, K.; Nishide, H. *J. Am. Chem. Soc.* **2007**, *129*, 14128–14129.
18. Yonekuta, Y.; Honda, K.; Nishide, H. *Polym. Adv. Technol.* **2008**, *19*, 281–284.
19. Suga, T.; Aoki, K.; Nishide, H. *ACS Macro Lett.* **2015**, *4*, 892–896.
20. Suguro, M.; Iwasa, S.; Nakahara, K. *Macromol. Rapid Commun.* **2008**, *29*, 1635–1639.
21. Qu, J.; Katsumata, T.; Satoh, M.; Wada, J.; Masuda, T. *Polymer* **2009**, *50*, 391–396.
22. Wang, Y.-H.; Hung, M.-K.; Lin, C.-H.; Lin, H.-C.; Lee, J.-T. *Chem. Commun.* **2011**, *47*, 1249–1251.
23. Hung, M.-K.; Wang, Y.-H.; Lin, C.-H.; Lin, H.-C.; Lee, J.-T. *J. Mater. Chem.* **2012**, *22*, 1570–1577.
24. Janoschka, T.; Teichler, A.; Krieg, A.; Hager, M. D.; Schubert, U. S. *J. Polym. Sci., Part A: Polym. Chem.* **2012**, *50*, 1394–1407.
25. Suga, T.; Sakata, M.; Aoki, K.; Nishide, H. *ACS Macro Lett.* **2014**, *3*, 703–707.

26. Ernould, B.; Devos, M.; Bourgeois, J.-P.; Rolland, J.; Vlad, A.; Gohy, J.-F. *J. Mater. Chem. A* **2015**, *3*, 8832–8839.
27. Kemper, T. W.; Larsen, R. E.; Gennett, T. *J. Phys. Chem. C* **2015**, *119*, 21369–21375.
28. Suga, T.; Sugita, S.; Ohshiro, H.; Oyaizu, K.; Nishide, H. *Adv. Mater.* **2011**, *23*, 751–754.
29. Qu, J.; Fujii, T.; Katsumata, T.; Suzuki, Y.; Shiotsuki, M.; Sanda, F.; Satoh, M.; Wada, J.; Masuda, T. *J. Polym. Sci., Part A: Polym. Chem.* **2007**, *45*, 5431–5445.
30. Nesvadba, P.; Bugnon, L.; Maire, P.; Novák, P. *Chem. Mater.* **2010**, *22*, 783–788.
31. Suga, T.; Pu, Y.-J.; Kasatori, S.; Nishide, H. *Macromolecules* **2007**, *40*, 3167–3173.
32. Suga, T.; Ohshiro, H.; Sugita, S.; Oyaizu, K.; Nishide, H. *Adv. Mater.* **2009**, *21*, 1627–1630.
33. Price, J. T.; Paquette, J. A.; Harrison, C. S.; Bauld, R.; Fanchini, G.; Gilroy, J. B. *Polym. Chem.* **2014**, *5*, 5223–5226.
34. Gilroy, J. B.; McKinnon, S. D. J.; Koivisto, B. D.; Hicks, R. G. *Org. Lett.* **2007**, *9*, 4837–4840.
35. Takahashi, Y.; Hayashi, N.; Oyaizu, K.; Honda, K.; Nishide, H. *Polym. J.* **2008**, *40*, 763–767.
36. Katsumata, T.; Qu, J.; Shiotsuki, M.; Satoh, M.; Wada, J.; Igarashi, J.; Mizoguchi, K.; Masuda, T. *Macromolecules* **2008**, *41*, 1175–1183.
37. Oyaizu, K.; Ando, Y.; Konishi, H.; Nishide, H. *J. Am. Chem. Soc.* **2008**, *130*, 14459–14461.

38. Sukegawa, T.; Omata, H.; Masuko, I.; Oyaizu, K.; Nishide, H. *ACS Macro Lett.* **2014**, *3*, 240–243.
39. Jähnert, T.; Häupler, B.; Janoschka, T.; Hager, M. D.; Schubert, U. S. *Macromol. Rapid Commun.* **2014**, *35*, 882–887.
40. Paré, E. C.; Brook, D. J. R.; Brieger, A.; Badik, M.; Schinke, M. *Org. Biomol. Chem.* **2005**, *3*, 4258–4261.
41. Ren, L.; Zhang, J.; Bai, X.; Hardy, C. G.; Shimizu, K. D.; Tang, C. *Chem. Sci.* **2012**, *3*, 580–583.
42. Love, J. A.; Morgan, J. P.; Trnka, T. M.; Grubbs, R. H. *Angew. Chem. Int. Ed.* **2002**, *41*, 4035–4037.
43. Hanack, M.; Stihler, P. *Eur. J. Org. Chem.* **2000**, *2000*, 303–311.
44. Jung, R.; Hanack, M. *Synth. Met.* **1999**, *102*, 1526.
45. Sheldrick, G. M. *Acta Crystallogr., Sect. C: Struct. Chem.* **2015**, *71*, 3–8.
46. Sheldrick, G. M. *Acta Crystallogr., Sect. A: Found. Adv.* **2015**, *71*, 3–8.
47. *CRC Handbook of Chemistry and Physics*. 94th ed.; CRC Press: Boca Ranton, FL, 2013.
48. Gilroy, J. B.; Koivisto, B. D.; McDonald, R.; Ferguson, M. J.; Hicks, R. G. *J. Mater. Chem.* **2006**, *16*, 2618–2624.
49. Brook, D. J. R.; Yee, G. T. *J. Org. Chem.* **2006**, *71*, 4889–4895.
50. Gilroy, J. B.; McKinnon, S. D. J.; Kennepohl, P.; Zsombor, M. S.; Ferguson, M. J.; Thompson, L. K.; Hicks, R. G. *J. Org. Chem.* **2007**, *72*, 8062–8069.
51. Chemistruck, V.; Chambers, D.; Brook, D. J. R. *J. Org. Chem.* **2009**, *74*, 1850–1857.

52. Anderson, K. J.; Gilroy, J. B.; Patrick, B. O.; McDonald, R.; Ferguson, M. J.; Hicks, R. G. *Inorg. Chim. Acta* **2011**, *374*, 480–488.

Chapter 4

4 Synthesis, Characterization, and Preceramic Properties of π -Conjugated Polymers Based on Ni(II) Complexes of Goedken's Macrocycle

Adapted from:

J. A. Paquette, E. R. Sauv , and J. B. Gilroy* *Macromol. Rapid Commun.* **2015**, *36*, 621–626.

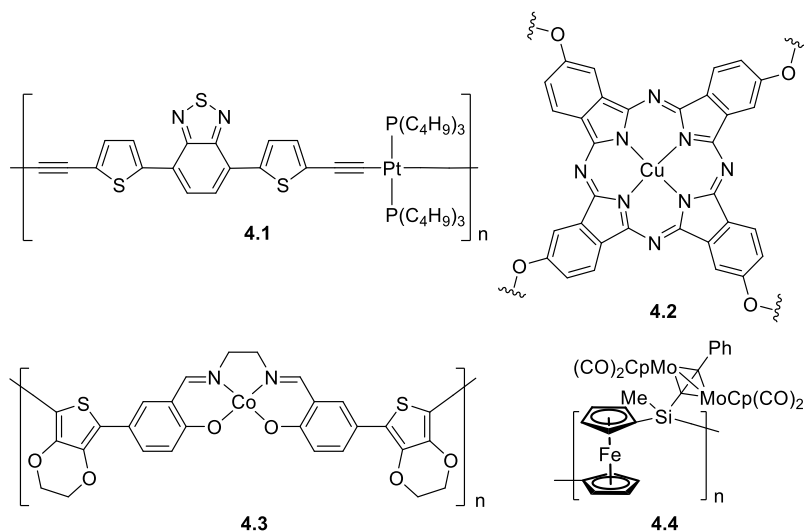
J. A. Paquette, J. G. Gilroy* *J. Polym. Sci., Part. A: Polym Chem.* **2016**, *54*, 3257–3266.

4.1 Introduction

Metallopolymers,¹⁻¹⁰ which combine the processability of macromolecules and the properties of transition metals, are an intriguing class of functional materials. As a result of these combined traits, metallopolymers have been used extensively, for example, as redox-active,¹¹⁻¹⁶ magnetic,¹⁷⁻²² and luminescent materials.²³⁻²⁷

The introduction of metals into π -conjugated polymer frameworks affords the ability to further expand their functionality.²⁸⁻³⁴ One of the most well-studied classes of π -conjugated metallopolymers are metal-polyynes.^{30, 35-38} Wong and co-workers have previously described platinum-based systems (*e.g.*, **4.1**) with π -conjugation along the polymer backbone and demonstrated their utility in photovoltaic devices³⁷ and as pre-ceramic materials.³⁸⁻⁴⁰ Another widely explored family of polymers based on π -conjugated units contain porphyrins and phthalocyanine complexes.⁴¹⁻⁴⁵ For example, Paik and co-workers realized a Cu(II)-containing phthalocyanine polymer (**4.2**) via intramolecular macrocyclization reactions in order to create single chain nanoparticles.⁴⁵ π -Conjugated metallopolymers composed of Schiff bases coordinated to transition metals have also shown widespread utility.^{28, 46-53} Notably, Swager and colleagues have reported polymers based on salen ligands coordinated to cobalt (*e.g.*, **4.3**) and demonstrated their utility as nitric oxide sensors.⁴⁸⁻⁴⁹

Most metallopolymers contain one metal atom in their repeating unit, which can limit their utility in some applications, including as pre-ceramic materials. The introduction of additional transition metal atoms to polymer scaffolds can afford highly metallized polymers.^{38, 54-58} One such example was synthesized by Manners and co-workers, where molybdenum cyclopentadienyl (Cp) carbonyl was used to append two MoCp(CO)₂ groups to each repeating unit of the backbone of a polyferrocenylsilane (**4.4**) to produce metallopolymers with utility in UV-photolithography applications.⁵⁴



Herein, we present a series of π -conjugated polymers containing Ni(II) complexes of Goedken's macrocycle and their comprehensive characterization, including comparison to model compounds. These copolymers have been specifically targeted in an effort to combine the redox and charge transfer properties of Ni(II)-complexes of Goedken's macrocycle⁵⁹⁻⁶⁰ with common traits associated with π -conjugated organic polymers (*e.g.*, low band-gaps, charge transport properties).^{28, 35, 61} Furthermore, we describe post-polymerization reactions used to transform one of the copolymers into a heterobimetallic polymer and its use as a pre-ceramic material.

4.2 Experimental

4.2.1 General Considerations

Reactions and manipulations were carried out under a nitrogen atmosphere using standard Schlenk or glove box techniques unless otherwise stated. Solvents were obtained from

Caledon Laboratories, dried using an Innovative Technologies Inc. solvent purification system, collected under vacuum, and stored under a nitrogen atmosphere over 4 Å molecular sieves. Reagents were purchased from Sigma-Aldrich, Alfa Aesar, or Oakwood Chemical and used as received unless otherwise stated. 4-[(trimethylsilyl)ethynyl]-benzoyl chloride,⁶² tetramethyldibenzo-tetraaza[14]annulene nickel(II),⁶³ 2,7-dibromo-9,9-dihexylfluorene,⁶⁴ 2-bromo-9,9-dihexylfluorene,⁶⁴ 2,5-dibromo-3-hexylthiophene⁶⁵, and 1,4-dibromo-2,5-bis(hexyloxy)benzene⁶⁶ were prepared according to previously published protocols. NMR Spectra were recorded on a 600 MHz (¹H: 599.3 MHz, ¹³C{¹H}: 150.7 MHz) Varian INOVA instrument or a 400 MHz (¹H 400.1 MHz, ¹³C{¹H}: 100.6 MHz) Varian Mercury instrument. ¹H NMR spectra were referenced to residual CHCl₃ (7.27 ppm) and ¹³C{¹H} NMR spectra were referenced to CDCl₃ (77.0 ppm). Mass spectrometry data were recorded in positive-ion mode with a Bruker microTOF II instrument using electrospray ionization. UV-vis absorption spectra were recorded in CH₂Cl₂ solutions using a Cary 300 Scan instrument. Four separate concentrations were run for each sample and molar extinction coefficients were determined from the slope of a plot of absorbance against concentration. FT-IR spectra were recorded on a PerkinElmer Spectrum Two instrument using an attenuated total reflectance accessory or as KBr pellets using a Bruker Vector 33 FT-IR spectrometer. Powder XRD diffractograms were acquired using an Inel CPS powder diffractometer with an Inel XRG 3000 generator and Inel CPS 120 detector using a CuK α radiation source. Elemental analyses (C, H, N) were carried out by Laboratoire d'Analyse Élémentaire de l'Université de Montréal, Montréal, QC, Canada.

4.2.2 Microwave Reactions

Microwave reactions were carried out in a 400 W Biotage Initiator 2.0 microwave reactor. A 5 mL glass vial was charged with the relevant solid or degassed liquid reagents/solvents, sealed in an inert atmosphere glove box, and subjected to microwave irradiation as described below.

4.2.3 Gel Permeation Chromatography (GPC)

GPC experiments were conducted in chromatography-grade THF at concentrations of 5 mg mL⁻¹ using a Viscotek GPCmax VE 2001 GPC instrument equipped with an Agilent

PolyPore guard column (PL1113-1500) and two sequential Agilent PolyPore GPC columns packed with porous poly(styrene-*co*-divinylbenzene) particles (MW range: 200–2,000,000 g mol⁻¹; PL1113-6500) regulated at a temperature of 30 °C. Signal responses were measured using a Viscotek VE 3580 RI detector, and molecular weights were determined by comparison of the maximum RI response with a calibration curve (10 points, 1,500–786,000 g mol⁻¹) established using monodisperse polystyrene standards purchased from Viscotek.

4.2.4 Thermal Analysis and Pyrolysis Studies

Thermal degradation studies were performed using a TA Instruments Q50 TGA. Samples were placed in platinum pan and heated at a rate of 10 °C min⁻¹ from 25 to 800/1000 °C under a flow of nitrogen (60 mL min⁻¹). Differential scanning calorimetry (DSC) traces were acquired on a TA Instruments DSC Q20 instrument. The polymer samples were placed in an aluminum T_{zero} pan and heated from room temperature to 150/250 °C at 10 °C min⁻¹ under a flow of nitrogen (50 mL min⁻¹) and cooled down to 0/–50 °C at 10 °C min⁻¹, before they underwent two more heating/cooling cycles.

Thin films of **4.10F** and **4.10F-[Co₂(CO)₆]₂** were prepared by drop-casting 250 μL of a 20 mg mL⁻¹ solution of each polymer in chlorobenzene onto a silicon wafer (area = 1 cm²). The samples were dried in air, transferred to a vacuum oven, and further dried under vacuum at 60 °C for 16 h before they were heated at a rate of 10 °C min⁻¹ to a temperature of 800 °C under a gentle flow of N₂/H₂ (95:5) in a quartz tube within a Lindberg Blue M tube furnace. The temperature was maintained at 800 °C for an additional 3 h before the furnace was cooled to room temperature at a rate of 10 °C min⁻¹. The samples were analyzed directly using scanning electron microscopy (SEM) at 1 keV beam energy and elemental analysis was performed at 10 keV beam energy on a LEO (Zeiss) 1540XB with an equipped Oxford X-sight X-ray detector and INCA analysis software at the Western Nanofabrication Facility.

4.2.5 Electrochemical Methods

CV experiments were performed with a Bioanalytical Systems Inc. (BASi) Epsilon potentiostat and analyzed using BASi Epsilon software. Typical electrochemical cells consisted of a three-electrode setup including a glassy carbon working electrode, platinum wire counter electrode, and silver wire *pseudo* reference electrode. Experiments were run at a scan rate of 100 mV s^{-1} in dry and degassed CH_2Cl_2 solutions of the analyte ($\sim 1 \text{ mM}$) and electrolyte ($0.1 \text{ M } [n\text{Bu}_4\text{N}][\text{PF}_6]$). CVs were internally referenced against the ferrocene/ferrocenium redox couple ($\sim 1 \text{ mM}$ internal standard) and corrected for internal cell resistance using the BASi Epsilon software.

4.2.6 X-ray Crystallography Details

A crystal of monomer **4.7** was mounted on a MiTeGen polyimide micromount with a small amount of Paratone-N oil. All X-ray measurements were made on a Bruker Kappa Axis Apex2 diffractometer at a temperature of 110 K. The unit cell dimensions were determined from a symmetry constrained fit of 9769 reflections with $6.16^\circ < 2\theta < 68.84^\circ$. The data collection strategy was a number of w and j scans which collected data up to 69.238° (2θ). The frame integration was performed using SAINT.⁶⁷ The resulting raw data was scaled and absorption corrected using a multi-scan averaging of symmetry equivalent data using SADABS.⁶⁸ The structure was solved by using a dual space methodology using the SHELXT program.⁶⁹ All non-hydrogen atoms were obtained from the initial solution. The hydrogen atoms were introduced at idealized positions and were allowed to ride on the parent atom. The structural model was fit to the data using full matrix least-squares based on F^2 . The calculated structure factors included corrections for anomalous dispersion from the usual tabulation. The structure was refined using the SHELXL-2014 program from the SHELX suite of crystallographic software.⁷⁰ Additional crystallographic data can be found in Table 4.1.

Table 4.1 Crystallography data for compound solid state structure of **4.7**.

Chemical Formula	$C_{42.50}H_{33}Cl_5N_4NiO_2$
Formula Weight (<i>g/mol</i>)	867.69
Crystal Dimensions (<i>mm</i>)	$0.494 \times 0.270 \times 0.126$
Crystal Color and Habit	green plate
Crystal System	monoclinic
Space Group	$P 2_1/c$
Temperature (K)	110
<i>a</i> (Å)	14.480(6)
<i>b</i> (Å)	16.295(4)
<i>c</i> (Å)	17.868(7)
α (°)	90
β (°)	112.466(16)
γ (°)	90
<i>V</i> (Å ³)	3896(2)
<i>Z</i>	4
ρ (<i>g/cm</i>)	1.483
λ , Å, (MoK α)	0.71073
μ , (<i>cm</i> ⁻¹)	0.884
Diffractometer Type	Bruker Kappa Axis Apex2
R_{merge}	0.0545
$R_1^{a)}$ [$2\sigma I > 2$]	0.0513
$wR_2^{b)}$ [$2\sigma I > 2$]	0.1277
R_1 (all data)	0.0776
wR_2 (all data)	0.1421
GOF	1.034

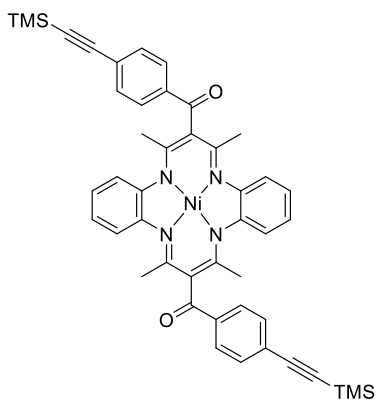
$$^a)R_1 = \Sigma (|F_o| - |F_c|) / \Sigma F_o$$

$$^b)wR_2 = [\Sigma (w(F_o^2 - F_c^2)^2) / \Sigma (w F_o^4)]^{1/2}$$

$$GOF = [\Sigma (w(F_o^2 - F_c^2)^2) / (No. of reflns. - No. of params.)]^{1/2}$$

4.2.7 Synthetic Procedures

Synthesis of complex **4.6**

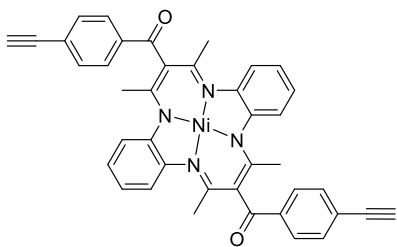


A Schlenk flask equipped with a stir bar was charged with complex **4.5** (0.81 g, 2.0 mmol), 4-[(trimethylsilyl)ethynyl]benzoyl chloride (1.00 g, 4.22 mmol) and dry toluene (90 mL) in a glove box before it was sealed and removed from the glove box. Et₃N (4.2 mL, 3.1 g, 30 mmol) was added and the vessel was fitted with a condenser and heated to 125 °C. After stirring for 16 h, the mixture was cooled to 20 °C and filtered *in vacuo*. The

solvent was then removed to yield a dark green solid. Precipitation of a saturated CH₂Cl₂ solution in pentane afforded TMS-substituted complex **4.6** as a green solid. Yield = 1.54 g, 96%. ¹H NMR (400.1 MHz, CDCl₃): δ 8.18 (d, 4H, ³J_{HH} = 8 Hz, aryl CH), 7.66 (d, 4H,

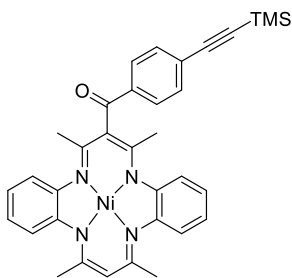
$^3J_{\text{HH}} = 8$ Hz, aryl *CH*), 6.67–6.59 (m, 8H, aryl *CH*), 1.90 (s, 12H, *CH*₃), 0.29 (s, 18H, Si*CH*₃). $^{13}\text{C}\{^1\text{H}\}$ NMR (100.6 MHz, CDCl₃) δ 199.5, 153.8, 147.2, 138.5, 132.5, 129.5, 128.3, 122.8, 121.9, 120.9, 104.1, 98.5, 20.5, -0.2. IR (KBr): $\nu = 2957$ (w, CH), 2158 (w, C \equiv C), 1653 (m, C=O), 1598 (m), 1533 (s), 1457 (m), 1429 (m), 1380 (s), 1054(m), 855 (s), 746 (m) cm⁻¹. UV-vis (CH₂Cl₂): λ_{max} (ϵ) 587 nm (5,975 M⁻¹ cm⁻¹), 435 nm (sh, 12,275 M⁻¹ cm⁻¹), 389 nm (30,075 M⁻¹ cm⁻¹), 300 nm (73,875 M⁻¹ cm⁻¹), 286 nm (78,775 M⁻¹ cm⁻¹). Mass Spec. (ESI, +ve mode) m/z : [M + H⁺] calcd for [C₄₆H₄₇N₄NiO₂Si₂]⁺, 801.2591; found, 801.2584; difference: -0.9 ppm. Anal. Calcd for C₄₆H₄₆N₄NiO₂Si₂: C, 68.91; H, 5.78, N, 6.99; found: C, 68.03, H, 5.83; N, 6.92.

Synthesis of monomer 4.7



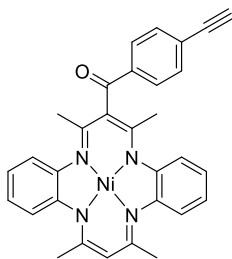
TMS-protected complex **4.6** (1.88 g, 2.34 mmol) was stirred with K₂CO₃ (1.30 g, 9.38 mmol) in THF/MeOH (3:1, 80 mL) for 16 h. CH₂Cl₂ was added and the organic layer was washed with 0.5 M aqueous NH₄Cl, dried with MgSO₄ and concentrated *in vacuo*. The resulting dark green solid was purified via column chromatography (silica gel, hexanes/EtOAc [8:2]), and precipitated from a saturated CH₂Cl₂ solution in pentane to afford compound **4.7** as a dark green microcrystalline solid. Yield = 1.39 g, 90%. ^1H NMR (400.1 MHz, CDCl₃): δ 8.21 (d, 4H, $^3J_{\text{HH}} = 8$ Hz, aryl *CH*), 7.70 (d, 4H, $^3J_{\text{HH}} = 8$ Hz, aryl *CH*), 6.68–6.60 (m, 8H, aryl *CH*), 3.31 (s, 2H, *CH*), 1.91 (s, 12H, *CH*₃). $^{13}\text{C}\{^1\text{H}\}$ NMR (100.6 MHz, CDCl₃): δ 199.4, 153.8, 147.2, 138.9, 132.7, 129.6, 127.2, 122.8, 121.8, 120.8, 82.9, 80.6, 20.5. IR (KBr): $\nu = 3284$ (w, C \equiv CH), 1656 (s, C=O), 1599 (m), 1533 (s), 1431 (m), 1380 (s), 1055 (m), 855 (s), 748 (m) cm⁻¹. UV-vis (CH₂Cl₂): λ_{max} (ϵ) 583 nm (6,525 M⁻¹ cm⁻¹), 389 nm (31,475 M⁻¹ cm⁻¹), 262 nm (76,900 M⁻¹–cm⁻¹). Mass Spec. (ESI, +ve mode) m/z : [M + H⁺] calcd for [C₄₀H₃₁N₄NiO₂]⁺: 657.1800; found: 657.1802; difference: +0.3 ppm. Anal. Calcd for C₄₀H₃₀N₄NiO₂: C, 73.08, H, 4.60, N, 8.52; found: C, 72.23, H, 4.46, N, 8.41.

Synthesis of complex 4.8



A Schlenk flask equipped with a stir bar was charged with complex **4.5** (1.68 g, 4.19 mmol), 4-[(trimethylsilyl)ethynyl]benzoyl chloride (1.00 g, 4.19 mmol) and dry toluene (100 mL) in a glove box. Upon removal, dry and degassed Et₃N (4.67 mL, 33.5 mmol) was added and the vessel was fitted with a condenser and heated to 125 °C. After stirring for 16 h, the mixture was cooled to room temperature and filtered *in vacuo*. The solvent was then removed. Column chromatography (CH₂Cl₂/Hexanes, 2:1, 100 mL silica gel) was performed to yield complex **4.8** as a dark green solid. Yield = 0.57 g, 23% yield (and **4.7**; 1.26 g, 38%). ¹H NMR (400.1 MHz, CDCl₃): δ 8.15 (d, 2H, *J*_{HH} = 8 Hz, aryl *CH*), 7.61 (d, 2H, *J*_{HH} = 8 Hz, aryl *CH*), 6.72 (dd, 2H, *J*_{HH} = 8, 1 Hz, aryl *CH*) 6.62–6.60 (m, 4H, aryl *CH*), 6.57–6.55 (m, 2H, aryl *CH*), 4.86 (s, 1H, *CH*), 2.10 (s, 6H, *CH*₃), 1.88 (s, 6H, *CH*₃), 0.28 (s, 9H, Si*CH*₃). ¹³C{¹H} NMR (100.6 MHz, CDCl₃) δ 199.5, 155.4, 153.8, 147.4, 147.2, 138.6, 132.4, 129.5, 128.1, 122.9, 121.8, 121.7, 120.9, 120.5, 111.3, 104.2, 98.3, 21.9, 20.7, -0.2. FT-IR (ATR): ν = 2957 (w, CH), 2158 (w, C≡C), 1638 (m, C=O), 1596 (m), 1529 (s), 1453 (m), 1430 (m), 1381 (s), 1168 (m), 1215 (s), 1168 (m), 913 (m), 840 (m), 743 (m) cm⁻¹. UV-vis (CH₂Cl₂): λ_{max} (ε) 589 nm (5,500 M⁻¹ cm⁻¹), 433 nm (sh, 14,100 M⁻¹ cm⁻¹), 392 nm (33,400 M⁻¹ cm⁻¹), 301 nm (sh, 52,800, M⁻¹ cm⁻¹), 285 nm (60,800 M⁻¹ cm⁻¹). Mass Spec. (ESI, +ve mode) *m/z*: [M]⁺ calc'd for [C₃₄H₃₄N₄NiOSi]⁺, 600.1855; found, 600.1853; difference: -0.3 ppm.

Synthesis of complex 4.9



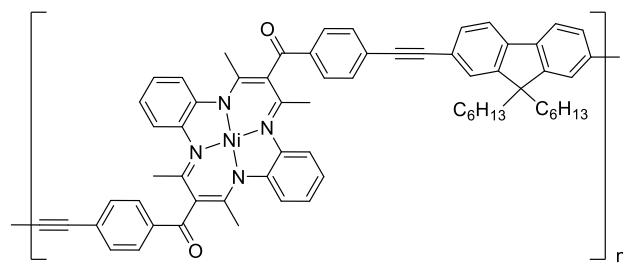
Complex **4.8** (0.20 g, 0.33 mmol) was stirred with K₂CO₃ (0.09 g, 0.7 mmol) in THF/MeOH (3:1, 16 mL) for 16 h. CH₂Cl₂ was added and the organic layer was washed with 0.5 M aqueous NH₄Cl (50 mL), dried with MgSO₄ and concentrated *in vacuo*. The resulting dark green solid was purified via precipitation from a saturated CH₂Cl₂ solution in pentane to afford **4.9** as a dark green microcrystalline solid. Yield = 0.14 g, 81%. ¹H NMR (400.1 MHz, CDCl₃): δ 8.18 (d, 2H, *J*_{HH} = 7 Hz, aryl *CH*), 7.65 (d, 2H, *J*_{HH} = 8 Hz,

aryl *CH*), 6.73 (d, 2H, $J_{\text{HH}} = 8$ Hz) 6.62–6.60 (m, 4H, aryl *CH*), 6.57–6.56 (m, 2H, aryl *CH*) 4.87 (s, 1H, *CH*), 3.28 (s, 1H, $\text{C}\equiv\text{C}-\text{H}$), 2.10 (s, 6H, CH_3), 1.90 (s, 6H, CH_3). $^{13}\text{C}\{^1\text{H}\}$ NMR (100.6 MHz, CDCl_3) δ 199.4, 155.4, 153.8, 147.4, 147.1, 139.0, 132.6, 129.5, 127.0, 123.0, 121.8, 121.7, 120.9, 120.4, 111.2, 82.9, 80.5, 21.9, 20.7. FT-IR (ATR): $\nu = 3301$ (w), 1663 (w, $\text{C}=\text{O}$), 1597 (w), 1530 (m), 1454 (m), 1429 (m), 1382 (s), 1365 (s), 1217 (m), 1166 (m), 1054 (m), 913 (m), 853 (s), 772 (m), 746 (s), 645 (m), 617 (m) cm^{-1} . UV-vis (CH_2Cl_2): λ_{max} (ϵ) 588 nm (4,100 $\text{M}^{-1} \text{cm}^{-1}$), 427 nm (sh, 9,200 $\text{M}^{-1} \text{cm}^{-1}$), 392 nm (23,700 $\text{M}^{-1} \text{cm}^{-1}$), 274 nm (33,700 $\text{M}^{-1} \text{cm}^{-1}$). Mass Spec. (ESI, +ve mode) m/z : $[\text{M}]^+$ calc'd for $[\text{C}_{31}\text{H}_{26}\text{N}_4\text{NiO}]^+$, 528.1460; found, 528.1452; difference: -1.5 ppm.

General synthetic procedure for copolymers 4.10F, 4.10T, and 4.10B

Compound **4.7** (0.10 g, 0.15 mmol), dibromoaryl monomer (0.15 mmol), $\text{Pd}(\text{PPh}_3)_4$ (0.004 g, 0.004 mmol, 10%) and CuI (0.002 g, 0.008 mmol, 5%) were combined in a microwave vial. The solvent mixture, 3 mL $\text{DMF}/\text{DIPA}/\text{H}_2\text{O}$ (2:1:0.03), was degassed by three freeze-pump-thaw cycles, brought into a glove box and added to the solids. The reaction vessel was sealed before it was heated to 100 °C for 60 min in a microwave reactor. The resulting dark green solution was diluted with CH_2Cl_2 (20 mL), filtered and column chromatography was performed (CH_2Cl_2 , 20 mL silica gel). The solvent was then removed and the resulting residue was dried overnight under vacuum. The solid was dissolved in *ca.* 2 mL CH_2Cl_2 and precipitated into Et_2O (3×100 mL) and pentane (2×50 mL), dried, dissolved in THF (*ca.* 5 mL) and precipitated into MeOH (2×50 mL). The resulting dark green polymers were isolated by centrifugation and dried overnight under vacuum.

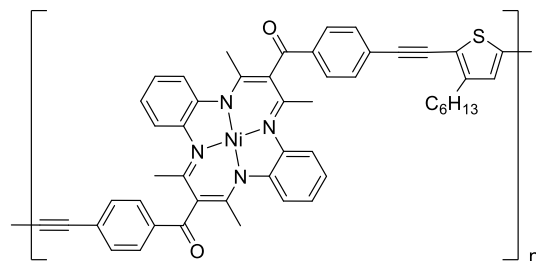
Copolymer 4.10F



From 2,7-dibromo-9,9-dihexylfluorene (0.20 g, 0.30 mmol). Yield = 0.16 g, 56%. ^1H NMR (399.8 MHz, CDCl_3): δ 8.25 (m, 4H, aryl *CH*), 7.75 (m, 6H, aryl *CH*), 7.58 (m, 4H, aryl *CH*), 6.66 (m, 8H, aryl *CH*), 2.02 (m, 4H, CH_2), 1.95 (s, 12H, CH_3), 1.09 (m, 12H, CH_2), 0.79 (t, 6H, $J_{\text{HH}} = 7.03$ Hz, CH_3), 0.65 (m, 4H, CH_2). IR (KBr): $\nu = 3426$ (w, $\text{C}\equiv\text{C}$), 2949 (w), 2926

(w), 2855 (w) 1654 (m, C=O), 1596 (m), 1532 (s), 1431 (m), 1381 (s), 1055 (m), 853 (s), 747 (m) cm^{-1} . UV-vis (CH_2Cl_2): λ_{max} (ϵ) = 588 nm ($6,000 \text{ M}^{-1} \text{ cm}^{-1}$), 378 nm ($100,750 \text{ M}^{-1} \text{ cm}^{-1}$), 275 nm ($50,850 \text{ M}^{-1} \text{ cm}^{-1}$).

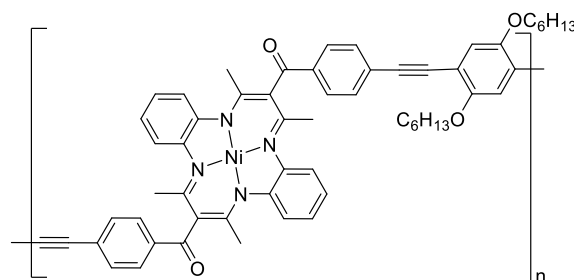
Copolymer 4.10T



From 2,5-dibromo-3-hexylthiophene (0.050 g, 0.15 mmol). Yield = 0.075 g, 60%. ^1H NMR (599.3 MHz, CDCl_3) δ 8.23 (4H, br s, aryl CH), 7.72–7.70 (4H, m, aryl CH), 7.18 (1H, s, thiophene-CH), 6.67–6.62 (8H, m, aryl CH),

2.81–2.77 (2H, t, $J_{\text{HH}} = 8 \text{ Hz}$, CH_2), 1.93 (12H, br s, CH_3), 1.74–1.69 (2H, m, CH_2), 1.40–1.29 (6H, m, CH_2), 0.93–0.89 (3H, m, CH_3). FT-IR (ATR): $\nu = 2953$ (w sh), 2926 (w), 2854 (w) 1655 (m, C=O), 1596 (m), 1527 (s), 1488 (w), 1449 (w), 1429 (m), 1362 (s), 1217 (m), 1168 (m), 1053 (w), 1013 (w), 911 (m), 852 (s), 743 (m) cm^{-1} . UV-vis (CH_2Cl_2): λ_{max} (ϵ) = 590 nm ($5,700 \text{ M}^{-1} \text{ cm}^{-1}$), 387 nm ($74,300 \text{ M}^{-1} \text{ cm}^{-1}$), 272 nm ($45,900 \text{ M}^{-1} \text{ cm}^{-1}$). GPC (THF, conventional calibration): $M_n = 6,575 \text{ g mol}^{-1}$, $M_w = 18,250 \text{ g mol}^{-1}$, $D = 2.77$.

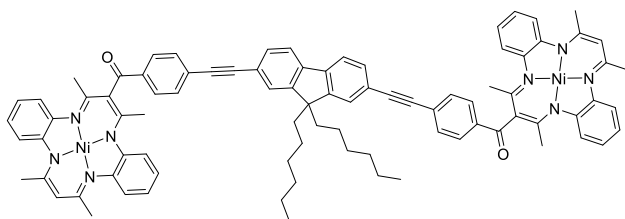
Copolymer 4.10B



From 1,4-dibromo-2,5-bis(hexyloxy)benzene (0.066 g, 0.15 mmol). Yield = 0.081 g, 57%. ^1H NMR (599.3 MHz, CDCl_3) δ 8.22–8.15 (4H, m, aryl CH), 7.74–7.72 (4H, m, aryl CH), 7.08 (2H, s, aryl CH), 6.68–6.62 (8H, m, aryl

CH), 4.11–4.00 (4H, m, OCH_2), 1.94 (12H, br. s, CH_3), 1.91–1.88 (4H, m, CH_2), 1.61–1.49 (4H, m, CH_2), 1.42–1.34 (8H, m, CH_2), 0.96–0.89 (6H, m, CH_3). FT-IR (ATR): $\nu = 3407$ (w, $\text{C}\equiv\text{C}$), 2949 (w sh), 2925 (w), 2856 (w) 1655 (m, C=O), 1596 (m), 1527 (s), 1429 (m), 1362 (s), 1217 (m), 1168 (m), 1053 (w), 1013 (w), 911 (m), 852 (s), 743 (m) cm^{-1} . UV-vis (CH_2Cl_2): λ_{max} (ϵ) = 589 nm ($5,700 \text{ M}^{-1} \text{ cm}^{-1}$), 387 nm ($57,400 \text{ M}^{-1} \text{ cm}^{-1}$), 330 nm ($38,300 \text{ M}^{-1} \text{ cm}^{-1}$), 302 (sh, $41,200 \text{ M}^{-1} \text{ cm}^{-1}$), 272 ($44,100 \text{ M}^{-1} \text{ cm}^{-1}$). GPC (THF, conventional calibration): $M_n = 7,700 \text{ g mol}^{-1}$, $M_w = 13,600 \text{ g mol}^{-1}$, $D = 1.76$.

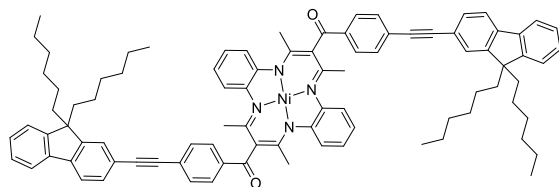
Synthesis of model compound **4.13**



Compound **4.9** (0.11 g, 0.21 mmol),
2,7-dibromo-9,9-dihexylfluorene
(0.05 g, 0.1 mmol), Pd(PPh₃)₄
(0.006 g, 0.005 mmol) and CuI

(2.0 g, 0.011 mmol) were combined in a 5 mL microwave vial. The solvent mixture, 3 mL DMF/DIPA/H₂O (2:1:0.03) was degassed by 3 freeze-pump-thaw cycles, brought into a glove box and added to the solid. The microwave vial was sealed and then heated at 100 °C for 45 min in a microwave reactor. Upon cooling, CH₂Cl₂ (10 mL) was added to the dark green solution and the entire mixture washed with H₂O (6 × 100 mL), dried with MgSO₄ and concentrated *in vacuo*. The resulting dark green residue was purified using a column chromatography (CH₂Cl₂, 25 mL silica gel) to afford **4.13** as a dark green microcrystalline solid after solvent removal *in vacuo*. Yield = 0.12 g, 83%. ¹H NMR (599.4 MHz, CDCl₃): δ 8.23 (d, 4H, ³J_{HH} = 8 Hz, aryl CH), 7.72 (m, 6H, aryl CH), 7.59–7.54 (m, 2H, aryl CH), 7.56 (s, 2H, aryl CH), 6.74 (m, 4H, aryl CH), 6.67–6.61 (m, 8H, aryl CH), 6.58–6.56 (m, 4H, aryl CH), 4.89 (s, 2H, CH), 2.12 (s, 12H, CH₃) 2.04–2.01 (m, 4H, CH₂), 1.94 (s, 12H, CH₃), 1.16–1.05 (m, 12H, CH₂), 0.78 (t, 6H, ³J_{HH} = 8 Hz, CH₃), 0.68–0.63 (m, 4H, CH₂). ¹³C{¹H} NMR (150.7 MHz, CDCl₃): δ 199.5, 155.4, 153.9, 151.3, 147.4, 147.2, 141.1, 138.4, 132.0, 131.0, 129.7, 128.5, 126.1, 122.9, 121.9, 121.8, 121.5, 120.9, 120.6, 120.2, 111.3, 94.0, 89.3, 55.4, 40.4, 31.5, 29.7, 23.7, 22.6, 21.9, 20.7, 14.0. FT-IR (ATR): ν = 2952 (s, hex CH), 2923 (s, hex CH), 2852 (s, hex CH), 1631 (m, C=O), 1595 (m), 1527 (s), 1454 (m), 1430 (m), 1381 (s), 1215 (m), 1051 (m), 1022 (m), 912 (m), 853 (m), 819 (m), 742 (m) cm⁻¹. UV-vis (CH₂Cl₂): λ_{max} (ε) = 584 nm (7,900 M⁻¹ cm⁻¹), 387 nm (91,100 M⁻¹ cm⁻¹), 273 nm (52,100 M⁻¹ cm⁻¹). Mass Spec. (ESI, +ve mode) *m/z*: [M + H]⁺ calc'd for [C₈₇H₈₃N₈Ni₂O₂]⁺, 1387.5346; found, 1387.5365; difference: +1.4 ppm.

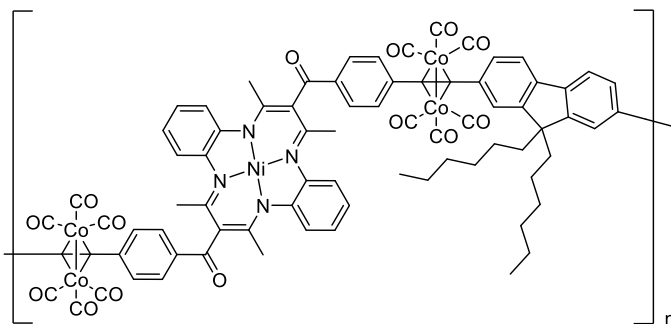
Synthesis of model complex **4.14**



Monomer **4.7** (0.08 g, 0.1 mmol), 9,9-dihexyl-6-bromofluorene (0.10 g, 0.24 mmol), Pd(PPh₃)₄ (0.007 g, 0.006 mmol) and CuI (0.002 g, 0.01 mmol)

were combined in a 5 mL microwave vial. The solvent mixture, 2 mL DMF/H₂O (100:1) and 1 mL DIPA were degassed by 3 freeze-pump-thaw cycles, brought into a glove box and added to the solid. The vessel containing the reaction mixture was sealed and then heated at 100 °C for 30 min in a microwave reactor. Upon cooling, CH₂Cl₂ was added to the dark green solution and the entire mixture washed with H₂O (6 × 100 mL), dried with MgSO₄ and concentrated *in vacuo*. The resulting dark green residue was purified using a short silica column (CH₂Cl₂ as eluent) afforded **4.14** as a dark green microcrystalline solid after solvent removal *in vacuo*. Yield = 0.13 g, 80%. ¹H NMR (400.1 MHz, CDCl₃): δ 8.25 (d, 4H, ³J_{HH} = 7 Hz, aryl CH), 7.77 (d, 4H, ³J_{HH} = 8 Hz, aryl CH), 7.73–7.71 (m, 4H, aryl CH), 7.59–7.56 (m, 4H, aryl CH), 7.37–7.34 (m, 6H, aryl CH), 6.70–6.61 (m, 8H, aryl CH), 2.00 (t, 8H, ³J_{HH} = 8 Hz, CH₂), 1.95 (s, 12H, CH₃), 1.15–1.03 (m, 24H, CH₂), 0.78 (t, 12H, ³J_{HH} = 8 Hz, CH₃), 0.63 (m, 8H, CH₂). ¹³C{¹H} NMR (100.6 MHz, CDCl₃): δ 199.5, 153.9, 151.1, 150.9, 147.3, 142.1, 140.2, 138.2, 132.0, 130.9, 129.7, 128.8, 127.7, 126.9, 126.1, 122.9, 122.8, 121.9, 120.9, 120.7, 120.1, 119.7, 94.4, 88.8, 55.2, 40.4, 31.5, 29.7, 23.7, 22.6, 20.5, 14.0. IR (KBr): ν = 3064 (w), 2954 (s, hex CH), 2923 (s, hex CH), 2855 (s, hex CH), 2205 (w), 1660 (m, C=O), 1597 (m), 1535 (s), 1382 (s), 1056 (m), 854 (s), 741 (m) cm⁻¹. UV-vis (CH₂Cl₂): λ_{max} (ε) = 587 nm (7,100 M⁻¹ cm⁻¹), 349 nm (109,150 M⁻¹ cm⁻¹), 283 nm (67 600 M⁻¹ cm⁻¹). Mass Spec. (ESI, +ve mode) *m/z*: [M]⁺ calcd for [C₉₀H₉₄N₄NiO₂]⁺, 1320.6730; found, 1320.6768; difference: -2.9 ppm. Anal. Calcd for C₉₀H₉₄N₄NiO₂: C, 81.74, H, 7.16, N, 4.24; found, C, 80.77, H, 7.40, N, 4.20.

Synthesis of copolymer **4.10F**-[Co₂(CO)₆]₂



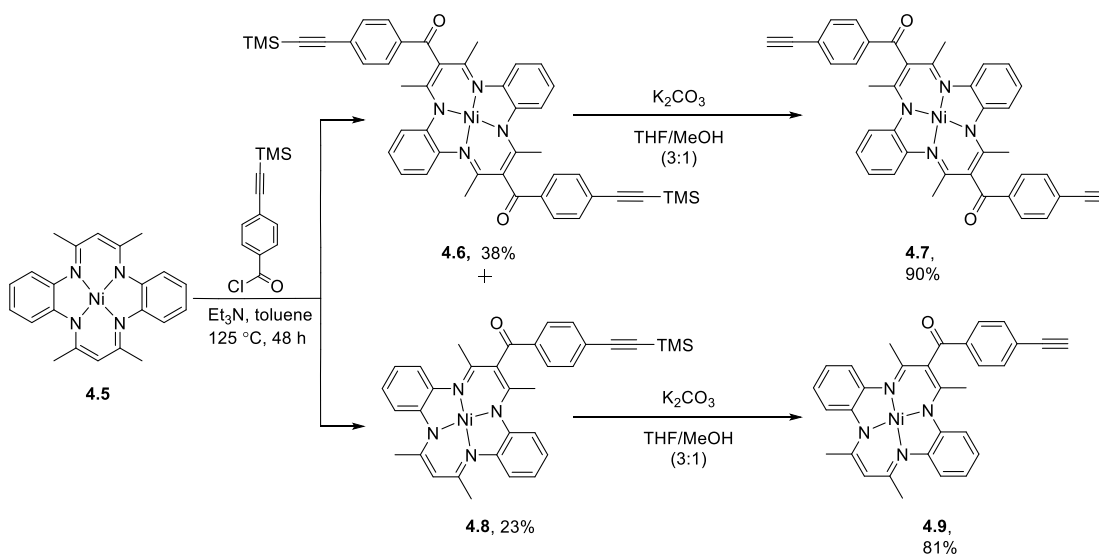
In a glovebox, **4.10F** (0.10 g, 0.10 mmol) was dissolved in 5 mL dry CH₂Cl₂. Co₂(CO)₈ (0.09 g, 0.25 mmol) was then added to the solution, causing the immediate evolution of gas. The reaction mixture was stirred at room temperature for 30 min. Once the reaction was complete, column chromatography was performed (CH₂Cl₂, 20 mL silica gel). The solvent was removed under reduced pressure, and the residue was dissolved in *ca.* 1 mL of CH₂Cl₂ and precipitated into pentane (1 × 50 mL, then 2 × 30 mL). The solvent was then decanted and the dark green solid was dried overnight under vacuum to give **4.10F**-[Co₂(CO)₆]₂ as a dark green/brown powder. Yield = 0.15 g, 95%. ¹H NMR (599.3 MHz, CDCl₃) δ 8.30–8.24 (4H, m, aryl CH), 7.84–7.49 (10H, m, aryl CH), 6.70 (4H, br. s, aryl CH), 6.62 (4 H, br. s, aryl CH), 2.00 (12H, s, CH₃), 1.94 (4H, s, CH₂), 1.33–1.08 (12H, m, CH₂), 0.90–0.71 (10H, m, CH₂, CH₃). FT-IR (ATR): ν = 2957 (m), 2920 (m), 2853 (m) 2088 (s, C=O), 2051 (s, C=O), 2019 (s, C=O), 1725 (w), 1658 (w, C=O), 1596 (w), 1551 (m), 1454 (w), 1377 (s), 1223 (m), 1055 (m), 910 (m), 799 (m), 744 (m) cm⁻¹. UV-vis (CH₂Cl₂): λ_{max} (ε) = 587 nm (9,900 M⁻¹ cm⁻¹), 385 nm (71,500 M⁻¹ cm⁻¹), 270 (85,900 M⁻¹ cm⁻¹). GPC (THF, conventional calibration): M_n = 7,700 g mol⁻¹, M_w = 10,900 g mol⁻¹, and Đ = 1.41.

4.3 Results and Discussion

4.3.1 Monomer Synthesis

In order to access the desired polymerizable macrocyclic Ni(II) complex, two equivalents of 4-[(trimethylsilyl)ethynyl]-benzoyl chloride⁶² was first combined with macrocycle **4.5** to afford complex **4.6** in 96% yield (Scheme 4.1, Figures A4.1, 4.2). The TMS protecting groups were removed by treating complex **4.6** with K₂CO₃ to afford monomer **4.7** in 90% yield (Scheme 4.1, and Figures A4.3, 4.4). Single crystals suitable for X-ray diffraction were grown via slow evaporation of a saturated CH₂Cl₂ solution of **4.7** (Figure 4.1). In the solid state, monomer **4.7** adopts a saddle-like geometry, although it must be noted that the

4-ethynylbenzoyl substituents are expected to rotate freely in solution and their orientation in the solid state may result from crystal-packing effects. The average C-C and C-N bond lengths within the -N-C(Me)-CR'-C(Me)-N- ligand backbones are 1.414 and 1.333 Å respectively, and are between the lengths of typical single and double bonds.⁷¹ The Ni(II) ion is coordinated by four nitrogen atoms with an average bond distance of 1.8550 Å in a square planar coordination environment described by angles of N1-Ni-N2 94.35(6), N2-Ni-N3 85.97(6), N3-Ni-N4 93.93(6), N1-Ni-N4 85.69(6)°. The torsion angles between the planes defined by N1-C2-C3-C4-N2 and N3-C16-C17-C18-N4 and the plane defined by the nickel-bound nitrogen atoms (N1-N2-N3-N4) are 28.29 and 29.76°, respectively.



Scheme 4.1 Synthesis of monomer **4.7** and macrocycle **4.9**.

Access to a Ni(II) complex of Goedken's macrocycle substituted with a single alkyne functionality was required in order to synthesize model complexes. Thus, a mixture of 4-[(trimethylsilyl)ethynyl]-benzoyl chloride and compound **4.5** was heated to reflux in the presence of triethylamine (Scheme 4.3). This reaction afforded a mixture of mono- (**4.8**) and di-substituted (**4.6**) macrocycles which could be separated using column chromatography, in 23 and 38% yield, respectively. The identity of complex **4.8** was confirmed by NMR spectroscopy (Figures A4.5, 4.6). Removal of the TMS group from compounds **4.8** and was achieved using potassium carbonate to afford compounds **4.9** and in 81% yield (Figures A4.7, 4.8).

Bromine-substituted 9,9-dihexylfluorene was chosen as a comonomer for **4.7** as it has been widely used in the synthesis of highly soluble π -conjugated polymers possessing interesting and useful electronic and optical properties.⁷² Comonomers 2,5-dibromo-3-hexylthiophene and 1,4-dibromo-2,5-bis(hexyloxy)benzene were also chosen due to their π -conjugated nature and ability to potentially solubilize the rigid, π -conjugated backbones of the targeted copolymers (Scheme 4.2).

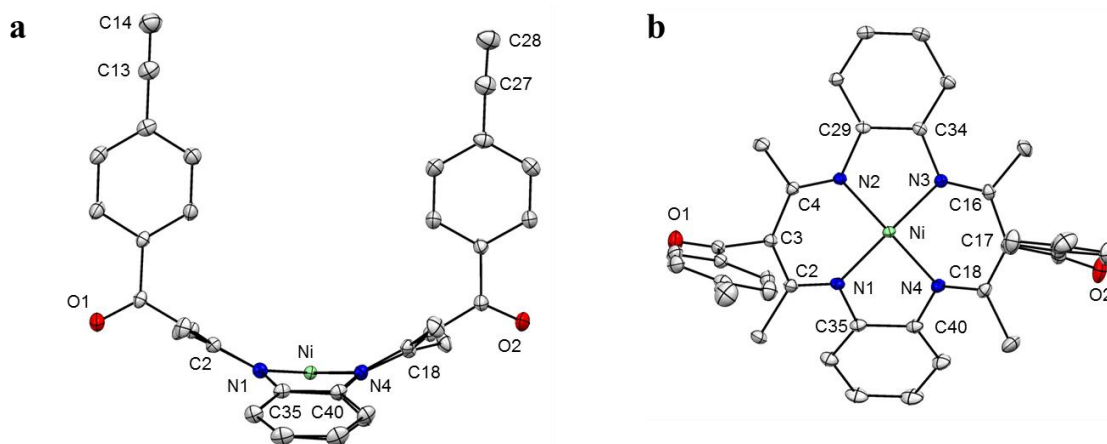
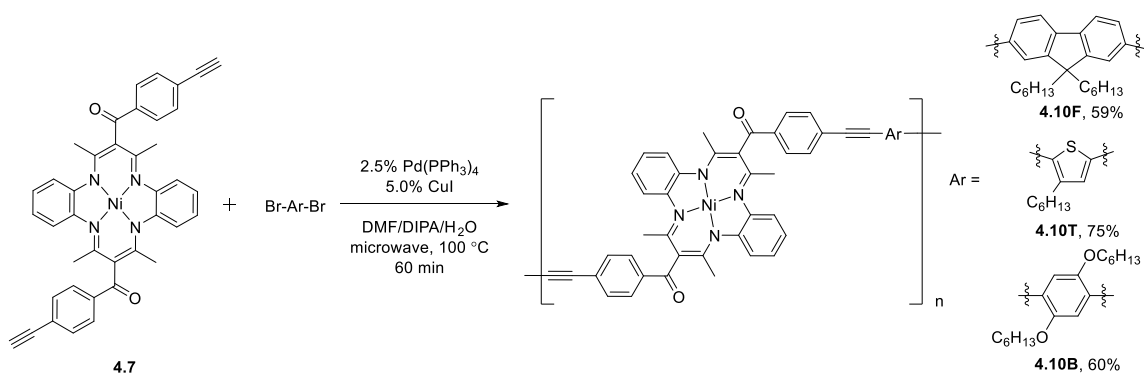


Figure 4.1 (a) Side view, and (b) top view of the solid-state structure of monomer **4.7**. Anisotropic displacement ellipsoids are shown at 50% probability. Hydrogen atoms and co-crystallized solvent molecules omitted for clarity. Selected bond lengths (Å): N1-C2 1.335(2), N1-C35 1.417(2), N1-Ni 1.8543(15), N2-C4 1.336(2), N2-C29 1.4156(19), N2-Ni 1.8590(13), N3-C16 1.333(2), N3-C34 1.4140(19), N3-Ni 1.8533(15), N4-C18 1.329(2), N4-C40 1.414(2), N4-Ni 1.8533(13), C2-C3 1.411(2), C3-C4 1.411(2), C16-C17 1.418(2), C17-C18 1.414(2). Selected bond angles (°): N1-Ni-N2 94.35(6), N2-Ni-N3 85.97(6), N3-Ni-N4 93.93(6), N1-Ni-N4 85.69(6).

4.3.2 Copolymer Synthesis

Polymers (**4.10F**, **4.10T**, and **4.10B**) containing 9,9-dihexylfluorene (**F**), 3-hexylthiophene (**T**), or 2,5-bis(hexyloxy)benzene (**B**) and a Ni(II) complex of Goedken's macrocycle (**4.5**) were synthesized using optimized polymerization conditions (Table 4.2, Scheme 4.2).⁷³ In order to optimize the copolymerization of **4.7** and **4.11** several microwave reactions were attempted. The mass balance for these reactions was typically made up of highly soluble oligomers, soluble polymers, and an unidentified insoluble gel (see below). Initially, three solvent combinations were screened for potential use in the production of polymer **4.10F** (Table 4.1, runs 1–3a). The polymers produced after 30 min of microwave irradiation at

100 °C in toluene/DIPA and DMF/DIPA had lower molecular weights than the polymer produced from a mixture of DMF/DIPA containing a small quantity of water. Using the latter solvent combination, the effect of catalyst loading on the production of polymer **4.10F** was studied (runs 4 and 5). In both cases, an increase in catalyst loading resulted in a decrease in polymer yield and molecular weight, perhaps due to the presence of an increased number of active oligomeric/polymeric species in solution.



Scheme 4.2 Synthesis of copolymers **4.10F**, **4.10B**, and **4.10T**.

Shorter and longer reaction times (runs 6 and 7) resulted in polymers with similar molecular weight distributions, but decreased yields compared to those isolated for run 3. Longer reaction times led to the formation of increased quantities of insoluble materials, while shorter reaction times led to increased quantities of oligomeric species. When the temperature was decreased to 75 °C (run 8) no reaction was observed. When the temperature was increased to 125 °C (run 9) an increased fraction of insoluble material was observed and the yield of soluble polymer was greatly diminished.

Table 4.2 Reaction conditions for the production of polymer **4.10F** (optimized conditions shown in bold).

Run	Solvent	Time (min)	Temp (°C)	Catalyst (%)		Yield (%)	M _n (g mol ⁻¹)	<i>D</i>	Gel (%)
				<i>Pd(PPh₃)₄</i>	<i>CuI</i>				
1	Toluene/DIPA	30	100	2.5	5.0	58	6,775	1.72	22
2	dry DMF/DIPA	30	100	2.5	5.0	50	5,825	1.65	22
3a	DMF/DIPA/H₂O	30	100	2.5	5.0	56	10,100	2.37	29
3b	DMF/DIPA/H₂O	30	100	2.5	5.0	59	12,050	2.43	30
3c	DMF/DIPA/H₂O	30	100	2.5	5.0	56	10,500	2.00	30
4	DMF/DIPA/H ₂ O	30	100	5.0	10.0	39	8,175	2.10	30
5	DMF/DIPA/H ₂ O	30	100	10.0	20.0	34	5,550	1.85	65
6	DMF/DIPA/H ₂ O	15	100	2.5	5.0	19	8,525	2.60	15
7	DMF/DIPA/H ₂ O	45	100	2.5	5.0	25	12,175	2.42	48
8	DMF/DIPA/H ₂ O	30	75	2.5	5.0	-	-	-	-
9	DMF/DIPA/H ₂ O	30	125	2.5	5.0	15	5,125	1.53	51

Upon completion of these experiments, we concluded that the optimal conditions for the production of polymer **4.10F** were those employed in run 3a. The reaction was performed in triplicate to demonstrate reproducibility (runs 3a–c). The average isolated yield over three runs, M_n, and *D* for the isolated polymers was 57%, 10,900 g mol⁻¹, and 2.27, respectively (Figures A4.9, 4.10). The mass balance for these reactions was made up of 12% oligomers (Figure A4.11) and 30% dark-green insoluble solid (gel). The dark-green, insoluble solid formed a gel when treated with a broad range of organic solvents. This behavior was consistent with a crosslinked structure and precluded further analysis as we were unable to purify or process the gels into powders or films. Copolymers **4.10T** and **4.10B** subjected to the same conditions produce significantly lower molecular weight polymers, therefore a longer microwave reaction time of 60 min was required. The isolated yields for copolymers **4.10T** and **4.10B** were 60 and 57% and a summary of the molecular weight data acquired by GPC can be found in Table 4.3. The relatively low molecular weights and broad molecular weight distributions observed are consistent with the step-growth polymerization method employed. ¹H NMR spectra of **4.10F** compared to the relevant monomer units is shown in Figure 4.2. Additional details, including thermal analysis and spectroscopic data (Figures A4.12, A4.13) are discussed below.

Table 4.3 Summary of GPC data for copolymers **4.10F**, **4.10F**-[Co₂(CO)₆]₂, **4.10B**, and **4.10T**.

Compound	M _n (g mol ⁻¹)	M _w (g mol ⁻¹)	<i>D</i>
4.10F	10,900	22,400	2.27
4.10F -[Co ₂ (CO) ₆] ₂ ^a	7,700	10,900	1.41
4.10T	6,575	18,250	2.77
4.10B	7,700	13,600	1.76

a) The post-polymerization was performed on polymer **4.10F** with a M_n = 7,825, M_w = 10,900 and *D* = 1.51.

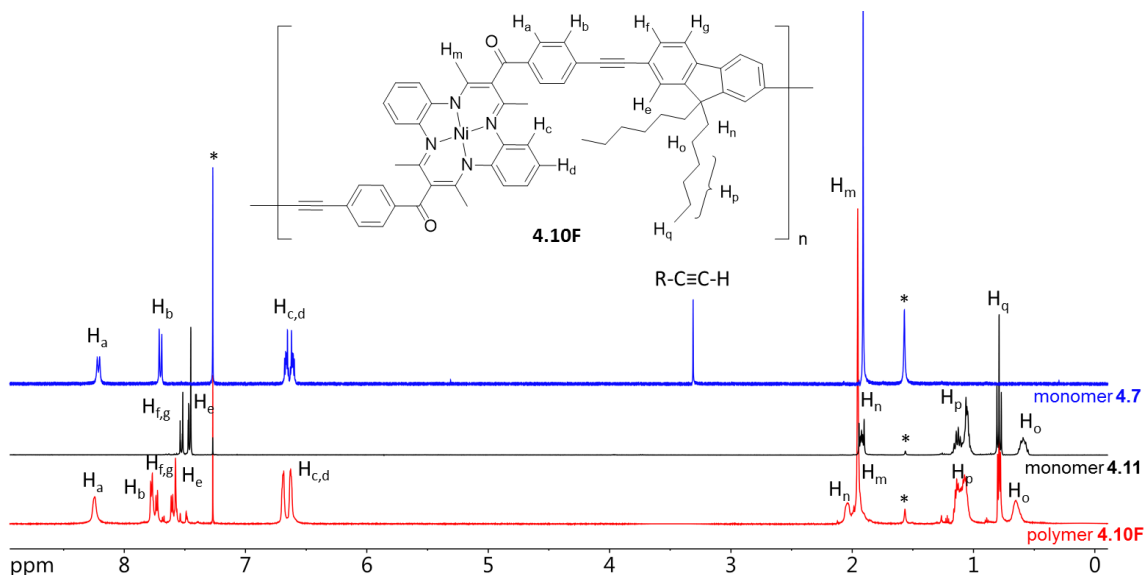
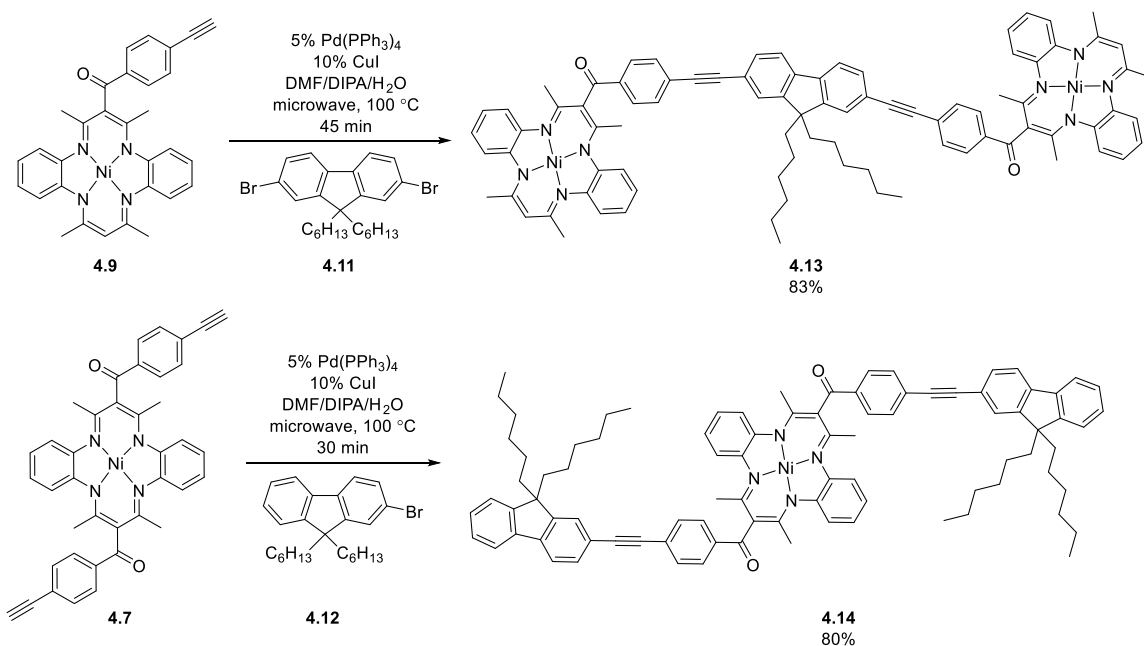


Figure 4.2 ¹H NMR spectra of comonomers **4.7** (blue), **4.11** (black), and polymer **4.10F** (red) recorded in CDCl₃ (asterisks denote residual CHCl₃ and H₂O).

4.3.3 Model Compound Synthesis

In order to gain further insight into the spectroscopic properties of the copolymers, specifically **4.10F**, model compounds **4.13** and **4.14** were prepared via similar Sonogashira cross-coupling reactions (Scheme 4.3). The first model compound consisted of two Ni(II) complexes of Goedken's macrocycles bridged by a 9,9-dihexylfluorene molecule (**4.13**). Microwave irradiation of a mixture of two equiv. of **4.9** with one equiv. of **4.11** for 30 min at 100 °C in the presence of Pd(PPh₃)₄ and CuI dissolved in DMF/DIPA/H₂O (2:1:0.03) produced compound **4.13** in 83% yield after purification by column chromatography (Figures A4.14, A4.15). The second model compound consisted of two 9,9-dihexylfluorene molecules bridged by a single Ni(II) complex of Goedken's

macrocycle (**4.14**). Microwave irradiation of a mixture of one equiv. of **4.7** with one equiv. of **4.12** for 30 min at 100 °C in the presence of Pd(PPh₃)₄ and CuI dissolved in DMF/DIPA/H₂O (2:1:0.03) produced compound **4.14** in 80% yield after purification by column chromatography (Figures A4.16, A4.17)



Scheme 4.3 Synthesis of model compounds **4.13** and **4.14**.

4.3.4 UV-vis Absorption Spectroscopy

The UV-vis absorption spectra of polymers **4.10F**, **4.10T**, and **4.10B** are presented in Figure 4.3 and the spectral features summarized in Table 4.4. The spectra of polymers **4.10T** and **4.10B** showed absorption maxima at 272 nm (**4.10T**, $\epsilon = 45,900$ and **4.10B**, $\epsilon = 44,100 \text{ M}^{-1} \text{ cm}^{-1}$), 387 nm (**4.10T**, $\epsilon = 74,300$ and **4.10B**, $\epsilon = 57,400 \text{ M}^{-1} \text{ cm}^{-1}$) and similar low-energy absorption maxima at *ca.* 590 nm ($5,700 \text{ M}^{-1} \text{ cm}^{-1}$). Similarly, polymer **4.10F** yielded absorption maxima at 275 nm ($50,900 \text{ M}^{-1} \text{ cm}^{-1}$), 378 nm ($100,800 \text{ M}^{-1} \text{ cm}^{-1}$), and 588 nm ($6,000 \text{ M}^{-1} \text{ cm}^{-1}$). The low energy absorption has been previously assigned in molecular analogues to a charge transfer (LMCT) from the ligand centred HOMO of the macrocyclic backbone to the lowest energy empty d orbital of Ni(II).⁷⁴ It was observed that

the absorption at *ca.* 590 nm remains essentially unchanged in the copolymers due to the lack of long range electronic delocalization via the orthogonal arrangement of the Ni(II) macrocycle units and the organic spacers, as inferred by the solid-state structure of **4.9**.⁷³ The high-energy absorptions at *ca.* 272 nm is thought to be a $\pi \rightarrow \pi^*$ transition associated with Goedken's macrocycle, while the transition at *ca.* 387 nm appears to originate primarily from a macrocycle centered $\pi \rightarrow \pi^*$ transition associated with the π -conjugated organic spacer in each structure. The $\pi \rightarrow \pi^*_2$ transition of copolymer **4.10F** is blue-shifted by *ca.* 10 nm compared to these of copolymers **4.10T** and **4.10B**. This trend is consistent with that observed for the wavelengths of maximum absorption of poly(9,9-dihexylfluorene) and poly(3-hexylthiophene) and may relate to the antiaromatic nature of the 9,9-dihexylfluorene spacer.⁷⁵⁻⁷⁶

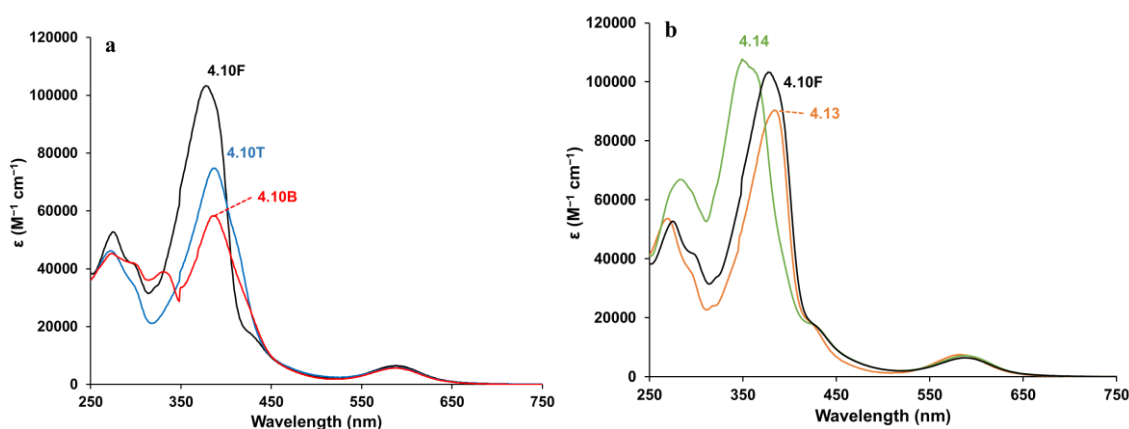


Figure 4.3 UV-vis absorption spectra recorded in CH_2Cl_2 . (a) Comparison of copolymers **4.10F**, **4.10T**, and **4.10B**. (b) Comparison of model compounds **4.13**, **4.14**, and copolymer **4.10F**.

In order to further understand the absorption properties of the copolymers, the absorption behavior of model complexes **4.13** and **4.14** were examined. Model compound **4.13**, which contains two Ni(II) complexes bridged by a 9,9-dihexylfluorene, shows absorption maxima at 584, 387, and 273 nm (Figure 1b). Model compound **4.14**, which contains two fluorene molecules and one Ni(II) complex, shows absorbance maxima at 587, 349, and 283 nm. The intermediate absorption maxima at 349 nm was blue-shifted with respect to **4.10F** and **4.13**, which both had maximum absorptions at 387 nm. This is thought to be due to the

presence of a shorter conjugated π -system [CO-Ph-alkyne-(9,9-dihexylfluorene)] within the backbone in compound **4.14**, compared to the relatively large [CO-Ph-alkyne-(9,9-dihexylfluorene)-alkyne-Ph-CO] system present in model compound **4.13** and copolymer **4.10F**. The increase in π -conjugation accounts for ten additional π -electrons and results in a red-shift in λ_{max} of 38 nm. The Ni(II) based absorption at *ca.* 590 nm for **4.13**, **4.14**, and **4.10F** were unchanged regardless of the degree of π -conjugation within the organic spacer (Table 4.4).

Table 4.4 UV-vis absorption spectroscopy data for copolymers **4.10F**, **4.10F**-[Co₂(CO)₆]₂, **4.10T**, and **4.10B**, and model compounds **4.13** and **4.14** in CH₂Cl₂.

Compound	λ_{max} (nm), ϵ (M ⁻¹ cm ⁻¹)		
	$\pi \rightarrow \pi^*_{1}$	$\pi \rightarrow \pi^*_{2}$	LMCT
4.10F ⁵⁹	275, 50,900	378, 100,800	588, 6,000
4.10F -[Co ₂ (CO) ₆] ₂	270, 85,900	385, 71,500	587, 9,900
4.10T	272, 45,900	387, 74,300	590, 5,700
4.10B	272, 44,100	387, 57,400	589, 5,700
4.13	273, 52,100	387, 91,100	584, 7,900
4.14 ⁵⁹	283, 67,600	349, 109,200	587, 7,100

4.3.5 Cyclic Voltammetry

The electrochemical properties of polymers **4.10F**, **4.10T**, and **4.10B** are summarized in Table 4.5. Cyclic voltammetry studies of the copolymers revealed two reversible one-electron oxidation events at $E^{\circ}_{\text{ox1}} = 0.24$ and $E^{\circ}_{\text{ox2}} = 0.74$ V for **4.10F**, $E^{\circ}_{\text{ox1}} = 0.23$ and $E^{\circ}_{\text{ox2}} = 0.74$ V for **4.10T**, and $E^{\circ}_{\text{ox1}} = 0.25$ and $E^{\circ}_{\text{ox2}} = 0.75$ V for **4.10B** in CH₂Cl₂, relative to the ferrocene/ferrocenium redox couple (Figure 4.4). Model compound **4.14** also produced two reversible one-electron oxidation waves at $E^{\circ}_{\text{ox1}} = 0.25$ and $E^{\circ}_{\text{ox2}} = 0.76$ V (Figure A4.18). The electrochemical behavior of model compound **4.13** was considerably more complicated, although similar to other unsubstituted Ni(II) complexes of Goedken's macrocycle (Figure A4.19).⁷⁴ Compound **4.13** gave rise to three irreversible oxidation waves at $E_{\text{pa}(1)} = 0.16$ V, $E_{\text{pa}(2)} = 0.92$ V, and $E_{\text{pa}(3)} = 1.11$ V and a single irreversible reduction wave $E_{\text{pc}(1)} = 0.74$ V. The irreversible oxidation at 1.11 V has been reported to arise due to the oxidation of a dimer formed via radical coupling of two equivalents of the radical cation form of similar Ni(II) complexes of Goedken's macrocycle.⁷⁷

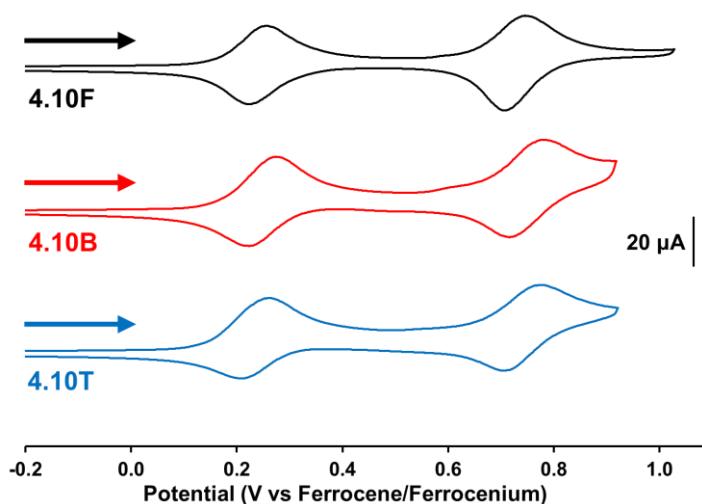


Figure 4.4 Cyclic voltammograms of **4.10F**, **4.10T**, and **4.10B** recorded at a scan rate of 100 mV s^{-1} in CH_2Cl_2 solutions containing $1 \times 10^{-3} \text{ M}$ analyte and 0.1 M $[\text{nBu}_4\text{N}][\text{PF}_6]$ as supporting electrolyte.

Furthermore, Ni(II) complexes of Goedken's macrocycle have been shown to form polymeric species on electrode surfaces.⁷⁸ Upon cycling repeatedly between 0.0 and 1.3 V, film formation was observed in the case of **4.13**, but there was a lack of current enhancement typically associated with electropolymerization (Figure A4.20).²⁸ Rather, we presume that a variety of oligomeric species are generated upon oxidation, leading to similar oxidation events ($E = 0.6\text{--}0.9 \text{ V}$) and electrode plating being observed.⁷⁹

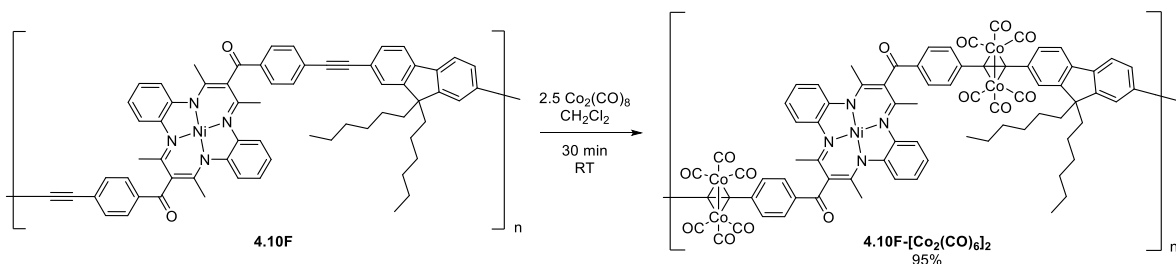
Table 4.5 Cyclic voltammetry data for polymers **4.10F**, **4.10T**, **4.10B** and model compounds **4.13** and **4.14**.^a

Compounds	$E_{\text{pa}(1)}^{\text{b}}$	$E_{\text{ox}1}^{\circ}$	$E_{\text{pc}(1)}^{\text{c}}$	$E_{\text{ox}2}^{\circ}$	$E_{\text{pa}(2)}^{\text{b}}$	$E_{\text{pa}(3)}^{\text{b}}$
4.10F ⁵⁹	-	0.24	-	0.74	-	-
4.10T	-	0.23	-	0.74	-	-
4.10B	-	0.25	-	0.75	-	-
4.13	0.16	-	0.74	-	0.92	1.11
4.14 ⁵⁹	-	0.25	-	0.76	-	-

^a Recorded at a scan rate of 100 mV s^{-1} in a CH_2Cl_2 solution containing $1 \times 10^{-3} \text{ M}$ analyte and 0.1 M $[\text{nBu}_4\text{N}][\text{PF}_6]$ as supporting electrolyte. Potentials reported in V relative to the ferrocene/ferrocenium redox couple.

4.3.6 Post-Polymerization Functionalization

In order to produce a heterobimetallic copolymer, **4.10F** was dissolved in CH_2Cl_2 and reacted with 2.5 equiv. of $\text{Co}_2(\text{CO})_8$. The resulting copolymer was purified using flash column chromatography on alumina and repeated precipitations from CH_2Cl_2 into pentane, to afford **4.10F**- $[\text{Co}_2(\text{CO})_6]_2$ in 95% yield (Scheme 4.4). GPC analysis of **4.10F**- $[\text{Co}_2(\text{CO})_6]_2$ yielded $M_n = 7,700 \text{ g mol}^{-1}$, $M_w = 10,900 \text{ g mol}^{-1}$, and $\mathcal{D} = 1.41$. The overall distribution and shape of the GPC traces are conserved when compared to the original polymer **4.10F** (Figure A4.21), which suggests the integrity of the polymer backbone was maintained after the introduction of the cobalt carbonyl clusters.



Scheme 4.4 Synthesis of **4.10F**- $[\text{Co}_2(\text{CO})_6]_2$.

UV-vis absorption spectroscopy confirmed the preservation of the absorption maxima at 587, 385, and 270 nm when compared to the parent polymer **4.10F** (Figure A4.22), although the molar absorptivity of the absorption maxima at 385 nm was reduced from $\epsilon = 100,800 \text{ M}^{-1} \text{ cm}^{-1}$ in **4.10F** to $\epsilon = 71,500 \text{ M}^{-1} \text{ cm}^{-1}$ in **4.10F**- $[\text{Co}_2(\text{CO})_6]_2$ and the molar absorptivity of the absorption maxima at 275 nm was increased from $\epsilon = 50,900 \text{ M}^{-1} \text{ cm}^{-1}$ in **4.10F** to $\epsilon = 85,900 \text{ M}^{-1} \text{ cm}^{-1}$ in **4.10F**- $[\text{Co}_2(\text{CO})_6]_2$. Furthermore, analysis of the FT-IR spectrum of **4.10F**- $[\text{Co}_2(\text{CO})_6]_2$ revealed the appearance of three diagnostic carbonyl stretches at 2019, 2051, and 2088 cm^{-1} , and the disappearance of the alkyne $\text{C}\equiv\text{C}$ stretch at 2196 cm^{-1} (Figure 4.5). ^1H NMR spectroscopy revealed similar chemical shifts for most of the proton signals present in **4.10F** and **4.10F**- $[\text{Co}_2(\text{CO})_6]_2$ copolymers, although there was a significant difference for some of the chemical shifts of the signals corresponding to

the protons present on the fluorene organic spacer, including the aromatic and aliphatic signals (Figure A4.23).

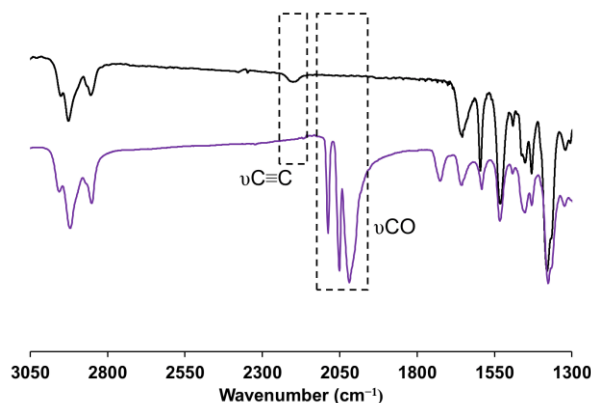


Figure 4.5 FT-IR spectra of **4.10F** (black) and **4.10F-[Co₂(CO)₆]₂** (purple). The dashed boxes highlight the energy regions of specific interest.

4.3.7 Thermal Analysis

The TGA of copolymers **4.10F**, **4.10T**, and **4.10B** demonstrated their thermal stability up to temperatures of 316, 284, and 252 °C, respectively (Figures 4.6, A4.24–A4.26). Differential scanning calorimetry studies did not reveal glass transitions between 0 and 250 °C (Figures A4.27–4.29). We speculate that the lack of observable glass transitions may be attributed to interdigitation of the alkyl chains present on the backbones of these polymers.

TGA data collected for copolymer **4.10F-[Co₂(CO)₆]₂** showed its thermal stability up to 177 °C before decomposition occurred in two steps. The first decomposition occurred to a temperature of *ca.* 300 °C with an initial mass loss of *ca.* 20%. This mass loss accounts for the expulsion of the carbonyl groups present on the polymer backbone, which corresponds to 21% of the total polymer mass. The second step resulted in a further mass loss of 46% to a temperature of 490 °C, and was followed by a slow thermal degradation until a char yield of 50% was achieved at 800 °C (Figure 4.6). For comparison, the char yield observed for **4.10F** was *ca.* 70%. Upon inspection of the TGA data for **4.10F** and **4.10F-[Co₂(CO)₆]₂**, there were similar degradation features after the initial loss of the carbonyl groups once the thermal stability limit was reached at 316 °C. The DSC data for **4.10F-**

$[\text{Co}_2(\text{CO})_6]_2$ did not reveal a glass transition within the stability window of the polymer (Figure A4.30).

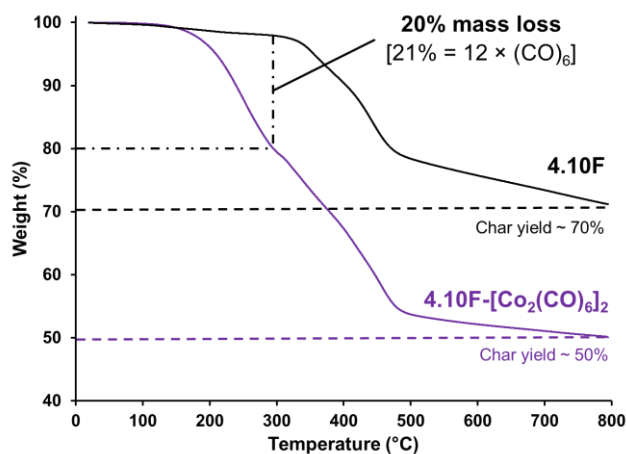


Figure 4.6 TGA data demonstrating the thermal decomposition of **4.10F** (black) and **4.10F-[Co₂(CO)₆]₂** (purple).

4.3.8 Pre-Ceramic Properties

The interesting thermal decomposition characteristics and significant char yields (> 50%) observed for **4.10F** and **4.10F-[Co₂(CO)₆]₂** suggested the formation of potentially useful ceramic materials. Specifically, Ni/Co alloys were targeted due to their demonstrated utility as magnetic materials,⁸⁰ their use in catalysis,⁸¹⁻⁸² and their high charge capacity.⁸³ Thin-films of **4.10F** and **4.10F-[Co₂(CO)₆]₂**, estimated to be approximately 5 μm thick (Figure A4.31), were created by drop-casting a 20 mg mL⁻¹ solution of each polymer in chlorobenzene onto a silicon wafer. The loaded wafers were then dried overnight in a vacuum oven at 60 °C before the samples were heated to 800 °C at a rate of 10 °C min⁻¹ and held at that temperature for an additional 3 h under a N₂/H₂ (95:5) atmosphere. Upon cooling, the samples were studied using SEM and energy-dispersive X-ray (EDX) spectroscopy.

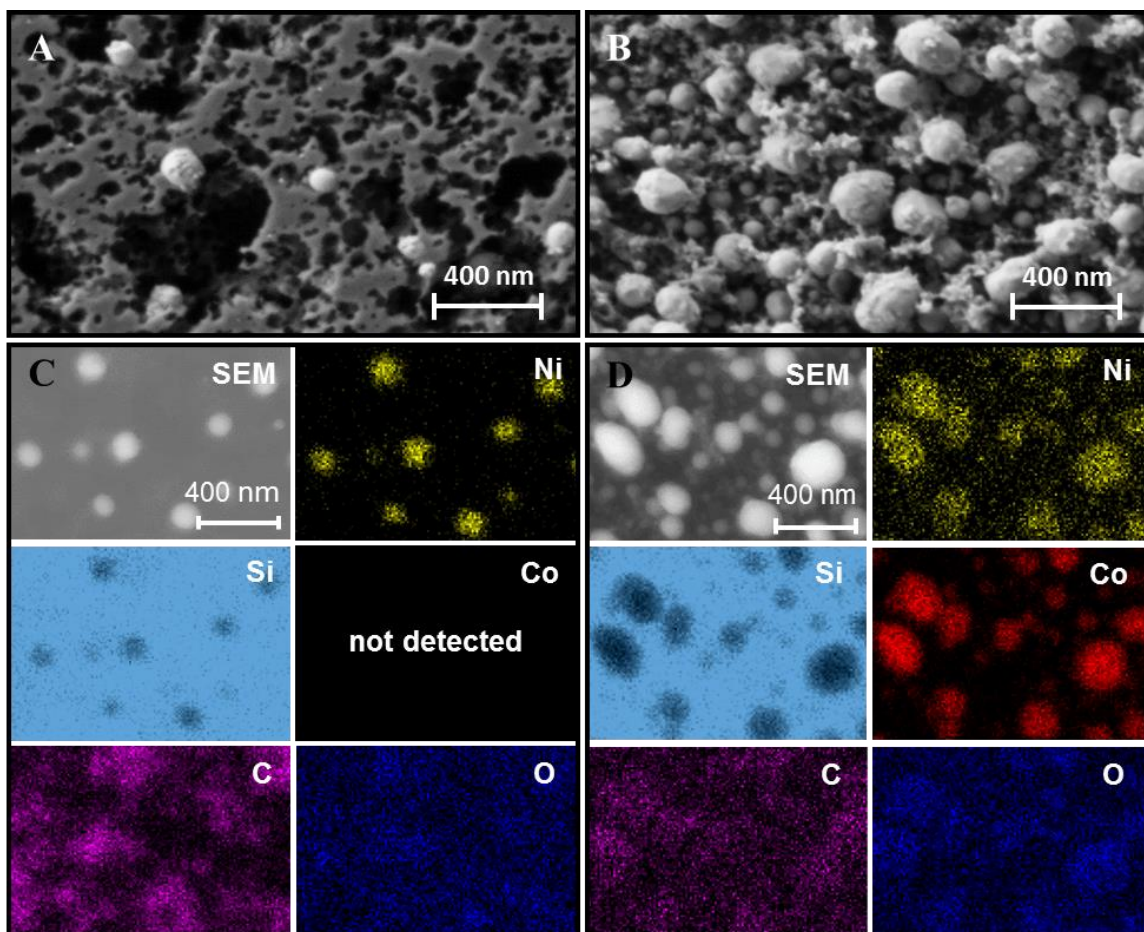


Figure 4.7 SEM of the nanomaterials resulting from pyrolysis of A) **4.10F** and B) **4.10F-[Co₂(CO)₆]₂**. Elemental maps (EDX spectroscopy) of the nanomaterials resulting from the pyrolysis of C) **4.10F** and D) **4.10F-[Co₂(CO)₆]₂**. Light areas indicate a positive response for the elements in question.

SEM images of the pyrolyzed films of **4.10F** and **4.10F-[Co₂(CO)₆]₂** are shown in Figure 4.7. The micrographs of the nanomaterials derived from **4.10F** show the presence of ill-defined nanoparticles within a porous matrix. Based on our EDX spectroscopy analysis we conclude that the nickel-rich nanoparticles are suspended in a porous and amorphous carbon matrix, presumably carbon black (Figures 4.7a,c). Oxygen appeared throughout the film and was concentrated in metal-rich areas. Although the pyrolysis experiments were performed in the absence of oxygen, brief exposure likely led to the formation of a thin layer of nickel-oxide. The micrograph of the nanomaterials that resulted from the pyrolysis of **4.10F-[Co₂(CO)₆]₂** showed a surface more densely populated with metallic nanoparticles within an amorphous carbon matrix (Figure 4.7b). The nanoparticles were

shown to be rich in cobalt and nickel (Figure 4.7d), while the cobalt and nickel alloys appeared to be more susceptible to oxidation based on the elemental maps obtained (Figure 4.7d). Furthermore, the ratio of cobalt to nickel (*ca.* 5.5:1) was measured by EDX spectroscopy, which deviated from the 4:1 ratio of metals present in **4.10F**-[Co₂(CO)₆]₂ (Figure A4.32). PXRD studies of the pyrolyzed thin-films of **4.10F** and **4.10F**-[Co₂(CO)₆]₂ indicated the presence of amorphous materials, consistent with the morphologies observed using SEM. These studies demonstrated our ability, through post-polymerization functionalization, to control the ratio of metals present within the nanomaterials.

4.4 Conclusion

The copolymerization of Ni(II) complexes of Goedken's macrocycle bearing alkyne substituents with 2,7-dibromo-9,9-dihexylfluorene via a microwave-induced Sonogashira cross-coupling reaction to produce copolymers **4.10F** was reported and optimized. An expansion of the series to include comonomers 2,5-dibromo-3-hexylthiophene and 1,4-dibromo-2,5-bis(hexyloxy)benzene, to produce copolymers **4.10T** and **4.10B** was explored. The copolymers exhibited high thermal stability (up to 300 °C) and two one-electron oxidation waves in their cyclic voltammograms. The spectroscopic properties of copolymer **4.10F** were probed by comparison with model compounds **4.13** and **4.14**, which provided insight into the observed spectroscopic properties for this family of copolymers. Specifically, the intermediate absorption maxima observed for the copolymers was shown to vary with the size and nature of the organic spacer within the polymer backbones. Post-polymerization functionalization via the alkyne synthetic handle present in **4.10F** led to the production of heterobimetallic copolymers that produced interesting amorphous nanomaterials rich in nickel and cobalt upon pyrolysis, with metal content influenced by the structure of the polymer.

4.5 References

1. Lu, Y.; Yeung, N.; Sieracki, N.; Marshall, N. M. *Nature* **2009**, *460*, 855–862.
2. Ho, C.-L.; Wong, W.-Y. *Coord. Chem. Rev.* **2011**, *255*, 2469–2502.
3. Whittell, G. R.; Hager, M. D.; Schubert, U. S.; Manners, I. *Nat. Mater.* **2011**, *10*, 176–188.
4. Bagh, B.; Gilroy, J. B.; Staubitz, A.; Muller, J. *J. Am. Chem. Soc.* **2010**, *132*, 1794–1795.
5. Zha, Y.; Thaker, H. D.; Maddikeri, R. R.; Gido, S. P.; Tuominen, M. T.; Tew, G. N. *J. Am. Chem. Soc.* **2012**, *134*, 14534–14541.
6. Wang, X.; Cao, K.; Liu, Y.; Tsang, B.; Liew, S. *J. Am. Chem. Soc.* **2013**, *135*, 3399–3402.
7. Hadadpour, M.; Liu, Y.; Chadha, P.; Ragogna, P. J. *Macromolecules* **2014**, *47*, 6207–6217.
8. Pawar, G. M.; Lalancette, R. A.; Bonder, E. M.; Sheridan, J. B.; Jäkle, F. *Macromolecules* **2015**, *48*, 6508–6515.
9. Sandmann, B.; Happ, B.; Kupfer, S.; Schacher, F. H.; Hager, M. D.; Schubert, U. S. *Macromol. Rapid Commun.* **2015**, *36*, 604–609.
10. Yan, Y.; Zhang, J.; Ren, L.; Tang, C. *Chem. Soc. Rev.* **2016**, 5232–5263.
11. Feng, X.; Zhang, K.; Hempenius, M. A.; Vancso, G. J. *RSC Adv.* **2015**, *5*, 106355–106376.
12. Rulkens, R.; Lough, A. J.; Manners, I.; Lovelace, S. R.; Grant, C.; Geiger, W. E. *J. Am. Chem. Soc.* **1996**, *118*, 12683–12695.
13. Ma, Y.; Dong, W.-F.; Hempenius, M. A.; Möhwald, H.; Vancso, G. J. *Nat. Mater.* **2006**, *5*, 724–729.

14. Staff, R. H.; Gallei, M.; Mazurowski, M.; Rehahn, M.; Berger, R.; Landfester, K.; Crespy, D. *ACS Nano* **2012**, *6*, 9042–9049.
15. Rabiee Kenaree, A.; Berven, B. M.; Ragogna, P. J.; Gilroy, J. B. *Chem. Commun.* **2014**, *50*, 10714–10717.
16. Zhang, K.; Feng, X.; Sui, X.; Hempenius, M. A.; Vancso, G. J. *Angew. Chem. Int. Ed.* **2014**, *53*, 13789–13793.
17. MacLachlan, M. J.; Ginzburg, M.; Coombs, N.; Coyle, T. W.; Raju, N. P.; Greedan, J. E.; Ozin, G. A.; Manners, I. *Science* **2000**, *287*, 1460–1463.
18. O'Sullivan, T. J.; Djukic, B.; Dube, P. A.; Lemaire, M. T. *Chem. Commun.* **2009**, 1903–1905.
19. Al-Badri, Z. M.; Maddikeri, R. R.; Zha, Y.; Thaker, H. D.; Dobriyal, P.; Shunmugam, R.; Russell, T. P.; Tew, G. N. *Nat. Commun.* **2011**, *2*, 482.
20. Baljak, S.; Russell, A. D.; Binding, S. C.; Haddow, M. F.; O'Hare, D.; Manners, I. *J. Am. Chem. Soc.* **2014**, *136*, 5864–7.
21. Braunschweig, H.; Damme, A.; Demeshko, S.; Dück, K.; Kramer, T.; Krummenacher, I.; Meyer, F.; Radacki, K.; Stellwag-Konertz, S.; Whittell, G. R. *J. Am. Chem. Soc.* **2015**, *137*, 1492–1500.
22. Jiang, B.; Hom, W. L.; Chen, X.; Yu, P.; Pavelka, L. C.; Kisslinger, K.; Parise, J. B.; Bhatia, S. R.; Grubbs, R. B. *J. Am. Chem. Soc.* **2016**, *138*, 4616–4625.
23. Ulbricht, C.; Beyer, B.; Friebe, C.; Winter, A.; Schubert, U. S. *Adv. Mater.* **2009**, *21*, 4418–4441.
24. Ulbricht, C.; Becer, C. R.; Winter, A.; Schubert, U. S. *Macromol. Rapid Commun.* **2010**, *31*, 827–833.
25. Soliman, A. M.; Fortin, D.; Zysman-Colman, E.; Harvey, P. D. *Macromol. Rapid Commun.* **2012**, *33*, 522–527.

26. Wild, A.; Teichler, A.; Ho, C.-L.; Wang, X.-Z.; Zhan, H.; Schlütter, F.; Winter, A.; Hager, M. D.; Wong, W.-Y.; Schubert, U. S. *J. Mater. Chem. C* **2013**, *1*, 1812–1822.
27. Matsumura, Y.; Fukuda, K.; Inagi, S.; Tomita, I. *Macromol. Rapid Commun.* **2015**, *36*, 660–664.
28. Holliday, B. J.; Swager, T. M. *Chem. Commun.* **2005**, 23–36.
29. Moorlag, C.; Sih, B. C.; Stott, T. L.; Wolf, M. O. *J. Mater. Chem.* **2005**, *15*, 2433–2436.
30. Wong, W.-Y.; Harvey, P. D. *Macromol. Rapid Commun.* **2010**, *31*, 671–713.
31. Friebe, C.; Hager, M. D.; Winter, A.; Schubert, U. S. *Adv. Mater.* **2012**, *24*, 332–345.
32. Edelman, K. R.; Stevenson, K. J.; Holliday, B. J. *Macromol. Rapid Commun.* **2012**, *33*, 610–615.
33. Friebe, C.; Schulze, B.; Görls, H.; Jäger, M.; Schubert, U. S. *Chem. Eur. J.* **2014**, *20*, 2357–2366.
34. Caraway, J. D.; Nguyen, M. T.; Mitchell, L. A.; Holliday, B. J. *Macromol. Rapid Commun.* **2015**, *36*, 665–670.
35. Wong, W.-Y.; Ho, C.-L. *Acc. Chem. Res.* **2010**, *43*, 1246–1256.
36. Yang, M.; Zhang, L.; Lei, Z.; Ye, P.; Si, J.; Yang, Q.; Wang, Y. *J. Appl. Polym. Sci.* **1998**, *70*, 1165–1172.
37. Wong, W.-Y.; Wang, X.-Z.; He, Z.; Djurišić, A. B.; Yip, C.-T.; Cheung, K.-Y.; Wang, H.; Mak, C. S. K.; Chan, W.-K. *Nat. Mater.* **2007**, *6*, 521–527.
38. Ho, C.-L.; Poon, S.-Y.; Liu, K.; Wong, C.-K.; Lu, G.-L.; Petrov, S.; Manners, I.; Wong, W.-Y. *J. Organomet. Chem.* **2013**, *744*, 165–171.

39. Dong, Q.; Li, G.; Ho, C.-L.; Faisal, M.; Leung, C.-W.; Pong, P. W.-T.; Liu, K.; Tang, B.-Z.; Manners, I.; Wong, W.-Y. *Adv. Mater.* **2012**, *24*, 1034–1040.
40. Liu, K.; Ho, C.-L.; Aouba, S.; Zhao, Y.-Q.; Lu, Z.-H.; Petrov, S.; Coombs, N.; Dube, P.; Ruda, H. E.; Wong, W.-Y.; Manners, I. *Angew. Chem. Int. Ed.* **2008**, *47*, 1255–1259.
41. Scamporrino, E.; Vitalini, D. *Macromolecules* **1992**, *25*, 1625–1632.
42. Eichhorn, H.; Sturm, M.; Wöhrle, D. *Macromol. Chem. Phys.* **1995**, *196*, 115–131.
43. Ding, X.; Guo, J.; Feng, X.; Honsho, Y.; Guo, J.; Seki, S.; Maitarad, P.; Saeki, A.; Nagase, S.; Jiang, D. *Angew. Chem. Int. Ed.* **2011**, *50*, 1289–1293.
44. Abel, M.; Clair, S.; Ourdjini, O.; Mossoyan, M.; Porte, L. *J. Am. Chem. Soc.* **2011**, *133*, 1203–1205.
45. Jeong, J.; Lee, Y.-J.; Kim, B.; Kim, B.; Jung, K.-S.; Paik, H.-j. *Polym. Chem.* **2015**, *6*, 3392–3397.
46. Leung, A. C. W.; MacLachlan, M. J. *J. Inorg. Organomet. Polym. Mater.* **2007**, *17*, 57–89.
47. Kingsborough, R. P.; Swager, T. M. *Chem. Mater.* **2000**, *12*, 872–874.
48. Shioya, T.; Swager, T. M. *Chem. Commun.* **2002**, 1364–1365.
49. Holliday, B. J.; Stanford, T. B.; Swager, T. M. *Chem. Mater.* **2006**, *18*, 5649–5651.
50. Fukumoto, H.; Yamane, K.; Kase, Y.; Yamamoto, T. *Macromolecules* **2010**, *43*, 10366–10375.
51. Yagi, K.; Ito, M.; Houjou, H. *Macromol. Rapid Commun.* **2012**, *33*, 540–544.
52. Nguyen, M. T.; Holliday, B. J. *Chem. Commun.* **2015**, *51*, 8610–8613.

53. Realista, S.; Viana, A. S.; Cardoso, B. d. P.; Botelho do Rego, A. M.; Vaz, P. D.; Melato, A. I.; Martinho, P. N.; Calhorda, M. J. *RSC Adv.* **2015**, *5*, 39495–39504.
54. Chan, W. Y.; Clendenning, S. B.; Berenbaum, A.; Lough, A. J.; Aouba, S.; Ruda, H. E.; Manners, I. *J. Am. Chem. Soc.* **2005**, *127*, 1765–1772.
55. Zamora, M.; Bruña, S.; Alonso, B.; Cuadrado, I. *Macromolecules* **2011**, *44*, 7994–8007.
56. Zhang, J.; Yan, Y.; Chen, J.; Chance, W. M.; Hayat, J.; Gai, Z.; Tang, C. *Chem. Mater.* **2014**, *26*, 3185–3190.
57. Dong, Q.; Li, G.; Wang, H.; Wing-Tat Pong, P.; Leung, C.-W.; Manners, I.; Ho, C.-L.; Li, H.; Wong, W.-Y. *J. Mater. Chem. C* **2015**, *3*, 734–741.
58. Ciganda, R.; Gu, H.; Castel, P.; Zhao, P.; Ruiz, J.; Hernández, R.; Astruc, D. *Macromol. Rapid Commun.* **2016**, *37*, 105–111.
59. Cotton, F. A.; Czuchajowska, J. *Polyhedron* **1990**, *9*, 2553–2566.
60. Mountford, P. *Chem. Soc. Rev.* **1998**, *27*, 105–115.
61. Abd-El-Aziz, A. S.; Shipman, P. O.; Boden, B. N.; McNeil, W. S. *Prog. Polym. Sci.* **2010**, *35*, 714–836.
62. Gwyther, J.; Gilroy, J. B.; Rugar, P. A.; Lunn, D. J.; Kynaston, E.; Patra, S. K.; Whittell, G. R.; Winnik, M. A.; Manners, I. *Chem. Eur. J.* **2013**, *19*, 9186–9197.
63. Niewahner, J. H.; Walters, K. A.; Wagner, A. *J. Chem. Educ.* **2007**, *84*, 477.
64. Bernard, R.; Barsu, C.; Baldeck, P. L.; Andraud, C.; Cornu, D.; Scharff, J.-P.; Miele, P. *Chem. Commun.* **2008**, 3765–3767.
65. Mulherin, R. C.; Jung, S.; Huettner, S.; Johnson, K.; Kohn, P.; Sommer, M.; Allard, S.; Scherf, U.; Greenham, N. C. *Nano Lett.* **2011**, *11*, 4846–4851.

66. Umezawa, K.; Oshima, T.; Yoshizawa-Fujita, M.; Takeoka, Y.; Rikukawa, M. *ACS Macro Lett.* **2012**, *1*, 969–972.
67. Bruker-AXS, SAINT version 2013.8, **2013**, Bruker-AXS, Madison, WI 53711, USA.
68. Bruker-AXS, SADABS version 2012.1, **2012**, Bruker-AXS, Madison, WI 53711, USA.
69. Sheldrick, G. M. *Acta Crystallogr., Sect. C: Struct. Chem.* **2015**, *71*, 3–8.
70. Sheldrick, G. M. *Acta Crystallogr., Sect. A: Found. Adv.* **2015**, *71*, 3–8.
71. Haynes, W. M., *CRC Handbook of Chemistry and Physics*. 94th ed.; CRC Press: Boca Raton, FL, 2013.
72. Scherf, U.; List, E. J. W. *Adv. Mater.* **2002**, *14*, 477–488.
73. Paquette, J. A.; Sauvé, E. R.; Gilroy, J. B. *Macromol. Rapid Commun.* **2015**, *36*, 621–626.
74. Bailey, C. L.; Bereman, R. D.; Rillema, D. P.; Nowak, R. *Inorg. Chem.* **1984**, *23*, 3956–3960.
75. Fomina, N.; Bradforth, S. E.; Hogen-Esch, T. E. *Macromolecules* **2009**, *42*, 6440–6447.
76. Chen, T.-A.; Wu, X.; Rieke, R. D. *J. Am. Chem. Soc.* **1995**, *117*, 233–244.
77. McElroy, F. C.; Dabrowiak, J. C. *J. Am. Chem. Soc.* **1976**, *98*, 7112–7113.
78. Bailey, C. L.; Bereman, R. D.; Rillema, D. P.; Nowak, R. *Inorg. Chem.* **1986**, *25*, 933–938.
79. Kim, D.; Kim, E.; Byun, J.; Choi, J.; Na, H.; Park, Y. *J. Coord. Chem.* **2002**, *55*, 505–516.

80. Barakat, N. A. M.; Kim, B.; Yi, C.; Jo, Y.; Jung, M.-H.; Chu, K. H.; Kim, H. Y. *J. Phys. Chem. C* **2009**, *113*, 19452–19457.
81. Lian, K.; Thorpe, S. J.; Kirk, D. W. *Electrochim. Acta* **1992**, *37*, 169–175.
82. Xu, R.; Xie, T.; Zhao, Y.; Li, Y. *Nanotechnology* **2007**, *18*, 055602.
83. Chang, J.; Sun, J.; Xu, C.; Xu, H.; Gao, L. *Nanoscale* **2012**, *4*, 6786–91.

Chapter 5

5 Side-Chain Polymers bearing Ni(II) Complexes of Goedken's Macrocycle

5.1 Introduction

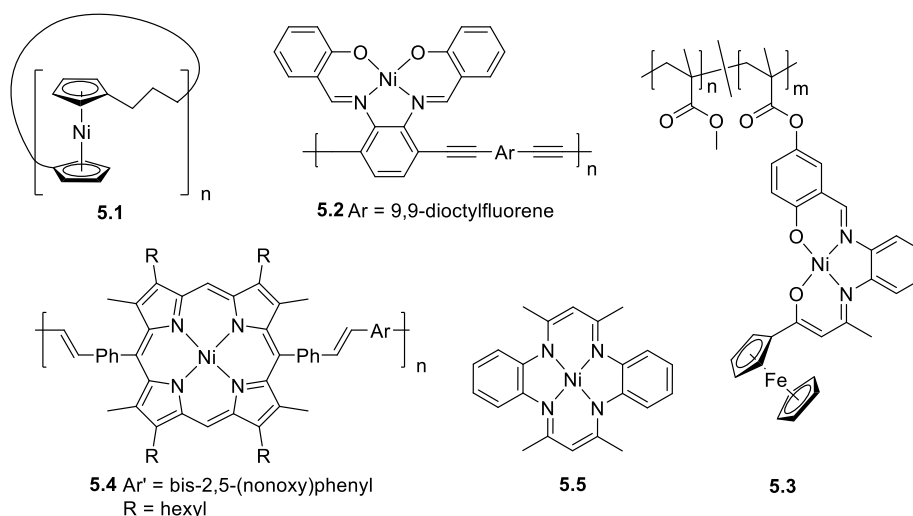
Metal-containing polymers (MCPs) have attracted significant attention due to their potential applications as functional materials.^{1-4,5-14} They gain their unique properties through the combination of the desirable properties of transition metals (*e.g.*, redox, catalytic, magnetic, pre-ceramic, and optical) and the processability and film-forming characteristics of polymers. As a result, MCPs have shown utility as, for example, the functional component of redox-active capsules¹⁵⁻¹⁶ and responsive surfaces,¹⁷ photonic crystal displays,¹⁸ antimicrobial surfaces,¹⁹ nanostructured magnetic materials,²⁰ and photovoltaic cells.²¹

While there has been impressive progress in the MCP field as a whole, there are relatively few examples of synthetic strategies that afford well-defined Ni-containing polymers. For example, the Manners group has expanded their ring-opening polymerization methods to include tricarb[3]nickelocenophanes, affording paramagnetic polymers (*e.g.*, **5.1**),²² and the Yamamoto group has prepared electrochemically-active copolymers based on Ni-salophen complexes and 9,9-dioctylfluorene (*e.g.*, **5.2**).²³

MCPs based on transition-metal complexes of macrocyclic ligands, including Schiff bases (*e.g.* **5.3**),²⁴ porphyrins (*e.g.*, **5.4**)²⁵⁻²⁶ and phthalocyanines²⁷⁻²⁹ have received significant attention due to their unique properties. However, polymers of the metal complexes are often produced by low-yielding and time-consuming synthetic routes, and examples of Ni-containing polymers are therefore relatively uncommon.

The Ni(II) complex of 4,11-dihydro-5,7,12,14-tetramethyldibenzo[b,i]-[1,4,8,11]tetraazacyclotetradecine (*aka*, Goedken's macrocycle) **5.5** exhibits unusual and potentially very useful electrochemical properties and can be produced via simple synthetic pathways in large quantities (> 10 g) and high yield (*ca.* 87%) from inexpensive starting

materials.³⁰⁻³¹ Although this complex has garnered significant interest from coordination chemists for over 5 decades,³²⁻³⁸ very little has been reported with respect to its incorporation into polymers with the only existing examples, prior to our work, produced in small quantities by electropolymerization.³⁹⁻⁴¹ A polymer-substituted derivative of complex **5.5** has also been used to template ladder-like nanostructures.⁴² In this chapter, we report the synthesis and characterization of a Ni-containing side-chain polymers produced by ring-opening metathesis polymerization (ROMP).



5.2 Experimental

5.2.1 General Considerations

Reactions and manipulations were carried out under a nitrogen atmosphere using standard Schlenk or glove box techniques unless otherwise stated. Solvents were obtained from Caledon Laboratories, dried using an Innovative Technologies Inc. solvent purification system, collected under vacuum, and stored under a nitrogen atmosphere over 4 Å molecular sieves. Reagents were purchased from Sigma-Aldrich, Alfa Aesar, or Oakwood Chemical and used as received unless otherwise stated. 4-[(trimethylsilyl)ethynyl]-benzoyl chloride,⁴³ tetramethyldibenzo-tetraaza[14]annulene Ni(II),³¹ 3-azido-1-propanol,⁴⁴ were prepared according to previously published protocols and isolation of *endo*-5-norbornene-2-carboxylic acid⁴⁵ was completed according to a literature procedure. NMR spectra were recorded on a 600 MHz (¹H: 599.3 MHz, ¹³C: 150.7 MHz) Varian INOVA instrument or a

400 MHz (^1H 400.1 MHz, $^{13}\text{C}\{^1\text{H}\}$: 100.6 MHz) Varian Mercury instrument. ^1H NMR spectra were referenced to residual CHCl_3 (7.27 ppm) and $^{13}\text{C}\{^1\text{H}\}$ NMR spectra were referenced to CDCl_3 (77.0 ppm). Mass spectrometry data were recorded in positive-ion mode with a Bruker microTOF II instrument using electrospray ionization. UV-vis absorption spectra were recorded in CH_2Cl_2 solutions using a Cary 5000 spectrophotometer. Four separate concentrations were run for each sample and molar extinction coefficients were determined from the slope of a plot of absorbance against concentration. FT-IR spectra were recorded on a PerkinElmer Spectrum Two instrument using an attenuated total reflectance accessory or as KBr pellets using a Bruker Vector 33 FT-IR spectrometer.

5.2.2 Gel Permeation Chromatography (GPC)

GPC experiments were conducted in chromatography-grade THF at concentrations of 5 mg mL^{-1} using a Viscotek GPCmax VE 2001 GPC instrument equipped with an Agilent PolyPore guard column (PL1113-1500) and two sequential Agilent PolyPore GPC columns packed with porous poly(styrene-*co*-divinylbenzene) particles (MW range: 200–2,000,000 g mol^{-1} ; PL1113-6500) regulated at a temperature of 30 °C. Signal responses were measured using a Viscotek VE 3580 RI detector, and molecular weights were determined by comparison of the maximum RI response with a calibration curve (10 points, 1,500–786,000 g mol^{-1}) established using monodisperse polystyrene standards purchased from Viscotek.

5.2.3 Thermal Analysis and Pyrolysis Studies

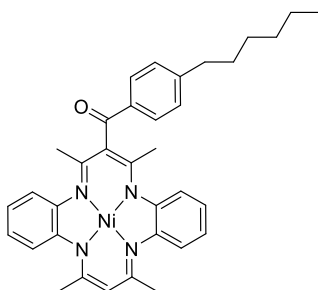
Thermal degradation studies were performed using a TA Instruments Q50 TGA. Samples were placed in a platinum pan and heated at a rate of 10 °C min^{-1} from 35 to 1000 °C under a flow of nitrogen (60 mL min^{-1}). Differential scanning calorimetry (DSC) traces were acquired on a TA Instruments DSC Q20 instrument. The polymer samples were placed in an aluminum T_{zero} pan and heated from room temperature to 250 °C at 10 °C min^{-1} under a flow of nitrogen (50 mL min^{-1}) and cooled down to -50 °C at 10 °C min^{-1} , before they underwent two additional heating/cooling cycles.

5.2.4 Electrochemical Methods

Cyclic voltammetry experiments were performed with a Bioanalytical Systems Inc. (BASi) Epsilon potentiostat and analyzed using BASi Epsilon software. Typical electrochemical cells consisted of a three-electrode setup including a glassy carbon working electrode, platinum wire counter electrode, and silver wire *pseudo* reference electrode. Experiments were run at a scan rate of 250 mV s⁻¹ in dry and degassed CH₂Cl₂ solutions of the analyte (~1 mM) and electrolyte (0.1 M [*n*Bu₄N][PF₆]). Cyclic voltammograms were internally referenced against the ferrocene/ferrocenium redox couple (~1 mM internal standard) and corrected for internal cell resistance using the BASi Epsilon software.

5.2.5 Synthesis

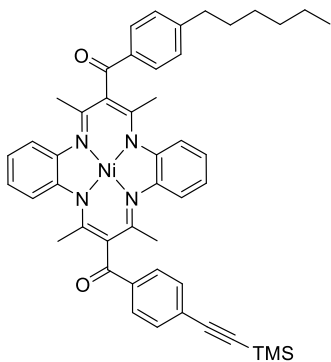
Synthesis of 4-hexylphenyl substituted macrocycle (**5.6**)



A Schlenk flask equipped with a stir bar was charged with complex **5.5** (10.0 g, 24.9 mmol), 4-hexylbenzoyl chloride (5.44 mL, 24.9 mmol) and dry toluene (250 mL). Dry and degassed Et₃N (27.8 mL, 199 mmol) was added and the vessel was fitted with a condenser and heated to 125 °C. After stirring for 16 h, the mixture was cooled to room temperature, filtered, and the solvent was removed *in vacuo*. Column chromatography (CH₂Cl₂/toluene, 1:1, 350 mL silica gel, R_f = 0.17) was performed to yield complex **5.6** as a dark green solid. Yield = 3.02 g, 21% (recovered starting material (**5.5**) 2.56 g and disubstituted product; 5.41 g, 28%). ¹H NMR (400.1 MHz, CDCl₃): δ 8.13 (d, 2H, J_{HH} = 8 Hz, aryl CH), 7.34 (d, 2H, J_{HH} = 9 Hz, aryl CH), 6.72 (d, 2H, J_{HH} = 8, 1 Hz, aryl CH) 6.64–6.59 (m, 4H, aryl CH), 6.56–6.53 (m, 2H, aryl CH), 4.86 (s, 1H, CH), 2.70 (t, 2H, J_{HH} = 8 Hz, CH₂), 2.10 (s, 6H, macrocycle CH₃), 1.91 (s, 6H, macrocycle CH₃), 1.67 (m, 2H, CH₂), 1.37–1.31 (m, 6H, CH₂), 0.91–0.88 (m, 3H, CH₃). ¹³C{¹H} NMR (150.7 MHz, CDCl₃) δ 200.1, 155.3, 153.7, 149.2, 147.4, 147.3, 136.9, 129.9, 128.9, 122.7, 121.8, 121.7, 121.1, 120.9, 111.2, 36.1, 31.7, 31.1, 29.0, 22.6, 21.9, 20.6, 14.1. FT-IR (ATR): ν = 2964 (w), 2923 (w), 2853 (w), 1653 (w), 1602 (w), 1530 (m), 1453 (m), 1430 (m), 1380 (s), 1260 (m), 1215 (m), 1171 (m), 1020 (m), 914 (m), 799 (m), 742 (s), 583 (w), 535 (w). UV-vis (CH₂Cl₂): λ_{max} (ε) 588

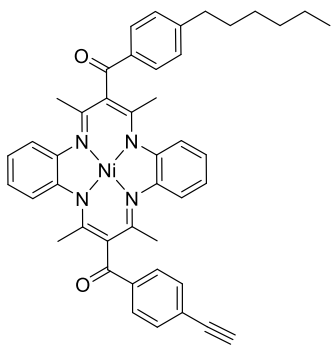
nm ($5,800 \text{ M}^{-1} \text{ cm}^{-1}$), 434 nm (sh, $12,200 \text{ M}^{-1} \text{ cm}^{-1}$), 393 nm ($32,800 \text{ M}^{-1} \text{ cm}^{-1}$), 269 nm ($44,000 \text{ M}^{-1} \text{ cm}^{-1}$). Mass Spec. (EI, +ve mode) m/z : $[M]^+$ calc'd for $[\text{C}_{35}\text{H}_{38}\text{N}_4\text{NiO}]^+$, 588.2399; found, 588.2387; difference: -2.0 ppm.

Synthesis of 4-hexylphenyl and (TMS-ethynyl)phenyl substituted macrocycle (5.7)



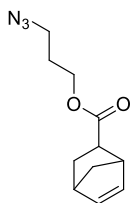
A Schlenk flask equipped with a stir bar was charged with complex **5.6** (0.45 g, 0.76 mmol), 4-[(trimethylsilyl)ethynyl]benzoyl chloride (0.22 g, 0.92 mmol) and dry toluene (45 mL). Dry and degassed Et_3N (0.85 mL, 6.1 mmol) was added and the vessel was fitted with a condenser and heated to 125°C under a N_2 atmosphere. After stirring for 16 h, the mixture was cooled to room temperature, filtered, and the solvent was removed *in vacuo*. Column chromatography ($\text{CH}_2\text{Cl}_2/\text{toluene}$, 2:1, 750 mL silica gel, $R_f = 0.12$) was performed to yield complex **5.7** as a dark green solid. Yield = 0.55 g, 91%. ^1H NMR (599.3 MHz, CDCl_3): δ 8.18–8.16 (m, 4H, aryl CH), 7.66 (d, 2H, $J_{\text{HH}} = 8$ Hz, aryl CH), 7.39 (d, 2H, $J_{\text{HH}} = 8$ Hz, aryl CH), 6.67–6.64 (m, 4H, aryl CH), 6.60–6.58 (m, 4H, aryl CH), 2.72 (t, 2H, $J_{\text{HH}} = 8$ Hz, CH_2), 1.92 (s, 6H, macrocycle CH_3), 1.90 (s, 6H, macrocycle CH_3), 1.71–1.66 (m, 2H, CH_2), 1.38–1.32 (m, 6H, CH_2), 0.91–0.89 (m, 3H, CH_3), 0.29 (s, 9H, SiCH_3). $^{13}\text{C}\{^1\text{H}\}$ NMR (150.7 MHz, CDCl_3) δ 200.0, 199.5, 153.7, 153.6, 149.3, 147.3, 147.2, 138.5, 136.7, 132.5, 129.9, 129.5, 129.0, 128.2, 122.7, 122.6, 121.8, 121.4, 120.8, 104.2, 98.4, 36.1, 31.6, 31.1, 29.0, 22.5, 20.5, 20.4, 14.1, -0.2 . FT-IR (ATR): $\nu = 3064$ (w), 2924 (w), 2854 (w), 1652 (m), 1598 (m), 1491 (m), 1449 (m), 1429 (m), 1362 (s), 1323 (m), 1222 (s), 1169 (m), 1053 (m), 919 (m), 841 (s), 743 (s) cm^{-1} . UV-vis (CH_2Cl_2): λ_{max} (ϵ) 590 nm ($6,000 \text{ M}^{-1} \text{ cm}^{-1}$), 430 nm (sh, $14,200 \text{ M}^{-1} \text{ cm}^{-1}$), 390 nm ($30,200 \text{ M}^{-1} \text{ cm}^{-1}$), 275 nm ($60,500 \text{ M}^{-1} \text{ cm}^{-1}$). Mass Spec. (ESI, +ve mode) m/z : $[M]^+$ calc'd for $[\text{C}_{47}\text{H}_{50}\text{N}_4\text{NiO}_2\text{Si}]^+$, 788.3056; found, 788.3059; difference: $+0.4$ ppm.

Synthesis of *n*-hexylphenyl and ethynylphenyl substituted macrocycle (**5.8**)



Compound **5.7** (0.40 g, 0.51 mmol) was stirred with K_2CO_3 (0.14 g, 1.0 mmol) in THF/MeOH (3:1, 20 mL) for 16 h at room temperature. CH_2Cl_2 (50 mL) was then added and the organic layer was washed with 0.5 M aqueous NH_4Cl (50 mL), dried with MgSO_4 and concentrated *in vacuo*. The resulting dark green solid was purified via precipitation from a saturated CH_2Cl_2 solution in pentane to afford **5.8** as a dark green microcrystalline solid. Yield = 0.31 g, 85%. ^1H NMR (599.3 MHz, CDCl_3): δ 8.22–8.21 (m, 2H, aryl CH), 8.15 (s, 2H, aryl CH), 7.70 (d, 2H, $J_{\text{HH}} = 8$, 1 Hz, aryl CH), 7.39 (d, 2H, $J_{\text{HH}} = 8$ Hz, aryl CH), 6.72–6.65 (m, 4H, aryl CH), 6.61–6.59 (m, 4H, aryl CH), 3.30 (s, 1H, CH), 2.72 (t, 2H, $J_{\text{HH}} = 7$ Hz, CH_2), 1.92 (s, 6H, macrocycle CH_3), 1.91 (s, 6H, macrocycle CH_3), 1.71–1.66 (m, 2H, CH_2), 1.40–1.32 (m, 6H, CH_2), 0.90 (t, 3H, $J_{\text{HH}} = 7$ Hz, CH_3). $^{13}\text{C}\{^1\text{H}\}$ NMR (150.7 MHz, CDCl_3) δ 200.1, 199.5, 153.8, 153.7, 149.4, 147.4, 147.2, 139.0, 136.7, 132.7, 129.9, 129.6, 129.0, 127.2, 122.8, 122.6, 121.8, 121.4, 120.8, 82.9, 80.5, 36.1, 31.7, 31.1, 29.0, 22.6, 20.5, 20.4, 14.1. FT-IR (ATR): $\nu = 3291, 2923, 2853, 1657, 1600$ (w), 1491 (w), 1530 (s), 1448 (m), 1428 (m), 1363 (s), 1323 (m), 1223 (s), 1170 (m), 1054 (m), 912 (m), 854 (m), 745 (s) cm^{-1} . UV-vis (CH_2Cl_2): λ_{max} (ϵ) 590 nm (5,700 $\text{M}^{-1} \text{cm}^{-1}$), 429 nm (sh, 13,400 $\text{M}^{-1} \text{cm}^{-1}$), 390 nm (28,500 $\text{M}^{-1} \text{cm}^{-1}$), 274 nm (62,300 $\text{M}^{-1} \text{cm}^{-1}$). Mass Spec. (ESI, +ve mode) m/z : $[\text{M}]^+$ calc'd for $[\text{C}_{44}\text{H}_{42}\text{N}_4\text{NiO}_2]^+$, 716.2661; found, 716.2658; difference: -0.4 ppm.

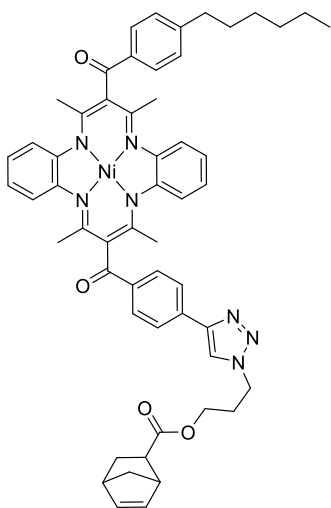
Synthesis of 3-azidopropyl *endo*-2-norbornene-2-carboxylate (**5.9**)



3-Azido-1-propanol (0.81 g, 8.0 mmol), *endo*-5-norbornene-2-carboxylic acid (1.10 g, 7.96 mmol), dicyclohexylcarbodiimide (1.64 g, 7.96 mmol), 4-(dimethylamino)pyridine (0.97 g, 7.96 mmol) were combined in dry/degassed CH_2Cl_2 (100 mL). Reaction progress was monitored by TLC and the reaction was stopped after 2 h, upon disappearance of the starting material. The solution was filtered and the solvent was removed *in vacuo*. Column chromatography (hexanes/EtOAc, 9:1, 75 mL silica gel, $R_f = 0.8$) was performed to yield **5.9** as a colourless oil. Yield = 1.08 g, 62%.

^1H NMR (400.1 MHz, CDCl_3): δ 6.21 (dd, 1H, $J_{\text{HH}} = 6, 3$ Hz C=CH), 5.93 (dd, 1H, $J_{\text{HH}} = 6, 3$ Hz C=CH), 4.12 (t, 2H, $J_{\text{HH}} = 6$ Hz, CH_2), 3.40 (t, 2H, $J_{\text{HH}} = 7$ Hz, CH_2), 3.22 (s, 1H, CH), 2.99–2.95 (m, 1H, CH), 2.92 (s, 1H, CH), 1.93–1.87 (m, 2H, CH_2), 1.47–1.41 (m, 2H, CH_2), 1.30–1.27 (m, 2H, CH_2). $^{13}\text{C}\{^1\text{H}\}$ NMR (150.7 MHz, CDCl_3) δ 174.6, 137.9, 132.2, 61.0, 49.7, 48.3, 45.7, 43.3, 42.5, 29.2, 28.2. FT-IR (ATR): $\nu = 3062$ (w), 2969 (w), 2878 (w), 2095 (s), 1729 (s), 1455 (w), 1336 (m), 1270 (m), 1172 (s), 1132 (m), 1066 (m), 991 (w), 905 (w), 838 (w) 710 (s) cm^{-1} . Mass Spec. (ESI, +ve mode) m/z : $[\text{M}]^+$ calc'd for $[\text{C}_{11}\text{H}_{15}\text{N}_3\text{O}_2]^+$, 221.1164; found, 221.1158; difference: -2.7 ppm.

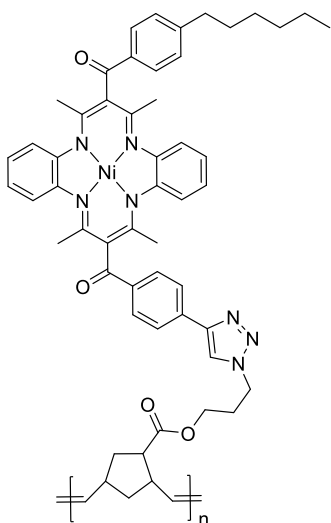
Synthesis of norbornene-functionalized macrocycle (5.10)



An oven-dried Schlenk flask was charged with CuI (1.3 mg, 0.068 mmol) and N,N,N',N'',N'' -pentamethyldiethylenetriamine (14.6 μL , 0.068 mmol) in dry/degassed THF (50 mL) and stirred for 10 min. To the reaction mixture was added compounds **5.8** (1.00 g, 1.40 mmol) and **5.10** (0.31 g, 1.40 mmol) and the mixture was stirred for 18 h at room temperature. The solvent was then removed *in vacuo*. Column chromatography (toluene/EtOAc, 19:1, 75 mL silica gel, $R_f = 0.13$) was performed to yield complex **5.10** as a dark green solid as the third fraction. Yield = 0.64 g, 54%. ^1H NMR (599.3 MHz, CDCl_3): δ 8.32–8.31 (m, 2H, aryl CH), 8.16 (s, 2H, aryl CH), 8.07 (d, 2H, $J_{\text{HH}} = 8$ Hz, aryl CH), 7.95 (s, 1H, triazole-CH), 7.40 (d, 2H, $J_{\text{HH}} = 8$ Hz, aryl CH), 6.68–6.66 (m, 4H, aryl CH), 6.60–6.58 (m, 4H, aryl CH), 6.23 (dd, 1H, $J_{\text{HH}} = 5, 3$ Hz, C=CH), 5.96 (dd, 1H, $J_{\text{HH}} = 6, 3$ Hz, C=CH), 4.55 (t, 2H, $J_{\text{HH}} = 6$ Hz, CH_2), 4.17–4.10 (m, 2H, CH_2), 3.23 (s, 1H, CH), 2.99–2.97 (m, 1H, CH), 2.94 (s, 1H, CH), 2.73 (t, 2H, $J_{\text{HH}} = 8$ Hz, CH_2), 2.36–2.33 (m, 2H, CH_2), 1.96–1.92 (m, 2H, CH_2), 1.92 (s, 6H, macrocycle CH_3), 1.90 (s, 6H, CH_3), 1.70–1.68 (m, 2H, CH_2), 1.47–1.28 (m, 10H, CH_2), 0.91–0.87 (m, 3H, macrocycle CH_3). $^{13}\text{C}\{^1\text{H}\}$ NMR (150.7 MHz, CDCl_3) δ 200.1, 199.7, 174.5, 153.7, 153.6, 149.4, 147.4, 147.3, 146.8, 138.6, 138.0, 136.7, 135.3, 132.0, 130.5, 130.4, 129.9, 129.0, 126.1, 122.7, 122.6, 121.8, 121.4, 121.0, 120.8, 60.5, 49.7, 47.4, 45.8, 43.3, 42.5, 36.1, 31.6, 31.1, 29.6, 29.2, 29.0, 22.6, 20.5, 20.4, 14.1. FT-IR (ATR): $\nu = 3058$

(w), 2928 (w), 2856 (w), 1729 (m), 1652 (m), 1603 (m), 1531 (s), 1448 (m), 1429 (m), 1363 (s), 1326 (m), 1224 (s), 1171 (s), 1054 (m), 912 (m), 839 (m), 732 (m), 704 (m), 535 (w) cm^{-1} . UV-vis (CH_2Cl_2): λ_{max} (ϵ) 590 nm ($5,900 \text{ M}^{-1} \text{ cm}^{-1}$), 429 nm (sh, $14,000 \text{ M}^{-1} \text{ cm}^{-1}$), 391 nm ($29,300 \text{ M}^{-1} \text{ cm}^{-1}$), 274 nm ($54,300 \text{ M}^{-1} \text{ cm}^{-1}$). Mass Spec. (ESI, +ve mode) m/z : $[\text{M}]^+$ calc'd for $[\text{C}_{55}\text{H}_{57}\text{N}_7\text{NiO}_4]^+$, 937.3825; found, 937.3853; difference: +2.8 ppm.

Polymerization of norbornene-functionalized macrocycle (5.11)



A grease-free Schlenk flask was charged with monomer **5.10** (0.100 g, 0.117 mmol) before dry and degassed CH_2Cl_2 (4 mL) was added. Once the monomer was dissolved a 10.4 mg mL^{-1} CH_2Cl_2 solution of Grubbs' 3rd generation catalyst (0.20 mL, 2.34×10^{-3} mmol) was rapidly added in one portion. The polymerization proceeded for 3 h before it was terminated with ethyl vinyl ether (0.28 mL, 2.93 mmol) and stirred for an additional 30 min. The crude mixture was filtered through a short neutral alumina column (4 cm \times 2.5 cm, CH_2Cl_2 then THF) before the solvent was removed *in vacuo*. The resultant polymer, a green solid was dissolved in THF (10 mL) and precipitated thrice into Et_2O (90, 90, and 15 mL) to afford **5.10** as a green powder. Yield = 0.084 g, 84%. ^1H NMR (599.3 MHz, CDCl_3): δ 8.22–8.03 (m, 7H, aryl CH and triazole CH), 7.36 (bs, 2H, aryl CH), 6.63 (s, 4H, aryl CH), 6.58 (s, 4H, aryl CH), 5.46–5.31 (m, 2H, C=CH), 4.56 (bs, 2H, CH_2), 4.14 (bs, 2H, CH_2), 3.19 (bs, 1H, CH), 2.94 (m, 2H, CH), 2.70 (s, 2H, CH_2), 2.33 (s, 2H, CH_2), 1.99–1.86 (m, 14H, macrocycle CH_3 and CH_2), 1.66 (s, 2H, CH_2), 1.36–1.31 (m, 10H, CH_2), 0.88 (s, 3H, CH_3). FT-IR (ATR): ν = 3062 (w), 2928 (w), 2856 (w), 1728 (m), 1652 (m), 1604 (m), 1532 (s), 1450 (m), 1429 (m), 1375 (s), 1326 (m), 1224 (s), 1172 (s), 1054 (m), 911 (m), 859 (w), 727 (s) cm^{-1} . UV-vis (CH_2Cl_2): λ_{max} (ϵ) 592 nm ($4,000 \text{ M}^{-1} \text{ cm}^{-1}$), 430 nm (sh, $9,600 \text{ M}^{-1} \text{ cm}^{-1}$), 391 nm ($19,800 \text{ M}^{-1} \text{ cm}^{-1}$), 274 nm ($36,900 \text{ M}^{-1} \text{ cm}^{-1}$). GPC (THF, conventional calibration): $M_n = 24,100 \text{ g mol}^{-1}$, $M_w = 26,500 \text{ g mol}^{-1}$, $D = 1.12$).

Variation of Feed Molar Ratio: Using 0.05 g of monomer **5.10** each, a series of five reactions were carried out according to the procedure described above. The catalyst molar feed stock ratios (monomer:catalyst) were: 20, 40, 60, 80, and 100. The polymerization times were held constant at 30 min. The number average degree of polymerization (DP_n) for each sample was measured by GPC analysis using conventional calibration relative to polystyrene standards.

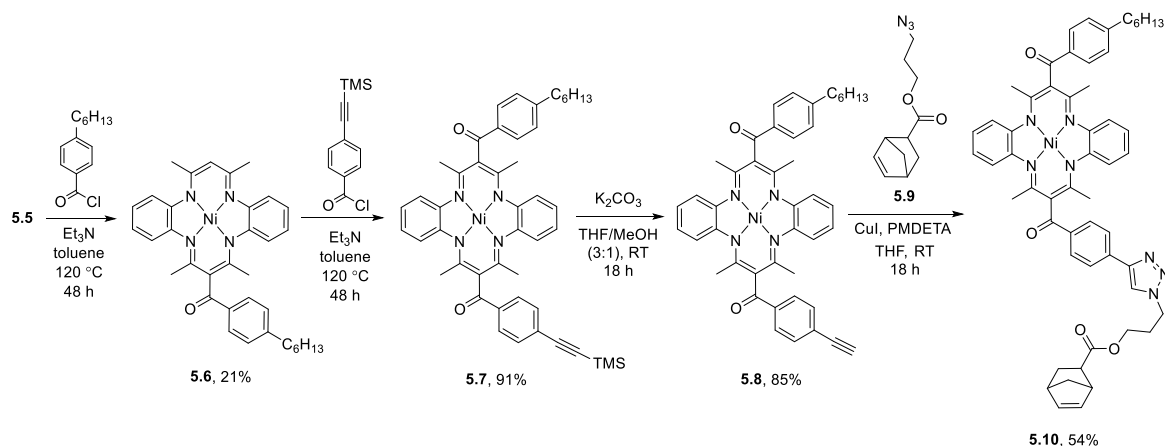
Monitoring Polymerization Progress with Timed Aliquots: A 1 mg mL⁻¹ CH₂Cl₂ solution of 3-bromopyridine derivative of Grubbs' 3rd generation catalyst (1.0 mL, 6.4 × 10⁻³ mmol) was rapidly added in one portion to a 27 mg mL⁻¹ CH₂Cl₂ solution of monomer **5.10** (11 mL, 0.32 mmol) and the mixture was stirred at 0 °C. Eight samples were removed at different time intervals (60, 120, 210, 300, 450, 600, 750, and 900 s) and added into separate reaction flasks containing excess ethyl vinyl ether to terminate the polymerization. The number average molecular weights (M_n) were measured by GPC analysis using conventional calibration relative to polystyrene standards and monomer to polymer ratios were monitored using NMR analysis.

5.3 Results and Discussion

5.3.1 Monomer Synthesis

The synthesis of monomer **5.10** (Scheme 5.1) began with the reaction of 4-hexylbenzoyl chloride with the Ni(II) complex of Goedken's macrocycle (**5.5**) in the presence of Et₃N. This condensation reaction afforded compound **5.6** in 21% yield. This transformation suffers from a low yield due to the statistical formation of unsubstituted (**5.5**), mono- and di-4-*n*-hexylbenzoyl substituted macrocycles, with yields of 26, 28, and 21%, respectively. The 4-hexylbenzoyl substituent was chosen to increase the solubility of the targeted polymers and to circumvent potential reactivity of the C-H present on the backbone. Next, 4-(TMS-ethynyl)benzoyl chloride was combined with **5.6** in the presence of Et₃N to afford compound **5.7** in 91% yield. The ethynyl functionality was deprotected using K₂CO₃ giving compound **5.8** in 85% yield. We chose to use the *endo*-norbornene derivative because it afforded the advantages of simplified ¹H and ¹³C{¹H} NMR spectra and slower reactions⁴⁶ which improves our ability to probe the reaction kinetics of this polymerization. The *endo*-

norbornene carboxylic acid was purified using an existing protocol.⁴⁵ Compound **5.9** was synthesized by combining 3-azido-1-propanol with *endo*-5-norbornene-2-carboxylic acid, using the Steglich esterification,⁴⁷ in 62% yield. Taking advantage of the azide and alkyne functional groups, a copper(I)-catalyzed azide-alkyne cycloaddition (CuAAC) reaction was performed to produce monomer **5.11** in 54% yield. Compounds **5.6–5.10** were characterized by high resolution mass spectrometry ¹H and ¹³C{¹H} NMR spectroscopy, FT-IR, and UV-vis absorption spectroscopy (see appendix 5).



Scheme 5.1 Synthesis of monomer **5.10**.

5.3.2 Polymerization

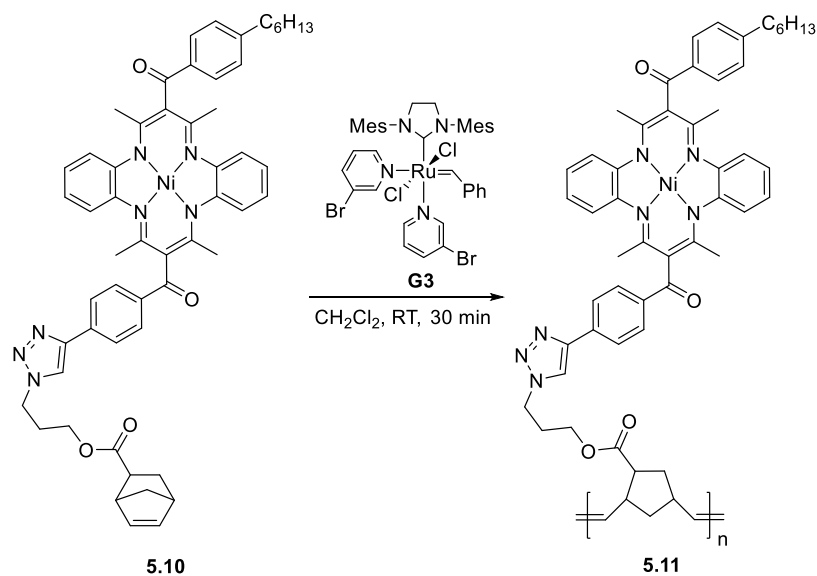
Once monomer **5.10** was synthesized, its polymerization behavior was studied. ROMP was chosen because it is tolerant of many organic solvents and functional groups. Solvent choice can effect the reaction kinetics of ROMP,⁴⁸ therefore, different solvents were screened for the polymerization. A typical polymerization reaction involved the rapid introduction of a solution of a 3-bromopyridine derivative of Grubbs' 3rd generation catalyst to a stirring solution of **5.10** at ambient temperature (21 °C) with a monomer to catalyst ratio of 50:1 (Scheme 5.2). The solvents that were tested included THF, DMF, and CH₂Cl₂ as the polymerization was not limited by the solubility of the monomer in these solvents. Monomer **5.10** was subjected to the same reaction conditions in each solvent and the resulting polymers were analyzed by GPC (Table 5.1). Polymerization in THF gave undesirable, broadened molecular weight distributions ($\mathcal{D} = 2.69$), and the reaction did not proceed when performed in DMF. The polymerization in CH₂Cl₂ produced polymers with

narrow molecular weight distributions ($\mathcal{D} = 1.12$), which is what is typically observed for a controlled polymerization protocol such as ROMP.

Table 5.1 MW data for the polymer **5.11** produced in different solvents.

Solvent	M_n (g mol ⁻¹)	M_w (g mol ⁻¹)	\mathcal{D}
THF	16,500	44,600	2.69
DMF	-	-	-
CH ₂ Cl ₂	24,100	26,500	1.12

Reaction progress in CH₂Cl₂ was monitored by the disappearance of signals associated with norbornene in the monomer (6.23 and 5.96 ppm) and appearance of olefinic signals associated with the polymer (5.46–5.31 ppm) in the corresponding ¹H NMR spectra. The reaction neared completion after approximately 15 min, and it was stirred for another 15 min to ensure complete conversion. This was followed by the addition of ethyl vinyl ether (EVE) to terminate the polymerization. The reaction mixture was passed through an alumina plug using THF to remove the catalyst, followed by precipitation from THF into Et₂O, and centrifugation and drying *in vacuo* to afford polymer **5.11** in 84% yield.



Scheme 5.2 ROMP of monomer **5.10** using Grubbs' 3rd generation catalyst.

5.3.3 Kinetic Studies

We performed two different studies on our norbornene-based monomers to further investigate the polymerization behaviour of our novel monomer. Typically, the molecular

weight of polymers can be determined by end-group analysis via ^1H NMR integration data. Unfortunately, the signals associated with the phenyl moiety on the end group were shrouded by the aromatic proton signals associated with Goedken's macrocycle (7.4–7.3 ppm), precluding end-group analysis for this polymer system. Therefore, the molecular weights of the polymers were estimated using GPC analysis (conventional calibration referencing PS). GPC analysis using triple detection methods were also unavailable as the absorbance maxima of the polymer at 593 nm overlaps with that of the laser used for the light scattering detector (630 nm). It is important to note that due to the significant difference between PS and the target polymer **5.11**, it is expected that the measured molecular weight will not accurately reflect the molecular weight of our polymer. However, GPC still allowed for a useful comparison of different molecular weights during kinetic experiments, and confirmed that high molecular weight polymers have been produced.

The first study involved a single ROMP reaction (monomer:catalyst 50:1) with the M_n measured as a function of time (Figure 5.1). The molecular weight of the polymer increased over time, with the reaction nearing completion around 300 s and complete conversion seen over 600 s made evident by the plateau appearing after 600 s (Figure 5.1a). This behaviour was consistent with a well-behaved ROMP reaction with limited side reactivity, whereby the rate of reaction decreases as the monomer is consumed. The consumption of monomer as a function of time was monitored by ^1H NMR spectroscopy using the ratio of olefinic signals of monomer (6.23 and 5.96 ppm) and polymer (5.46–5.31 ppm). A semilogarithmic plot (Figure 5.1b) as a function of time shows a linear trend between $\ln[M]_0/[M]$ and time, consistent with living polymerization (black line), where $[M]_0$ is the initial concentration of monomer and $[M]$ the concentration of monomer at different time intervals in solution.

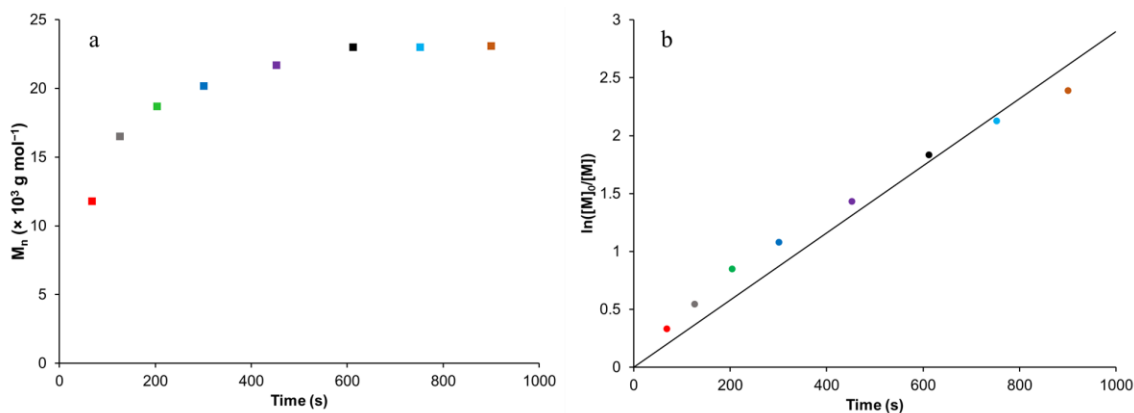


Figure 5.1 (a) Number average molecular weight (M_n) as a function of time from GPC, (b) semilogarithmic plot for the consumption of monomer **5.10** as a function of time. $[M]_0/[M]$ was determined using ^1H NMR integration data.

The second experiment was designed to further examine the ROMP of monomer **5.10** and involved several reactions with different feed molar (monomer:catalyst) ratios (Figure 5.2). The ratios (monomer:catalyst) studied were 20, 40, 60, 80, and 100. The molecular weights, and thus degree of polymerization, were analyzed by GPC. The measured molecular weight of the polymers increased as the feedstock ratios were increased from 20 to 100. The GPC traces of the different experiments are presented in Figure 5.2a and reveal increased average molecular weights as the molar feedstock ratio was increased. The linear relationship between monomer:feedstock and DP_n predicted was not maintained at high ratios as the increased number of ring-opening reactions required also increased the probability of side reactions (Figure 5.2b). The deviation of polymer molecular weights from ideal behaviour (black line, Figure 5.2b) may be due to the underestimation of the molecular weights by conventional calibration GPC. The upward tailing at higher feed molar ratio may imply early termination and/or side reactivity. These results demonstrate that this ROMP is well-behaved, although does not exhibit perfect living character.

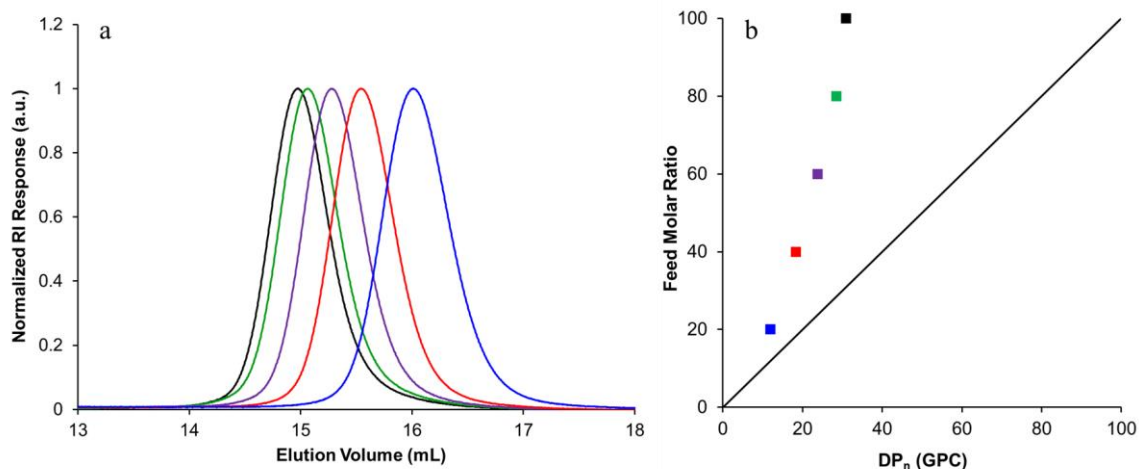


Figure 5.2 (a) GPC traces of polymer samples at different catalyst loadings. The graphs have been colour coded for ease of comparison. (b) Relationship of feed molar ratio and DP_n determined by GPC using conventional calibration. The black line depicts ideal behaviour.

5.3.4 Polymer Characterization

TGA analysis of a representative sample of polymer **5.11** revealed its stability up to a temperature of 278 °C, followed by a rapid decomposition to *ca.* 40% mass, then a slow decomposition to an overall char yield of 6% when heated to 1000 °C (Figure A5.12). A sample of polymer **5.11** was also analyzed by DSC where it was heated to 250 °C followed by a cooling to -50 °C, and the cycle was repeated twice more. The second heating/cooling cycle was used to determine a $T_g = 211$ °C (Figure A5.13).

The UV-vis absorption spectra of monomer **5.10** and polymer **5.11** were very similar (Figure 5.3). The characteristic absorption maxima for Ni(II) complexes of Goedken's macrocycle in monomer **5.10** [590 nm ($5,900 \text{ M}^{-1} \text{ cm}^{-1}$), 429 nm (sh, $14,000 \text{ M}^{-1} \text{ cm}^{-1}$), 391 nm ($19,800 \text{ M}^{-1} \text{ cm}^{-1}$), and 274 nm ($54,300 \text{ M}^{-1} \text{ cm}^{-1}$) nm] were conserved in the polymer [592 nm ($4,000 \text{ M}^{-1} \text{ cm}^{-1}$), 430 nm (sh, $9,600 \text{ M}^{-1} \text{ cm}^{-1}$), 391 nm ($19,800 \text{ M}^{-1} \text{ cm}^{-1}$), and 274 nm ($36,900 \text{ M}^{-1} \text{ cm}^{-1}$) nm].

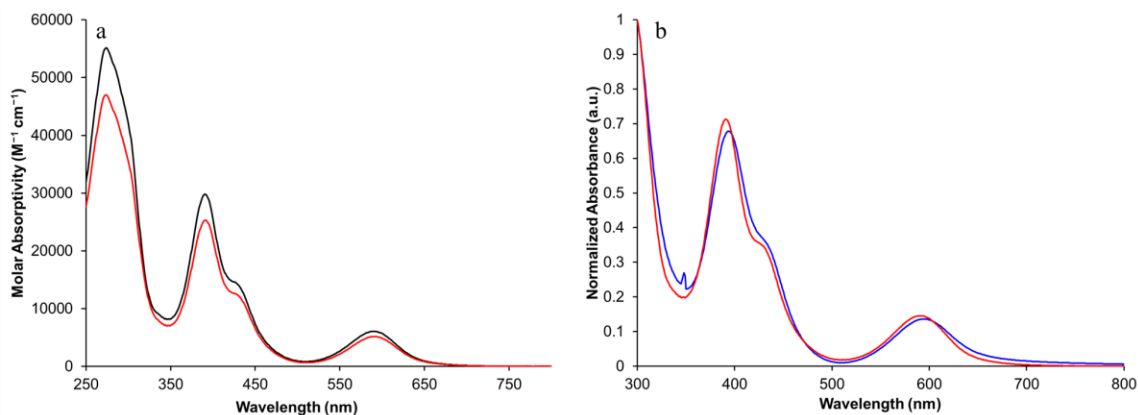


Figure 5.3 (a) UV-vis absorption spectra recorded in CH_2Cl_2 of monomer **5.10** (black) and polymer **5.11** (red). (b) UV-vis absorption spectra of polymer **5.11** in CH_2Cl_2 (red) and as a thin-film (blue).

The thin-film absorption properties of polymer **5.11** were also studied. The film was produced by spin coating a solution of the polymer in chlorobenzene (15 mg mL^{-1}) on a glass slide at 3000 rpm. The UV-vis spectrum was similar to that of the solution sample with absorption maxima at 396, 438 (sh), and 596 nm, confirming the conservation of the Ni(II) macrocycle in the side-chain polymer and the lack of significant interactions between macrocycle units in the solid state (Figure 5.3b).

The electrochemical properties of monomer **5.10** and polymer **5.11** were explored in CH_2Cl_2 (Figure 5.4, Table 5.2). In the cyclic voltammogram (CV) of the monomer, two reversible oxidation waves with half-wave potentials at 0.21 and 0.72 V vs the ferrocene/ferrocenium redox couple were observed. These waves correspond to the oxidation of the Ni-macrocycle (NiL) to the radical cation ($\text{NiL} \rightarrow \text{NiL}^{\bullet+}$) followed by the oxidation to the dication ($\text{NiL}^{\bullet+} \rightarrow \text{NiL}^{2+}$). In unfunctionalized derivatives, oxidative dimerization occurs during electrochemical studies.^{39, 49} Our monomer design has shut down this reactive pathway. An irreversible reduction was also observed for the monomer at $E_{\text{pc}(2)} = -2.14 \text{ V}$, which was previously assigned to the reduction of Ni.⁴⁹ The irreversibility of the electrochemical reduction wave suggests decomposition of the newly formed species.

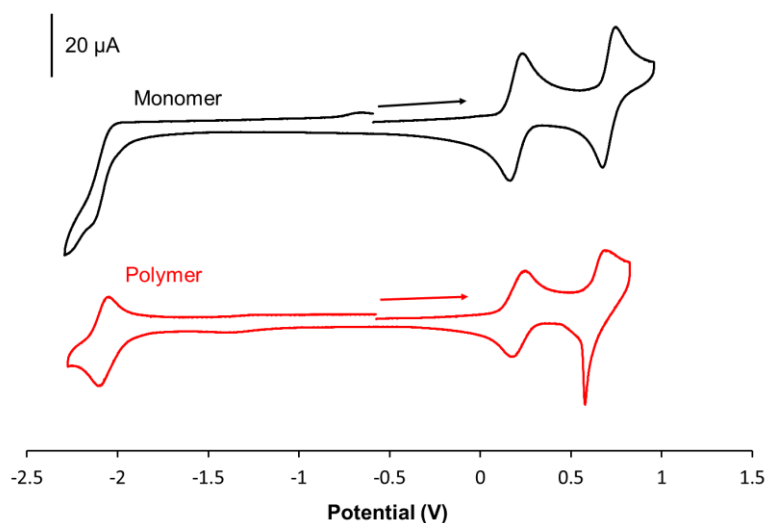


Figure 5.4 CVs of **5.10** (black) and **5.11** (red) recorded at a scan rate of 250 mV s^{-1} in CH_2Cl_2 solutions containing $1 \times 10^{-3} \text{ M}$ analyte and 0.1 M $[\text{nBu}_4\text{N}][\text{PF}_6]$ as supporting electrolyte.

Table 5.2 Cyclic voltammetry data for monomer **5.10** and polymer **5.11**.

Compound	$E_{\text{pc}(2)}$	$E_{\text{red}1}^\circ$	$E_{\text{ox}1}^\circ$	$E_{\text{pc}(1)}$	$E_{\text{pa}(1)}$	$E_{\text{ox}2}^\circ$
5.10	-2.14	-	0.21	-	-	0.72
5.11	-	-2.07	0.21	0.57	0.70	-

In the CV of the polymer, two oxidation events with half-wave potentials at 0.21 and 0.62 V were observed (Table 5.2). The first oxidation appears to be fully reversible, while the second oxidation showed E_{pa} at *ca.* 0.70 V, with a sharp cathodic peak ($E_{\text{pc}(1)} = 0.57 \text{ V}$) most likely caused by the plating of the dicationic species onto the working electrode surface, a common observation for redox-active polymers. To address the insolubility of the dicationic species different solvents were employed. CV experiments were run in THF, although the first oxidation to the radical cation demonstrated similar behaviour with a sharp cathodic reduction most likely caused by insolubility. The oxidation to the dicationic species was improved and did not show any significant electrode plating. Unfortunately, the combination of THF and CH_2Cl_2 (1:1 mixture) did not result in improved electrochemical behaviour and the oxidation of the macrocycle units in this solvent system were irreversible (Figure 5.5). DMF, and DMF: CH_2Cl_2 (1:1 mixture) solutions were also studied, but were plagued by the poor solubility of the analyte.

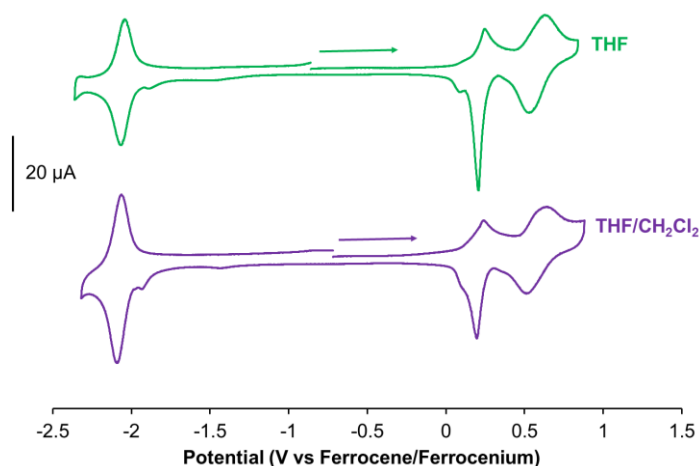


Figure 5.5 CVs of polymer **5.11** in THF (green) and THF/CH₂Cl₂ (1:1) solvent mixture (purple) recorded at a scan rate of 250 mV s⁻¹ in CH₂Cl₂ solutions containing 1 × 10⁻³ M analyte and 0.1 M [*n*Bu₄N][PF₆] as supporting electrolyte.

Furthermore, the polymer exhibited a reversible one-electron reduction wave associated with Ni (Ni²⁺ → Ni⁺),⁴⁹⁻⁵⁰ with a half-wave potential of -2.07 V. The difference in electrochemical behaviour of the monomer and polymer must arise from the macromolecular nature of the polymer, where the electrogenerated Ni⁺ species is protected by the tertiary structure of the polymer. This behaviour has been observed for related molecular species in the past.^{39, 50-53}

5.4 Conclusion

This chapter describes the design of a novel side-chain polymer **5.11**, incorporating Ni(II)-complexes of Goedken's macrocycle, one of the few examples of side-chain Ni-containing MCPs. ROMP was performed using a Grubbs' 3rd generation catalyst and a norbornene polymerizable group. The reaction was well behaved, although did not formally satisfy the criteria for a living polymerization. Polymer **5.11**, in solution and the solid state, exhibited UV-vis absorbance spectra similar to the monomeric unit and characteristic of Ni(II)-complexes of Goedken's macrocycle. The polymer also demonstrated three redox events, including two separate macrocycle-centred oxidations and a reversible reduction

associated with Ni. This behaviour was unique to the polymer, as the discrete monomer **5.10** showed an irreversible reduction at similar potential.

5.5 References

1. Holliday, B. J.; Swager, T. M. *Chem. Commun.* **2005**, 23–36.
2. Wong, W.-Y.; Harvey, P. D. *Macromol. Rapid Commun.* **2010**, *31*, 671–713.
3. Whittell, G. R.; Hager, M. D.; Schubert, U. S.; Manners, I. *Nat. Mater.* **2011**, *10*, 176–188.
4. Friebe, C.; Hager, M. D.; Winter, A.; Schubert, U. S. *Adv. Mater.* **2012**, *24*, 332–345.
5. Khramov, D. M.; Rosen, E. L.; Lynch, V. M.; Bielawski, C. W. *Angew. Chem. Int. Ed.* **2008**, *47*, 2267–2270.
6. O'Sullivan, T. J.; Djukic, B.; Dube, P. A.; Lemaire, M. T. *Chem. Commun.* **2009**, 1903–1905.
7. Gilroy, J. B.; Patra, S. K.; Mitchels, J. M.; Winnik, M. A.; Manners, I. *Angew. Chem. Int. Ed.* **2011**, *50*, 5851–5855.
8. Ren, L.; Zhang, J.; Hardy, C. G.; Ma, S.; Tang, C. *Macromol. Rapid Commun.* **2012**, *33*, 510–516.
9. Soliman, A. M.; Fortin, D.; Zysman-Colman, E.; Harvey, P. D. *Macromol. Rapid Commun.* **2012**, *33*, 522–527.
10. Padhy, H.; Ramesh, M.; Patra, D.; Satapathy, R.; Pola, M. K.; Chu, H.-C.; Chu, C.-W.; Wei, K.-H.; Lin, H.-C. *Macromol. Rapid Commun.* **2012**, *33*, 528–533.
11. Friebe, C.; Görls, H.; Jäger, M.; Schubert, U. S. *Eur. J. Inorg. Chem.* **2013**, *2013*, 4191–4202.

12. Wild, A.; Teichler, A.; Ho, C.-L.; Wang, X.-Z.; Zhan, H.; Schlütter, F.; Winter, A.; Hager, M. D.; Wong, W.-Y.; Schubert, U. S. *J. Mater. Chem. C* **2013**, *1*, 1812–1822.
13. Yan, Y.; Zhang, J.; Qiao, Y.; Ganewatta, M.; Tang, C. *Macromolecules* **2013**, *46*, 8816–8823.
14. Wang, X.; Cao, K.; Liu, Y.; Tsang, B.; Liew, S. *J. Am. Chem. Soc.* **2013**, *135*, 3399–3402.
15. Ma, Y.; Dong, W.-F.; Hempenius, M. A.; Möhwald, H.; Vancso, G. J. *Nat. Mater.* **2006**, *5*, 724–729.
16. Staff, R. H.; Gallei, M.; Mazurowski, M.; Rehahn, M.; Berger, R.; Landfester, K.; Crespy, D. *ACS Nano* **2012**, *6*, 9042–9049.
17. Péter, M.; Lammertink, R. G. H.; Hempenius, M. A.; Vancso, G. J. *Langmuir* **2005**, *21*, 5115–5123.
18. Arsenault, A. C.; Puzzo, D. P.; Manners, I.; Ozin, G. A. *Nat. Photonics* **2007**, *1*, 468–472.
19. Zhang, J.; Chen, Y. P.; Miller, K. P.; Ganewatta, M. S.; Bam, M.; Yan, Y.; Nagarkatti, M.; Decho, A. W.; Tang, C. *J. Am. Chem. Soc.* **2014**, *136*, 4873–4876.
20. Al-Badri, Z. M.; Maddikeri, R. R.; Zha, Y.; Thaker, H. D.; Dobriyal, P.; Shunmugam, R.; Russell, T. P.; Tew, G. N. *Nat. Commun.* **2011**, *2*, 482.
21. Wong, W.-Y.; Wang, X.-Z.; He, Z.; Djurišić, A. B.; Yip, C.-T.; Cheung, K.-Y.; Wang, H.; Mak, C. S. K.; Chan, W.-K. *Nat. Mater.* **2007**, *6*, 521–527.
22. Baljak, S.; Russell, A. D.; Binding, S. C.; Haddow, M. F.; O'Hare, D.; Manners, I. *J. Am. Chem. Soc.* **2014**, *136*, 5864–7.
23. Fukumoto, H.; Yamane, K.; Kase, Y.; Yamamoto, T. *Macromolecules* **2010**, *43*, 10366–10375.

24. Novoa, N.; Soto, J. P.; Henríquez, R.; Manzur, C.; Carrillo, D.; Hamon, J.-R. *J. Inorg. Organomet. Polym. Mater.* **2013**, *23*, 1247–1254.
25. Scamporrino, E.; Vitalini, D. *Macromolecules* **1992**, *25*, 1625–1632.
26. Eichhorn, H.; Sturm, M.; Wöhrle, D. *Macromol. Chem. Phys.* **1995**, *196*, 115–131.
27. Ding, X.; Guo, J.; Feng, X.; Honsho, Y.; Guo, J.; Seki, S.; Maitarad, P.; Saeki, A.; Nagase, S.; Jiang, D. *Angew. Chem. Int. Ed.* **2011**, *50*, 1289–1293.
28. Abel, M.; Clair, S.; Ourdjini, O.; Mossoyan, M.; Porte, L. *J. Am. Chem. Soc.* **2011**, *133*, 1203–1205.
29. Colson, J. W.; Dichtel, W. R. *Nat. Chem.* **2013**, *5*, 453–465.
30. Goedken, V. L.; Weiss, M. C.; Place, D.; Dabrowiak, J. *Inorg. Synth.* **1980**, 115–119.
31. Niewahner, J. H.; Walters, K. A.; Wagner, A. *J. Chem. Educ.* **2007**, *84*, 477.
32. Cotton, F. A.; Czuchajowska, J. *Polyhedron* **1990**, *9*, 2553–2566.
33. Mountford, P. *Chem. Soc. Rev.* **1998**, *27*, 105–115.
34. Raston, C. L.; Nichols, P. J.; Baranyai, K. *Angew. Chem. Int. Ed.* **2000**, *39*, 1842–1845.
35. Basiuk, E. V.; Rybak-Akimova, E. V.; Basiuk, V. A.; Acosta-Najarro, D.; Saniger, J. M. *Nano Lett.* **2002**, *2*, 1249–1252.
36. Liu, S.-J. *Electrochim. Acta* **2004**, *49*, 3235–3241.
37. Williams, U. J.; Mahoney, B. D.; DeGregorio, P. T.; Carroll, P. J.; Nakamaru-Ogiso, E.; Kikkawa, J. M.; Scheluter, E. J. *Chem. Commun.* **2012**, *48*, 5593–5595.
38. Basiuk, E. V.; Martinez-Herrera, M.; Álvarez-Zauco, E.; Henao-Holguin, L. V.; Puente-Lee, I.; Basiuk, V. A. *Dalton Trans.* **2014**, *43*, 7413–7428.

39. Bailey, C. L.; Bereman, R. D.; Rillema, D. P.; Nowak, R. *Inorg. Chem.* **1986**, *25*, 933–938.
40. Deronzier, A.; Marques, M. J. *J. Electroanal. Chem.* **1989**, *265*, 341–353.
41. Deronzier, A.; Marques, M. J. *J. Electroanal. Chem.* **1992**, *334*, 247–261.
42. Huang, H.-H.; Chao, C.-G.; Lee, S.-L.; Wu, H.-J.; Chen, C.-H.; Luh, T.-Y. *Org. Biomol. Chem.* **2012**, *10*, 5948–5953.
43. Gwyther, J.; Gilroy, J. B.; Rugar, P. A.; Lunn, D. J.; Kynaston, E.; Patra, S. K.; Whittell, G. R.; Winnik, M. A.; Manners, I. *Chem. Eur. J.* **2013**, *19*, 9186–9197.
44. Bertoldo, M.; Zampano, G.; Terra, F. L.; Villari, V.; Castelvetro, V. *Biomacromolecules* **2011**, *12*, 388–398.
45. Berson, J. A.; Ben-Efraim, D. A. *J. Am. Chem. Soc.* **1959**, *81*, 4083–4087.
46. *Handbook of Metathesis: Polymer Synthesis*. 2nd ed.; WILEY-VCH Verlag GmbH & Co.: Weinheim, 2015.
47. Neises, B.; Steglich, W. *Angew. Chem. Int. Ed.* **1978**, *17*, 522–524.
48. Bielawski, C. W.; Grubbs, R. H. *Prog. Polym. Sci.* **2007**, *32*, 1–29.
49. Kim, D.; Kim, E.; Byun, J.; Choi, J.; Na, H.; Park, Y. *J. Coord. Chem.* **2002**, *55*, 505–516.
50. Na, H. G.; Lee, D. C.; Lim, J. W.; Choi, J. H.; Byun, J. C.; Park, Y. C. *Polyhedron* **2002**, *21*, 917–923.
51. Streeky, J. A.; Pillsbury, D. G.; Busch, D. H. *Inorg. Chem.* **1980**, *19*, 3148–3159.
52. Bailey, C. L.; Bereman, R. D.; Rillema, D. P.; Nowak, R. *Inorg. Chem.* **1984**, *23*, 3956–3960.
53. Ricciardi, G.; Lelj, F. *Polyhedron* **1992**, *11*, 2089–2097.

Chapter 6

6 Conclusions and Future Work

6.1 Conclusions

The work presented throughout this thesis describes the incorporation of two different stable radicals into polymer scaffolds and the study of their physical and chemical properties. The incorporation of a 6-oxoverdazyl stable organic radical group appended to a methacrylate polymerizable functionality (Figure 6.1) yielded the first well-characterized example of a 6-oxoverdazyl being incorporated into a polymer. This methodology required the polymerization of the tetrazane precursor in order to use AIBN free radical polymerization followed by oxidation to the radical species. Post-polymerization reactions often suffer from poor conversions, but our methodology showed conversion of *ca.* 95% of the neutral species to radical species. We were able to demonstrate the tunability of the redox behaviour by modifying the substituents attached to the verdazyl moiety (*i*Pr and Ph) to shift the reduction half wave potential from -1.5 to -1.0 V vs. the ferrocene redox couple. The ability to modify the redox potentials will allow for incorporation into devices that may require different potentials to efficiently communicate electronically within the device. This system also displayed minimal change in the structural metrics upon oxidation, which is a crucial feature when they are to be used as redox-active materials for organic electronics.

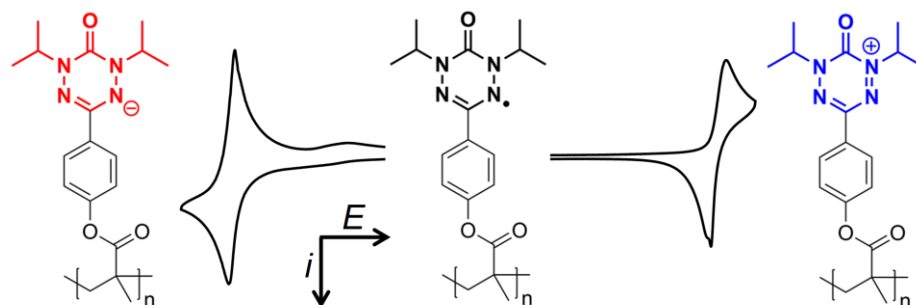


Figure 6.1 Graphical summary of Chapter 1.

Taking this system further, we combined *isopropyl-6-oxoverdazyl* stable organic radicals with a *cis-5-norbornene-*exo*-2,3-dicarboximide* polymerizable group. With this system, we were able to directly polymerize the 6-oxoverdazyl radical monomer using ROMP with Grubbs' 3rd generation catalyst, ensuring high radical content in the resulting polymer. This polymerization protocol led to the creation of polymers with controllable and narrow molecular weight distributions. The redox properties of this polymer were explored further by incorporation into different organic electronics. Initially, it was incorporated into thin-film devices that exhibited high and low conductivity states based on the applied voltage bias, creating a switchable conducting-insulating device. This material was also incorporated into an ultrathin memristor device (10 nm) that demonstrated three tunable charge states: positive, neutral, and negative (Figure 6.2). As the field of organic radical polymers is heavily focused on the design of battery systems, this research shows that the unique reactivity and stability of these materials are useful beyond charge storage and illustrate the suitability for different applications.

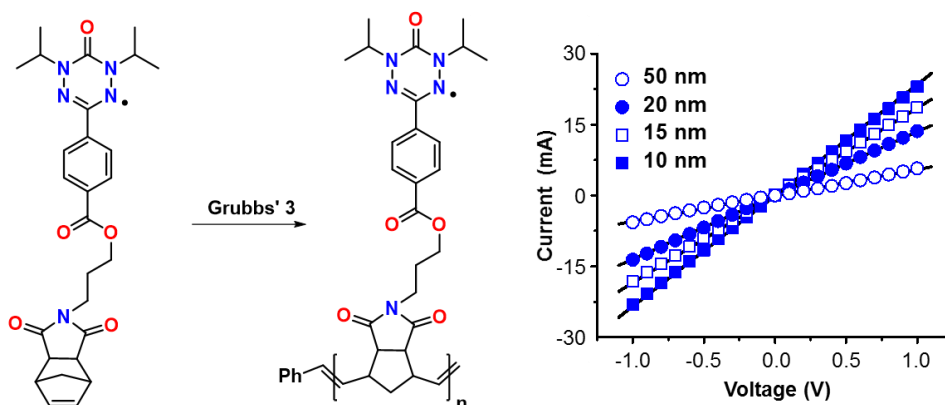


Figure 6.2 Graphical summary of Chapter 2.

The second family of polymers studied in this thesis incorporated Ni(II) complexes of Goedken's macrocycle into main-chain and side-chain architectures. The electronic and spectroscopic properties of this macrocycle have been extensively explored, but their incorporation into polymers was unprecedented. We utilized an alkyne functionalized version of Goedken's macrocycle in tandem with a variety of organic spacers in order to produce a highly π -delocalized copolymer via a step-growth Sonogashira cross-coupling reaction. The resulting polymers showed impressive thermal stability, conservation of

electronic spectra, and preserved redox behaviour. As a result of having an alkyne functionality available, we introduced a cobalt carbonyl into the system to create a heterobimetallic copolymer (Figure 6.3). Due to the macromolecular nature of this system, we were also able to take advantage of the processability of the materials. Thin-films of the system, before and after incorporation of cobalt, were cast and pyrolyzed in a reducing atmosphere to create nanomaterials, where the composition was influenced by the structure of the polymer. Control of elemental composition at the nanoscale becomes a more important research area as technology and electronics require less space to fulfill more demanding tasks. This study was successful in demonstrating some degree of control over molecular structure, although it requires an extensive synthesis pathway which may be a barrier to the scale-up of this polymer for commercialization.

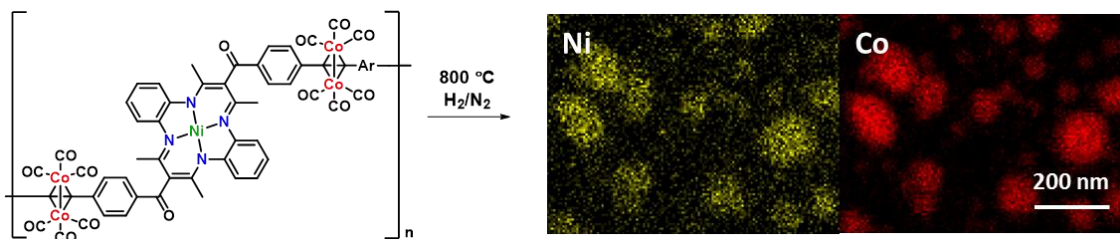


Figure 6.3 Graphical summary of Chapter 4.

To expand the functionality of the Ni(II) complex of Goedken's macrocycle we also produced side-chain polymers via a chain-growth mechanism utilizing norbornene polymerizable group and ROMP (Figure 6.4). This polymerization method produced well-defined polymers with narrow molecular weight distributions. The spectroscopic and electronic properties of the macrocycle were preserved in the polymer, which even showed the reversible redox behaviour of Ni²⁺ during cyclic voltammetry measurements in CH₂Cl₂, a process that was observed to be irreversible in the discrete monomer. The developed synthetic methodologies will allow for the expansion of this polymers series in order to tune electronic and physical properties for the incorporation into organic electronic devices or nanomaterials in the future.

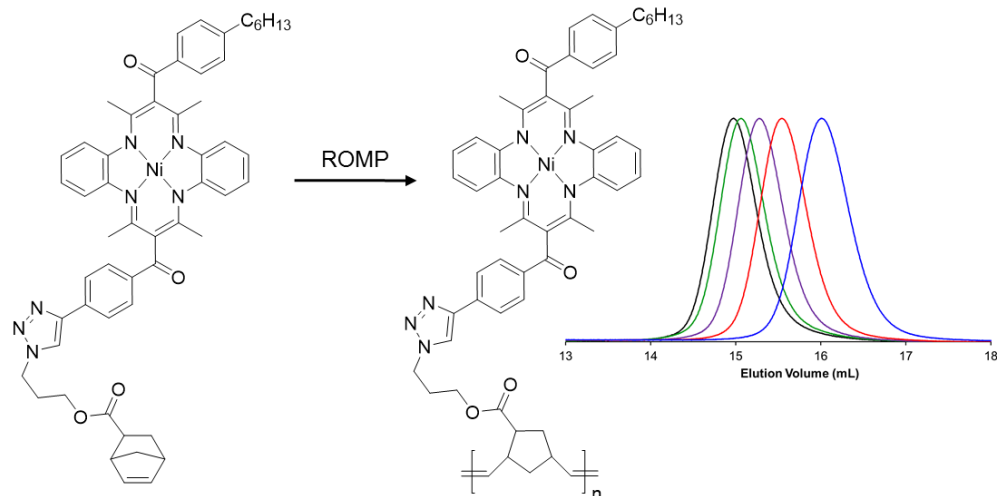
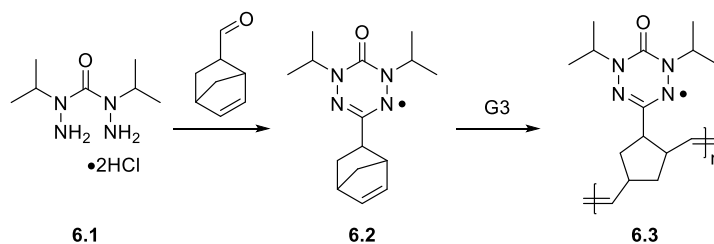


Figure 6.4 Graphical summary of Chapter 5.

6.2 Future Work

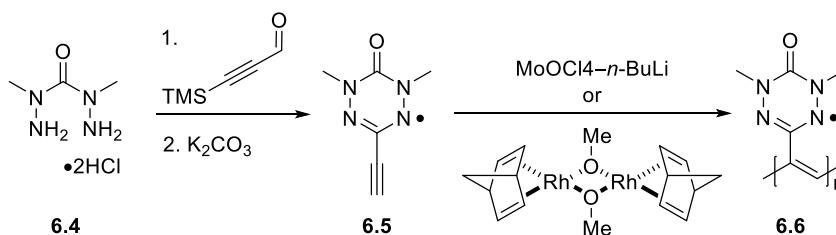
6.2.1 6-Oxoverdazyl Radical Polymers

Stable organic radicals incorporated into polymer systems has revealed many interesting applications for these materials that take advantage of their unique redox behaviour. The 6-oxoverdazyl system, compared to other radicals, offers distinct advantages in terms of stability and tunability of the redox potentials. However, the 6-oxoverdazyl polymers discussed in this thesis have relatively low radical content, considering the molecular weight of the repeating unit. By decreasing the overall molecular weight of the repeating unit we can target organic electronic devices that require increased radical content. The proposed synthetic route (Scheme 6.1), would produce an *isopropyl*-6-oxoverdazyl radical monomer (**6.2**) with a much lower molecular weight monomer unit, while still allowing for a controlled polymerization by ROMP utilizing a norbornene polymerizable group to produce **6.3**.



Scheme 6.1 Proposed synthesis of an *isopropyl-6-oxoverdazyl* polymer with higher radical content using ROMP.

One of the most popular applications for stable organic radical polymers involves their incorporation into batteries, as the charge storage material. Important criteria for these battery materials are high charge capacity, high radical content, robust redox cycling, and minimal distance between adjacent radical sites.¹⁻³ Most of these factors are dependent on the molecular weight of the repeating unit, therefore the design of a 6-oxoverdazyl with a relatively low molecular weight would be ideal. The proposed synthesis would take advantage of a methyl-6-oxoverdazyl radical unit⁴ appended to an ethynyl group (**6.5**) which would then be polymerized with a living mechanism using a molybdenum⁵ or rhodium⁶ catalyst to produce polymer **6.6** (Scheme 6.2).



Scheme 6.2 Proposed synthetic route towards 6-oxoverdazyl polymers with higher radical content metal-catalyzed polymerization.

The resulting polymers would have the highest theoretical charge density and the smallest distance between radical units of any polymer reported to date (Figure 6.5).^{2,7} Furthermore, the stability of the verdazyl radical may even rival that of polymers used in existing radical battery technologies which are based on nitroxide radicals. This synthetic strategy may also afford an advantage due to the direct polymerization of the radical species circumventing post-polymerization modification and ensuring each repeating unit contains a radical. This approach could be expanded to include other variations of the verdazyl polymer, including

the phenyl-6-oxoverdazyl and the phenyl-verdazyl radicals in order to study the effect of different redox potentials in the electronic materials.

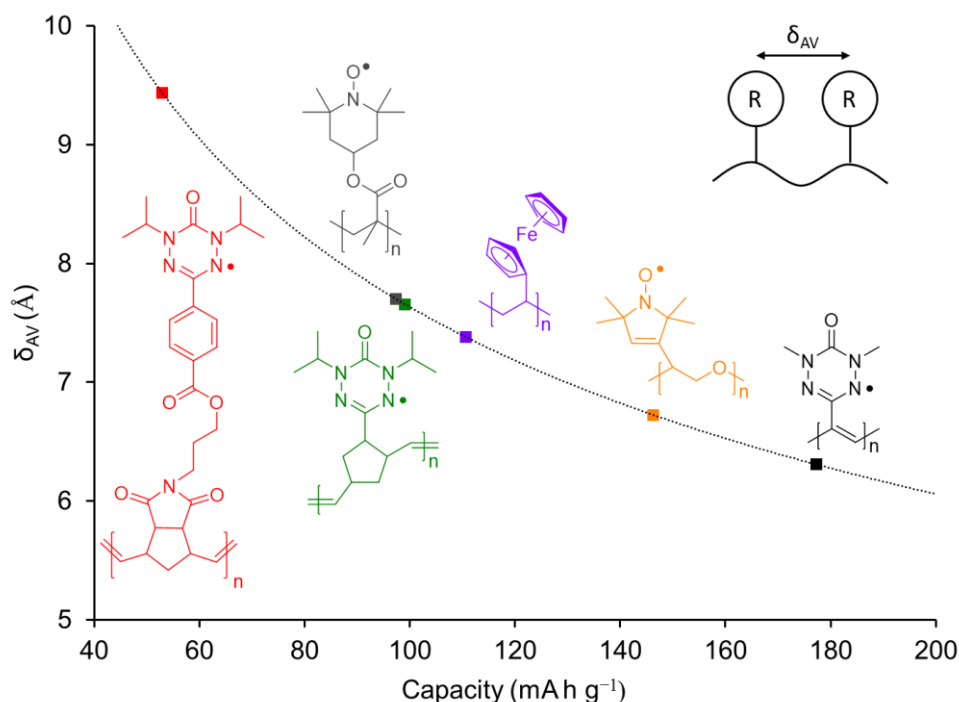


Figure 6.5 Plot of mean intersite distance (δ_{AV}) versus redox capacities for various redox active polymers. Polymers from left to right: **3.13**, **1.2**, **6.3**, poly(vinylferrocene), poly(ethernitroxide), and **6.6**. The dotted curve represents the mean intersite distance calculated per repeating unit. Inset: R represents redox-active sites.

6.2.2 Incorporation of Goedken's Macrocycle into Copolymers

Developing a side-chain polymer that incorporates Goedken's macrocycle using a controlled polymerization method such as ROMP affords us the ability to create copolymers. A new system would include the copolymerization of a polymer system similar to that presented in Chapter 5 with a water soluble *cis*-5-norbornene-*endo*-2,3-dicarboxylic acid (Figure 6.6). Once the appropriate ratio of hydrophobic (Goedken's macrocycle) to hydrophilic (norbornenedicarboxylic acid) blocks are achieved micelles can be targeted by self-assembly. A payload can be introduced into the micelle during the self-assembly process. Upon targeted oxidation of Goedken's macrocycle (using NOBF_4 , for example) both blocks become water-soluble which results in the disassembly of the micelles releasing the payload into the system.

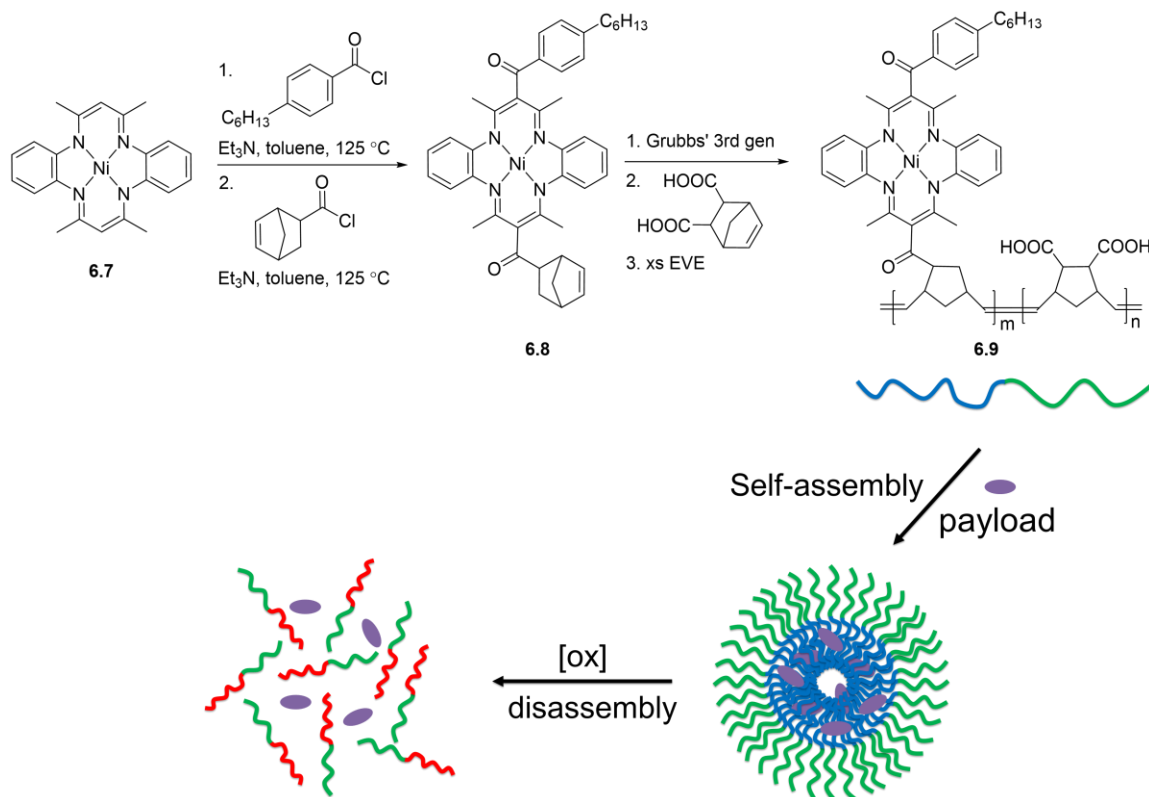


Figure 6.6 Synthesis of a block copolymer based on Goedken's macrocycle, followed by their self-assembly into micelles and targeted payload release.

The importance of non-covalent self-assembly is the driving force for many studies of supramolecular chemistry. By creating monodisperse macromolecules we can imitate the properties of biomacromolecules such as folding, coiling and multiplex formation through these non-covalent interactions. It is difficult to achieve the same degree of three dimensional (3D) control as biological systems, although by creating new two-dimensional (2D) systems with increasing complexity and size, we can progress towards creating and understanding the factors at play for 3D organization and self-assembly.⁸ The 2D system proposed requires an asymmetric M(II) complex of Goedken's macrocycle (M = Mn,⁹ Fe,¹⁰ Zn,⁹ Ru¹¹) with an iodine functionalized benzoyl moiety and a alkyne functionalized benzoyl moiety (**6.11**, Figure 6.7a) paired with a template molecule (**6.12**, Figure 6.7b). These metals were chosen as they have demonstrated coordination to pyridine or nitrogen containing molecules. It is important to note that the template molecule may require optimization in order to properly align the macrocycles for an efficient cross-coupling reaction.

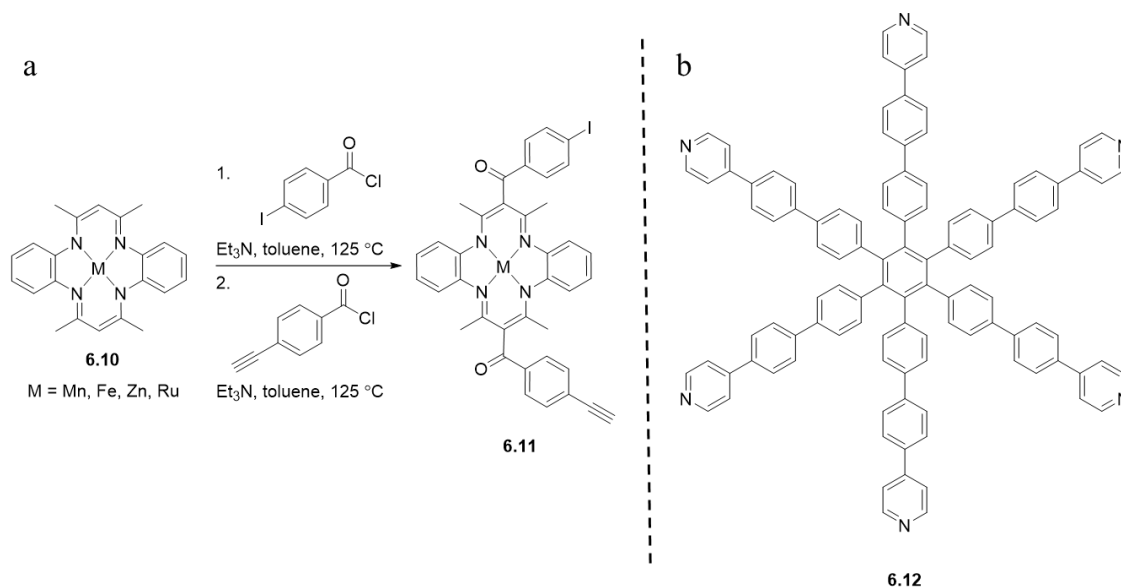


Figure 6.7 (a) Synthesis of an asymmetric Goedken's macrocycle and (b) potential template molecule **6.12**.

The template molecule **6.12** will coordinate to the metal centres present in the macrocycle ensuring the correct physical orientation for an efficient Sonogashira cross-coupling reaction. After the reaction has completed, pyridine will be introduced into the system to remove the template molecules from the newly formed cyclic oligomers (Figure 6.8). The macrocycles will then be studied on various surfaces (*e.g.* gold) in order to observe their self-assembly behaviour.

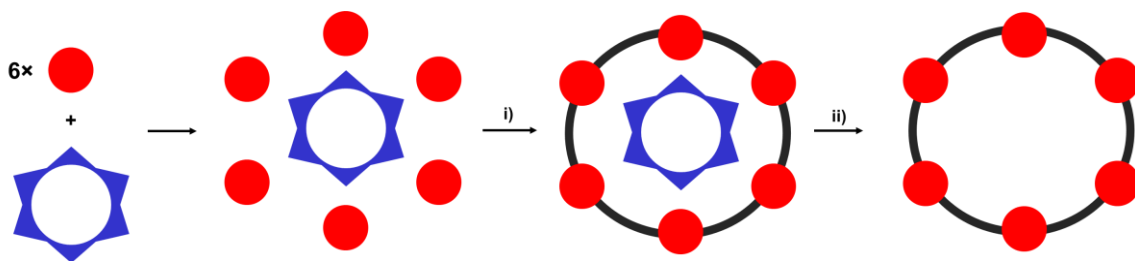


Figure 6.8 Template synthesis of cyclic oligomers composed of M(II) complexes of Goedken's macrocycle (**6.11**) with template molecule (**6.12**). i) $\text{PdCl}_2(\text{PPh}_3)_2$, CuI , Et_3N , THF. ii) pyridine.

6.3 References

- Tomlinson, E. P.; Hay, M. E.; Boudouris, B. W. *Macromolecules* **2014**, *47*, 6145–6158.

2. Suga, T.; Sugita, S.; Ohshiro, H.; Oyaizu, K.; Nishide, H. *Adv. Mater.* **2011**, *23*, 751–754.
3. Janoschka, T.; Hager, M. D.; Schubert, U. S. *Adv. Mater.* **2012**, *24*, 6397–6409.
4. Rayner, G.; Smith, T.; Barton, W.; Newton, M.; Deeth, R. J.; Prokes, I.; Clarkson, G. J.; Haddleton, D. M. *Polym. Chem.* **2012**, *3*, 2254–2260.
5. Hayano, S.; Masuda, T. *Macromolecules* **1998**, *31*, 3170–3174.
6. Kishimoto, Y.; Eckerle, P.; Miyatake, T.; Kainosho, M.; Ono, A.; Ikariya, T.; Noyori, R. *J. Am. Chem. Soc.* **1999**, *121*, 12035–12044.
7. Oyaizu, K.; Kawamoto, T.; Suga, T.; Nishide, H. *Macromolecules* **2010**, *43*, 10382–10389.
8. Kondratuk, D. V.; Perdigão, L. M. A.; Esmail, A. M. S.; O'Shea, J. N.; Beton, P. H.; Anderson, H. L. *Nat. Chem.* **2015**, *7*, 317–322.
9. Neves, D. R.; Dabrowiak, J. C. *Inorg. Chem.* **1976**, *15*, 129–134.
10. Goedken, V. L.; Park, Y.-A. *J. Chem. Soc., Chem. Commun.* **1975**, 214–215.
11. Warren, L. F.; Goedken, V. L. *J. Chem. Soc., Chem. Commun.* **1978**, 909–910.

Appendices

Appendix 1 – Permission to Reuse Copyrighted Material





[Home](#)
[Account Info](#)
[Help](#)
[Live Chat](#)

Title: An aqueous, polymer-based redox-flow battery using non-corrosive, safe, and low-cost materials
Author: Tobias Janoschka, Norbert Martin, Udo Martin, Christian Friebe, Sabine Morgenstern et al.
Publication: Nature
Publisher: Nature Publishing Group
Date: Oct 21, 2015
 Copyright © 2015, Rights Managed by Nature Publishing Group

Logged in as:
 Joseph Paquette
[LOGOUT](#)

Order Completed

Thank you for your order.

This Agreement between Joseph A Paquette ("You") and Nature Publishing Group ("Nature Publishing Group") consists of your license details and the terms and conditions provided by Nature Publishing Group and Copyright Clearance Center.

Your confirmation email will contain your order number for future reference.

[Get the printable license.](#)

License Number	3957121307992
License date	Sep 27, 2016
Licensed Content Publisher	Nature Publishing Group
Licensed Content Publication	Nature
Licensed Content Title	An aqueous, polymer-based redox-flow battery using non-corrosive, safe, and low-cost materials
Licensed Content Author	Tobias Janoschka, Norbert Martin, Udo Martin, Christian Friebe, Sabine Morgenstern et al.
Licensed Content Date	Oct 21, 2015
Licensed Content Volume	527
Licensed Content Issue	7576
Type of Use	reuse in a dissertation / thesis
Requestor type	academic/educational
Format	print and electronic
Portion	figures/tables/illustrations
Number of figures/tables/illustrations	1
High-res required	no
Figures	Figure 1.6
Author of this NPG article	no
Your reference number	
Title of your thesis / dissertation	SYNTHESIS OF METAL-CONTAINING POLYMERS AND STABLE ORGANIC RADICAL-CONTAINING POLYMERS AND THEIR USE AS ADVANCED FUNCTIONAL MATERIALS
Expected completion date	Dec 2016
Estimated size (number of pages)	250
Requestor Location	Joseph A Paquette 1151 Richmond St Department of Chemistry London, ON N6A 3K7 Canada Attn: Joseph A Paquette



RightsLink®

Home

Create Account

Help



ACS Publications
Most Trusted. Most Cited. Most Read.

Title: Battery-Inspired, Nonvolatile, and Rewritable Memory Architecture: a Radical Polymer-Based Organic Device

Author: Yasunori Yonekuta, Kentaro Susuki, Kenichi Oyaizu, et al

Publication: Journal of the American Chemical Society

Publisher: American Chemical Society

Date: Nov 1, 2007

Copyright © 2007, American Chemical Society

LOGIN

If you're a [copyright.com](#) user, you can login to RightsLink using your [copyright.com](#) credentials. Already a [RightsLink](#) user or want to [learn more?](#)

PERMISSION/LICENSE IS GRANTED FOR YOUR ORDER AT NO CHARGE

This type of permission/license, instead of the standard Terms & Conditions, is sent to you because no fee is being charged for your order. Please note the following:

- Permission is granted for your request in both print and electronic formats, and translations.
- If figures and/or tables were requested, they may be adapted or used in part.
- Please print this page for your records and send a copy of it to your publisher/graduate school.
- Appropriate credit for the requested material should be given as follows: "Reprinted (adapted) with permission from (COMPLETE REFERENCE CITATION). Copyright (YEAR) American Chemical Society." Insert appropriate information in place of the capitalized words.
- One-time permission is granted only for the use specified in your request. No additional uses are granted (such as derivative works or other editions). For any other uses, please submit a new request.

If credit is given to another source for the material you requested, permission must be obtained from that source.

BACK

CLOSE WINDOW

Copyright © 2016 [Copyright Clearance Center, Inc.](#) All Rights Reserved. [Privacy statement.](#) [Terms and Conditions.](#) Comments? We would like to hear from you. E-mail us at customer@copyright.com



RightsLink®

Home

Account Info

Help



Title: Supramolecular nesting of cyclic polymers
Author: Dmitry V. Kondratuk, Luís M. A. Perdigão, Ayad M. S. Esmail, James N. O'Shea, Peter H. Beton, Harry L. Anderson

Logged in as:
Joseph Paquette
Account #:
3001067126

LOGOUT

Publication: Nature Chemistry
Publisher: Nature Publishing Group
Date: Feb 16, 2015

Copyright © 2015, Rights Managed by Nature Publishing Group

Order Completed

Thank you for your order.

This Agreement between Joseph A Paquette ("You") and Nature Publishing Group ("Nature Publishing Group") consists of your license details and the terms and conditions provided by Nature Publishing Group and Copyright Clearance Center.

Your confirmation email will contain your order number for future reference.

[Get the printable license.](#)

License Number	3957171004941
License date	Sep 27, 2016
Licensed Content Publisher	Nature Publishing Group
Licensed Content Publication	Nature Chemistry
Licensed Content Title	Supramolecular nesting of cyclic polymers
Licensed Content Author	Dmitry V. Kondratuk, Luís M. A. Perdigão, Ayad M. S. Esmail, James N. O'Shea, Peter H. Beton, Harry L. Anderson
Licensed Content Date	Feb 16, 2015
Licensed Content Volume	7
Licensed Content Issue	4
Type of Use	reuse in a dissertation / thesis
Requestor type	academic/educational
Format	print and electronic
Portion	figures/tables/illustrations
Number of figures/tables/illustrations	1
High-res required	no
Figures	Figure 1.9
Author of this NPG article	no
Your reference number	
Title of your thesis / dissertation	SYNTHESIS OF METAL-CONTAINING POLYMERS AND STABLE ORGANIC RADICAL-CONTAINING POLYMERS AND THEIR USE AS ADVANCED FUNCTIONAL MATERIALS
Expected completion date	Dec 2016
Estimated size (number of pages)	250
Requestor Location	Joseph A Paquette 1151 Richmond St Department of Chemistry London, ON N6A 3K7 Canada Attn: Joseph A Paquette
Billing Type	Invoice



RightsLink®

Home

Account Info

Help



Title: Single Layer of Polymeric Fe-Phthalocyanine: An Organometallic Sheet on Metal and Thin Insulating Film

Author: Mathieu Abel, Sylvain Clair, Oualid Ourdjini, et al

Publication: Journal of the American Chemical Society

Publisher: American Chemical Society

Date: Feb 1, 2011

Copyright © 2011, American Chemical Society

Logged in as:
Joseph Paquette
Account #:
3001067126

LOGOUT

PERMISSION/LICENSE IS GRANTED FOR YOUR ORDER AT NO CHARGE

This type of permission/license, instead of the standard Terms & Conditions, is sent to you because no fee is being charged for your order. Please note the following:

- Permission is granted for your request in both print and electronic formats, and translations.
- If figures and/or tables were requested, they may be adapted or used in part.
- Please print this page for your records and send a copy of it to your publisher/graduate school.
- Appropriate credit for the requested material should be given as follows: "Reprinted (adapted) with permission from (COMPLETE REFERENCE CITATION). Copyright (YEAR) American Chemical Society." Insert appropriate information in place of the capitalized words.
- One-time permission is granted only for the use specified in your request. No additional uses are granted (such as derivative works or other editions). For any other uses, please submit a new request.

If credit is given to another source for the material you requested, permission must be obtained from that source.

BACK

CLOSE WINDOW

Copyright © 2016 Copyright Clearance Center, Inc. All Rights Reserved. [Privacy statement](#). [Terms and Conditions](#). Comments? We would like to hear from you. E-mail us at customercare@copyright.com



RightsLink®

Home

Account
Info

Help



ACS Publications
Most Trusted. Most Cited. Most Read.

Title: Genesis of Nanostructured, Magnetically Tunable Ceramics from the Pyrolysis of Cross-Linked Polyferrocenylsilane Networks and Formation of Shaped Macroscopic Objects and Micron Scale Patterns by Micromolding Inside Silicon Wafers

Author: Madlen Ginzburg, Mark J. MacLachlan, San Ming Yang, et al

Publication: Journal of the American Chemical Society

Publisher: American Chemical Society

Date: Mar 1, 2002

Copyright © 2002, American Chemical Society

Logged in as:
Joseph Paquette
Account #:
3001067126

LOGOUT

PERMISSION/LICENSE IS GRANTED FOR YOUR ORDER AT NO CHARGE

This type of permission/license, instead of the standard Terms & Conditions, is sent to you because no fee is being charged for your order. Please note the following:

- Permission is granted for your request in both print and electronic formats, and translations.
- If figures and/or tables were requested, they may be adapted or used in part.
- Please print this page for your records and send a copy of it to your publisher/graduate school.
- Appropriate credit for the requested material should be given as follows: "Reprinted (adapted) with permission from (COMPLETE REFERENCE CITATION). Copyright (YEAR) American Chemical Society." Insert appropriate information in place of the capitalized words.
- One-time permission is granted only for the use specified in your request. No additional uses are granted (such as derivative works or other editions). For any other uses, please submit a new request.

If credit is given to another source for the material you requested, permission must be obtained from that source.

BACK

CLOSE WINDOW

Copyright © 2016 [Copyright Clearance Center, Inc.](#) All Rights Reserved. [Privacy statement](#). [Terms and Conditions](#).
Comments? We would like to hear from you. E-mail us at customercare@copyright.com

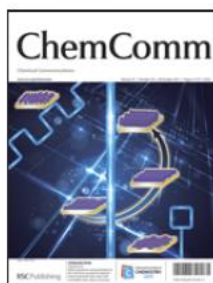


RightsLink®

Home

Account
Info

Help



Title: Redox-responsive organometallic microgel particles prepared from poly(ferrocenylsilane)s generated using microfluidics

Author: Xiaofeng Sui, Lingling Shui, Jin Cui, Yanbo Xie, Jing Song, Albert van den Berg, Mark A. Hempenius, G. Julius Vancso

Publication: Chemical Communications (Cambridge)

Publisher: Royal Society of Chemistry

Date: Jan 28, 2014

Copyright © 2014, Royal Society of Chemistry

Logged in as:
Joseph Paquette
Account #:
3001067126

LOGOUT

Order Completed

Thank you for your order.

This Agreement between Joseph A Paquette ("You") and Royal Society of Chemistry ("Royal Society of Chemistry") consists of your license details and the terms and conditions provided by Royal Society of Chemistry and Copyright Clearance Center.

Your confirmation email will contain your order number for future reference.

[Get the printable license.](#)

License Number	3957171508358
License date	Sep 27, 2016
Licensed Content Publisher	Royal Society of Chemistry
Licensed Content Publication	Chemical Communications (Cambridge)
Licensed Content Title	Redox-responsive organometallic microgel particles prepared from poly(ferrocenylsilane)s generated using microfluidics
Licensed Content Author	Xiaofeng Sui, Lingling Shui, Jin Cui, Yanbo Xie, Jing Song, Albert van den Berg, Mark A. Hempenius, G. Julius Vancso
Licensed Content Date	Jan 28, 2014
Licensed Content Volume	50
Licensed Content Issue	23
Type of Use	Thesis/Dissertation
Requestor type	academic/educational
Portion	figures/tables/images
Number of figures/tables/images	1
Distribution quantity	5
Format	print and electronic
Will you be translating?	no
Order reference number	
Title of the thesis/dissertation	SYNTHESIS OF METAL-CONTAINING POLYMERS AND STABLE ORGANIC RADICAL-CONTAINING POLYMERS AND THEIR USE AS ADVANCED FUNCTIONAL MATERIALS
Expected completion date	Dec 2016
Estimated size	250
Requestor Location	Joseph A Paquette 1151 Richmond St Department of Chemistry London, ON N6A 3K7



RightsLink®

Home

Account Info

Help



Title: Colour-tunable fluorescent multiblock micelles

Author: Zachary M. Hudson, David J. Lunn, Mitchell A. Winnik, Ian Manners

Publication: Nature Communications

Publisher: Nature Publishing Group

Date: Mar 5, 2014

Copyright © 2014, Rights Managed by Nature Publishing Group

Logged in as:
Joseph Paquette
Account #:
3001067126

LOGOUT

Order Completed

Thank you for your order.

This Agreement between Joseph A Paquette ("You") and Nature Publishing Group ("Nature Publishing Group") consists of your license details and the terms and conditions provided by Nature Publishing Group and Copyright Clearance Center.

Your confirmation email will contain your order number for future reference.

[Get the printable license.](#)

License Number	3957180249302
License date	Sep 27, 2016
Licensed Content Publisher	Nature Publishing Group
Licensed Content Publication	Nature Communications
Licensed Content Title	Colour-tunable fluorescent multiblock micelles
Licensed Content Author	Zachary M. Hudson, David J. Lunn, Mitchell A. Winnik, Ian Manners
Licensed Content Date	Mar 5, 2014
Licensed Content Volume	5
Type of Use	reuse in a dissertation / thesis
Requestor type	academic/educational
Format	print and electronic
Portion	figures/tables/illustrations
Number of figures/tables/illustrations	1
High-res required	no
Figures	Figure 1.11c
Author of this NPG article	no
Your reference number	
Title of your thesis / dissertation	SYNTHESIS OF METAL-CONTAINING POLYMERS AND STABLE ORGANIC RADICAL-CONTAINING POLYMERS AND THEIR USE AS ADVANCED FUNCTIONAL MATERIALS
Expected completion date	Dec 2016
Estimated size (number of pages)	250
Requestor Location	Joseph A Paquette 1151 Richmond St Department of Chemistry London, ON N6A 3K7 Canada Attn: Joseph A Paquette
Billing Type	Invoice
Billing address	Joseph A Paquette 1151 Richmond St Department of Chemistry

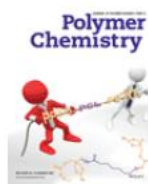


RightsLink®

Home

Account Info

Help



Title: Synthesis, characterization, and thin-film properties of 6-oxoverdazyl polymers prepared by ring-opening metathesis polymerization

Author: Joseph A. Paquette, Sabastine Ezugwu, Vishal Yadav, Giovanni Fanchini, Joe B. Gilroy

Publication: Journal of Polymer Science Part A: Polymer Chemistry

Publisher: John Wiley and Sons

Date: Jan 18, 2016

© 2016 Wiley Periodicals, Inc.

Logged in as:
Joseph Paquette
Account #:
3001067126

LOGOUT

Order Completed

Thank you for your order.

This Agreement between Joseph A Paquette ("You") and John Wiley and Sons ("John Wiley and Sons") consists of your license details and the terms and conditions provided by John Wiley and Sons and Copyright Clearance Center.

Your confirmation email will contain your order number for future reference.

[Get the printable license.](#)

License Number	3957231066737
License date	Sep 27, 2016
Licensed Content Publisher	John Wiley and Sons
Licensed Content Publication	Journal of Polymer Science Part A: Polymer Chemistry
Licensed Content Title	Synthesis, characterization, and thin-film properties of 6-oxoverdazyl polymers prepared by ring-opening metathesis polymerization
Licensed Content Author	Joseph A. Paquette, Sabastine Ezugwu, Vishal Yadav, Giovanni Fanchini, Joe B. Gilroy
Licensed Content Date	Jan 18, 2016
Licensed Content Pages	11
Type of use	Dissertation/Thesis
Requestor type	Author of this Wiley article
Format	Print and electronic
Portion	Full article
Will you be translating?	No
Title of your thesis / dissertation	SYNTHESIS OF METAL-CONTAINING POLYMERS AND STABLE ORGANIC RADICAL-CONTAINING POLYMERS AND THEIR USE AS ADVANCED FUNCTIONAL MATERIALS
Expected completion date	Dec 2016
Expected size (number of pages)	250
Requestor Location	Joseph A Paquette 1151 Richmond St Department of Chemistry London, ON N6A 3K7 Canada Attn: Joseph A Paquette
Publisher Tax ID	EU826007151
Billing Type	Invoice
Billing address	



RightsLink®

Home

Account Info

Help



Title: Polymers Containing Nickel(II) Complexes of Goedken's Macrocycle: Optimized Synthesis and Electrochemical Characterization

Author: Joseph A. Paquette, Ethan R. Sauvé, Joe B. Gilroy

Publication: Macromolecular Rapid Communications

Publisher: John Wiley and Sons

Date: Oct 31, 2014

© 2014 WILEY-VCH Verlag GmbH & Co. KGaA, Weinheim

Logged in as:
Joseph Paquette
Account #:
3001067126

LOGOUT

Order Completed

Thank you for your order.

This Agreement between Joseph A Paquette ("You") and John Wiley and Sons ("John Wiley and Sons") consists of your license details and the terms and conditions provided by John Wiley and Sons and Copyright Clearance Center.

Your confirmation email will contain your order number for future reference.

[Get the printable license.](#)

License Number	3957230943102
License date	Sep 27, 2016
Licensed Content Publisher	John Wiley and Sons
Licensed Content Publication	Macromolecular Rapid Communications
Licensed Content Title	Polymers Containing Nickel(II) Complexes of Goedken's Macrocycle: Optimized Synthesis and Electrochemical Characterization
Licensed Content Author	Joseph A. Paquette, Ethan R. Sauvé, Joe B. Gilroy
Licensed Content Date	Oct 31, 2014
Licensed Content Pages	6
Type of use	Dissertation/Thesis
Requestor type	Author of this Wiley article
Format	Print and electronic
Portion	Full article
Will you be translating?	No
Title of your thesis / dissertation	SYNTHESIS OF METAL-CONTAINING POLYMERS AND STABLE ORGANIC RADICAL-CONTAINING POLYMERS AND THEIR USE AS ADVANCED FUNCTIONAL MATERIALS
Expected completion date	Dec 2016
Expected size (number of pages)	250
Requestor Location	Joseph A Paquette 1151 Richmond St Department of Chemistry London, ON N6A 3K7 Canada Attn: Joseph A Paquette
Publisher Tax ID	EU826007151
Billing Type	Invoice
Billing address	Joseph A Paquette 1151 Richmond St

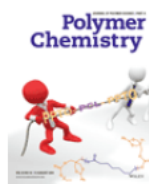


RightsLink®

Home

Account Info

Help



Title: Synthesis, characterization, and preceramic properties of n-conjugated polymers based on Ni(II) complexes of goedken's macrocycle

Author: Joseph A. Paquette, Joe B. Gilroy

Publication: Journal of Polymer Science Part A: Polymer Chemistry

Publisher: John Wiley and Sons

Date: Jul 2, 2016

© 2016 Wiley Periodicals, Inc.

Logged in as:
Joseph Paquette
Account #:
3001067126

LOGOUT

Order Completed

Thank you for your order.

This Agreement between Joseph A Paquette ("You") and John Wiley and Sons ("John Wiley and Sons") consists of your license details and the terms and conditions provided by John Wiley and Sons and Copyright Clearance Center.

Your confirmation email will contain your order number for future reference.

[Get the printable license.](#)

License Number	3957230696931
License date	Sep 27, 2016
Licensed Content Publisher	John Wiley and Sons
Licensed Content Publication	Journal of Polymer Science Part A: Polymer Chemistry
Licensed Content Title	Synthesis, characterization, and preceramic properties of n-conjugated polymers based on Ni(II) complexes of goedken's macrocycle
Licensed Content Author	Joseph A. Paquette, Joe B. Gilroy
Licensed Content Date	Jul 2, 2016
Licensed Content Pages	10
Type of use	Dissertation/Thesis
Requestor type	Author of this Wiley article
Format	Print and electronic
Portion	Full article
Will you be translating?	No
Title of your thesis / dissertation	SYNTHESIS OF METAL-CONTAINING POLYMERS AND STABLE ORGANIC RADICAL-CONTAINING POLYMERS AND THEIR USE AS ADVANCED FUNCTIONAL MATERIALS
Expected completion date	Dec 2016
Expected size (number of pages)	250
Requestor Location	Joseph A Paquette 1151 Richmond St Department of Chemistry London, ON N6A 3K7 Canada Attn: Joseph A Paquette
Publisher Tax ID	EU826007151
Billing Type	Invoice
Billing address	Joseph A Paquette 1151 Richmond St Department of Chemistry

Appendix 2 – Supporting Information for Chapter 2

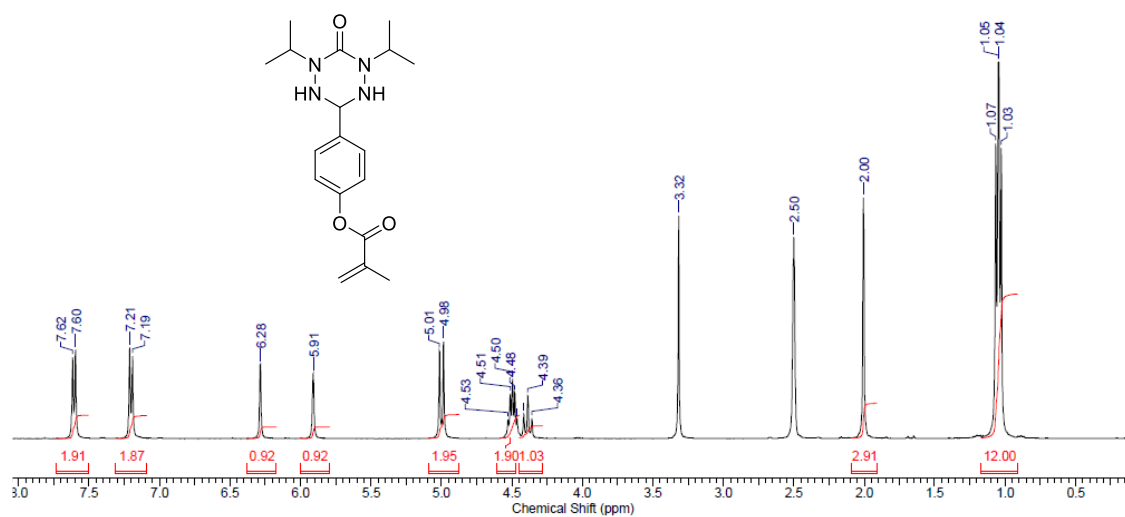


Figure A2.1 ¹H NMR spectrum of tetrazane monomer **2.5a** in *d*₆-DMSO.

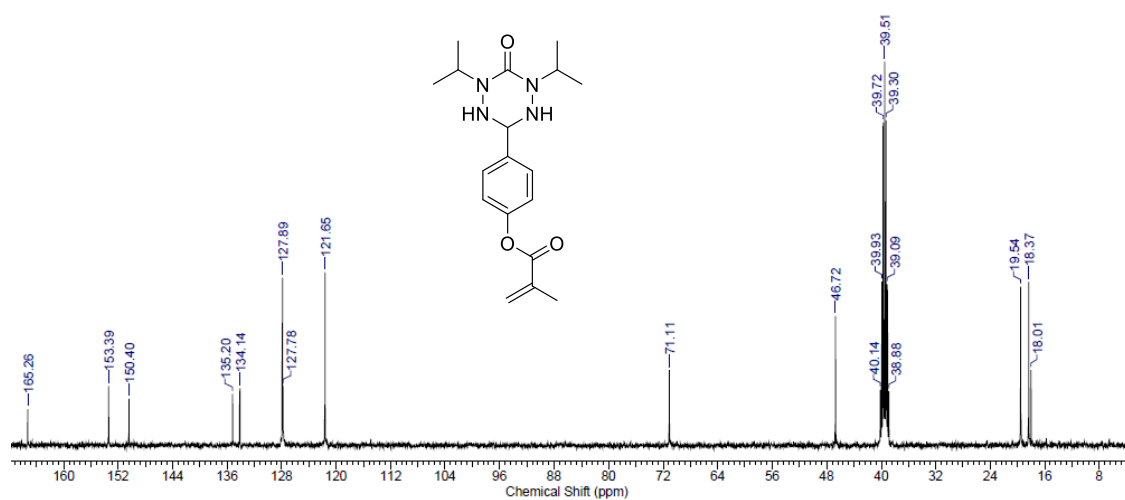


Figure A2.2 ¹³C{¹H} NMR spectrum of tetrazane monomer **2.5a** in *d*₆-DMSO.

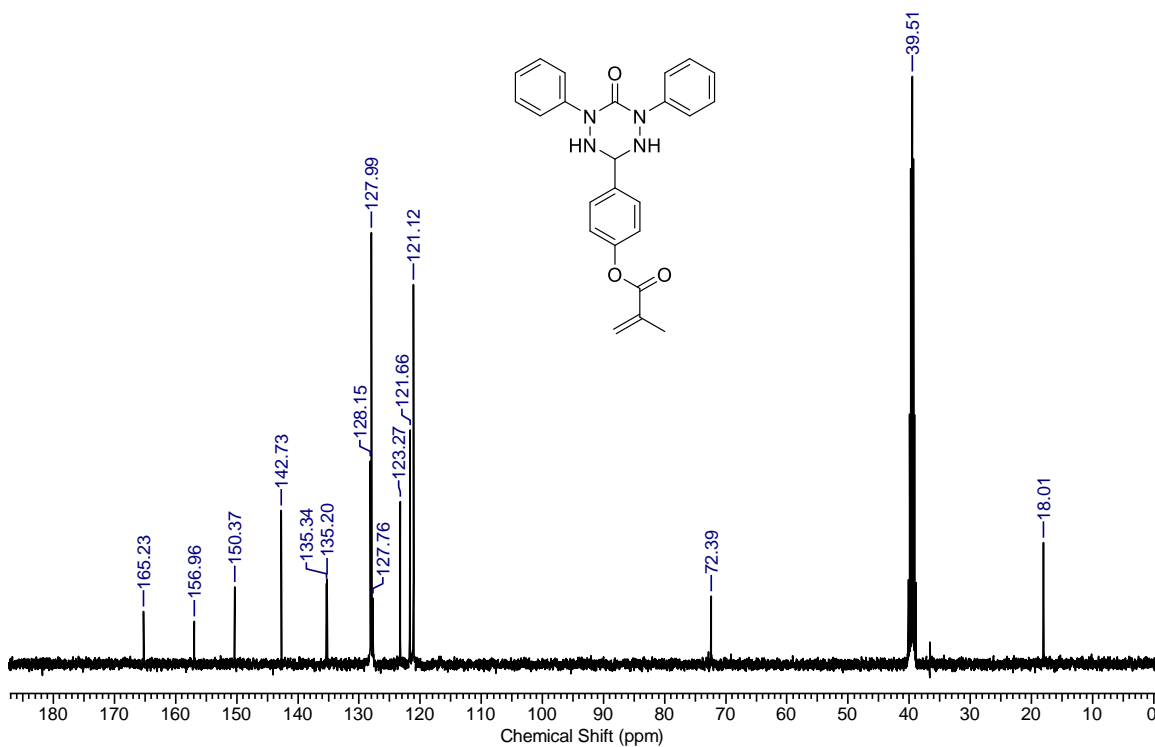


Figure A2.3 $^{13}\text{C}\{^1\text{H}\}$ NMR triaryl-6-oxotetrazane monomer **2.5b** in d_6 -DMSO.

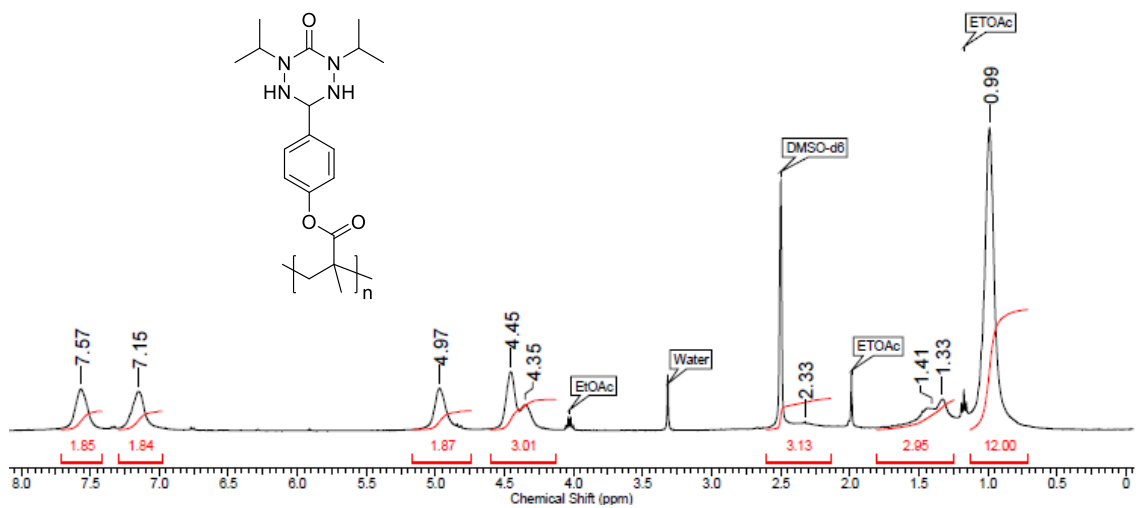


Figure A2.4 ^1H NMR spectrum of tetrazane polymer **2.6a** in d_6 -DMSO.

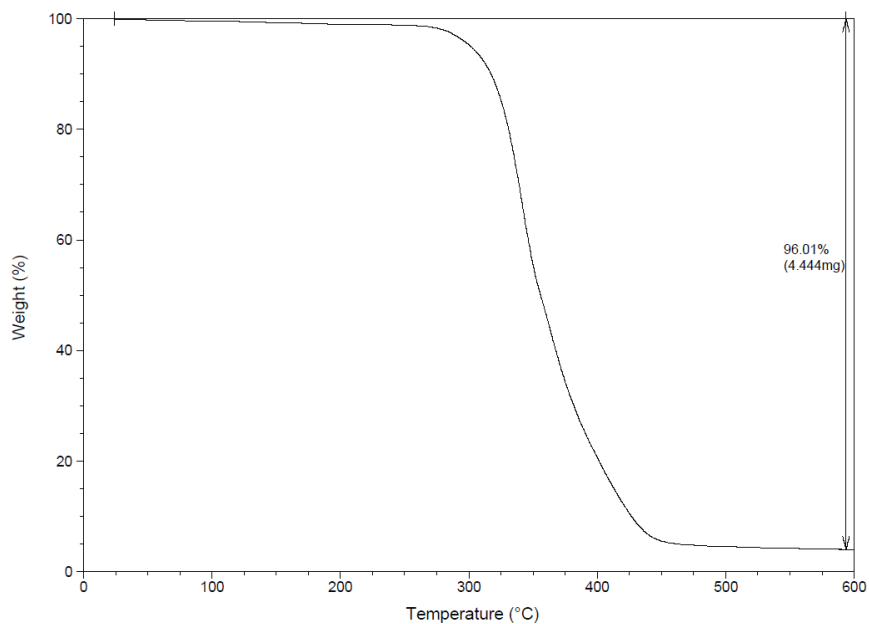


Figure A2.5 TGA trace for tetrazane polymer **2.6a**.

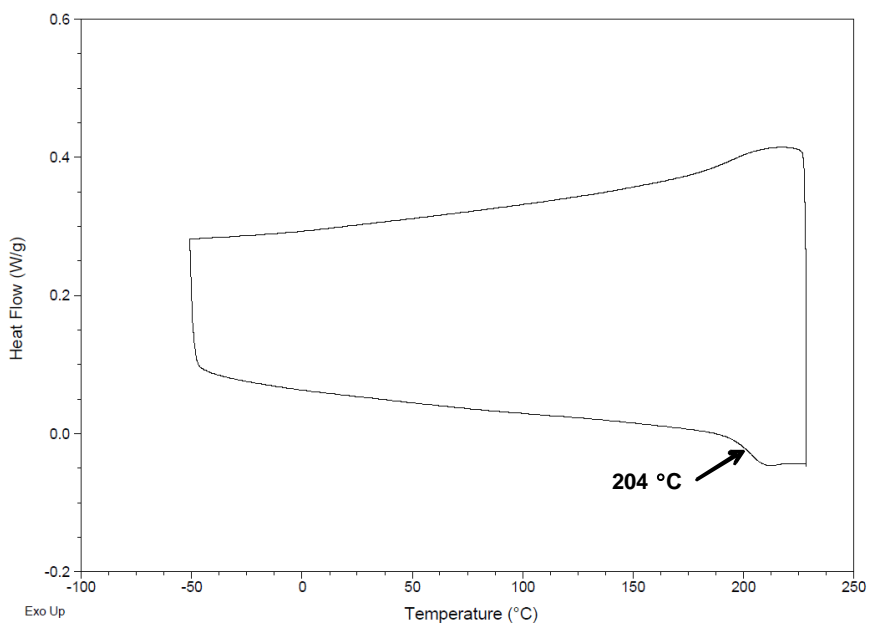


Figure A2.6 DSC thermogram for tetrazane polymer **2.6a**.

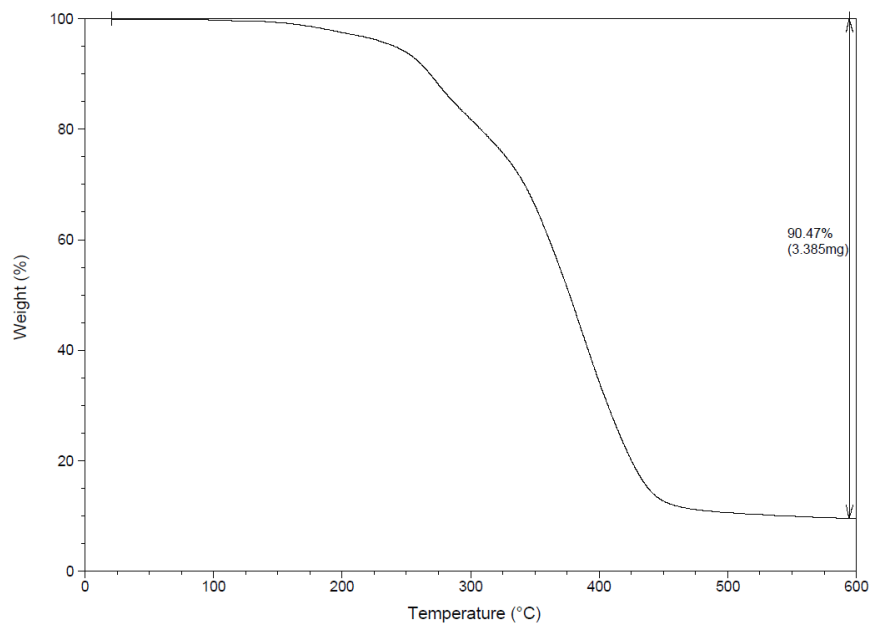


Figure A2.7 TGA trace for 6-oxoverdazyl polymer **2.7a**.

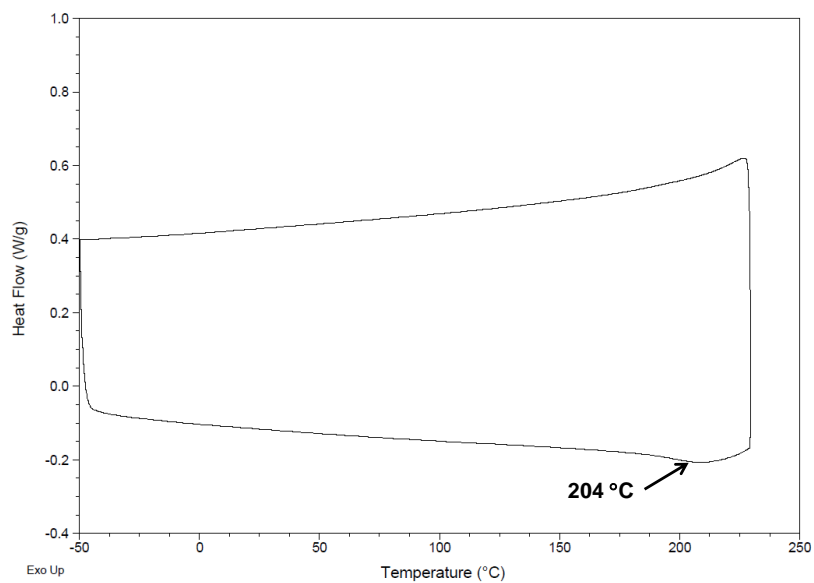


Figure A2.8 DSC thermogram of 6-oxoverdazyl polymer **2.7a**.

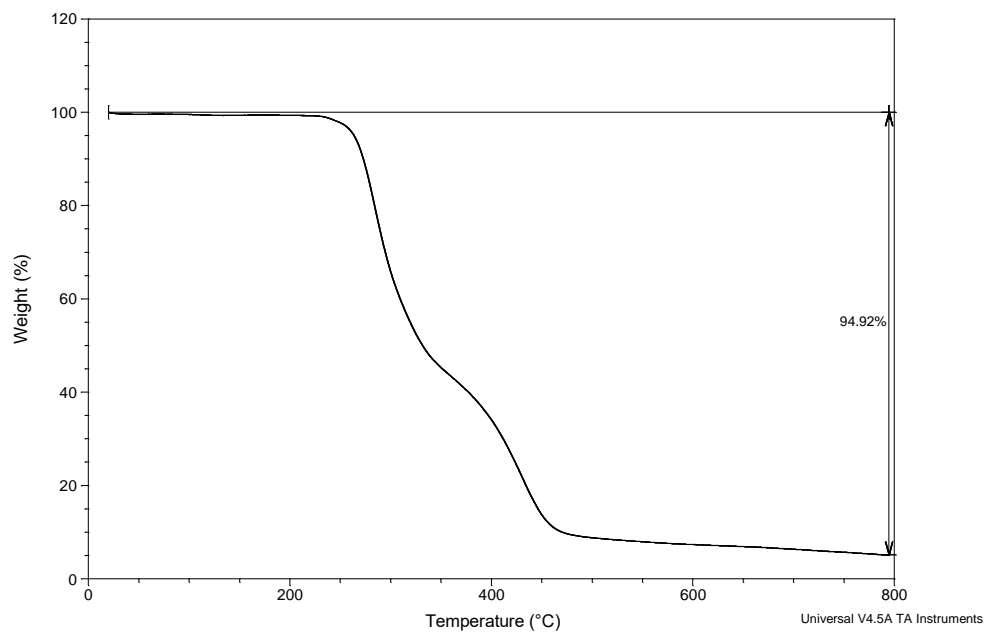


Figure A2.9 TGA trace for 6-oxoverdazyl polymer **2.6b**.

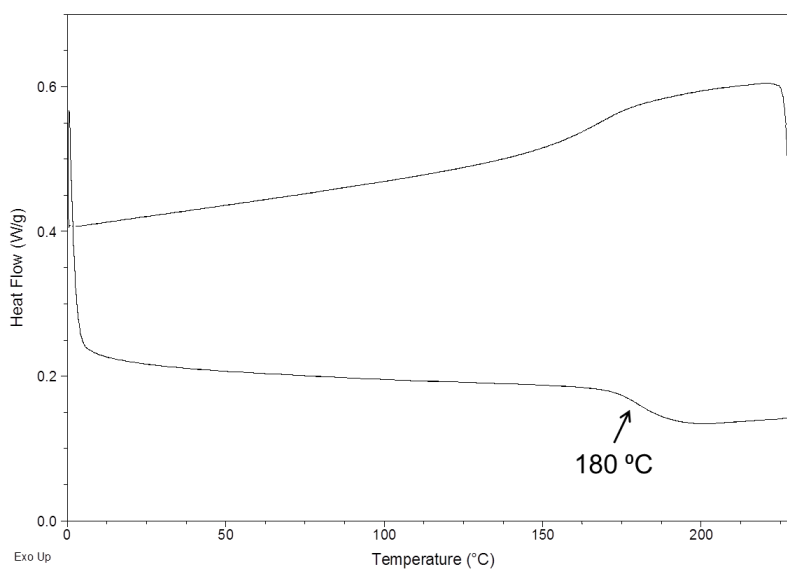


Figure A2.10 DSC thermogram of 6-oxoverdazyl polymer **2.6b**.

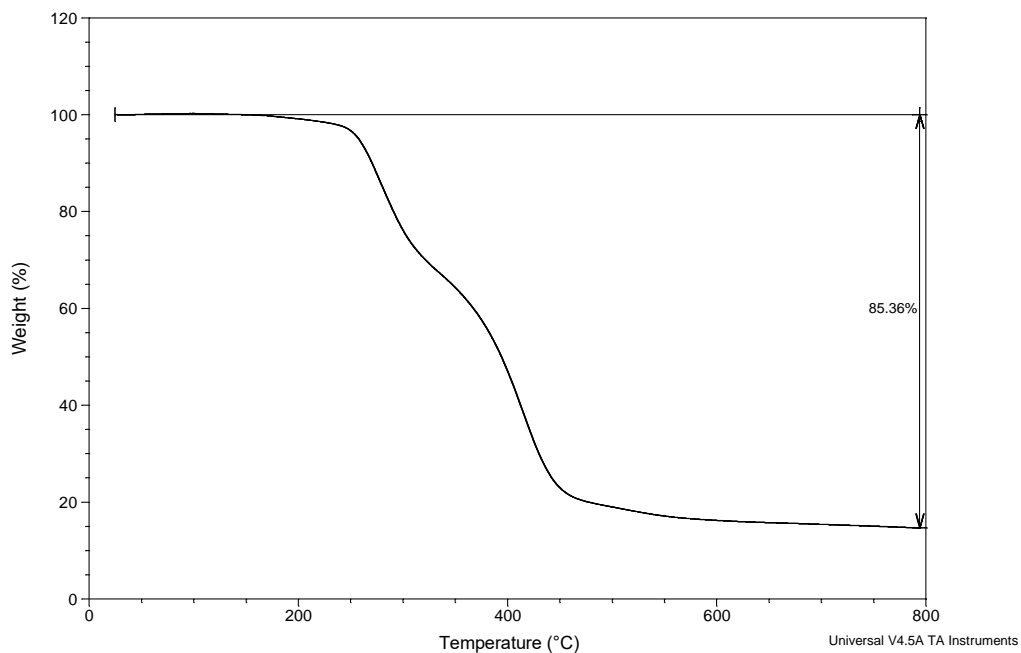


Figure A2.11 TGA trace for 6-oxoverdazyl polymer **2.7b**.

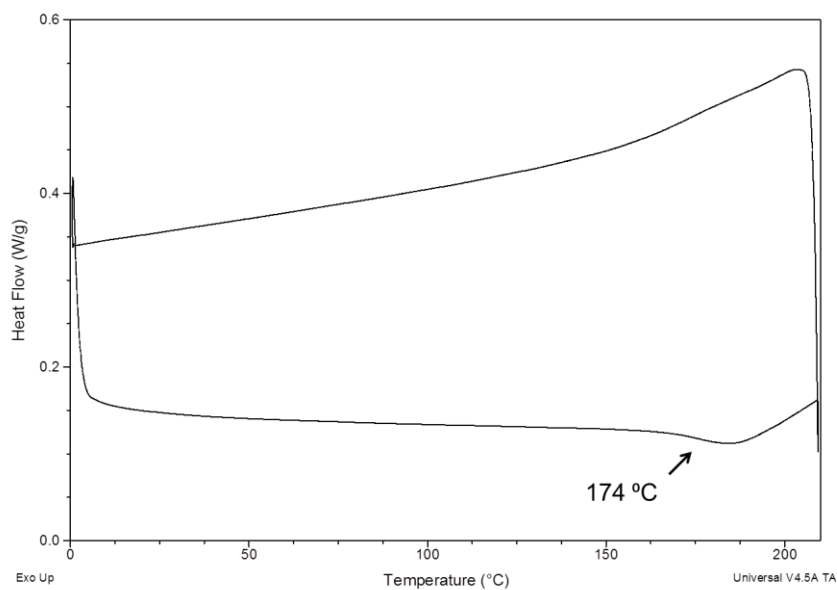


Figure A2.12 DSC thermogram of 6-oxoverdazyl polymer **2.7b**.

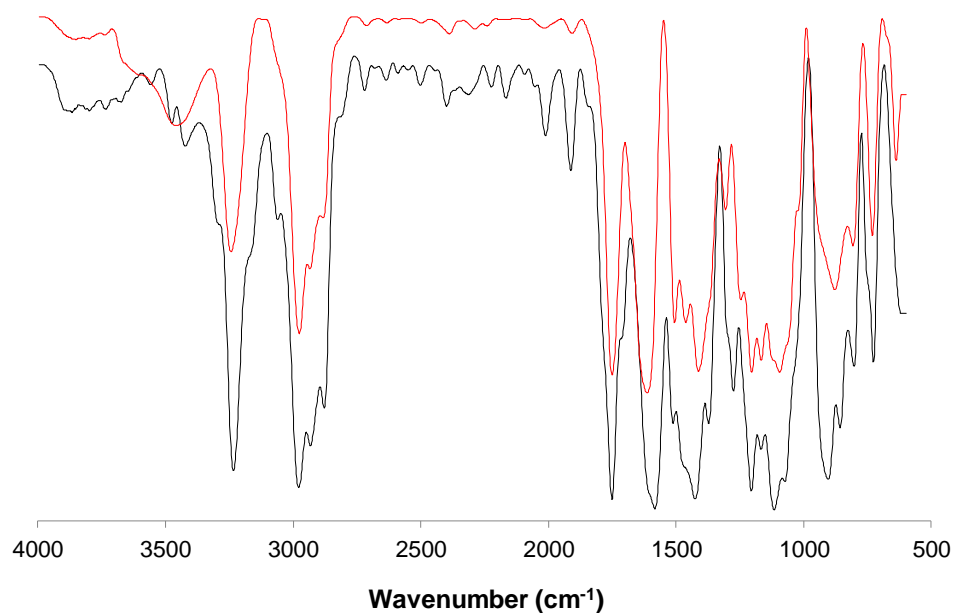


Figure A2.13 IR spectra of tetrazane polymer **2.6a** (red) and tetrazane **2.10a** (black) recorded as KBr pellets. The baselines have been offset for ease of comparison.

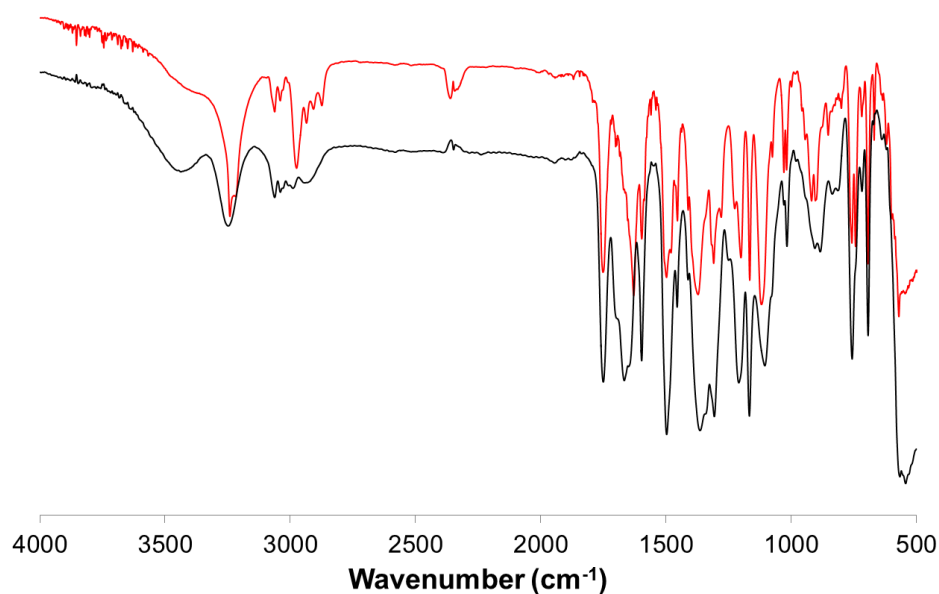


Figure A2.14 IR spectra for tetrazane polymer **2.6b** (black) and tetrazane **2.10b** (red) recorded as KBr pellets. The baselines have been offset for ease of comparison.

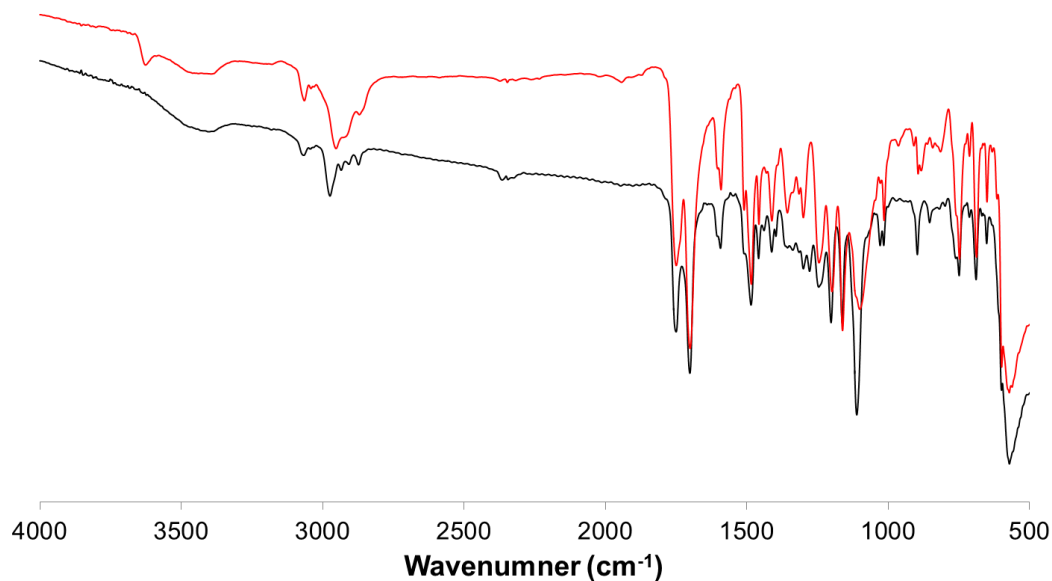


Figure A2.15 IR spectra of 6-oxoverdazyl polymer **2.7b** (red) and 6-oxoverdazyl **2.11b** (black) recorded as KBr pellets. The baselines have been offset for ease of comparison.

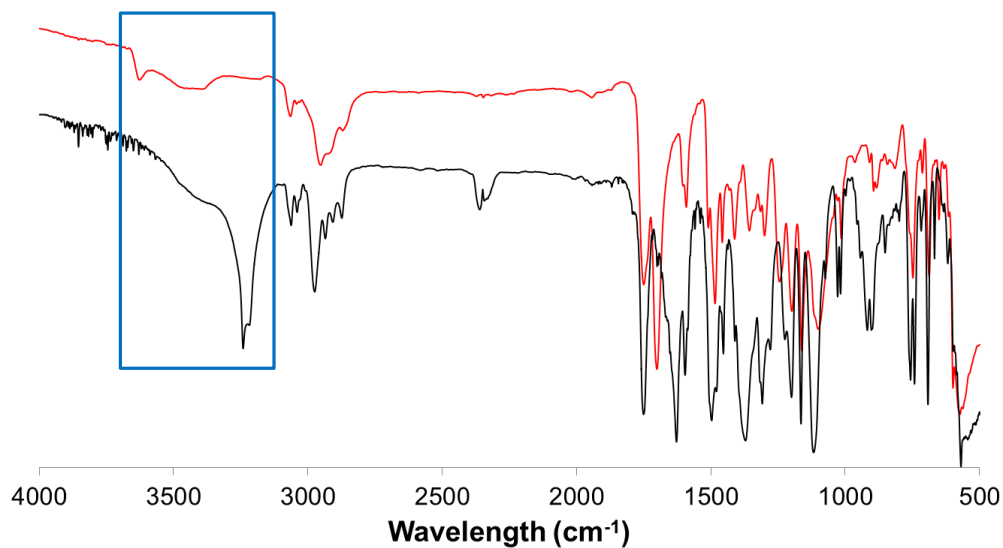


Figure A2.16 IR spectra for tetrazane polymer **2.6b** (black) and 6-oxoverdazyl polymer **2.7b** (red) recorded as KBr pellets. The baselines have been offset for ease of comparison. The rectangle highlights the NH region of the spectrum.

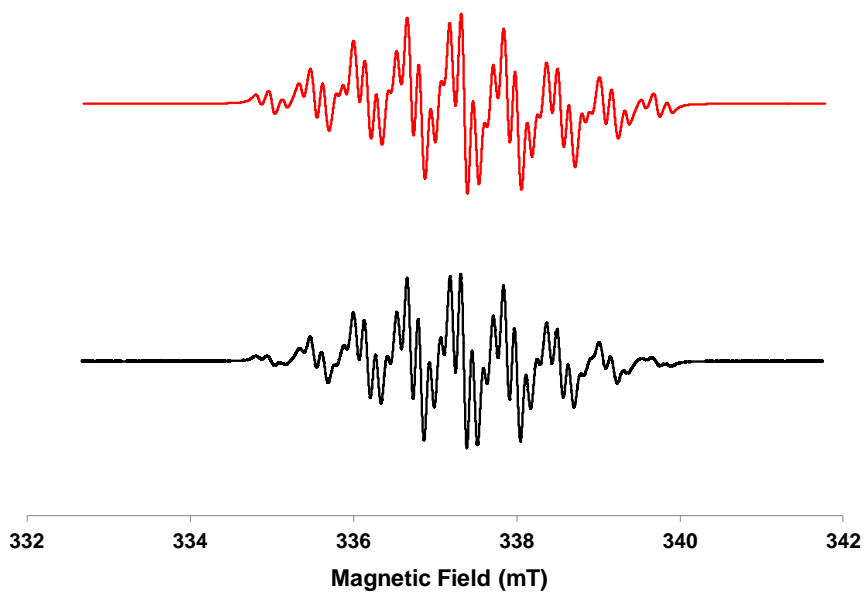


Figure A2.17 Simulated (top, red) and collected (bottom, black) EPR spectra of 6-oxoverdazyl **2.11a** in dichloromethane. Parameters used for simulation: $g = 2.0043$, line width = 0.85 mT, $a_{N1,5} = 0.533$ mT, $a_{N2,4} = 0.656$ mT, $a_H = 0.132$ mT.

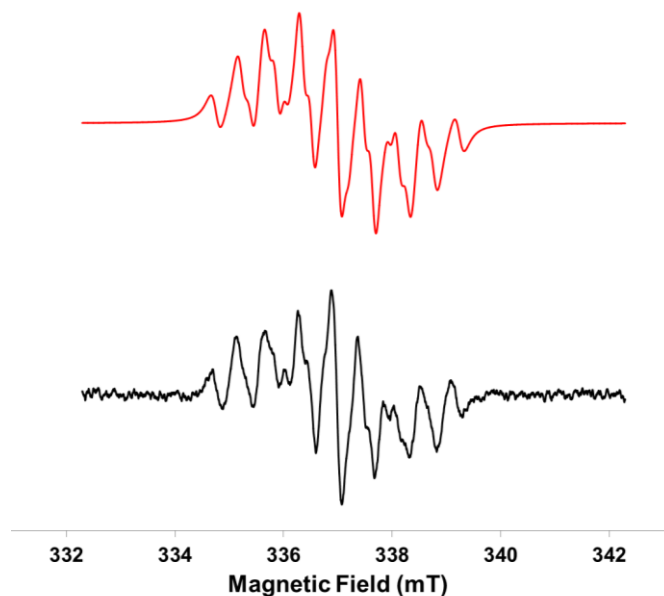


Figure A2.18 Simulated (top, red) and collected (bottom, black) EPR spectra of 6-triaryloxoverdazyl **2.11b** in dichloromethane. Parameters used for simulation: $g = 2.0038$, line width = 0.20 mT, $a_{N1,5} = 0.645$ mT, $a_{N2,4} = 0.475$ mT.

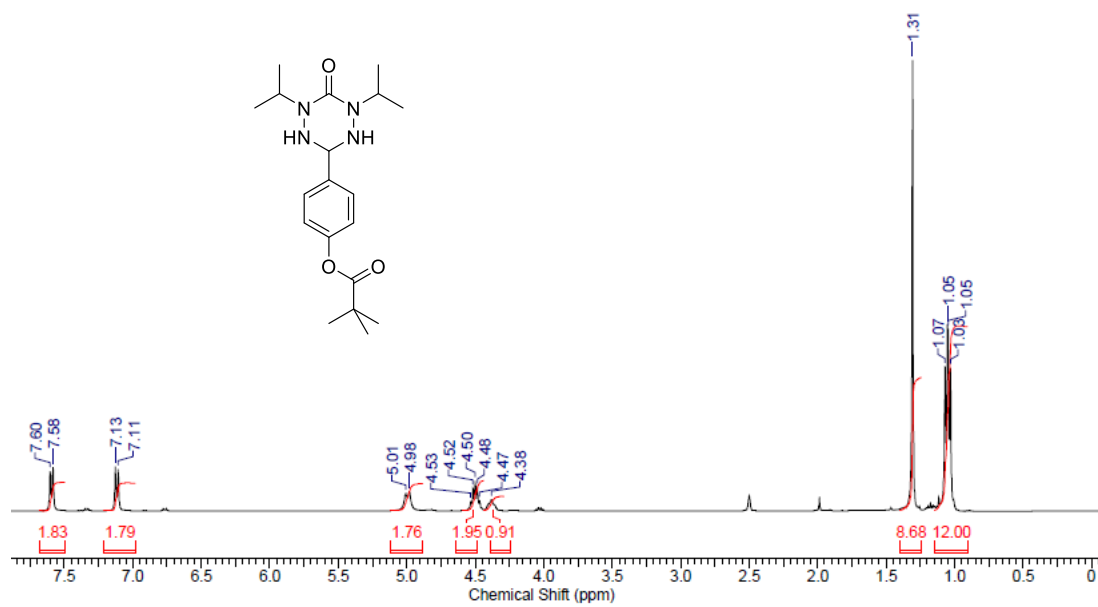


Figure A2.19 ^1H NMR spectrum of tetrazane **2.10a** in d_6 -DMSO.

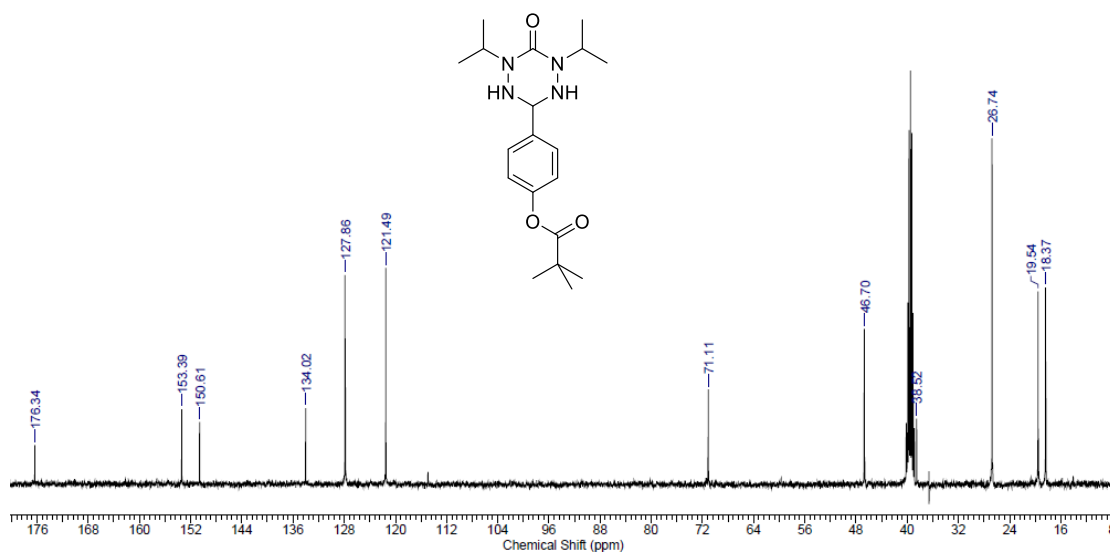


Figure A2.20 $^{13}\text{C}\{^1\text{H}\}$ NMR spectrum of tetrazane **2.10a** in d_6 -DMSO.

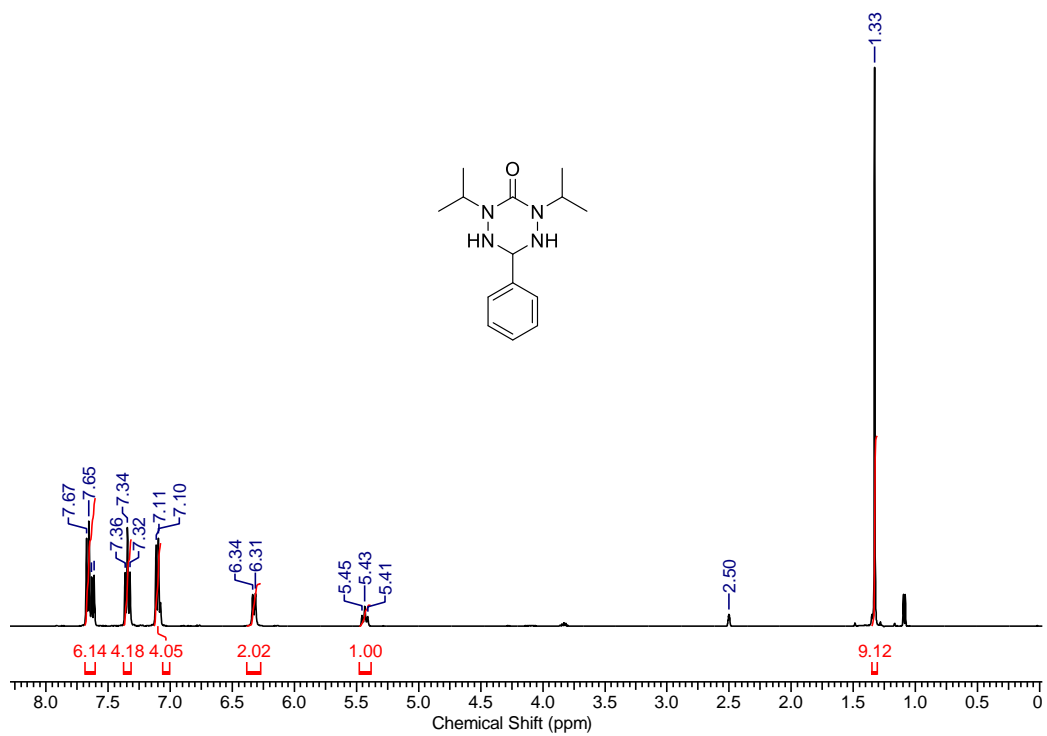


Figure A2.21 ¹H NMR of triaryl-6-oxotetrazane **2.10b** in *d*₆-DMSO.

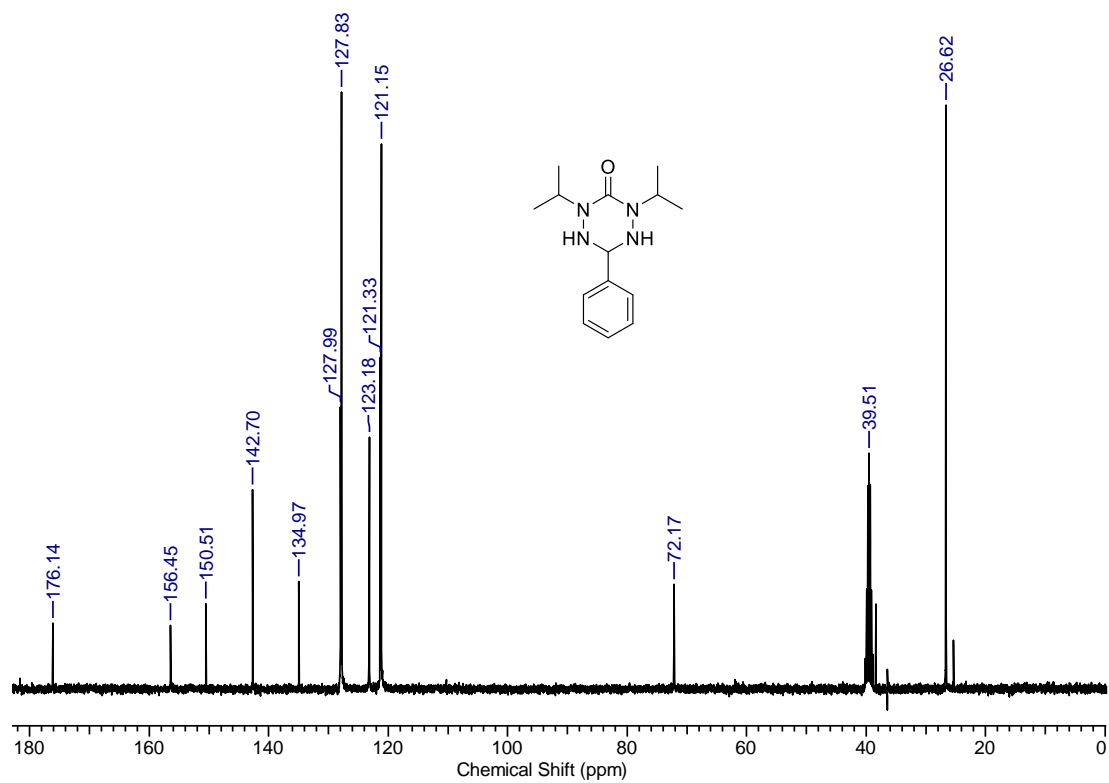


Figure A2.22 ¹³C{¹H} NMR triaryl-6-oxotetrazane **2.10b** in *d*₆-DMSO.

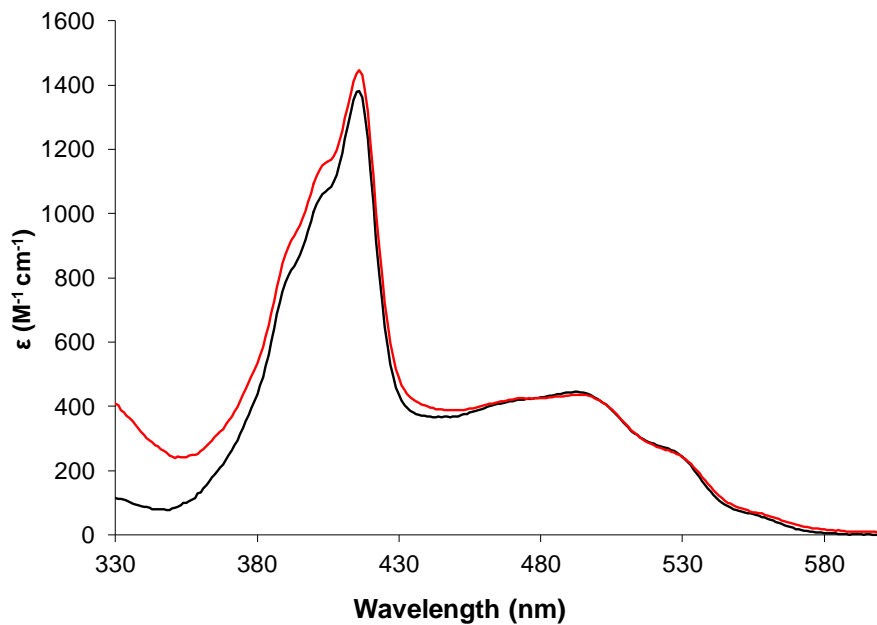


Figure A2.23 UV-Vis absorption spectrum of 6-oxoverdazyl polymers **2.7a** (red) and model 6-oxoverdazyl **2.11a** (black) recorded in CH_2Cl_2 .

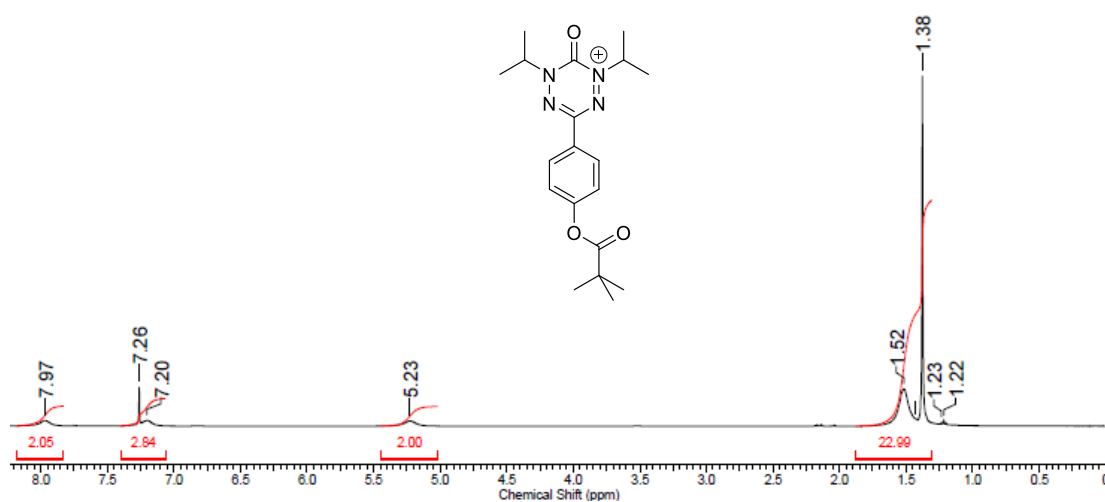


Figure A2.24 1H NMR spectrum of tetrazinium cation **2.12a** in $CDCl_3$.

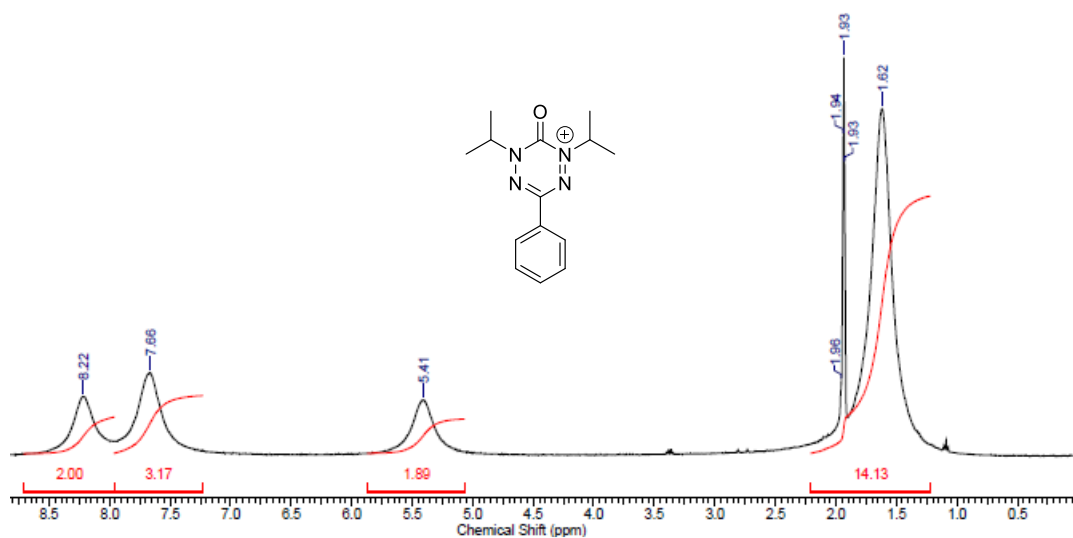


Figure A2.25 ^1H NMR spectrum of tetrazinium cation **2.12c** in CD_3CN at $-40\text{ }^\circ\text{C}$.

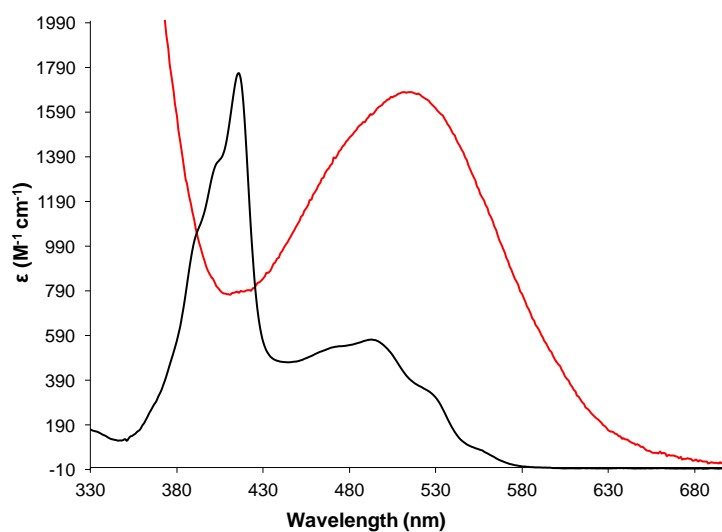


Figure A2.26 UV-Vis absorption spectra of 6-oxoverdazyl **2.11a** (black) and tetrazinium cation **2.12a** (red) recorded in CH_2Cl_2 .

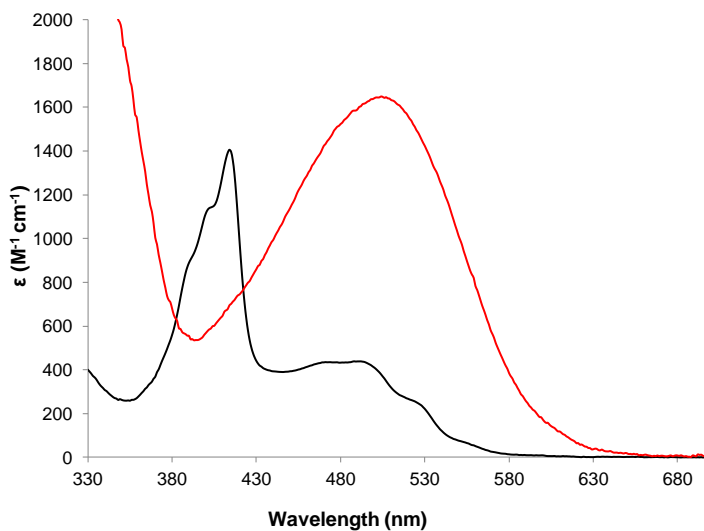


Figure A2.27 UV-Vis absorption spectra of 6-oxoverdazyl **2.11c** (black) and tetrazinium cation **2.12c** (red) recorded in CH_2Cl_2 .

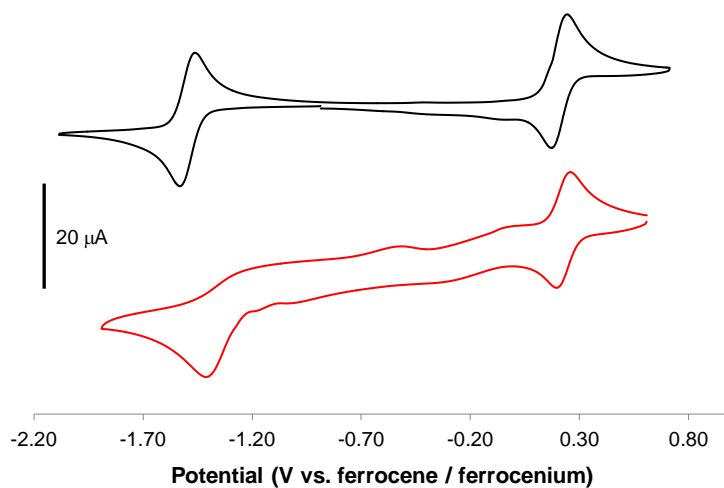


Figure A2.28 CVs of 6-oxoverdazyl **2.11a** (black) and tetrazinium cation **2.12a** (red) recorded at scan rate 100 mV s^{-1} in THF solutions containing 1 mM analyte and 0.1 M tetrabutylammonium hexafluorophosphate.

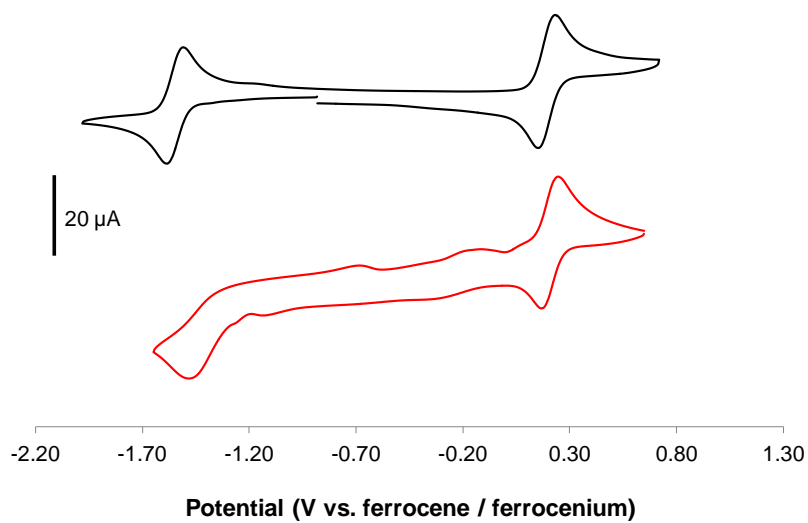


Figure A2.29 CVs of 6-oxoverdazyl **2.11c** (black) and tetrazinium cation **2.12c** (red) recorded at scan rate 100 mV s^{-1} in THF solutions containing 1 mM analyte and 0.1 M tetrabutylammonium hexafluorophosphate.

Appendix 3 – Supporting Information for Chapter 3

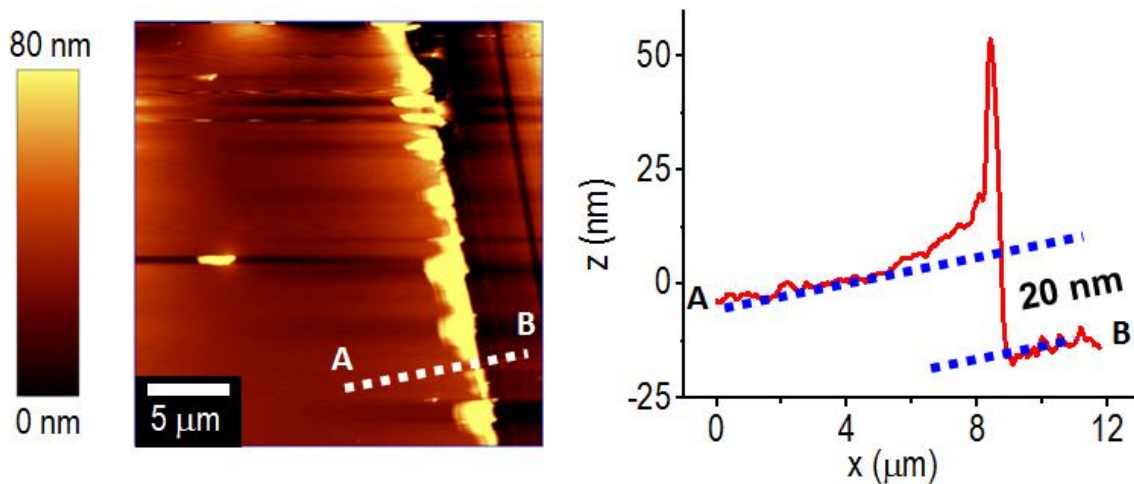


Figure A3.1 (a) Atomic Force Microscopy (AFM) image of a 20 nm thin film of polymer **3.13** (left side of the image) and indium-tin oxide (ITO) substrate (right side of the image). (b) Z-axis profile of the “step” at the edge of polymer **3.13** used to determine the thin film thickness. From the right side of the profile, root mean squared (RMS) roughness of ITO could be estimated to be about 4 nm, much less than the polymer thickness, which is about 20 nm with an RMS roughness of about 2 nm, significantly less than the RMS roughness of ITO. This suggests the polymeric film is continuous with no outstanding ITO pinholes.

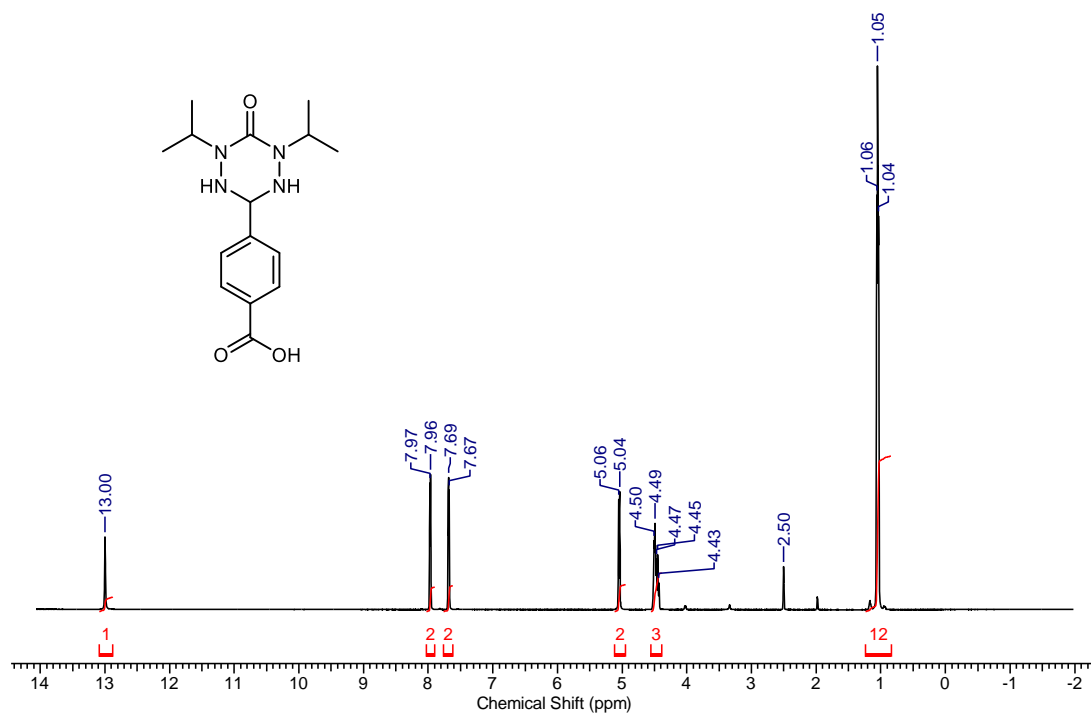


Figure A3.2 ^1H NMR spectrum of tetrazane **3.9** in d_6 -DMSO. The asterisk denotes residual $\text{CD}_3\text{SOCD}_2\text{H}$.

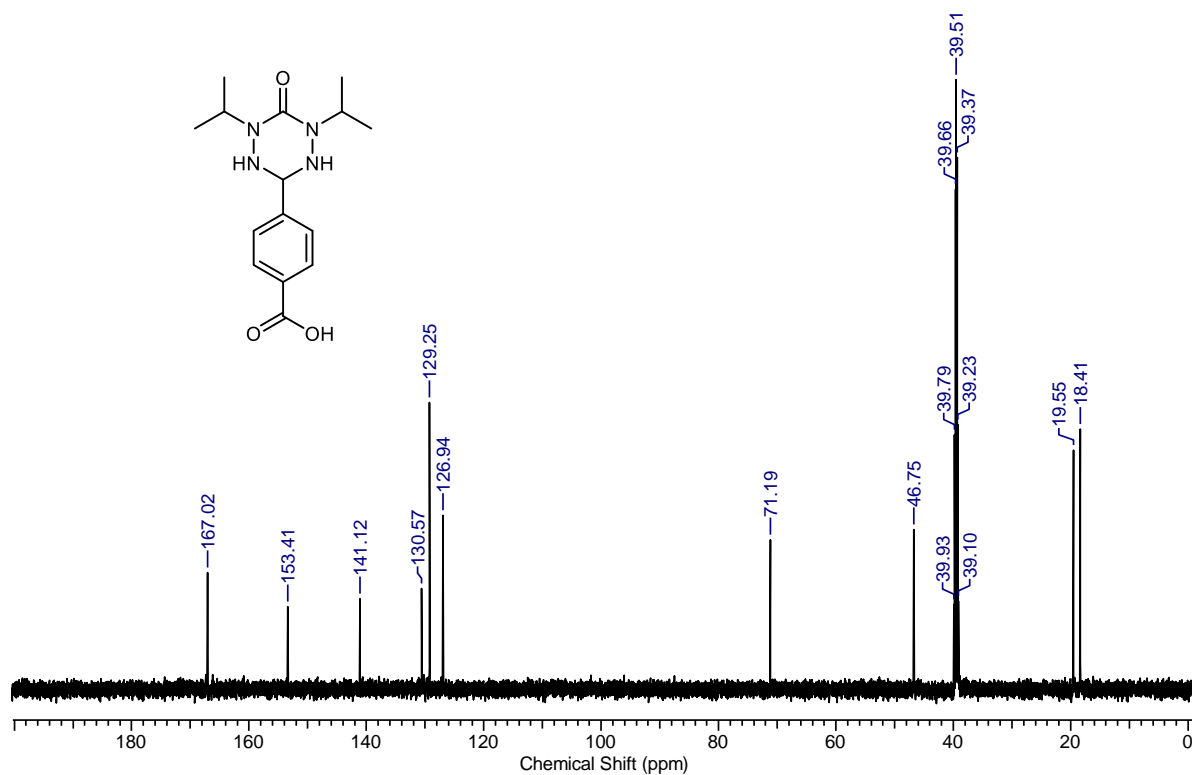


Figure A3.3 $^{13}\text{C}\{^1\text{H}\}$ NMR spectrum of tetrazane **3.9** in d_6 -DMSO. The asterisk denotes d_6 -DMSO.

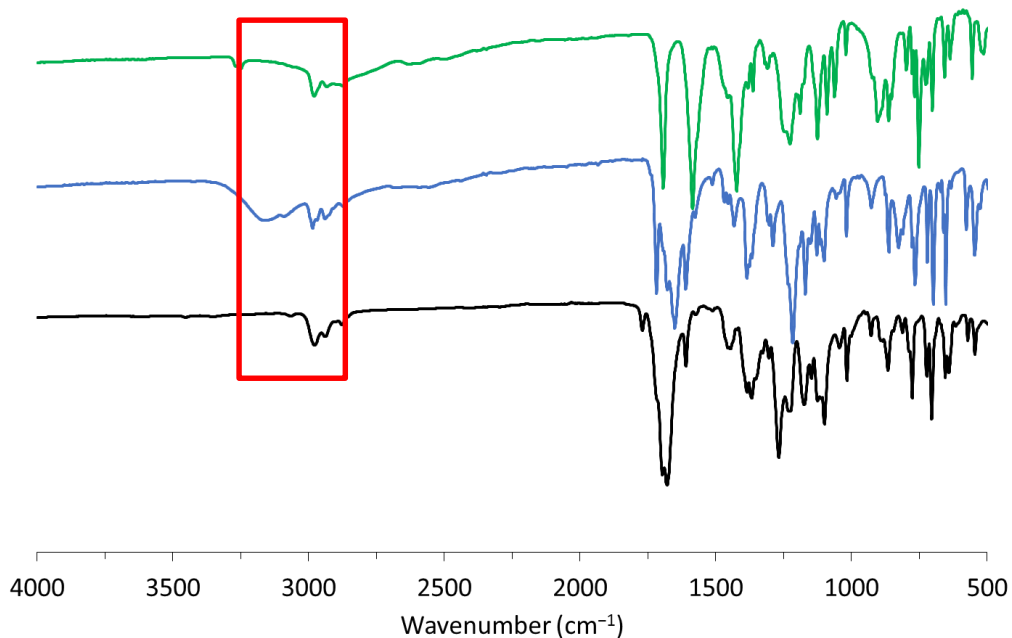


Figure A3.4 FT-IR spectra of tetrazane **3.9** (green line), 6-oxoverdazyl **3.10** (blue line), and monomer **3.12** (black line). Baselines have been offset for ease of comparison. Note the disappearance of the stretch at 3249 cm^{-1} upon oxidation of tetrazane **3.9** to verdazyl **3.10**, and the disappearance of the broad COOH stretch at 3434 cm^{-1} after the DCC coupling reaction (**3.10** \rightarrow **3.12**).

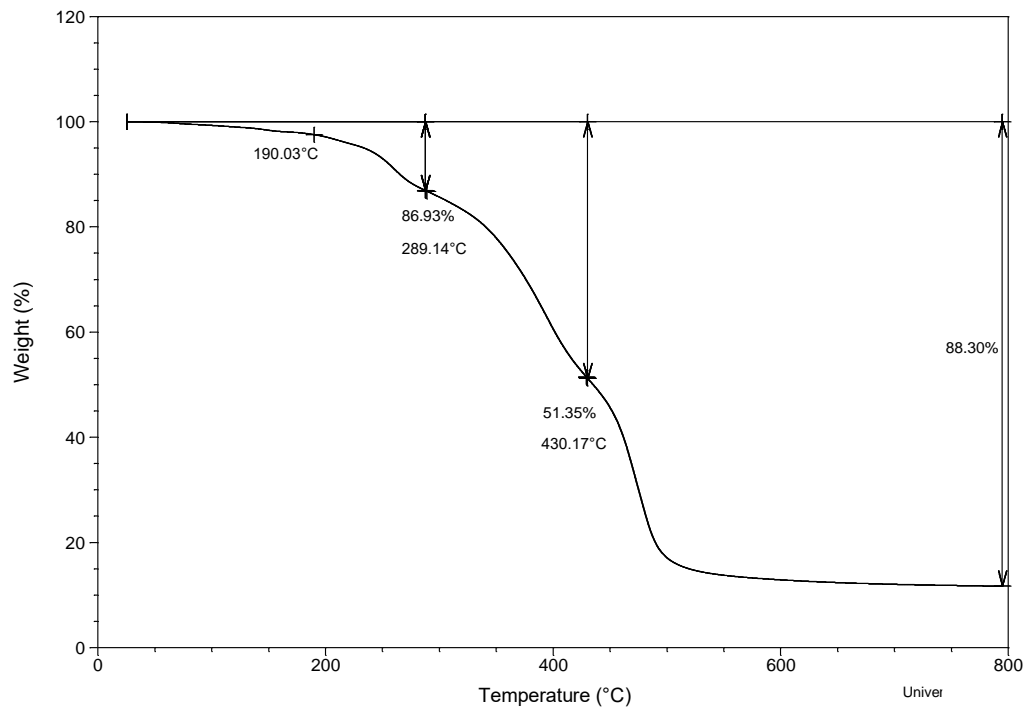


Figure A3.5 TGA trace for 6-oxoverdazyl polymer **3.13**.

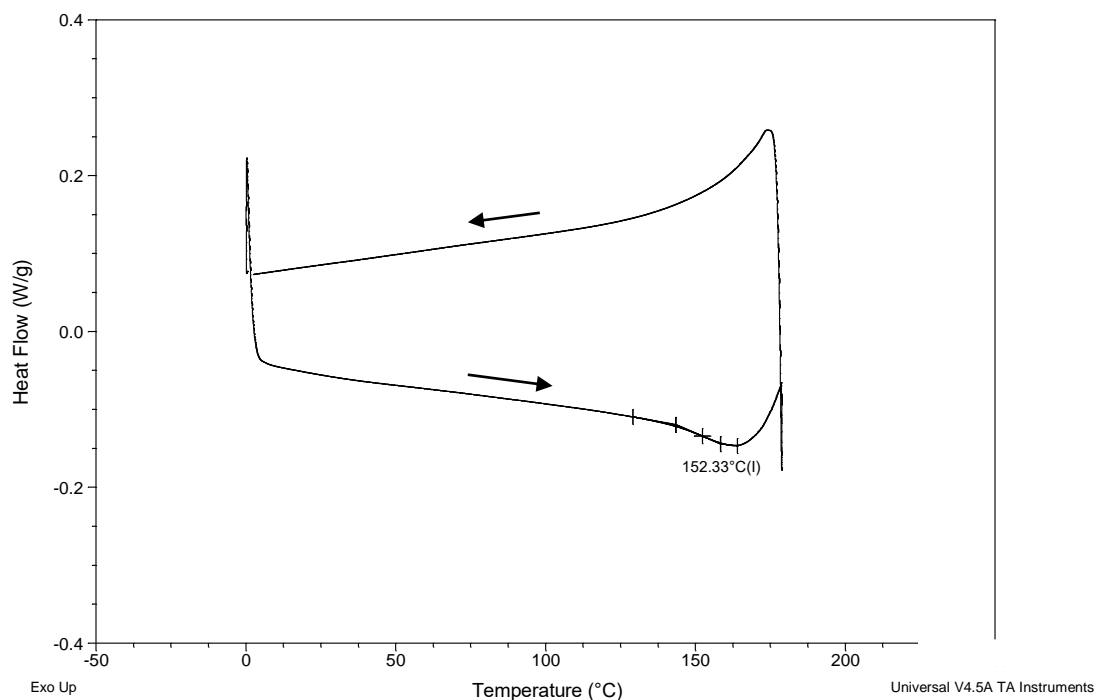


Figure A3.6 DSC data (second heating/cooling cycle) for 6-oxoverdazyl polymer **3.13**.

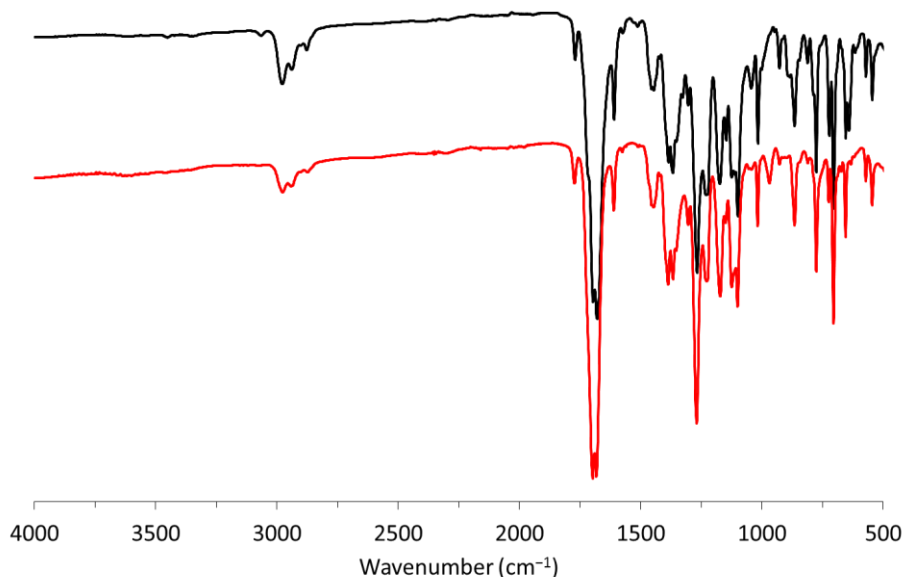


Figure A3.7 FT-IR spectra of 6-oxoverdazyl monomer **3.12** (red line) and polymer **3.13** (black line). Baselines have been offset for ease of comparison.

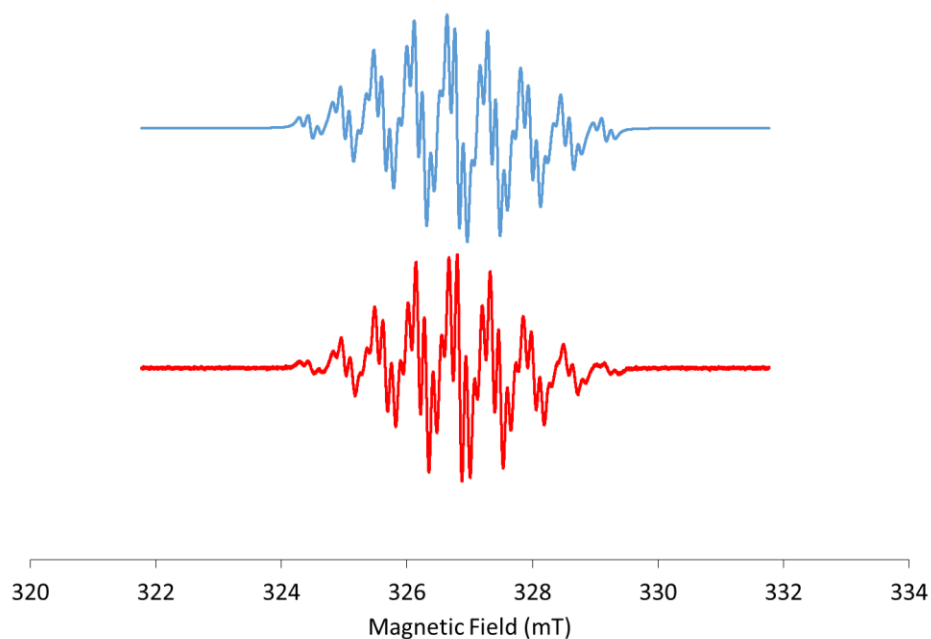


Figure A3.8 Simulated (top, blue line) and experimental (bottom, red line) EPR spectra of 6-oxoverdazyl monomer **3.12** in CH₂Cl₂. Parameters for simulation: $g = 2.0045$, line width = 0.089 mT, $a_{N1,3} = 0.529$ mT, $a_{N2,4} = 0.640$ mT, $a_H = 0.140$ mT.

Appendix 4 – Supporting Information for Chapter 4

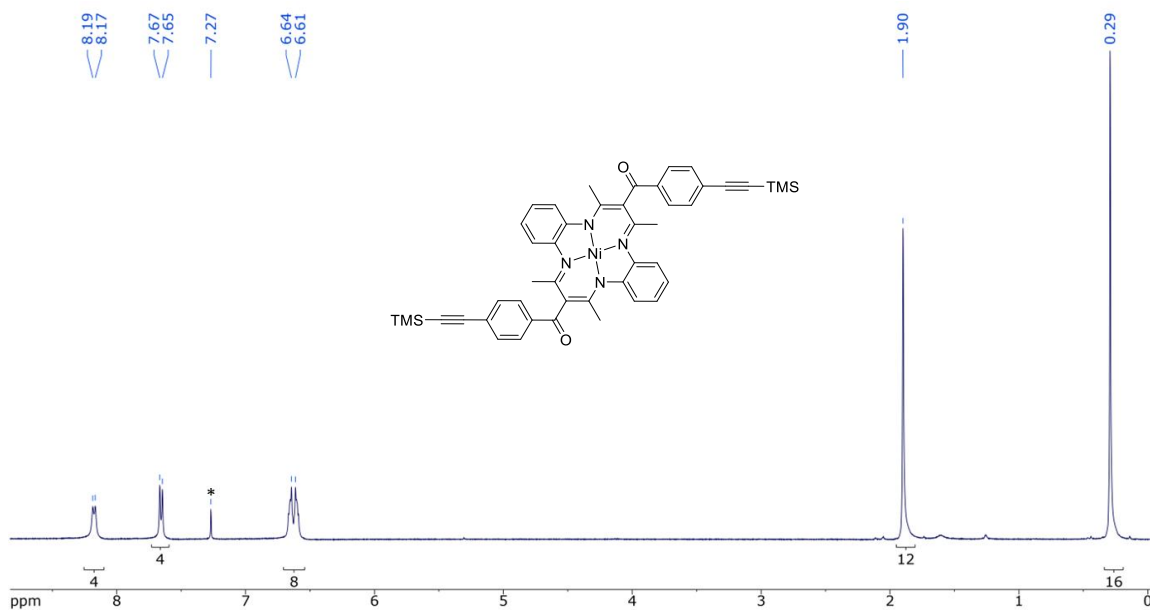


Figure A4.1. ^1H NMR spectrum of compound **4.6** in CDCl_3 . The asterisk denotes residual CHCl_3 .

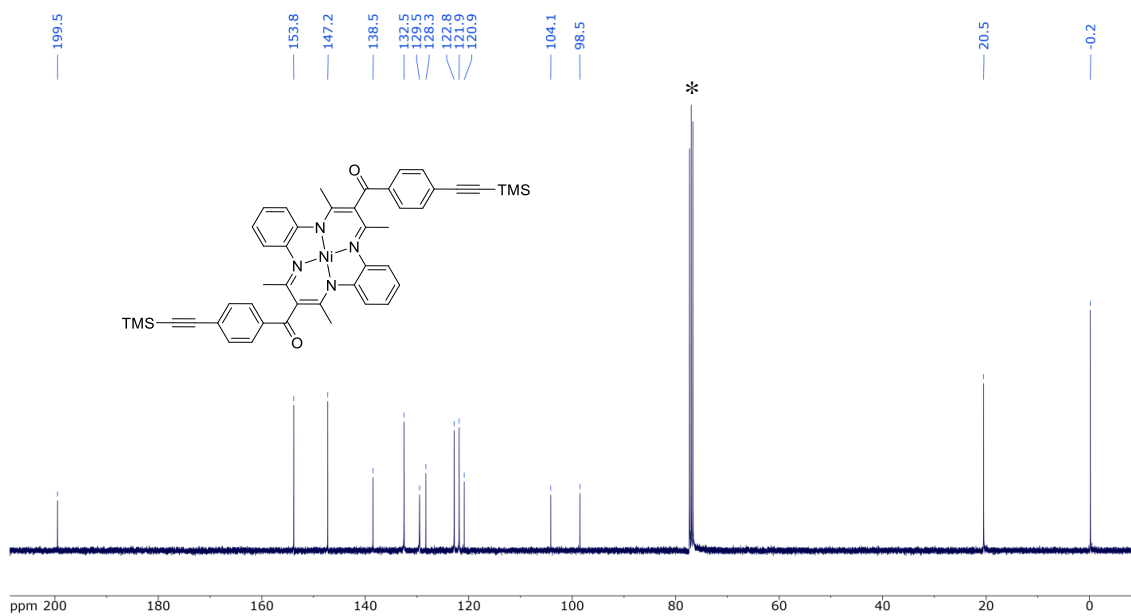


Figure A4.2 $^{13}\text{C}\{^1\text{H}\}$ NMR spectrum of compound **4.6** in CDCl_3 . The asterisk denotes CDCl_3 .

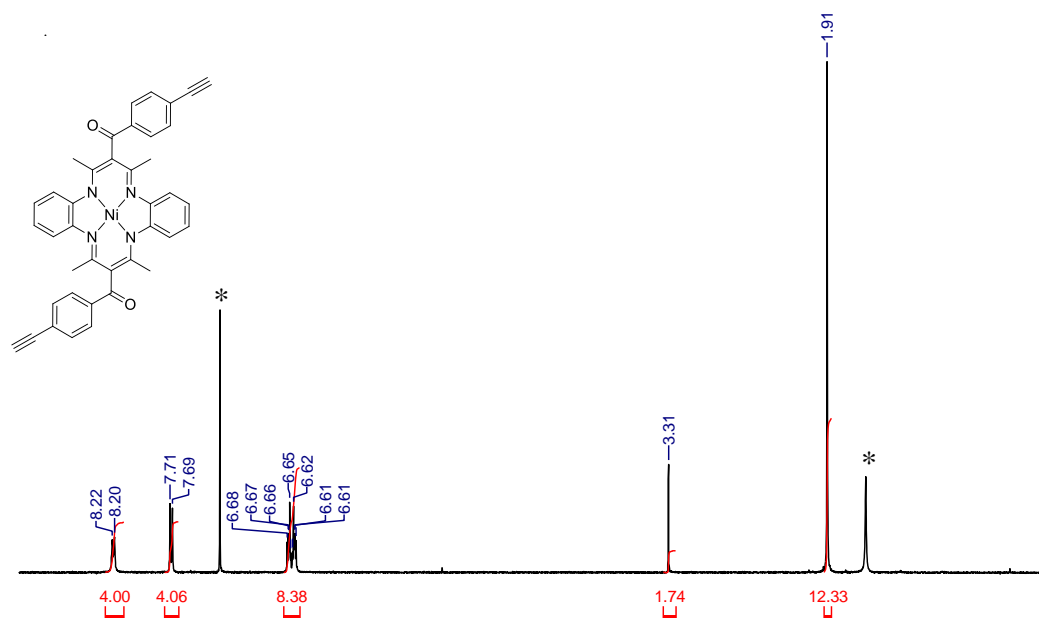


Figure A4.3. ^1H NMR spectrum of **4.7** in CDCl_3 . The asterisk denotes residual CHCl_3 and H_2O .

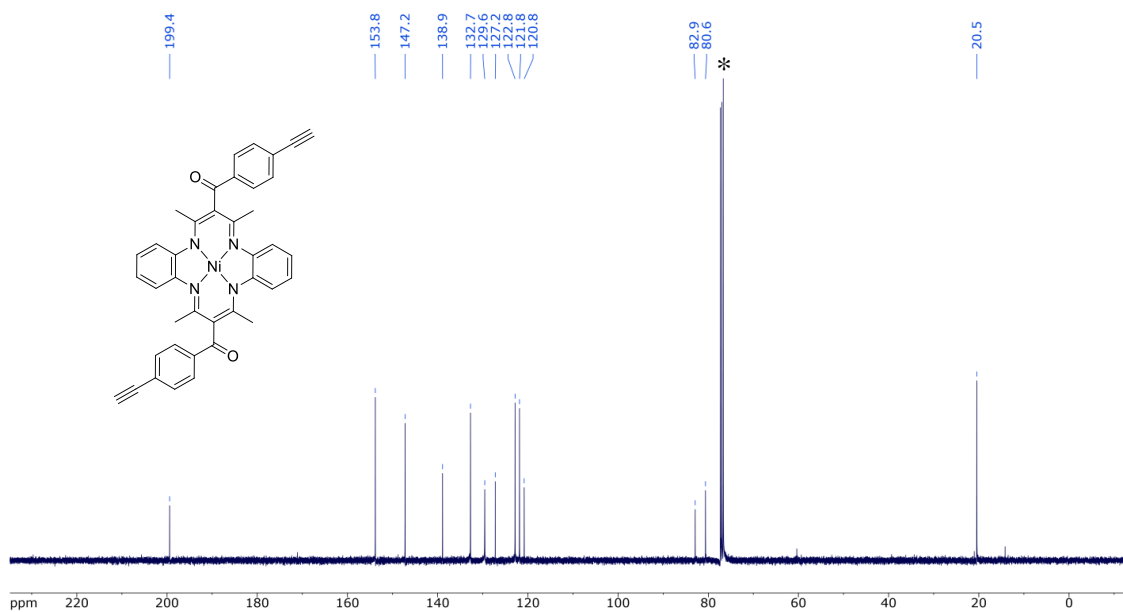


Figure A4.4. $^{13}\text{C}\{^1\text{H}\}$ NMR spectrum of **4.7** in CDCl_3 . The asterisk residual CDCl_3 .

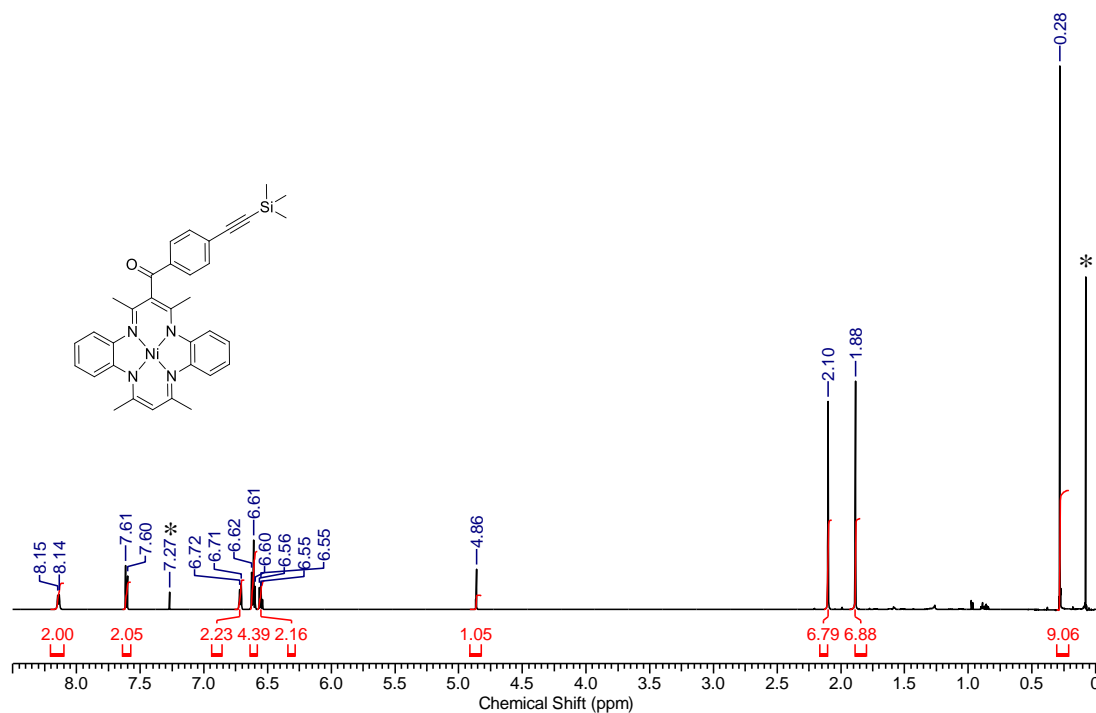


Figure A4.5. ^1H NMR spectrum of **4.8** in CDCl_3 . Asterisks denote residual solvent and grease signals.

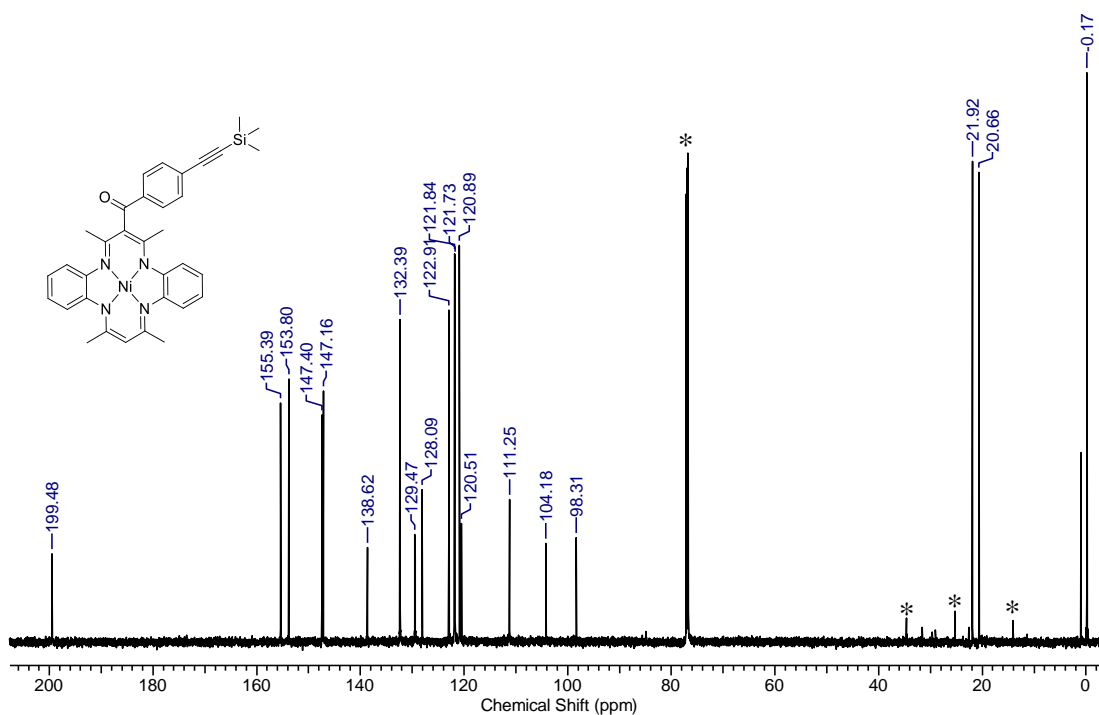


Figure A4.6. $^{13}\text{C}\{^1\text{H}\}$ NMR spectrum of **4.8** in CDCl_3 . Asterisks denote solvent and grease signals.

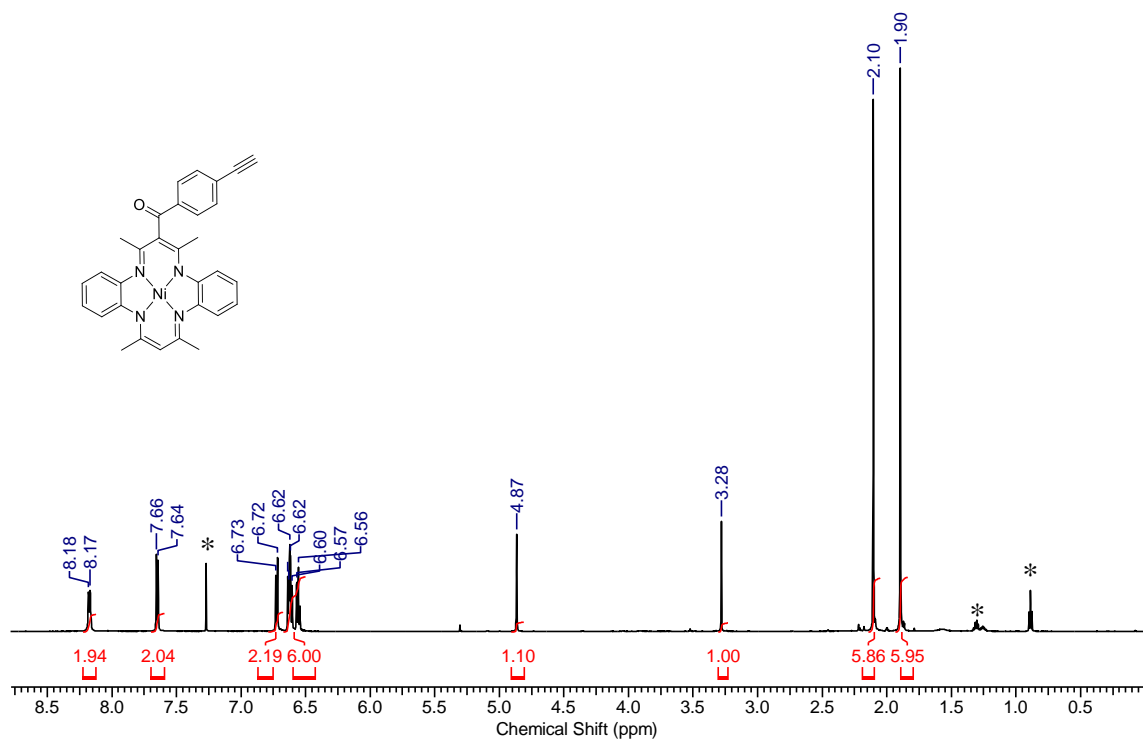


Figure A4.7. ^1H NMR spectrum of **4.9** in CDCl_3 . Asterisks denote residual solvent signals.

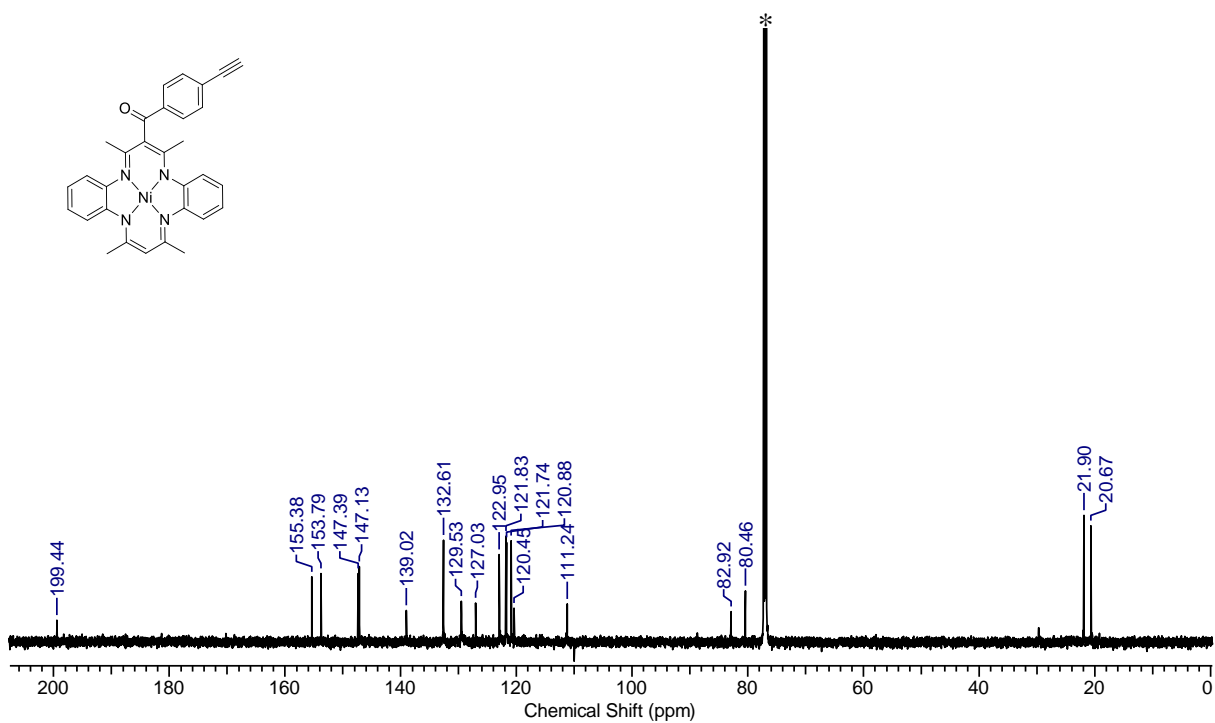


Figure A4.8. $^{13}\text{C}\{^1\text{H}\}$ NMR spectrum of **4.9** in CDCl_3 . Asterisk denotes solvent signal.

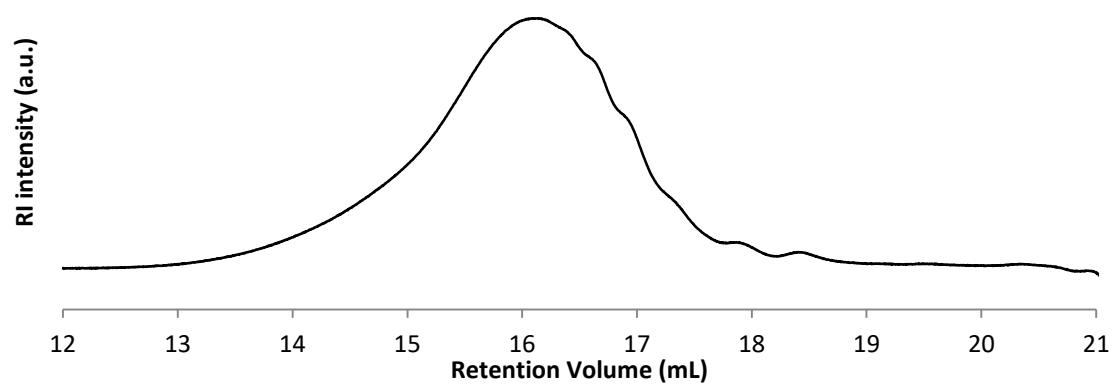


Figure A4.9. GPC trace for copolymer **4.10F** (run 3a) recorded in THF at 30 °C.

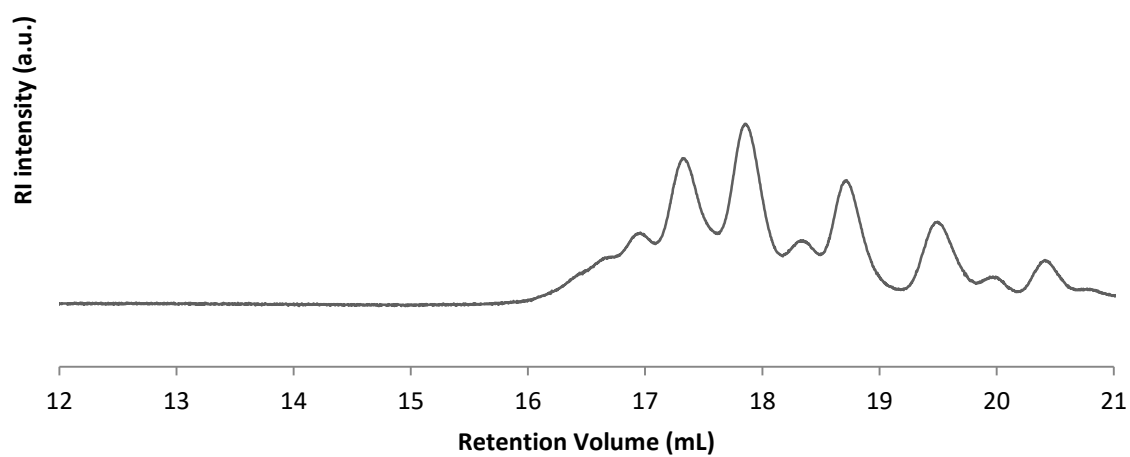


Figure A4.10. GPC trace for the Et₂O soluble oligomers (run 3a) recorded in THF.

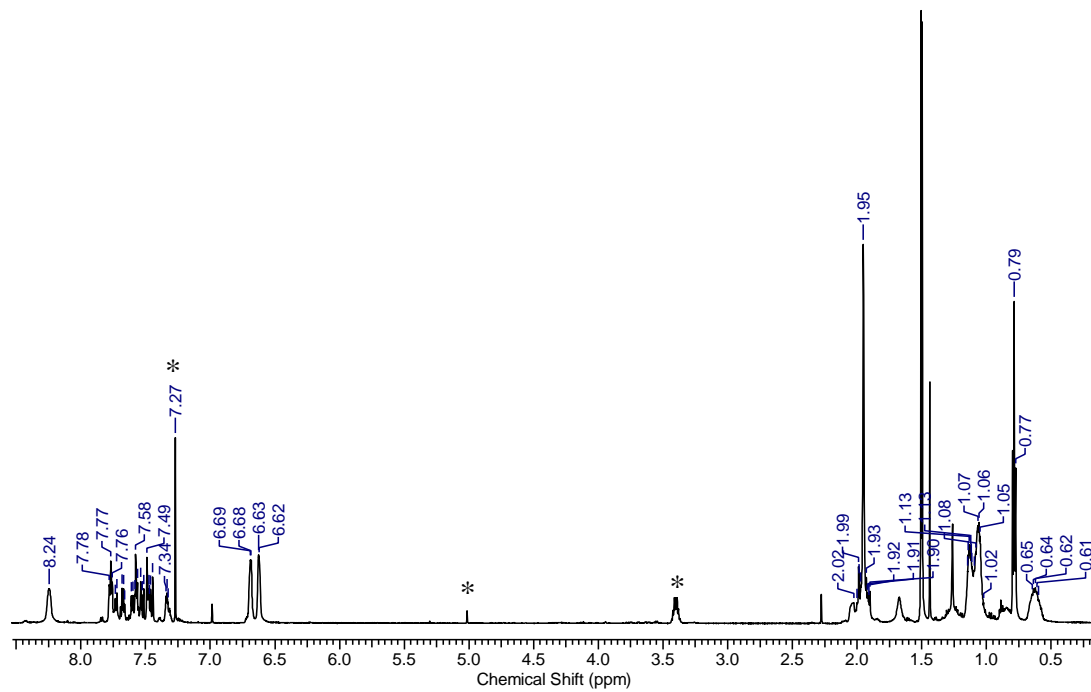


Figure A4.11. ^1H NMR spectrum of the Et_2O soluble oligomers (run 3a) recorded in CDCl_3 . The asterisks denote residual CHCl_3 , CH_2Cl_2 , MeOH and H_2O (from left to right).

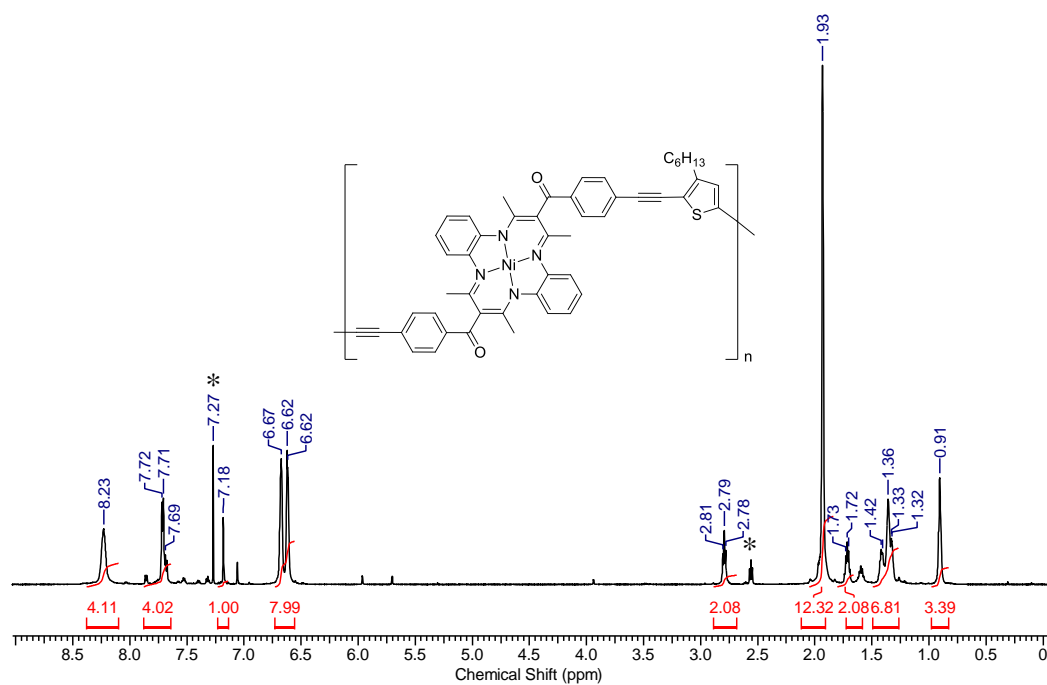


Figure A4.12. ^1H NMR spectra of copolymer **4.10T** in CDCl_3 . Asterisks denote residual solvent signals.

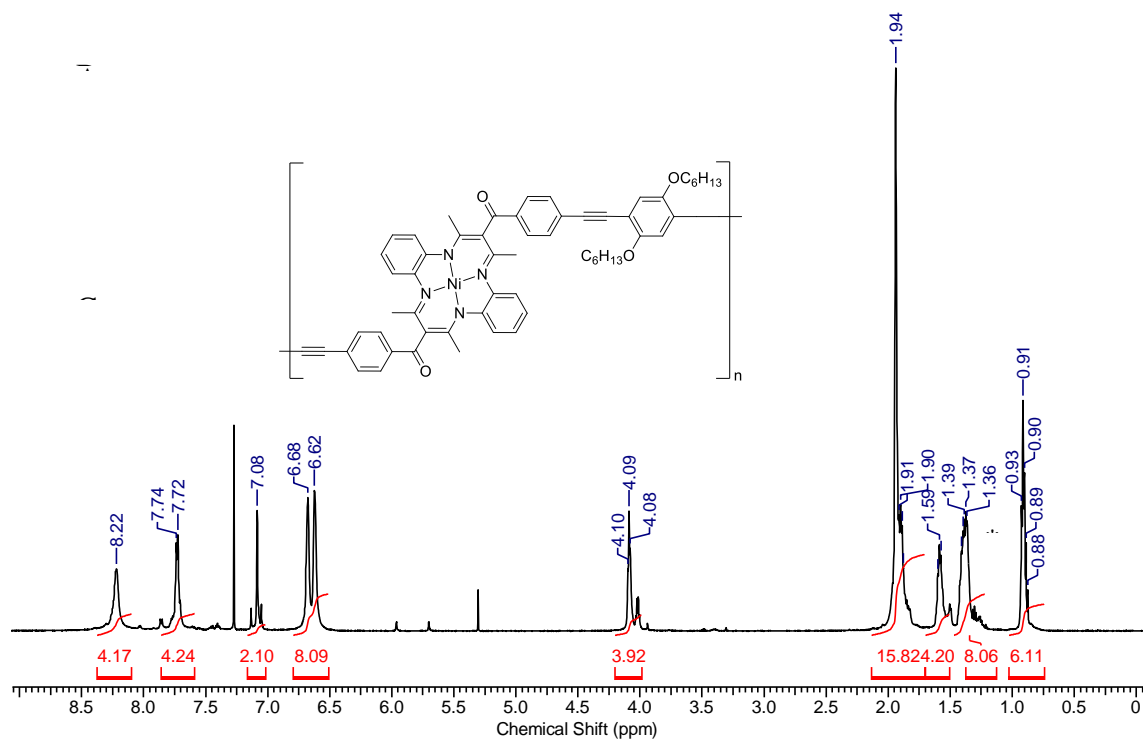


Figure A4.13. ¹H NMR spectra of copolymer **4.10B** in CDCl₃. Asterisks denote residual solvent signals.

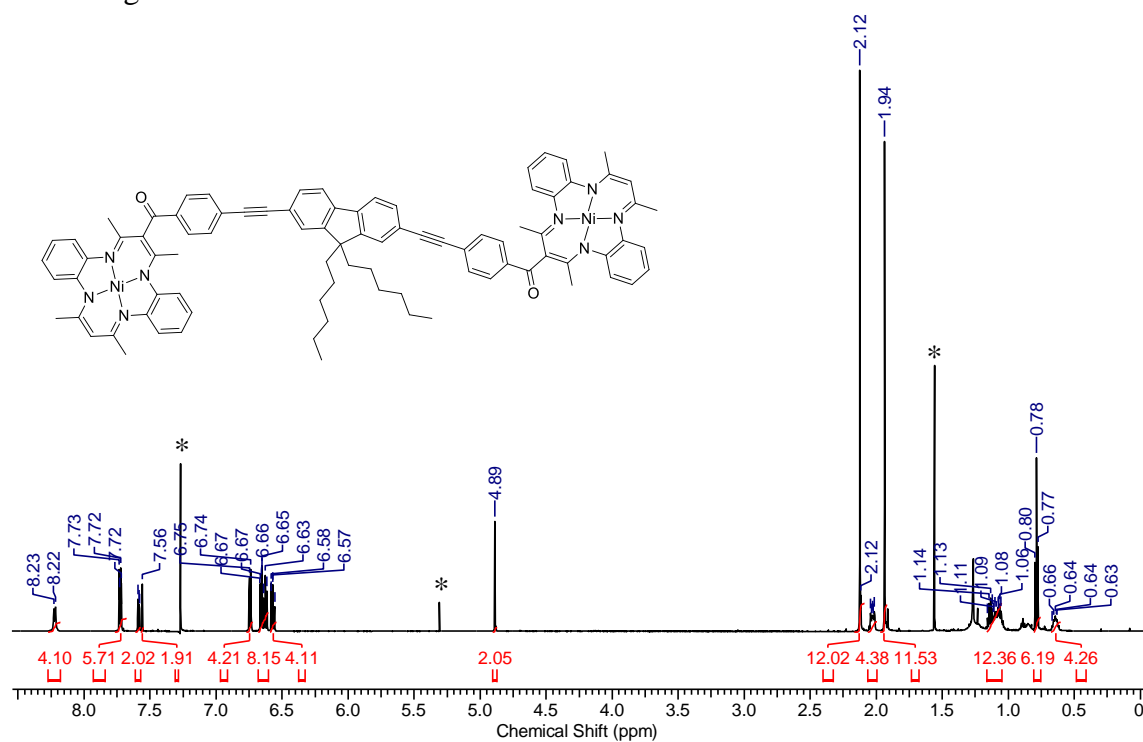


Figure A4.14. ¹H NMR spectrum of **4.13** in CDCl₃. Asterisks denote residual solvent signals.

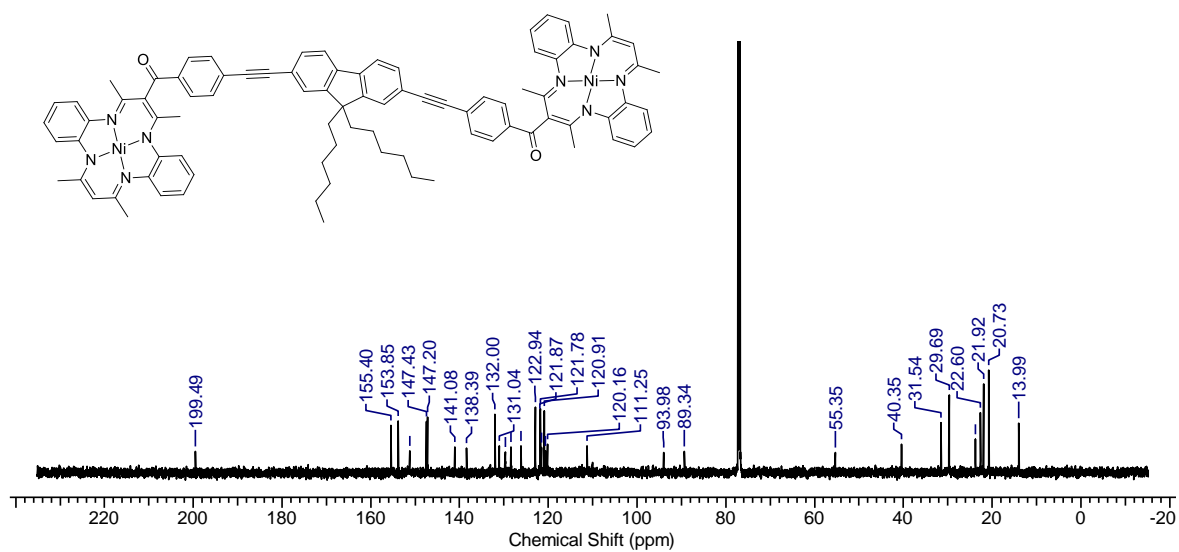


Figure A4.15. $^{13}\text{C}\{^1\text{H}\}$ NMR spectrum of **4.13** in CDCl_3 . Asterisk denotes solvent signal.

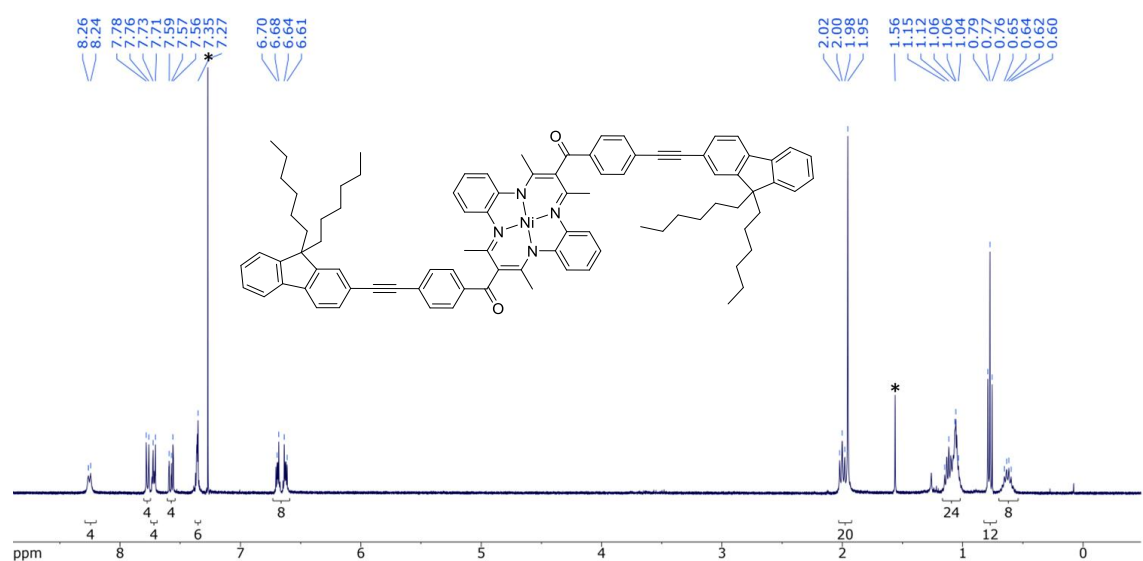


Figure A4.16. ^1H NMR spectrum of **4.14** in CDCl_3 . The asterisks denote residual CHCl_3 and H_2O .

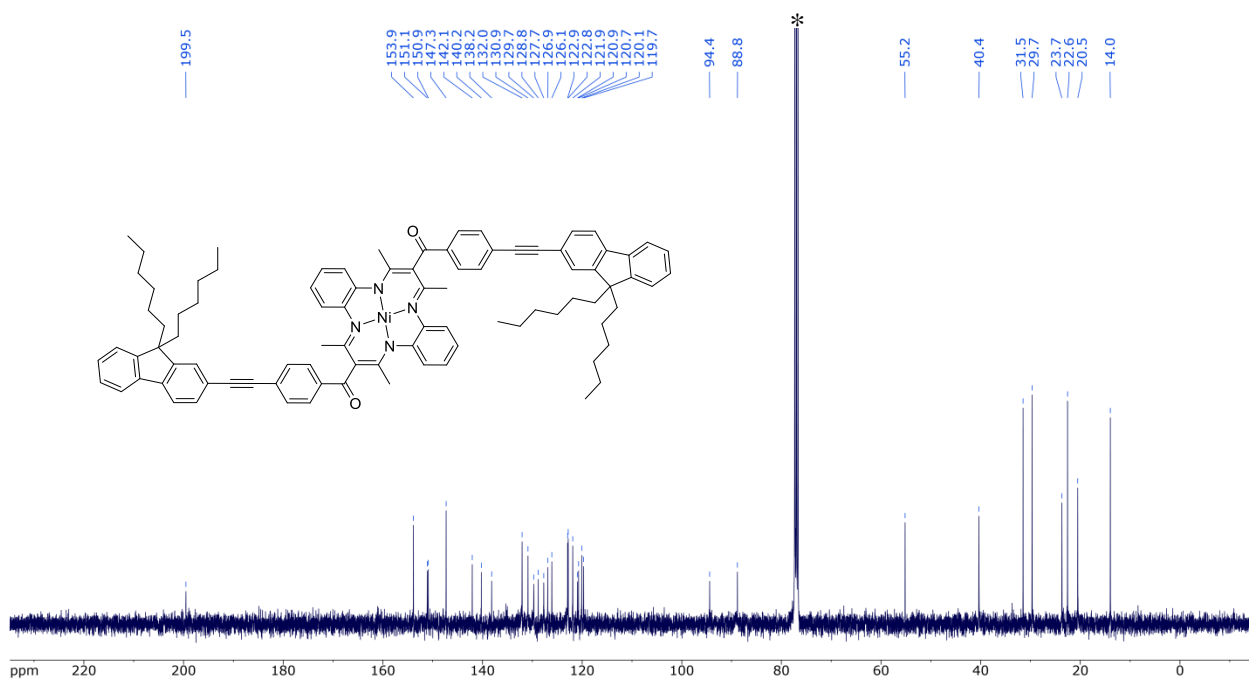


Figure A4.17. $^{13}\text{C}\{^1\text{H}\}$ NMR spectrum of **4.14** in CDCl_3 . The asterisk denotes CDCl_3 .

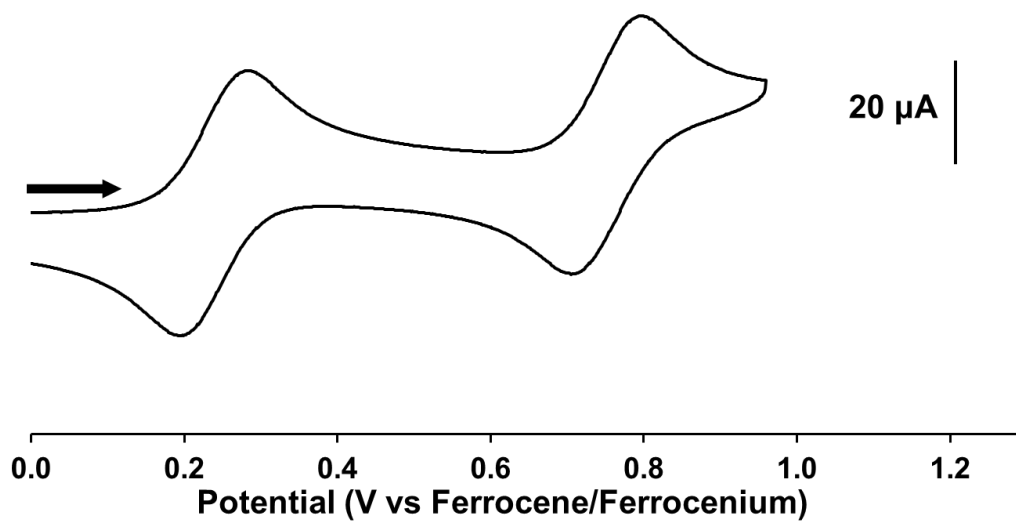


Figure A4.18. CV of model compound **4.14** recorded at a scan rate of 100 mVs^{-1} in a CH_2Cl_2 solution containing $1 \times 10^{-3} \text{ M}$ analyte and 0.1 M $[\text{nBu}_4\text{N}][\text{PF}_6]$ as supporting electrolyte.

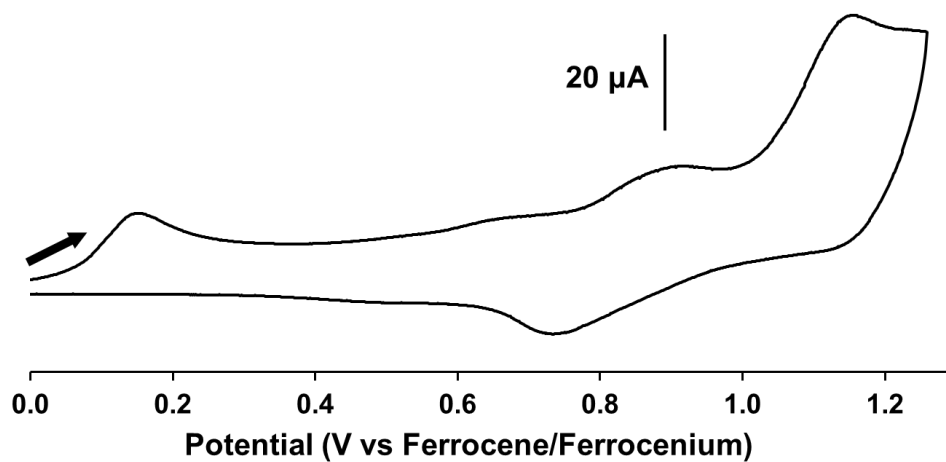


Figure A4.19. CV of model compound **4.13** recorded at a scan rate of 100 mV s^{-1} in a CH_2Cl_2 solution containing $1 \times 10^{-3} \text{ M}$ analyte and 0.1 M $[\text{nBu}_4\text{N}][\text{PF}_6]$ as supporting electrolyte.

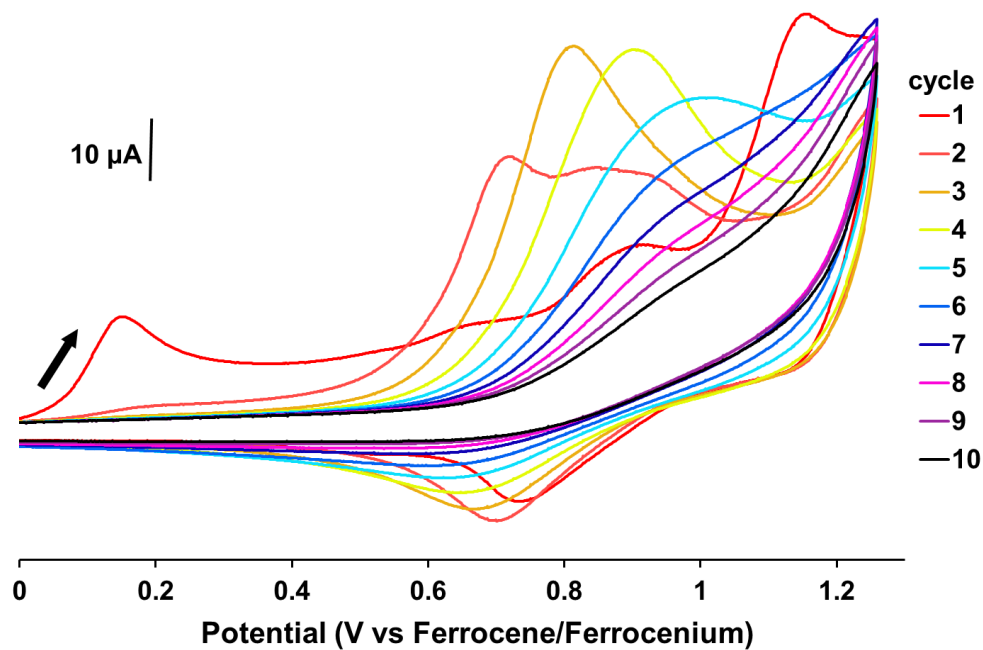


Figure A4.20. CVs of **4.13** cycled 10 times and recorded at a scan rate of 250 mV s^{-1} in a CH_2Cl_2 solution containing $1 \times 10^{-3} \text{ M}$ analyte and 0.1 M $[\text{nBu}_4\text{N}][\text{PF}_6]$ as supporting electrolyte.

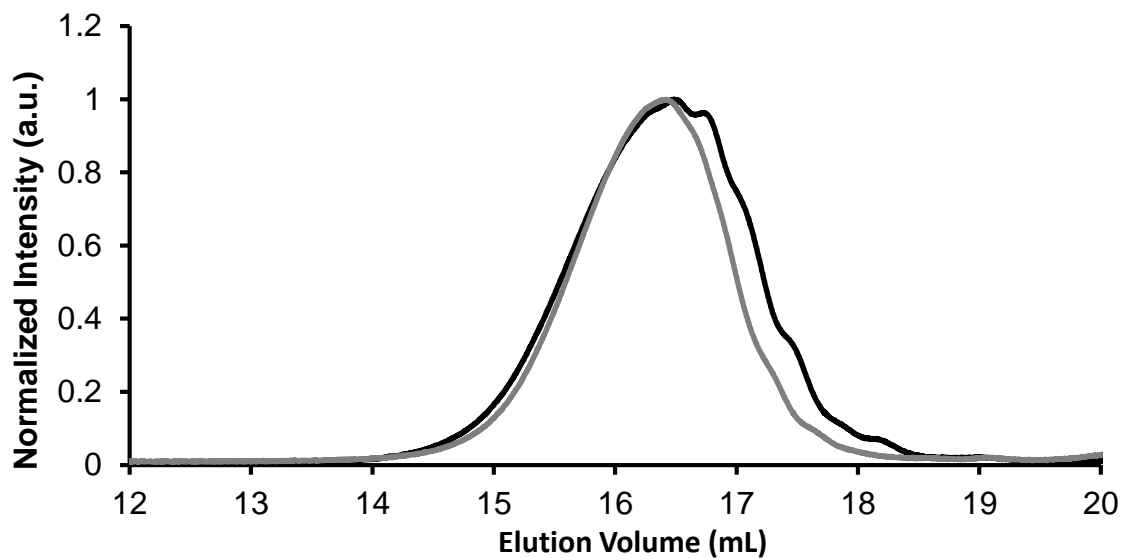


Figure A4.21. GPC traces for **4.10F** (black) and **4.10F-[Co₂(CO)₆]₂** (grey).

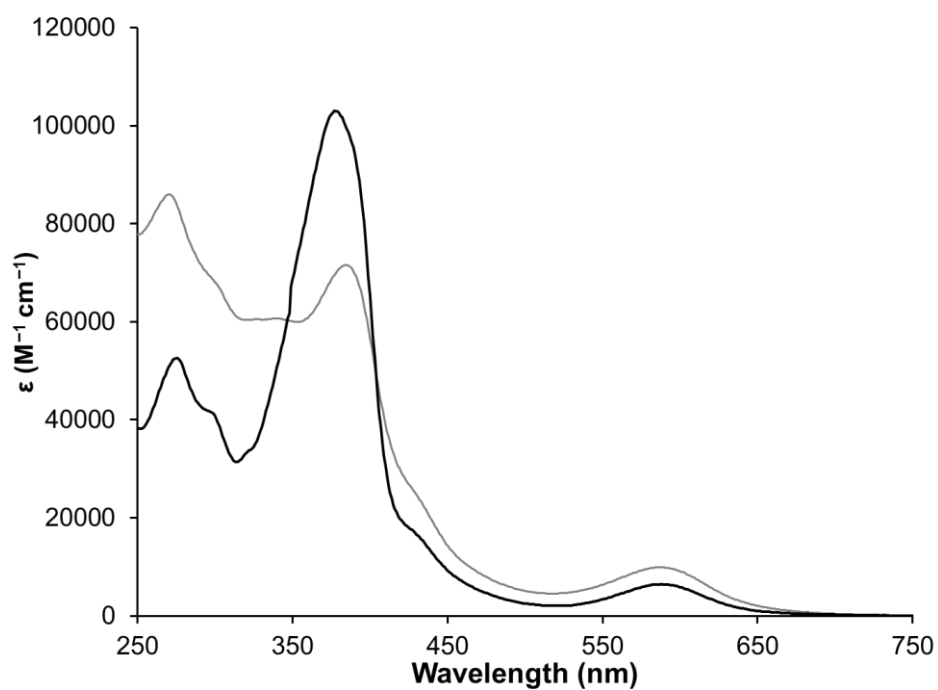


Figure A4.22. UV-vis absorption spectra of **4.10F** (black) and **4.10F-[Co₂(CO)₆]₂** (grey) in CH₂Cl₂.

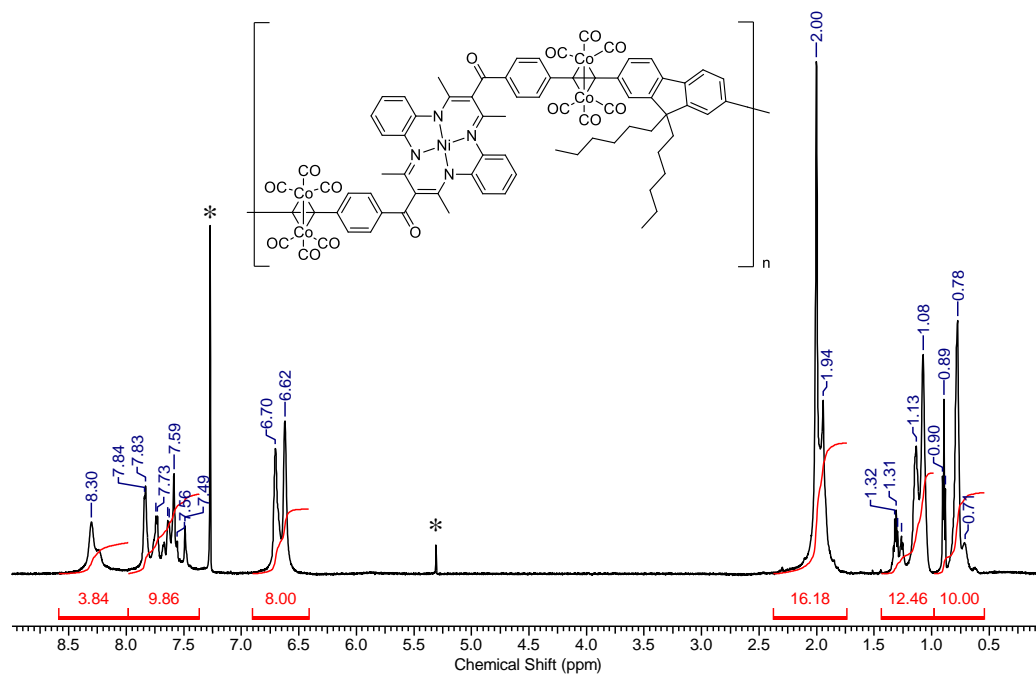


Figure A4.23. ¹H NMR spectrum of **4.10F** and **4.10F**-[Co₂(CO)₆]₂ in CDCl₃. Asterisks denote residual solvent signals.

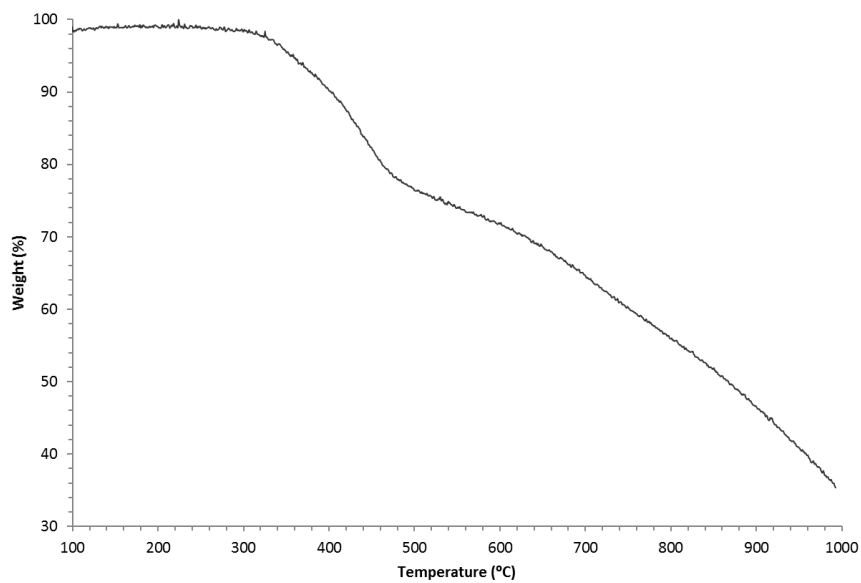


Figure A4.24. TGA trace data for **4.10F**.

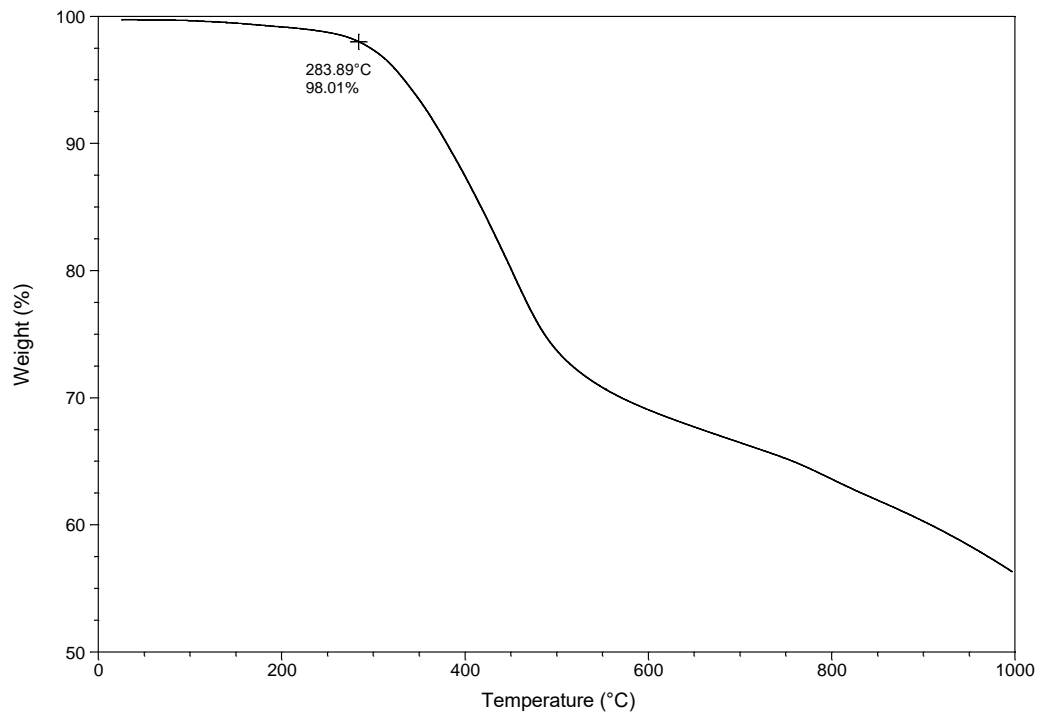


Figure A4.25. TGA trace data for **4.10T**.

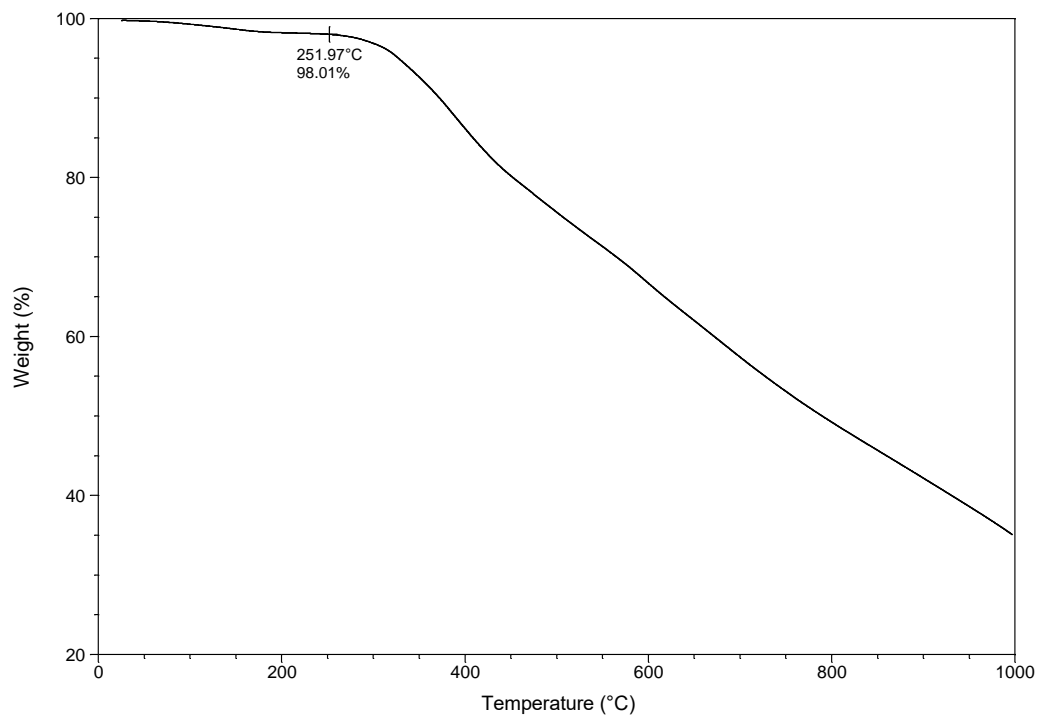


Figure A4.26. TGA trace for **4.10B**.

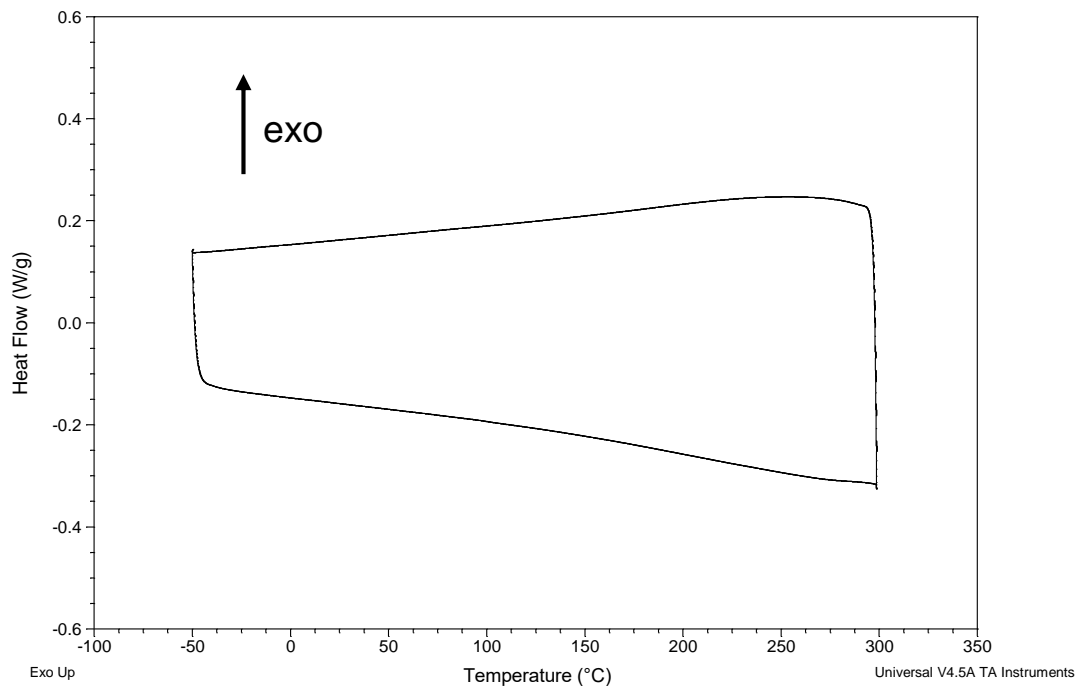


Figure A4.27. DSC trace for **4.10F**. The second heating/cooling cycle is shown.

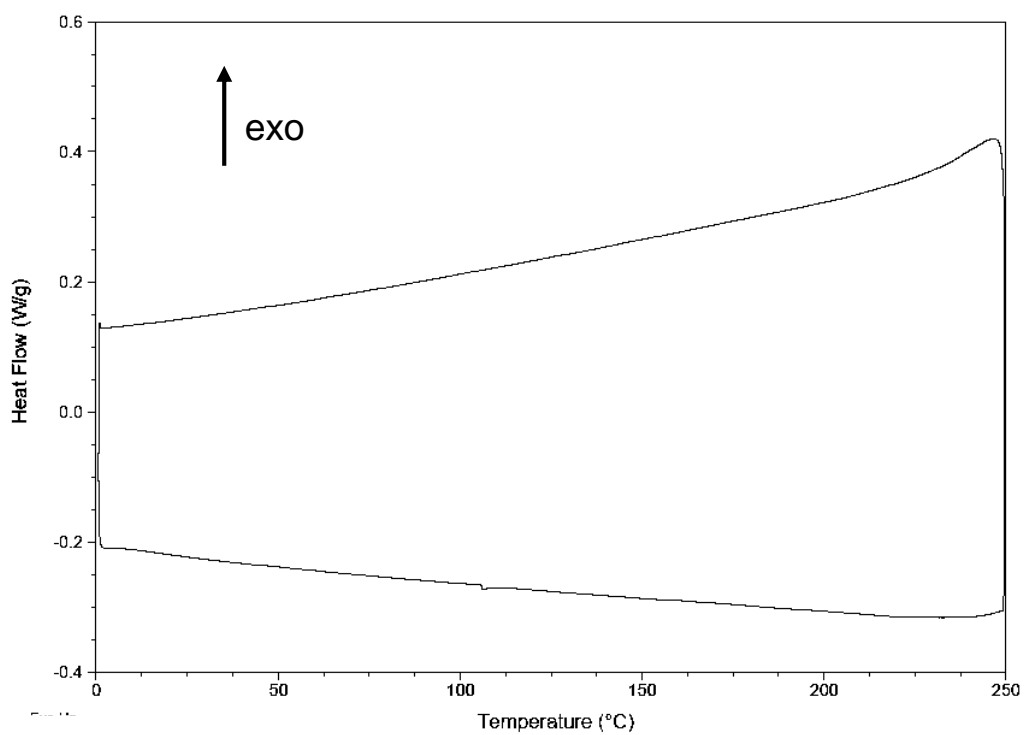


Figure A4.28. DSC trace for **4.10T**. The second heating/cooling cycle is shown.

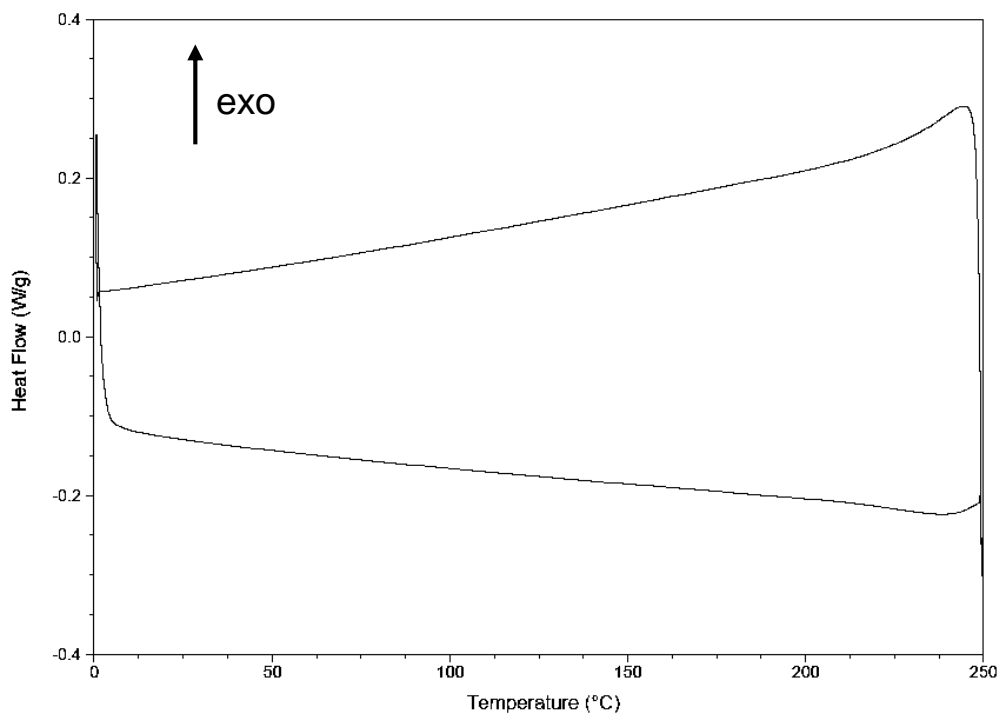


Figure A4.29. DSC trace for **4.10B**. The second heating/cooling cycle is shown.

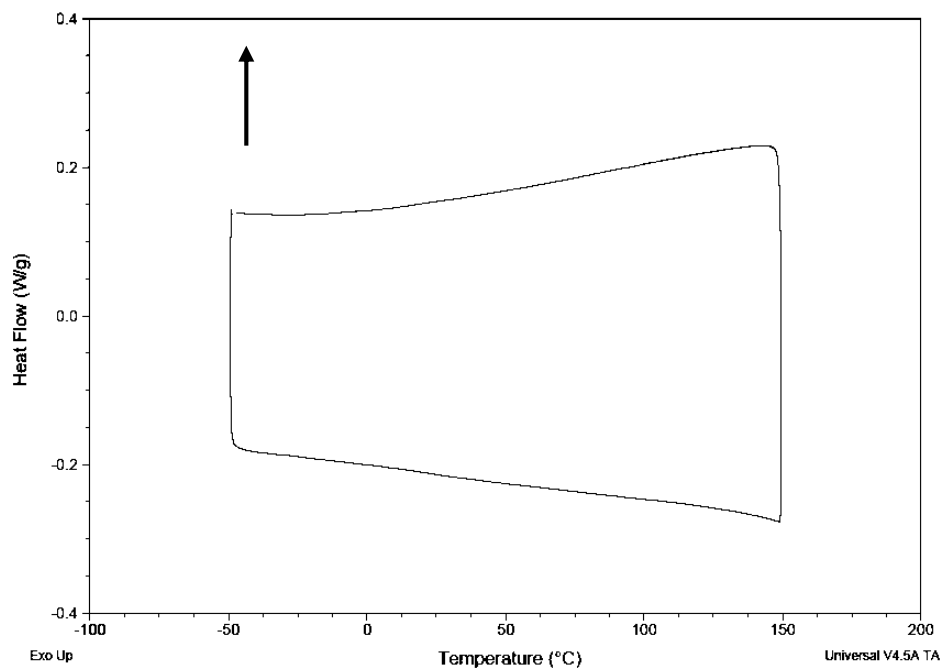


Figure A4.30. DSC trace for **4.10F-[Co₂(CO)₆]**. The second heating/cooling cycle is shown.



Figure A4.31. SEM of a cross-section of a thin film prepared by drop casting **4.10F-[Co₂(CO)₆]₂** onto a silicon wafer.

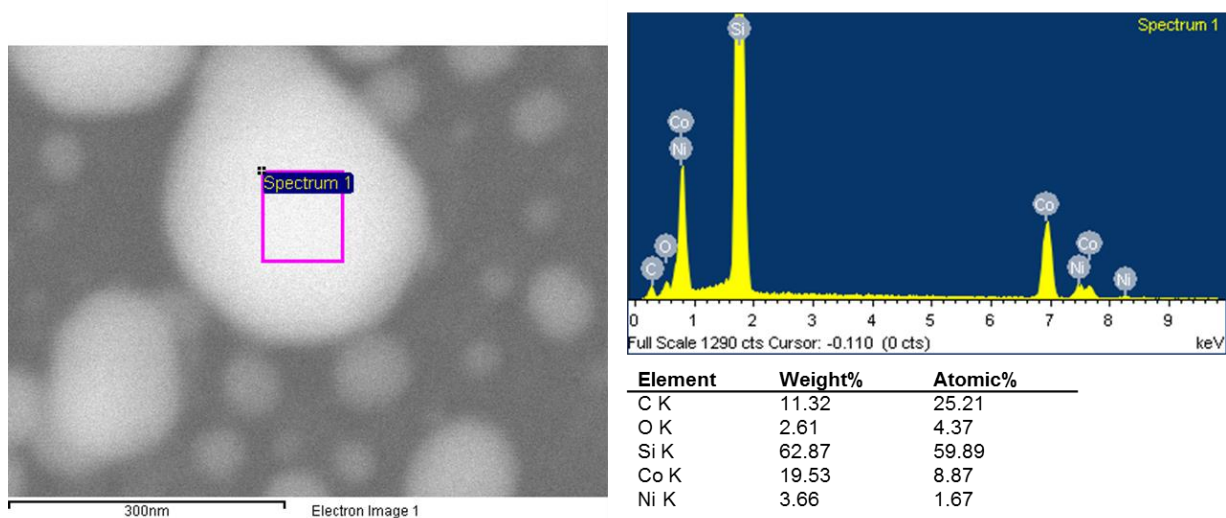


Figure 4.32. EDX spectroscopy data collected from the nanomaterials produced from the pyrolysis of thin film of **4.10F-[Co₂(CO)₆]₂** on a silicon wafer.

Appendix 5 – Supporting Information for Chapter 5

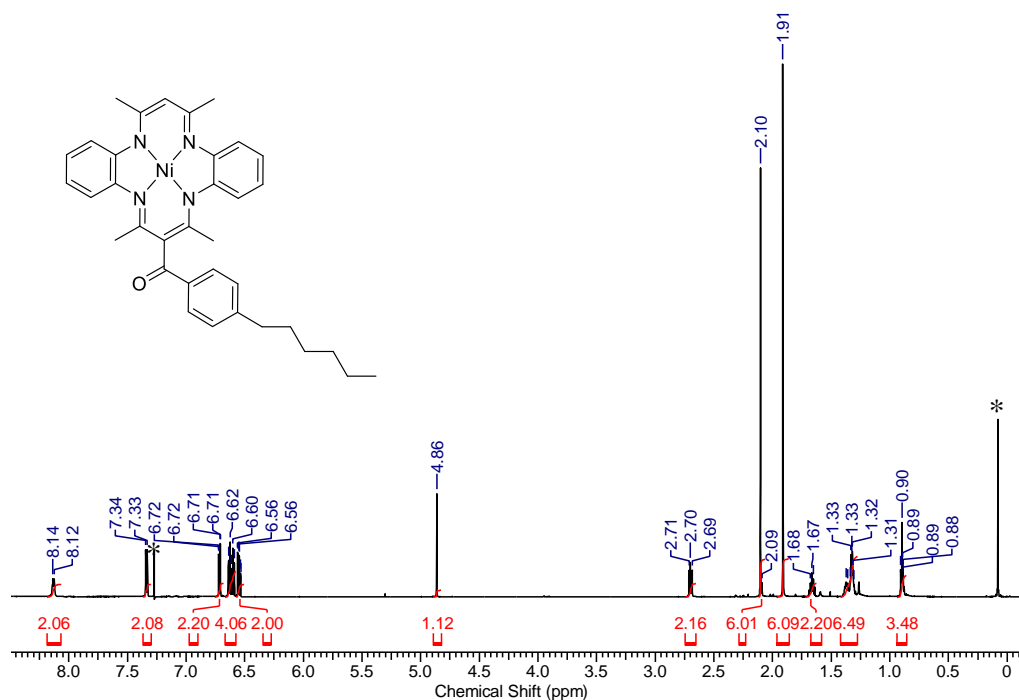


Figure A5.1 ^1H NMR spectrum of compound **5.6**. Asterisks denotes residual CHCl_3 and grease.

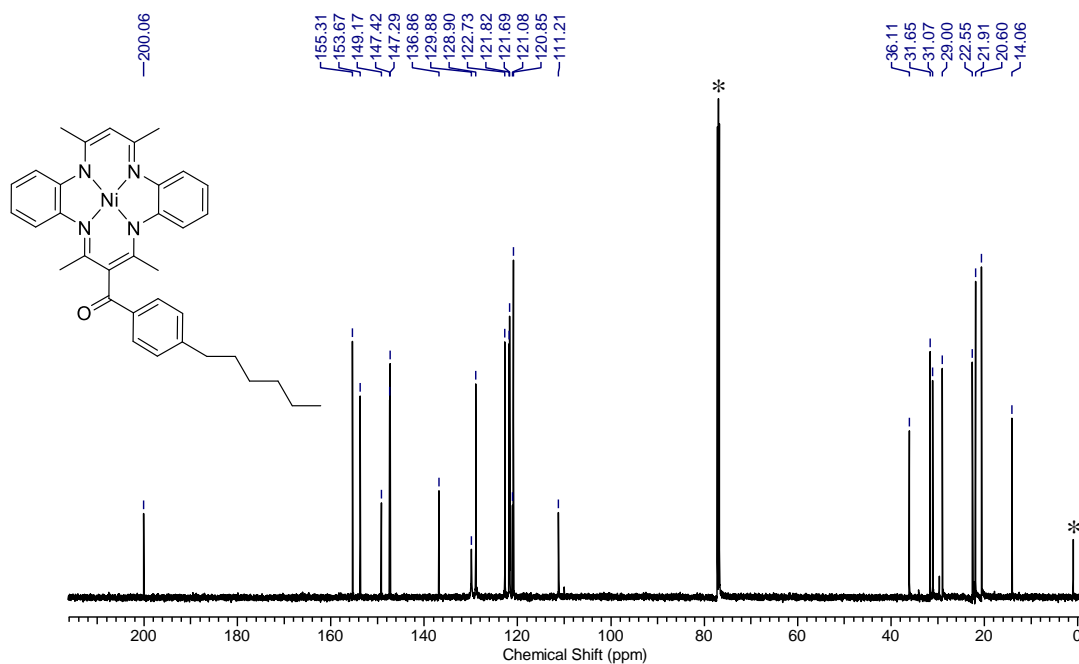


Figure A5.2 $^{13}\text{C}\{^1\text{H}\}$ NMR spectrum of **5.6** in CDCl_3 . Asterisks denote CDCl_3 and grease.

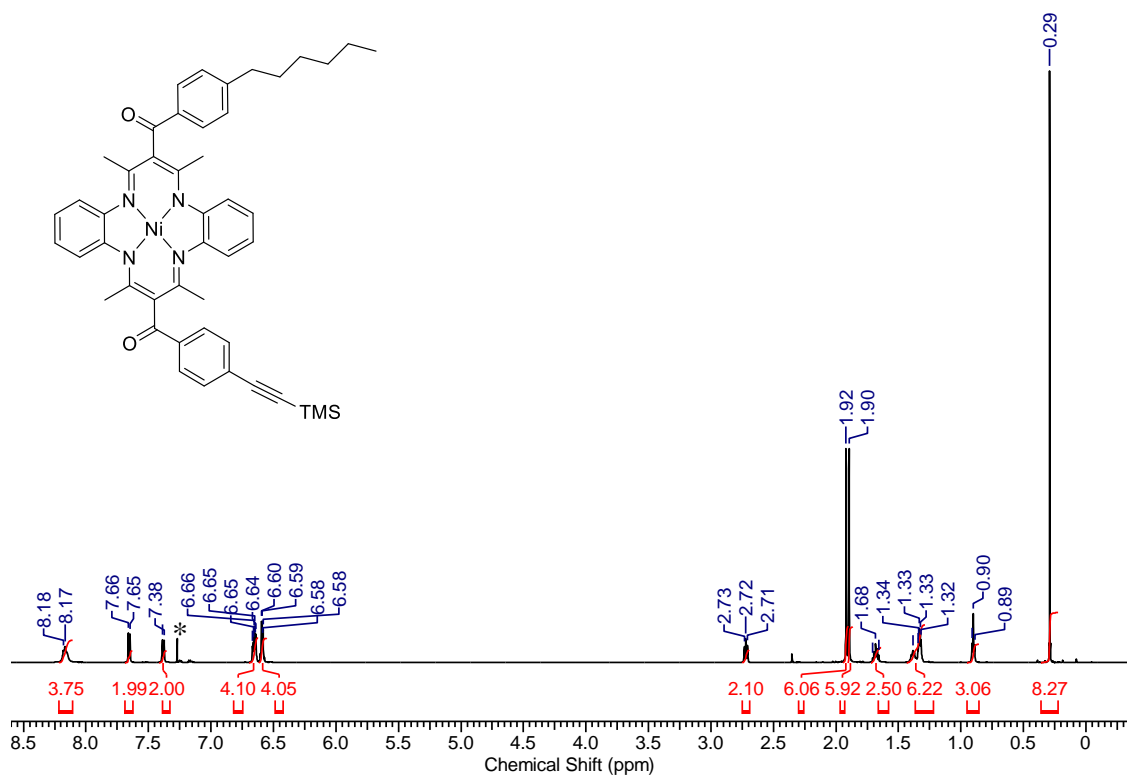


Figure A5.3 ^1H NMR spectrum of compound **5.7**. Asterisk denotes residual CHCl_3 .

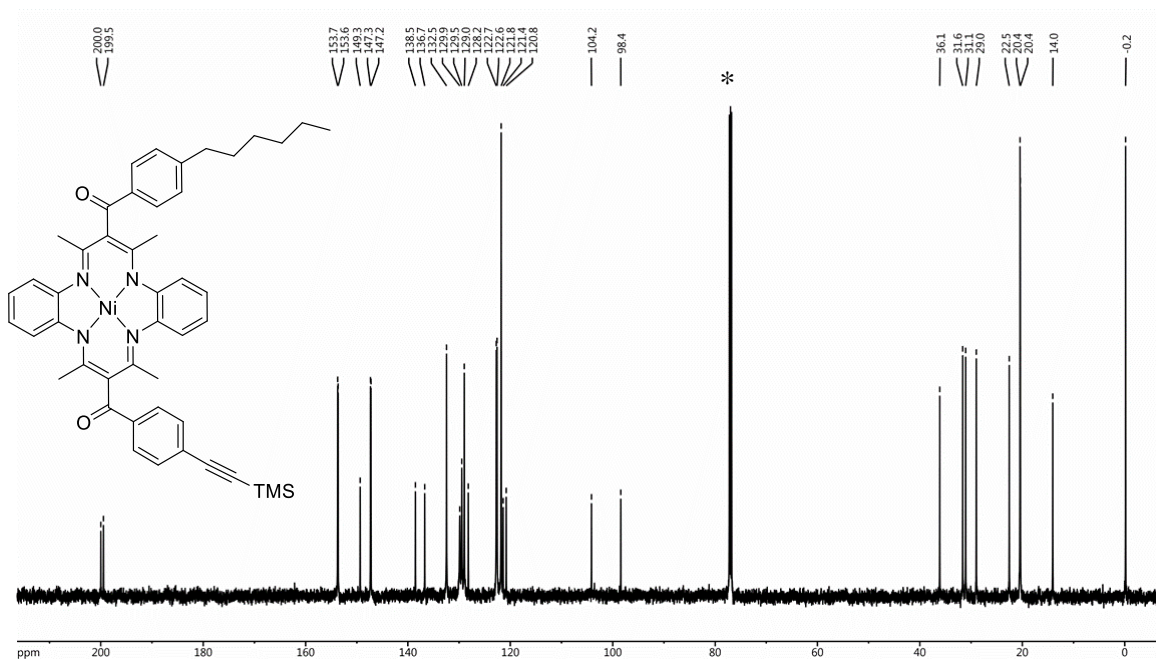


Figure A5.4 $^{13}\text{C}\{^1\text{H}\}$ NMR spectrum of **5.7** in CDCl_3 . Asterisk denotes CDCl_3 .

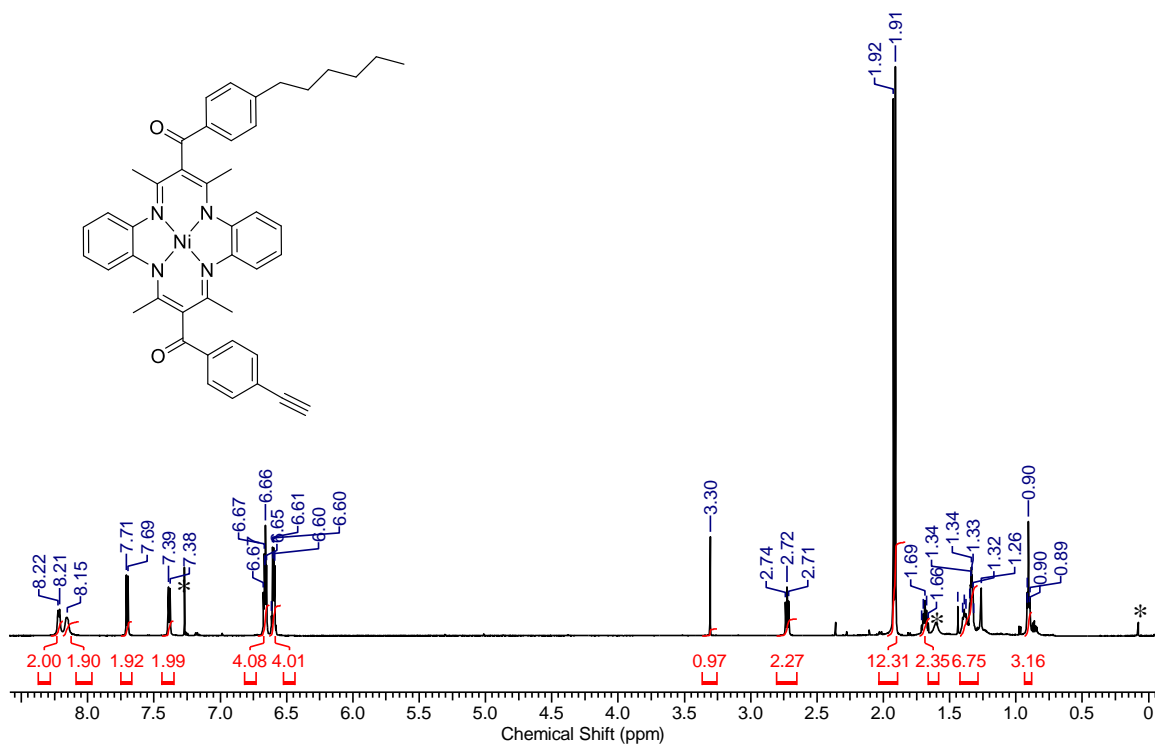


Figure A5.5 ^1H NMR spectrum of compound **5.8**. Asterisks denote residual CHCl_3 , water, and grease.

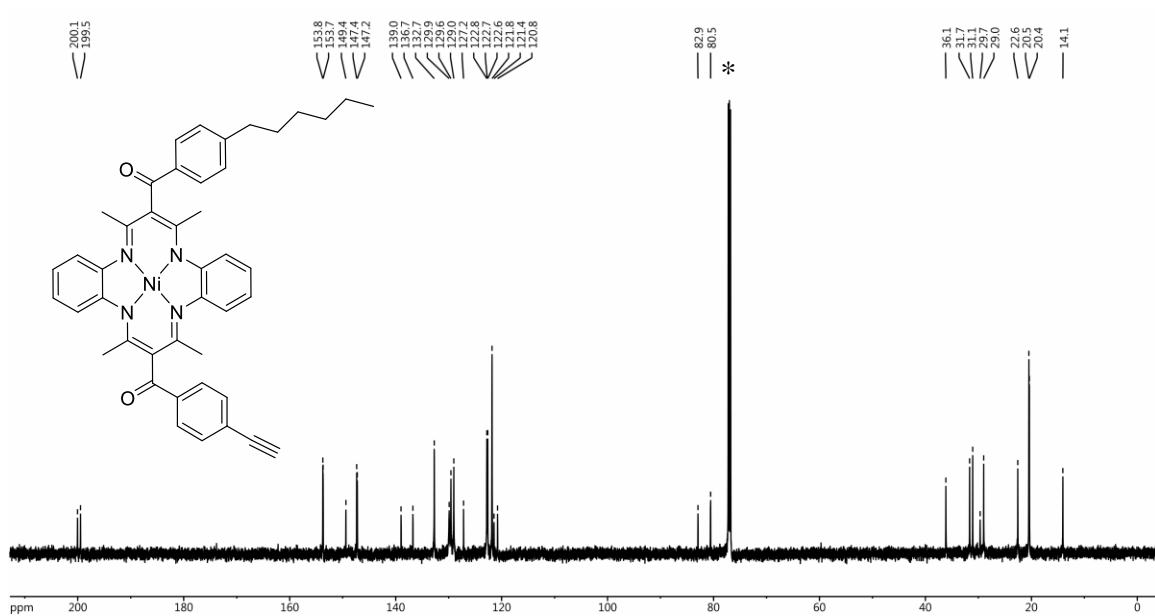


Figure A5.6 $^{13}\text{C}\{^1\text{H}\}$ NMR spectrum of **5.8** in CDCl_3 . Asterisk denotes CDCl_3 .

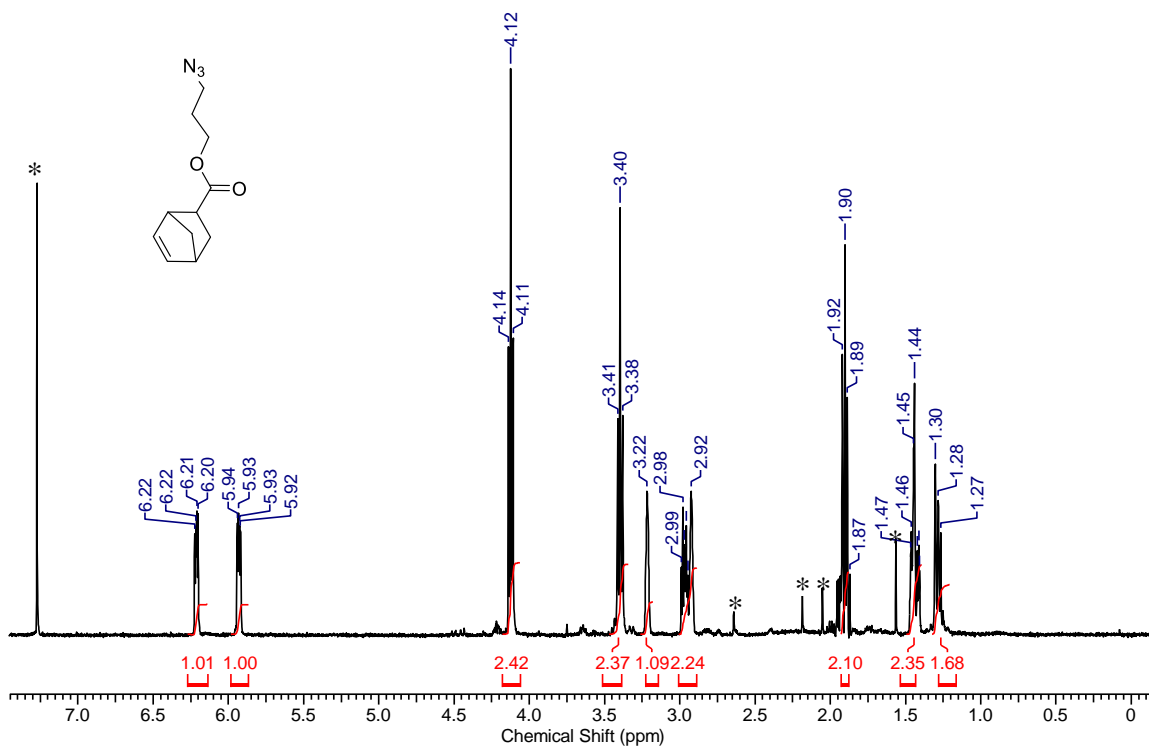


Figure A5.7 ^1H NMR spectrum of compound **5.9**. Asterisks denote residual CHCl_3 and water.

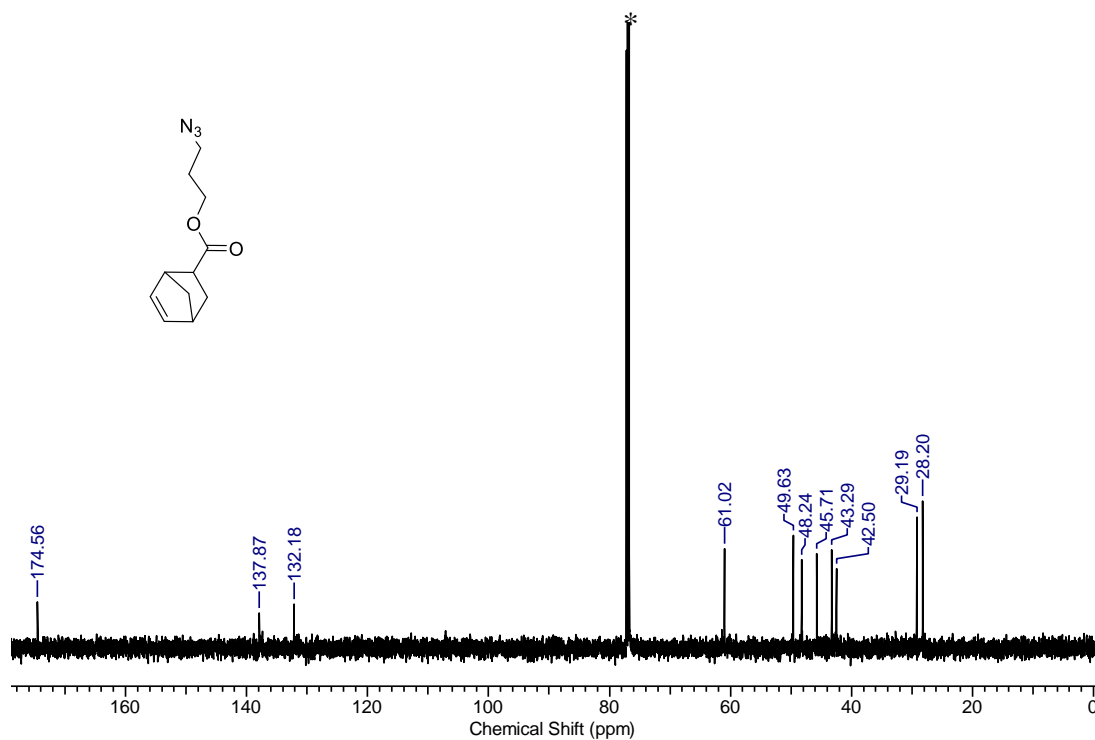


Figure A5.8 $^{13}\text{C}\{^1\text{H}\}$ NMR spectrum of **5.9** in CDCl_3 . Asterisk denotes CDCl_3 .

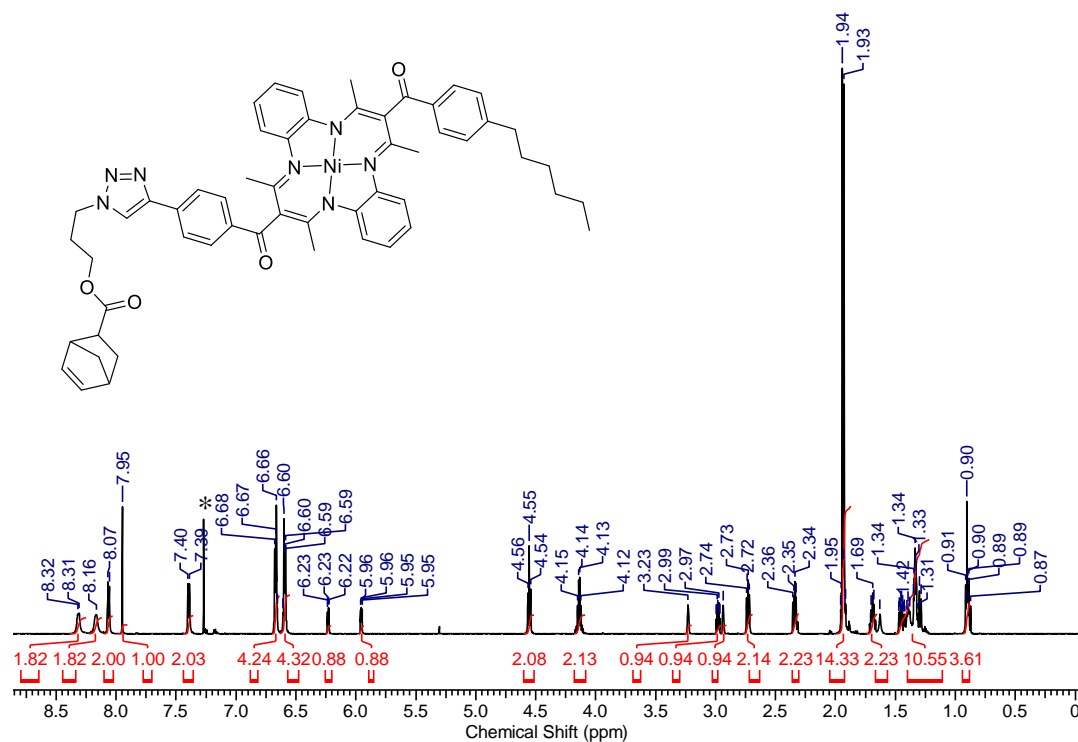


Figure A5.9 ^1H NMR spectrum of compound **5.10**. Asterisk denotes residual CHCl_3 .

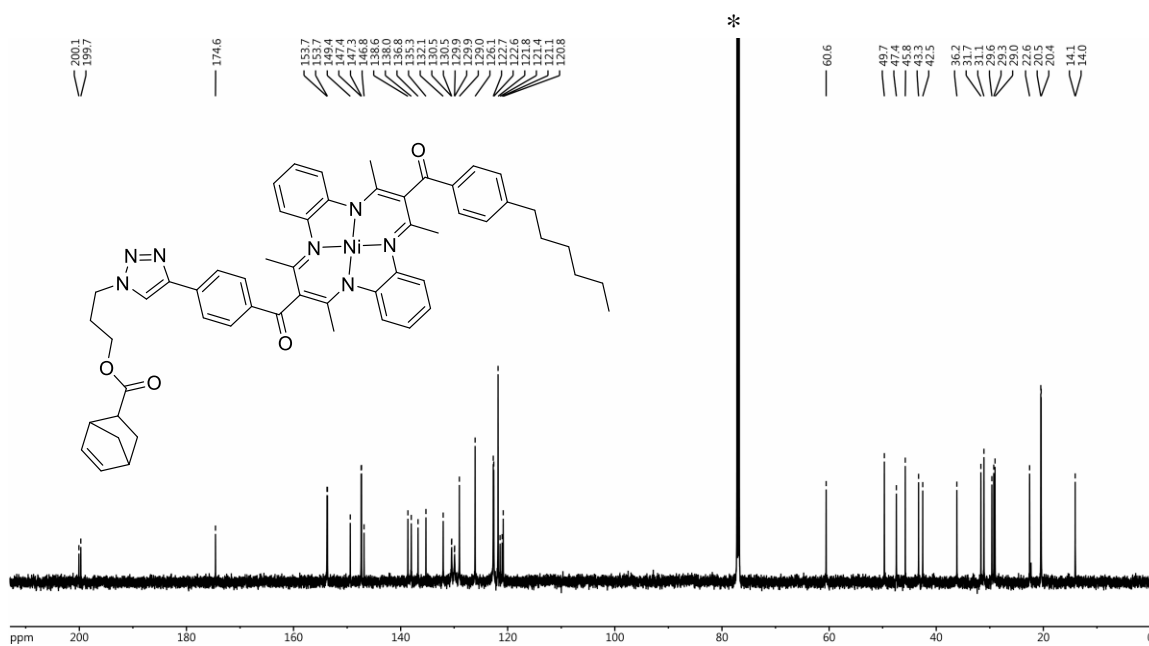


Figure A5.10 $^{13}\text{C}\{^1\text{H}\}$ NMR spectrum of **5.10** in CDCl_3 . Asterisk denotes CDCl_3 .

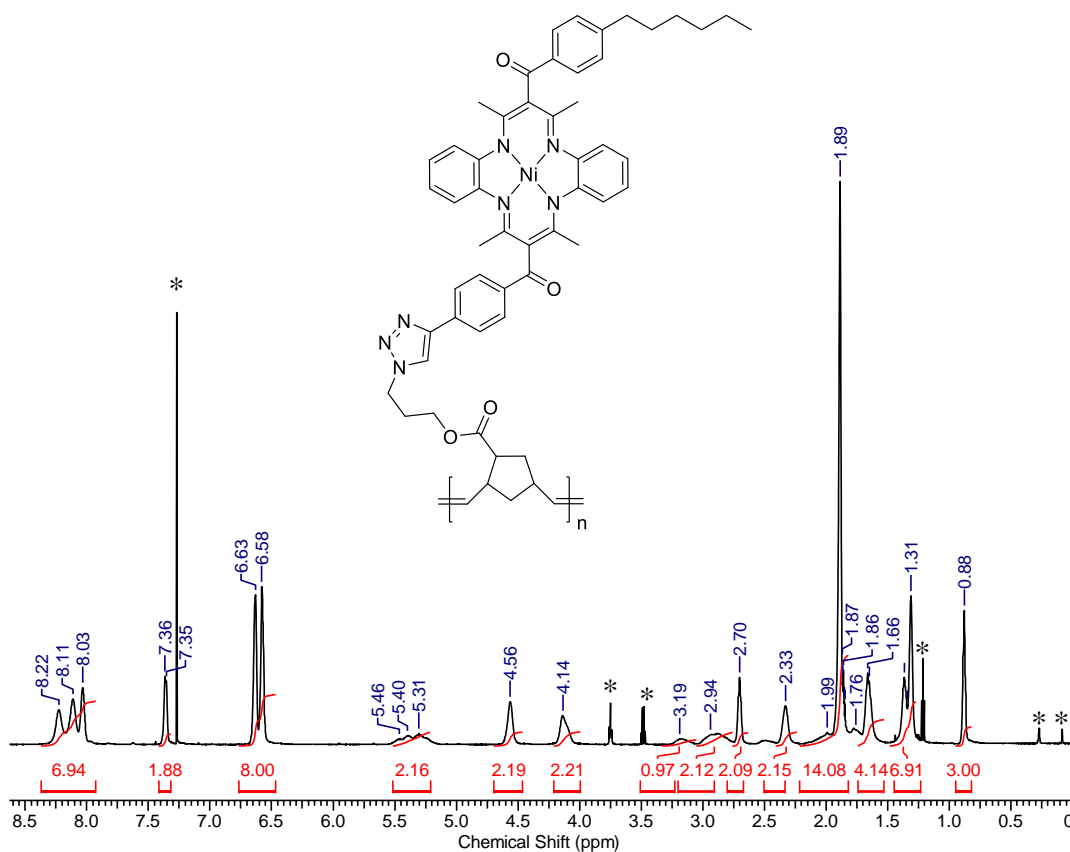


Figure A5.11 ^1H NMR spectrum of polymer 5.11. Asterisk denotes residual CHCl_3 , THF, and Et_2O .

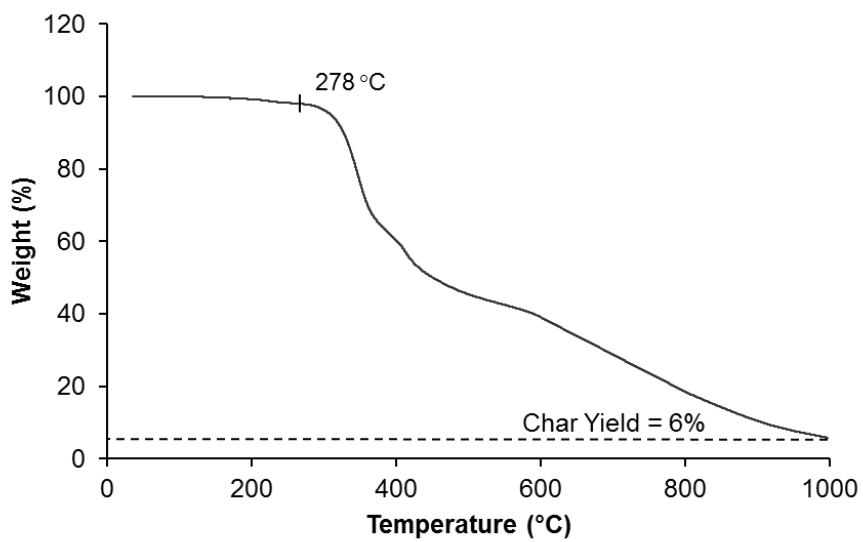


Figure A5.12 TGA trace for polymer 5.11.

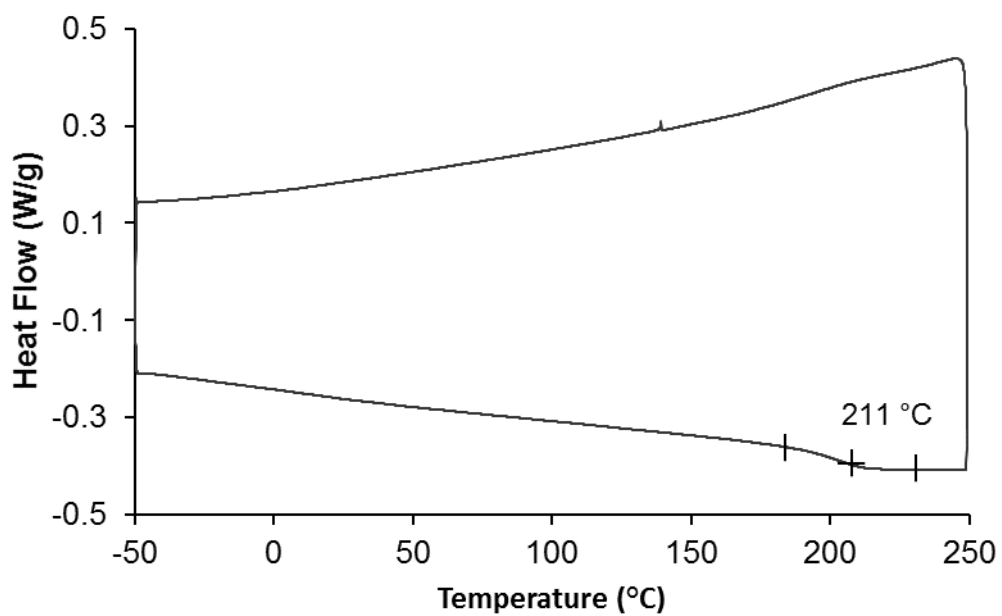


Figure A5.13 DSC of polymer **5.11**. The trace is taken from the second heating/cooling cycle.

Curriculum Vitae

Name:	Joseph A. Paquette	
Post-secondary Education and Degrees:	University of Guelph Guelph, Ontario, Canada 2006–2010	B.Sc.
	Wilfrid Laurier University Waterloo, Ontario, Canada 2010–2012	M.Sc.
	The University of Western Ontario London, Ontario, Canada 2013–2016	Ph.D.
Honours and Awards:	National Science and Engineering Research Council (NSERC) Doctoral Fellowship 2015–2017	\$42,000
	Province of Ontario Graduate Scholarship 2015–2016 (declined)	\$15,000
	Province of Ontario Graduate Scholarship 2014–2015	\$15,000
	1 st Place Poster Prize Interdisciplinary Research Showcase	\$100
Related Work Experience	Teaching Assistant Lab Coordinator – CH2271 The University of Western Ontario 2014–2016	
	Teaching Assistant – CH1200b, CH1024a, CH2281, and CH2273 The University of Western Ontario 2013–2014	
Publications:		
11.	J. A. Paquette , K. M. Psutka, C. J. Yardley, K. E. Maly* Probing the Structural Features that Influence the Mesomorphic Properties of Substituted Dibenz[a,c]anthracenes. <i>Can. J. Chem.</i> 2016 , DOI: 10.1139/cjc-2016-0505.	

10. S. Ezugwu, **J. A. Paquette**, V. Yadav, J. B. Gilroy*, G. Fanchini* Design Criteria for Ultrathin Single-Layer Flash Memristors from Organic Polyradicals. *Adv. Electron. Mater.* **2016**, *2*, 1600253.
9. **J. A. Paquette**, J. G. Gilroy* Synthesis, Characterization, and Pre-Ceramic Properties of π -Conjugated Polymers Based on Ni(II) Complexes of Goedken's Macrocyclic. *J Polym. Sci., Part. A: Polym Chem.* **2016**, *54*, 3257–3266.
8. **J. A. Paquette**, R. E. Yardley, J. W.-Y. Yu, S. H. Eichhorn, K. E. Maly* Anthra- and Pentacenequinone Derivatives as Building Blocks for Columnar Organic Semiconductors. *New J. Chem.* **2016**, *40*, 5985–5988.
7. S. Novoa, **J. A. Paquette**, S. M. Barbon, R. R. Maar, J. B. Gilroy* Side-Chain Boron Difluoride Formazanate Polymers via Ring-Opening Metathesis Polymerization, *J. Mater. Chem. C* **2016**, *4*, 3987–3994.
6. **J. A. Paquette**, S. Ezugwu, V. Yadav, G. Fanchini*, J. B. Gilroy* Synthesis, Characterization, and Thin-Film Properties of 6-Oxoverdazyl Polymers Prepared by Ring-Opening Metathesis Polymerization, *J. Polym. Sci., Part A: Polym. Chem.* **2016**, *54*, 1803–1813.
5. **J. A. Paquette**, E. R. Sauv e, and J. B. Gilroy* Polymers Containing Nickel(II) Complexes of Goedken's Macrocyclic: Optimized Synthesis and Electrochemical Characterization, *Macromol. Rapid Commun.* **2015**, *36*, 621–626.
4. S. Kandeepan, **J. A. Paquette**, J. B. Gilroy and S. Mittler* OMCVD Gold Nanoparticles Covalently Attached to Polystyrene for Biosensing Applications., *Chem. Vap. Deposition* **2015**, *21*, 275–280.
3. K. M. Psutka, J. Williams, **J. A. Paquette**, O. Calderon, K. J. A. Bozek, V. E. Williams, and K. E. Maly* Synthesis of Substituted Dibenz[a,c]anthracene and an Investigation of Their Liquid Crystalline Properties. *Eur. J. Org. Chem.* **2015**, *7*, 1456–1463.
2. J. T. Price, **J. A. Paquette**, C. S. Harrison, R. Bauld, G. Fanchini,* and J. B. Gilroy* 6-Oxoverdazyl radical Polymers with Tunable Electrochemical Properties. *Polym. Chem.* **2014**, *5*, 5223–5226.
1. **J. A. Paquette**, C. J. Yardley, K. M. Psutka, M. A. Cochran, O. Calderon, V. E. Williams, and K. E. Maly* Dibenz[a,c]anthracene Derivatives

Exhibiting Columnar Mesophases Over Broad Temperature Ranges *Chem. Commun.* **2012**, 48, 8210–8212.

Selected Conferences:

13. **J. A. Paquette**, J. B. Gilroy*. Oral Presentation, “*Synthesis, Characterization, and Switchable Thin-Film Conductivity of 6-Oxoverdazyl Radical Polymers Prepared via ROMP*” High Polymer Forum, Ganonoque, ON, August 9–11, **2016**.
12. **J. A. Paquette**, J. B. Gilroy*. Oral Presentation, “*Organic-inorganic hybrid polymers based on nickel(II) complexes of Goedken’s macrocycle.*” Pacificchem 2015, Honolulu, HI. December 15–20, **2015**.
11. **J. A. Paquette**, E. R. Sauve, J. B. Gilroy*. Oral Presentation, “*Polymers Containing Nickel(II) Complexes of Goedken’s Macrocycle.*” 98th Canadian Chemistry Conference and Exhibition, Ottawa, ON. June 13–17, **2015**.
10. **J. A. Paquette**, J. T. Price, C. S. Harrison, R. R. Maar, R. Bauld, G. Fanchini*, and J. B. Gilroy*. Poster Presentation (1st place poster prize) “*Stable Organic Radical Polymers as Hydrophobic Hole-Transport Materials.*” Interdisciplinary Research Symposium, The University of Western Ontario, London, ON. December 2, **2014**.
9. **J. A. Paquette**, J. T. Price, C. S. Harrison, R. R. Maar, R. Bauld, G. Fanchini*, J. B. Gilroy*. Poster Presentation “*Stable Radical Polymers as Hydrophobic Hole-Transport Materials.*” Interdisciplinary Research Showcase, The University of Western Ontario, London, ON. Nov. 27, **2014**. *1st place poster prize.
8. **J. A. Paquette**, J. B. Gilroy*. Oral Presentation. “*Synthesis and Characterization of Redox-Active 6-Oxoverdazyl Polymers.*” Chemistry Graduate Student Symposium, Oral Presentation, Buffalo, NY. May 19–21, **2014**.
7. **J. A. Paquette**, J. B. Gilroy*. Poster Presentation. *Polymerizable Analogues of Goedken’s Macrocycle*. CAMBR Distinguished Lecturer and Research Day, The University of Western Ontario, London, ON, Nov. 1, **2013**.

6. **J. A. Paquette**, J. B. Gilroy*. Poster Presentation, “*Efforts Towards the Polymerization of Goedken’s Macrocycle.*” 46th Inorganic Discussion Weekend, York University, Toronto, ON. Nov. 8–10, **2013**.
5. **J. A. Paquette**, K. M. Psutka and K. E. Maly*. Poster Presentation, “*Synthesis and Mesomorphic Properties of Novel Discotic 1,2:3,4-Dibenzanthracene Derivatives*” 95th Canadian Chemistry Conference and Exhibition, Calgary, AB, May 26–30, **2012**.
4. **J. A. Paquette**, C. Yardley, K. Psutka, M. Cochran, K. E. Maly*. Oral Presentation, “*Synthesis and Investigation of the Liquid Crystalline Properties of 1,2:3,4-Dibenzanthracene Derivatives*”. 39th Physical Organic Minisymposium, London, ON, Nov. 4–6, **2011**.
3. **J. A. Paquette**, C. Yardley, K. Psutka, M. Cochran, K. E. Maly*. Poster Presentation, “*Synthesis and Investigation of the Liquid Crystalline Properties of 1,2:3,4-Dibenzanthracene Derivatives*”. 94th Canadian Chemistry Conference, Montreal, QC, June 5–9, **2011**.
2. **J. A. Paquette**, C. Yardley, K. Psutka, M. Cochran and K. E. Maly*. Poster Presentation, “*Synthesis and Investigation of the Liquid Crystalline Properties of 1,2:3,4-Dibenzanthracene Derivatives*”. 38th Physical Organic Mini-Symposium, Guelph, ON, November 12–14, **2010**.
1. **J. A. Paquette**, A. Michaelides, A. L. Schwan*. Oral Presentation “*Preparation of a Selection of N-Protected Homoserine Lactones from Enantiopure L-Aspartic Acid*”. 38th Southern Ontario Undergraduate Student Chemistry Conference, London, ON, **2010**.